IAEA TECDOC SERIES

Trends of Synchrotron Radiation Applications in Cultural Heritage, Forensics and Materials Science

IAEA

International Atomic Energy Agency

TRENDS OF SYNCHROTRON RADIATION APPLICATIONS IN CULTURAL HERITAGE, FORENSICS AND MATERIALS SCIENCE

The following States are Members of the International Atomic Energy Agency:

AFGHANISTAN	GEORGIA	OMAN
ALBANIA	GERMANY	PAKISTAN
ALGERIA	GHANA	PALAU
ANGOLA	GREECE	PANAMA
ANTIGUA AND BARBUDA	GUATEMALA	PAPUA NEW GUINEA
ARGENTINA	GUYANA	PARAGUAY
ARMENIA	HAITI	PERU
AUSTRALIA	HOLY SEE	PHILIPPINES
AUSTRIA	HONDURAS	POLAND
AZERBAIJAN	HUNGARY	PORTUGAL
BAHAMAS	ICELAND	QATAR
BAHRAIN	INDIA	REPUBLIC OF MOLDOVA
BANGLADESH	INDONESIA	ROMANIA
BARBADOS	IRAN, ISLAMIC REPUBLIC OF	RUSSIAN FEDERATION
BELARUS	IRAQ	RWANDA
BELGIUM	IRELAND	SAN MARINO
BELIZE	ISRAEL	SAUDI ARABIA
BENIN	ITALY	SENEGAL
BOLIVIA, PLURINATIONAL	JAMAICA	SERBIA
STATE OF	JAPAN	SEYCHELLES
BOSNIA AND HERZEGOVINA	JORDAN	SIERRA LEONE
BOTSWANA	KAZAKHSTAN	SINGAPORE
BRAZIL	KENYA	SLOVAKIA
BRUNEI DARUSSALAM	KOREA, REPUBLIC OF	SLOVENIA
BULGARIA	KUWAIT	SOUTH AFRICA
BURKINA FASO	KYRGYZSTAN	SPAIN
BURUNDI	LAO PEOPLE'S DEMOCRATIC	SRI LANKA
CAMBODIA	REPUBLIC	SUDAN
CAMEROON	LATVIA	SWAZILAND
CANADA	LEBANON	SWEDEN
CENTRAL AFRICAN	LESOTHO	SWITZERLAND
REPUBLIC	LIBERIA	SYRIAN ARAB REPUBLIC
CHAD	LIBYA	TAJIKISTAN
CHILE	LIECHTENSTEIN	THAILAND
CHINA	LITHUANIA	THE FORMER YUGOSLAV
COLOMBIA	LUXEMBOURG	REPUBLIC OF MACEDONIA
CONGO	MADAGASCAR	TOGO
COSTA RICA	MALAWI	TRINIDAD AND TOBAGO
CÔTE D'IVOIRE	MALAYSIA	TUNISIA
CROATIA	MALI	TURKEY
CUBA	MALTA	TURKMENISTAN
CYPRUS	MARSHALL ISLANDS	UGANDA
CZECH REPUBLIC	MAURITANIA	UKRAINE
DEMOCRATIC REPUBLIC	MAURITIUS	UNITED ARAB EMIRATES
OF THE CONGO	MEXICO	UNITED KINGDOM OF
DENMARK	MONACO	GREAT BRITAIN AND
DJIBOUTI	MONGOLIA	NORTHERN IRELAND
DOMINICA	MONTENEGRO	UNITED REPUBLIC
DOMINICAN REPUBLIC	MOROCCO	OF TANZANIA
ECUADOR	MOZAMBIQUE	UNITED STATES OF AMERICA
EGYPT	MYANMAR	URUGUAY
EL SALVADOR	NAMIBIA	UZBEKISTAN
ERITREA	NEPAL	VANUATU
ESTONIA	NETHERLANDS	VENEZUELA, BOLIVARIAN
ETHIOPIA	NEW ZEALAND	REPUBLIC OF
FIJI	NICARAGUA	VIET NAM
FINLAND	NIGER	YEMEN
FRANCE	NIGERIA	ZAMBIA
GABON	NORWAY	ZIMBABWE

The Agency's Statute was approved on 23 October 1956 by the Conference on the Statute of the IAEA held at United Nations Headquarters, New York; it entered into force on 29 July 1957. The Headquarters of the Agency are situated in Vienna. Its principal objective is "to accelerate and enlarge the contribution of atomic energy to peace, health and prosperity throughout the world".

IAEA-TECDOC-1803

TRENDS OF SYNCHROTON RADIATION APPLICATIONS IN CULTURAL HERITAGE, FORENSICS AND MATERIALS SCIENCE

PROCEEDINGS OF A TECHNICAL MEETING HELD IN VIENNA, AUSTRIA 17–21 OCTOBER 2011

INTERNATIONAL ATOMIC ENERGY AGENCY
VIENNA, 2016

FOREWORD

Synchrotron radiation (SR) has been used as a tool for analytical research for over three decades, leading to exponential growth of research in many scientific disciplines. More than sixty synchrotron light sources have been built worldwide, and others are in the construction or planning phase. The IAEA has recognized the importance of SR sources for advanced research and analytical applications. In particular, within the framework of an interregional technical cooperation project, the IAEA supports the training of end users and beamline scientists, as well as the commissioning and operation of the International Centre for Synchrotron Light for Experimental Science and Applications in the Middle East (SESAME).

SR offers remarkable analytical capabilities owing to its unique properties, including its high brilliance, wide spectral range (from the infrared to the hard X ray energy region), wavelength (energy) tunability, high degree and selection of polarization, and well defined time–space structure and coherence. These SR features, dynamically coupled with various modes of photon–matter interactions, have led to the development of a wide range of analytical techniques offering structural characterization, high elemental sensitivity, chemical specificity, and three dimensional spatial resolution at the micrometre scale or below. This in turn has boosted analytical applications in a diverse range of scientific disciplines such as materials sciences, energy research, protein crystallography, environmental sciences, chemistry, life sciences/biosciences, microelectronics, geological sciences including extraterrestrial matter and paleoenvironment studies, and industrial applications such as automotive applications, pharmaceuticals and biotechnology, semi-conductors, metallurgy, cosmetics and bulk chemical synthesis. Among the emerging scientific fields are characterization of energy storage and conversion related micro- and nanoscale heterogeneous materials such as batteries, fuel cells, photovoltaics and organic semiconductors, and analysis of cultural heritage materials and materials related to forensics.

This publication provides an overview of the analytical applications of SR sources in the fields of cultural heritage, forensics and materials science, and presents relevant research projects carried out by 14 IAEA Member States. The papers included in this TECDOC were presented by experts during a Technical Meeting held at the IAEA on 17–21 October 2011. The meeting aimed at providing a forum for specialists in SR applications to review the current status of, and developments and trends in, SR applications, with an emphasis on the fields of cultural heritage, forensics and characterization of energy related materials; to identify and map needs for further improvement in SR instrumentation and analytical methodologies to improve and optimize the analytical performance of SR based techniques; to explore means to exchange and share cross-cutting information and know-how between scientists in the relevant SR applications; and to provide information on how to enhance and support training of young scientists in SR applications (e.g. training courses, advanced schools). The present publication presents all the scientific information and ideas exchanged among the experts at the Technical Meeting, including participants from 14 IAEA Member States (Austria, Australia, Belgium, China, France, Germany, India, Italy, Lebanon, Portugal, Serbia, Thailand, Ukraine and the United States of America) and IAEA staff members. It offers a summary of the state of the art of SR applications.

The IAEA would like to thank all the participants, and in particular J. Koen (Belgium), for their valuable contributions. The IAEA officer responsible for this publication was A. Karydas of the Division of Physical and Chemical Sciences.

CONTENTS

INTRODUCTION

The synergistic application of synchrotron radiation (SR) analytical techniques can provide nowadays an integrated characterization of materials based on complementary analytical information revealed from: (i) chemical analysis, including elemental composition, chemical state (speciation) and coordination site analysis of the absorbing atom, identification of molecular groups and structures (X ray fluorescence (XRF), X ray absorption spectroscopy (XAS), X ray emission spectroscopy (XES), inelastic X ray scattering (IXS), resonant inelastic X ray scattering (RIXS), X ray absorption near edge structure / Near edge X ray absorption fine structure (XANES/NEXAFS), extended X ray absorption fine structure (EXAFS), Fourier Transform infra-red spectroscopy (FTIR), ultra violet / visible luminescence (UV/Vis)), (ii) structural analysis to understand the modifications induced to crystalline of heterogeneous materials (X ray diffraction (XRD), small angle X ray scattering (SAXS)), (iii) investigation of electronic and magnetic properties of surfaces, thin films, and buried interfaces (Soft X ray emission, Photoemission electron microscopy (PEEM), angular resolved photoemission spectroscopy (ARPES), low energy electron microscopy (LEEM), X ray magnetic circular dichroism (XMCD)), and (iv) morphological characterization, i.e. visualization in two or three dimensions of the very fine details of complex structures (Micro-tomography (μCT) and Phase contrast tomography PhC CT).

Despite the aforementioned analytical possibilities new challenges have already emerged in certain scientific fields including the needs for the characterization of advanced, energy storage and conversion related materials and materials related to cultural heritage investigations and forensics.

The modern approach for the characterization of the electrochemical systems (battery systems, fuel cells) requires both off-line and in situ analysis using a probe that can penetrate electrodes and electrolytes at depths up to several mm and appropriate detectors to allow time resolved studies of the electrochemical reactivity. In the case of nano-scaled structured photovoltaic and novel nano-structured battery materials new variants of standard techniques such as the Grazing Incidence XRF (GIXRF) are explored nowadays for in depth profiling of the elemental concentration gradients that affect crucially the band energy gap and the density of free charge carriers, and consequently the efficiency of the solar cell.

In the field of CH applications, the non-destructive character of examination renders the SR as an inevitable analytical tool. New SR analytical modalities by means of 3D-XRF, 3D-XANES provide in-depth element-specific compositional and chemical state analysis which helps to understand degradation phenomena in ancient glass and the formation of ancient nanomaterials (attic ceramics black gloss), the fading and alteration of pigments in painting masterpieces etc. Further on, the features of SR-FTIR (high spatial resolution- 10 μm range and improved noise-to-signal ratio) have considerably increased the possibility to understand and characterize simultaneously organic (binders, mordants, varnishes, glazes, pigments) and inorganic (pigments, fillers) materials in paintings, organic coatings on furniture, varnishes in organic instruments, corrosion compounds in bronze artefacts etc. In forensics related investigations SR-FTIR can be applied without the need for any special sample treatment for the analysis of minute complex and vibrationally active samples (blood smears on surfaces, mixed tissue and body fluids on clothing, fingerprints on a weapon) from crime scenes. In this sense, the use of synchrotron based infrared fingerprinting looks promising in the future of forensics offering characterization of trace amounts of explosives, tiny fragments of paint and plastic from cars, clothing, carpet fibres, hair dyes, illicit drugs and poisons.

1. SYNCHROTRON RADIATION APPLICATIONS FOR CULTURAL HERITAGE AND FORENSIC MATERIALS

1.1 Main advantages and limitations – current status

The main advantages of synchrotron radiation in this field of research are:

- The low destructiveness of the methods which are based on light-matter interactions (from IR to X rays) allowing protocols involving complementary characterization, essential due to the complexity and heterogeneity of the samples studied;
- The abundance of information that can be reached (from the atomic to the structural levels), also because of the multimodal character and the interaction between the various user community that takes place on the same instrument;
- The quality of information, thanks to the high beam brightness, which enables to obtain data rapidly and on a limited quantity of matter;
- The high spatial resolution offered by the beam spot size, in particular for micro-imaging, which allows a selective analysis;
- Some methods are non-invasive and allow for internal inspection of entire objects (hard X ray, THz);
- The capability to perform real-time in-situ analyses.

Main limitations are that:

- Objects and people need to be transferred;
- Most techniques are invasive (sampling required);
- There is a limited access to beam time, and skills in getting beam time may not always be accessible to new users;
- Communication and knowledge transfer between physical scientists and specialists in the fields of Cultural Heritage, Archaeology and Forensics

1.2. Research areas and methods covered

1.2.1 Currently

1. The current use of synchrotron-radiation techniques for Cultural heritage has been reviewed in a number of articles (see: Table 1 and [1-21]).
2. Main issues at stake are shortly summarized below:

- Provenance, strong at the beginning but going down in terms of applications except on specific areas of research where statistic is needed on small particles/inclusions (aboriginal ochres, iron metal artefacts)
- Ancient technology,
- Visualization of hidden/vanished art and historical documents,
- Degradation
- Evaluation, monitoring, optimization of consolidation, stabilization and conservation procedures

Forensics is often driven by specific cases: strong interest for organic residuals from crime sciences.

Materials studied in the field are represented in FIG. 1 and the list of beam lines used is represented in FIG. 2, with output from beamlines exemplified by the situation at ID21 from the ESRF.

1.2.2. To be explored

Some of the points listed below have been demonstrated as feasible, however more stabilization is needed to make them more widely accessible to the user communities.

Emerging fields of research:
- Evaluation of active and passive conservation treatments, including study of past interventions and building materials
- Forensics per se
- Works on corpuses and collections of artworks and artefacts
- Contemporary art materials: polymers, waxes, etc.
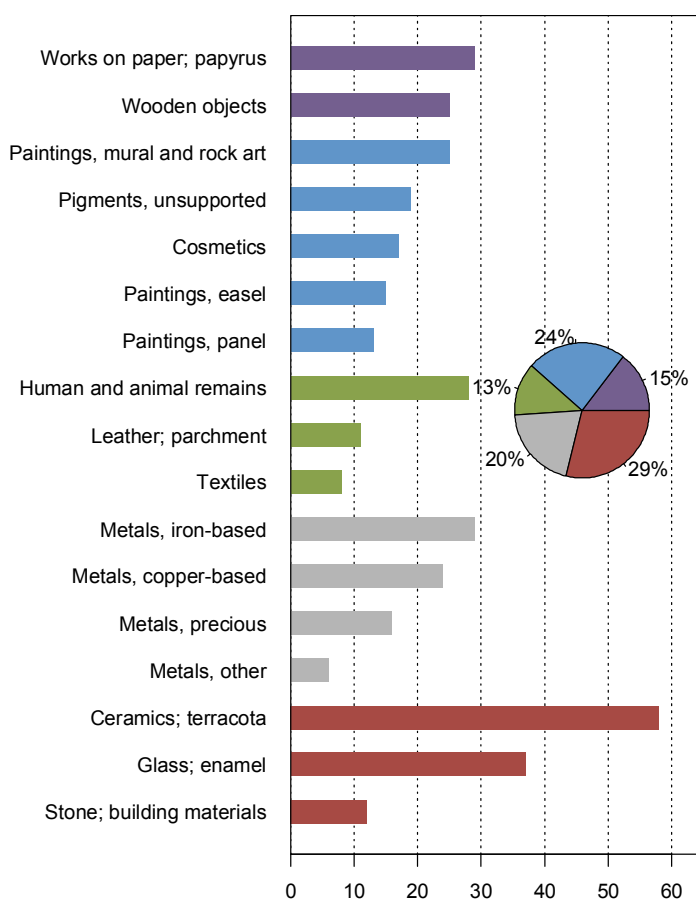
FIG. 1. Classes of materials from Archaeology and Cultural Heritage studied using synchrotron-radiation techniques based on review of the literature in the 1986–2010 period. Data: L. Bertrand et al.

Consolidation of methodological topics:
- Synergetic use of complementary synchrotron-based techniques (3D/2D, imaging/spectroscopy, morphology/chemistry, coupling of several energy ranges)
- Advanced analytics applied to complete objects
- More systematic multi-spectral view on materials
- Switching capabilities in terms of beam size

- Depth selectivity, particularly in confocal setups
- Sample preparation methods
- Data processing software
- In-situ characterizations
- Enhanced possibilities of quantitative approaches in 2D/3D micro- and macro-characterization.

New feasibility to be assessed:
- New energy ranges in the field: THz, near infrared, UV/visible;
- Full-field XRF, XAS, X ray macro-scanning and new coherence-based imaging modalities;
- Developments in the use of small-angle X ray scattering techniques.
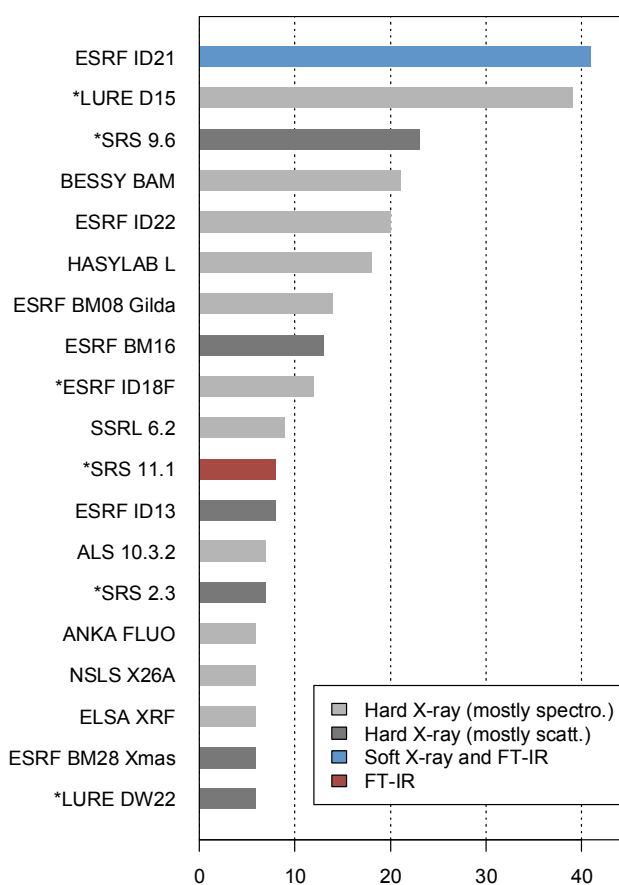
FIG. 2. Synchrotron beam lines used for Archaeology and Cultural heritage with more than 5 resulting publications, based on a review of the literature in the 1986–2010 period. The six beam lines marked with a star (*) are now shut down. Data: Bertrand et al.

Crossovers between similar fields employing synchrotron radiation such as environmental science and materials science could be more strongly supported.

1.3.   Instrumental and methodological needs

Cultural heritage is connected to many instrumental developments, including that of nano-investigation; however we focus here more on the major aspects of interest raised. Needs expressed by the countries specifically can be found in the attached table in annex to this document.

1.3.1. Full-field X ray (XRF, XAS) imaging

Current developments in full-field XAS (ESRF ID21; SSRL 6-2) and XRF (BESSY BAMline) allow recording hyper spectral images without sample scanning and the need of single spot spectra. The data collection time is therefore strongly reduced and some artefacts connected to scanning can be avoided. It also offers more possibilities for tomography imaging and real time in-situ characterization. It will also allow XRF tomography to yield full 3D elemental reconstructions, as shown by current developments with the MAIA detector.

1.3.2. Scanning tomography

If XRF tomography at the micrometer level might be achieved in the near future in stable conditions using full-field setups avoiding the scanning, there is still a marked interest for higher resolution works. Potentially more important are scanning XRD and SAXS 3D reconstructions using micro-focused beams.

1.3.3. μCT and laminography capabilities

The interests of synchrotron μCT are several: increased spatial resolution, increased contrast speed, phase-contrast capabilities compared to standard lab sources. Synchrotron μCT also offers more possibilities for in-situ studies, an approach largely used for material sciences but not regularly for Cultural Heritage. Current development includes the research of enhanced contrast and elimination of physical constraints due to artefact shapes.

1.3.4. Macro-scanning

X ray macro-scanning was shown to provide pictorial information in relation to morphology of macroscopic artefacts (artworks), including through visualization of the trace-elemental patterning. Today efforts are put in the careful design of objects holders and stages since the objects have to be moved relative to the fixed beam.

1.3.5. New energy ranges

THz depth imaging of entire objects is currently investigated. UV/visible spectroscopy and imaging appear as a promising complements to soft X ray characterization and to the more usual FT-IR spectroscopy. Methodological developments in the hard X ray region are also relevant to the field, for instance for XRF/XRD mapping and 3D imaging.

1.3.6. Processing and analysis of multi-/hyper spectral data

Data processing is very demanding when coming to multi-/hyper spectral data, and many new questions are raised regarding data reduction, clustering, fusion, statistical analysis and also data storage and consultation. Recovery of quantitative data from 3D characterizations is also a challenging topic. In addition, there is a recurrent constraint connected to access from users to software, particularly for expensive pieces of software. IAEA could therefore support funding of freely available software for processing of synchrotron data.

1.3.7. Databases of reference materials

Many Cultural Heritage works require reference materials (particularly for X ray absorption spectroscopy). Having access to numeric data is a first useful step and should be encouraged before characterization of standards during experiments. Intercomparison tests during round robins can also be favored by IAEA both for accurate data recording and training purposes.

1.3.8. New beam lines with a program connected to Cultural Heritage

- P63 (PETRA III), a general-purpose microprobe beam line (XRF, XRD, XAS) and macro-scanning for Cultural heritage artefacts.
- PUMA (SOLEIL) optimized for ancient materials with two end stations on X ray micro focused characterization and full-field imaging.
- The imaging beam line ID19 at ESRF currently being fully upgraded.

1.4. Support needs

1.4.1. Support for travel for synchrotron experiments

The current schemes in force in various countries (in Europe for instance) allows for support of travel to synchrotron facilities to perform synchrotron characterization on cultural heritage, however, this is not the case for many countries and a limited scheme, even on a restricted set of selected projects, that would answer this need was identified as priority if it could fit under the possibility for funding by IAEA. A specific scheme has been put in place for SESAME that could possibly benefit to other user countries. Ideally, this support could include elongated stays for sample preparation and data processing, particularly for newcomers.

1.4.2. Synchrotron schools including hands-on training

Past training activities in several synchrotron facilities devoted to Cultural Heritage proved very efficient in fostering research in the field. Such schools at synchrotrons devoted to Cultural Heritage were performed in the past at SRS (Daresbury, UK), SOLEIL (Saint-Aubin, France), ESRF (Grenoble, France), ELETTRA (Trieste, Italy). More generalist schools are organized in several countries (among others: HERCULES in Europe, CHEIRON in Japan, 'ASEAN workshops on synchrotron-based techniques' at SLRI, Thailand, - Stanford Synchrotron Radiation Summer School, Canadian Synchrotron Summer School, NESY Winter School on Research with Neutrons and Synchrotron radiation, Synchrotron radiation school in SSRF for users with potential interest. Here, we identified the need for (a) specific Cultural Heritage training courses that could be organized at synchrotrons in other regions of the world and (b) support for the attendance of students from 'developing' countries (in the IAEA sense) with new users in the field. Training on data processing should also be included and supported in training schools, including on software such as PyMCA, GeoPIXE and FEFF, etc. for EXAFS/XANES processing.

1.4.3. Experience in equivalent laboratory techniques for preliminary characterization and training (μXRF, PIXE, μCT, FTIR, Raman, UV/visible spectroscopy), including for sample preparation

Experience in equivalent laboratory techniques for preliminary characterization and training was shown as a major initial step for new synchrotron users. The extent of corresponding techniques is large: μXRF, PIXE, μCT, FTIR, Raman, UV/visible spectroscopy, etc., some of them being also available through the NSIL IAEA laboratory. These techniques are both useful in that they provide necessary preliminary characterization of Cultural Heritage and forensics materials, and also because they are an efficient training to the use of corresponding or similar techniques at synchrotron facilities. Cultural heritage could be identified as an area of application of NSIL, particularly in 2D/3D X ray spectro-imaging and diffraction, and coordination with access to synchrotron facilities could be favoured. Sample preparation is also recognized as a strong need for the field, as it is dealing with complex heterogeneous materials. For these reasons, we advise that support is provided to exchanges also on these topics aside direct support to synchrotron activities.

1.4.4. Support to international conferences

There are many events worldwide where synchrotron users convene to present and discuss their work. There is one international conference in the field of Cultural Heritage, called "Synchrotron radiation in Art and Archaeology" (SR2A) that was organised:
- at SSRL, SLAC, California, USA, 18 October 2000;
- at the ESRF and CNRS, Grenoble, France, 9–11 February 2005;
- at BESSY, Berlin, Germany, 27–29 September 2006;
- in Barcelona, Spain, 22–24 October 2008;
- at the Van Gogh museum in Amsterdam, The Netherlands, 8–9 November 2010.

The next editions are scheduled at the Metropolitan museum of Art in New York, USA (6-8 June 2012), and the 2014 edition is scheduled in Paris, France. For the 2012, 2014 and future editions, IAEA could potentially support the travel of users from 'developing' countries, as well as for instance a specific session putting the emphasis in new developments in these countries. We would also like to suggest here the idea that IAEA would formally support that the 2016 edition be organized in a region were this event did not took place in the past, such as Asia which has a strong tradition of research in the field of Cultural Heritage, a large patrimony and many very recent developments in synchrotron-based research in the field.

1.4.5. Support to regional conferences

Aside the SR2A conference, a possible evolution, as seen for many other fields of research, would be the organization of regional conferences, between two meetings of SR2A, in various part of the world which could benefit from IAEA funding support. Such a conference could be combined with a relevant training school.

1.4.6. Documentation

Participants raised the interest for an IAEA book that would be freely available over the internet and deal with "Synchrotron radiation for Cultural Heritage Research", as a complement to the existing "Nuclear Techniques for Cultural Heritage Research" published in September 2011. A first step would be that the result of the current meeting is published in the IAEA Technical Report series.

TABLE 1. SYNCHROTRON RADIATION IN CULTURAL HERITAGE AND FORENSICS BY MEMBER STATES

Country	Field of SR applications	SR techniques utilized/complementary techniques	Facility	SR Instrumentation development current status and specificities	Results obtained on Materials Analyzed	Challenges for the analysis and methodologies to be developed
Australia	Cultural Heritage, Forensics [22]	XAS, XRF, XRF Tomography, Tomography	Australian Synchrotron (AS), Australian National Beamline Facility (Photon Factory, Japan), Advanced Photon Source	Large area chemical (XANES) mapping (AS). Maia detector – ultrafast XRF mapping enabling MPixel images in ~5-10 hours (AS), [23] GeoPIXE software for statistical analysis of XRF spectra/maps and quantification (AS), Fast, full 3D reconstruction for samples <~3mm diameter	Hair (possible proof of metabolism by changes in speciation) [24] Paintings (mapped underlying paint layers), Egyptian artefacts (provenance and manufacturing technique), [25] Aboriginal Ochres (mineralogical profiles for provenance)	Access/availability/cost of analysis software for individual users Computing/algorithms/expertise for quantification of 3D reconstructions.
		XRF, XAS	XOR-CAT, Advanced Photon Source	High sensitivity and high resolution XRF	Characterizing preservatives in cultural heritage materials [26],[27]	
		CT and Transmission X ray microscopy (TXM)	NSRRC, Taiwan	High resolution zone plates (down to 17nm @ 8keV) for CT and TXM [28]	Otolith fossils (evidence of possible microbial degradation, NSRRC)	

Country	Field	Technique	Instrumentation	Beamline	Research topics	Future developments
Belgium	Cultural Heritage, Environmental materials	MA-XRF Micro-XANES Micro-XRD 2d+ tomography Micro-XRF 2d+tomography Confocal micro-XRF	MAR CCD Polycapillary lenses (confocal)	DESY – BL L	Materials use/hidden layers in paintings. Provenance of historical Glass [29] Degradation of (a) artists pigments, (b) historical glass, (c) ferro-gallic inks on historic documents [30],[31] Methodological developments (MAXRF, confocal XRF, FF-XRF imaging, XRF/XRD scanning, XRD tomography.[32], [33], [34], [25], [36] Degradation /reactivity of environmental particles	Upgrade plan for BL P63 Petra III
France	Cultural Heritage	Micro-XANES Micro-XRF, FTIR mapping	KB, FZP, submicron beam, IR microscope	ESRF – ID21	Insights into degradation mechanism of pigments [37], [38], [39], [40], [41] Evaluation of historical glass conservation treatments [42]	Side branch with XRD scanning, Full field XAS imaging
France	Cultural Heritage	Absorption tomography Phase Contrast Tomography	High-resolution Frelon camera	ESRF – ID19	Evaluation of conservation treatments of (a) archaeological wood, (b) historical glass, (c) limestone[46], [47] Method development: laminography of paintings [48]	Laminography under development, Enhanced phase contrast imaging under development

France		SOLEIL – SMIS & DIFFABS			
Cultural Heritage	XANES, XRD, FTIR mapping		IR microscope	Evaluation of conservation treatments of (a) historical documents with ferro-gallicinks and (b) limestone. [49],[50]	Puma beamline proposed and designed
Cultural Heritage Sciences (30%), Environmental Sciences (23%), Earth and Planetary Sciences (16%), Life Sciences and Medicine (10%)	μXRF, μXANES [43]	ESRF, ID21	Excitation: 2-9keV, beam focused with Zone plates, or KB system, down to $0.3\mu m$(ver.) $\times 0.7\mu m$ (hor.) flux: 10^9-10^{10} detection: photodiode (fluorescence, transmission) EDS (SDD, 7element Ge) WDS. High efficiency for low Z elements Development of a full-field set-up Data analysis: PyMca [44], [45]	Pigment (identification, degradation) painting (degradation), glass and ceramics (manufacturing, color, opacity; degradation), metal (manufacturing, corrosion), bones (color), papers and ink (manufacturing and degradation), textile (manufacturing, degradation), wood (degradation), [51], [52], [53], [54], [55], [56], [57], [58], [59], [60], [61], [62] Patina on African sculpture (identification of blood)[63]	Sample preparation (thin sections), Full 2D XANES

ESRF, ID21	μFTIR	700-4000 cm⁻¹ Confocal microscope (Thermo) MCT detector Transmission, reflection, ATR Data analysis: PyMca Easy combination with X ray (same sample holder)	painting (identification of pigments and binders; degradation), glass (degradation) [64] (identification of blood) varnishes on music instruments (identification)[65], plastics (degradation), wax (degradation), mummy (degradation), papers and ink (manufacturing, degradation), textile (manufacturing, degradation), wood (degradation)	Sample preparation (thin sections)[66] Improved resolution
France	Cultural Heritage / Environment	XRF / XAS	SOLEIL synchrotron[1], DIFFABS, LUCIA, SAMBA, ODE, (NANOSCOPIUM, PUMA)	EXAFS data collection at low X ray energies Quick EXFAS and XANES Corrosion cells	Pigments (alteration processes)[67] Metal (corrosion processes)	Few micrometer beam spatial resolution for hard X rays (to be added through the new funded PUMA beamline) Corpus analysis XRF/XRF macro-scanning

Country	Field	Technique	Synchrotron, beamline	Characteristics	Application / samples	Future developments
France	Cultural Heritage / Environment	XRD / SAXS	SOLEIL synchrotron, DIFFABS, CRISTAL, SWING, (PUMA)	High-temperature setups; Small to wide angle SAXS data collection	Metal (corrosion processes)	Few micrometer beam spatial resolution for hard X rays (to be added through the new funded PUMA beamline); Corpus analysis; XRF/XRF macro-scanning, full-field imaging
	Cultural Heritage / Environment	FTIR spectro-microscopy	SOLEIL synchrotron, SMIS	Diffraction-limited spectral imaging	Historical instruments (varnish composition, alteration) [68]; Paintings and rock art (alteration, pigment identification); Archaeological bones (alteration)	Easier use of ATR setups for historical cross-sections
	Cultural Heritage / Environment	UV/visible luminescence microspectroscopy and imaging	SOLEIL synchrotron, DISCO, DESIRS	Unique setup adapted to Cultural Heritage samples; High-spatial (300-500 nm) and spectral resolution. Mpixel data collection in 10 s^{-1} min	Paintings and historical instruments cross-section (organic material identification, semiconductor pigments identification, alteration feature imaging) [69]	Better coupling between UV/visible microspectroscopy and imaging; Hyperspectral setup
	Cultural Heritage / Environment	CT	SOLEIL synchrotron, METROLOGY, (PSICHE, PUMA)	Test setup for the moment	Test setup for the moment	Development of a phase-contrast CT setup underway with the PUMA beamline
Portugal	Cultural Heritage	Confocal XRF	ANKA	Stable X ray confocal XRF setup	Metal objects (inclusion analysis) [70]	Higher lateral and depth resolution

13

Country	Field	Techniques	Facility	Details	Applications	Comments
	Cultural Heritage,	XANES, EXAFS, XRF	ESRF, Grenoble, France	BM 29 6-20 Kev XRD wave length 0,7 – 2,1 Å	Faience, porcelains and tiles glazes and painting decoration (Co speciation and coordination; coloring causes; dating criterion) [71], [72], [73], [74], [75], [76],	Analysis of heterogeneous material Analysis of organic materials Availability of additional support programs for visits to SR facilities in order to develop methodologies adapted to samples to be analyzed
	Environment/ Geology	(XRD, INAA, SEM, Neutron Tomography, TL-OSL)	(Instituto Tecnológico e Nuclear)			
Lebanon	Cultural heritage	1.7 MV Tandem accelerator (PIXE, PIGE, RBS, NRS)	PIXE, microPIXE	Installation of an in air microbeam	Provenance of byzantine, roman and Ottoman ceramics and Omayyad coins, ancient glass	Segregation process Availability of statistical program with higher performance Heterogeneity in some samples.

14

Thailand	Cultural heritage (6%) Material Science (73%) Environmental Science (13%) Geological Science (4%) Biology (4%)	XAS and XRF Complimented with PIXE and SEM-EDX	Synchrotron Light Research Institute (SLRI), Beamline 8	Bending magnet beamlime (1.25 keV-10 keV) with a large beam size (13mm x 1 mm), detection limit ~ 50 ppm with a 13-element germanium detector	Decorative red and blue glasses (oxidation states of copper and cobalt) Decorative red and blue glasses (identification on main glass composition and traced elements, qualitative analysis)	Higher photon flux to improve sensitivity and shortening dwell time (collimating and/or focusing mirrors) Adjustable beam size (slits) to probe small specific area Higher photon energy (wavelength shifter) Quantitative analysis (signal-concentration calibration), Visibility of light elements (commission of silicon drift detector in vacuum and/or helium-filled sample chamber) Micro beam (capillary lenses) 2D Mapping (motorized sample stages)

2. SYNCHROTRON RADIATION APPLICATIONS FOR MATERIAL SCIENCE

2.1. Main advantages and limitations – current status

Besides the advantages already described in 1.1 the main advantages of synchrotron radiation in this field of research can be summarized as following:

- Probing with complementary modalities on different length scales from the atom to m sized objects
- High time resolution <ps
- the ability to follow in real time dynamic processes and phase transitions
- mostly non destructive

- Main limitations are:
- There is a limited access to beam time, and skills in getting beam time may not always be accessible to new users;
- Sometimes complicated experimental conditions with long set up times
- For small sized low contrast objects radiation damage.

2.2. Research areas and methods covered

2.2.1. Currently

A substantial percentage of beam lines at synchrotron radiation sources are dedicated to material science (e.g. FIG. 3) and the current use of synchrotron radiation techniques in the field has been reviewed in a number of articles [77-91].

The regions of application of synchrotron radiation are X ray microscopy, X ray phase imaging including Computed Tomography (CT), different X ray absorption spectroscopy techniques (such as XANES, EXAFS, XMCD, GIXRS, XES, RIXS, X ray Raman) for local atomic and electronic structure determination in multi-component complex solid-state systems and techniques probing surfaces (such as PEEM, LEEM, ARPES, etc.).
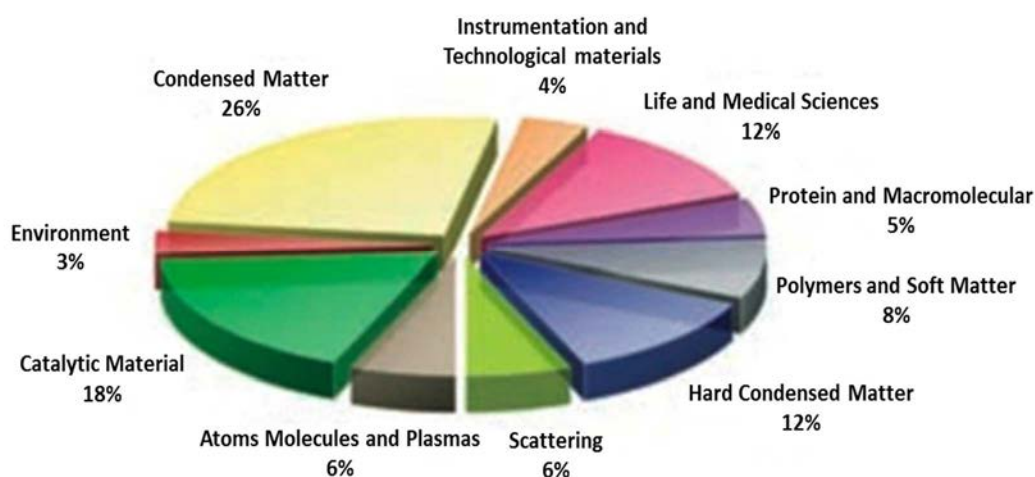
FIG. 3. Allocated Proposals by research area at Elettra for the period July 2009 - June 2010: From a total of 438 accepted proposals around 80% can be identified with material science.

Main issues are concerned with the investigation of:
- surfaces
- interfaces
- depth profiling and chemical speciation at buried interfaces contamination
- bulk materials
- morphological structure
- nano materials
- Graphene
- nanostructures and organic films
- Magnetism and highly correlated systems
- in
- (semimagnetic) semiconductors,
- in energy storage and energy conversion related materials
- advanced materials
- geological samples
- porous materials
- nanotechnology

2.2.2. *To be explored*

Some of the points listed below have been demonstrated as feasible, however, more stabilization is needed to make them more widely accessible to the user communities.

- Emerging fields of research:
- bio- nano interfaces
- nano structured (functionalized) materials
- intelligent polymers
- ceramics
- light metals and alloys
- electronics and magnetic materials

2.3. Instrumental and methodological needs

Material Science relies on many instrumental developments, including that of nano-investigation. The final quality of the data is depending on the accelerators, the optics, the detectors and the data mining. Specific needs expressed by the countries can be found in ANNEX IV: Table 2. The general overview of instrumentation needs can be summarized as in the following:

2.3.1. *Machine performance*

Machine performance in terms of brightness, photon flux, stability (spatial and in intensity), lateral and temporal coherence should be generally increased.

2.3.2. Optics and diagnostics

High fidelity beam line optics is required that does not effect the phase of the associated wave field. Focusing optics to generate nm sized focal spots will be needed in future applications. High quality gratings and mirrors as well as bended single crystals might be a bottleneck. In-situ, non-invasive beam intensity and position monitoring especially for small sized foci will be mandatory. With respect to substantial power-load at XFELS diamond optics and diamond based detectors.

2.3.3. Multi-element spectroscopic detectors

To increase the throughput of XRF beam lines the data collection time has to be strongly reduced thus scanning approaches should be avoided or dwell times reduced. This can be obtained using multi element spectroscopic detectors such as MAIA detector or multi element silicon drift detectors (SDD). The use of such devices offers real time in-situ characterization. It will also allow XRF tomography to yield full 3D elemental reconstructions.

2.3.4. Energy resolving imaging detectors

Some applications, for instance micro level or nano level in one dimension for depth profiling require large area pixel detectors of about 10 cm x 10 cm (e.g. pnCCDs) combining energy dispersive measurements and imaging applications (energy resolution < 200 eV at 6 keV) and at count rate per pixel of 1000 photons (50 μm x 50 μm). Good peak to background ratio (1000 for soft X rays (< Si K edge) and 10,000 for hard X rays (> Si K-edge)) would be required for the experimental setting of the next decade. These requirements are ambitious but are definitely needed for future XFELs. A later transition of such detection systems to ERL and SR facilities can be anticipated.

2.3.5. μCT and laminography capabilities

Dedicated imaging detectors featuring small pixel size (~ 1μm × 1μm), large field of view (~ 5 cm × 5 cm), high dynamic (> 16 bit) and fast frame rates (> 1 kHz frame rate) are needed. Local tomography can reduce the requirements on the field of view but would rely on quantitative reconstruction algorithm. Especially for large aspect ratio samples (like turbine blades) reconstruction algorithms from limited projection sets similar to laminography are mandatory.

2.3.6. Sample holders

New XRF sample holders' concepts should be developed that contribute little with impurities and do not contaminate the spectra; this is also valid for the entire environment in the vicinity of the sample / detector. For complementary (imaging) methods interchangeable sample holders with well-defined fiducially markers will be needed in future.

2.4. Needs in analytical methodologies

2.4.1. Data mining for imaging

There is a strong need for quantitative phase retrieval in phase based radiography and CT. Moreover, quantitative morphological information from 3-D and 4 -D data sets should be extracted. New concepts in data acquisition, data handling, data-storage, data transfer will be needed especially when large data sets of complementary imaging or time sequences are recorded. Data reduction already in the front-end electronics might be mandatory use as it is used in high-energy physics experiments. Development of quantitative local CT algorithms is required as well as a reduction of reconstruction artefacts. Spiral CT might be an option to reduce the data acquisition times. Phase CT should be combined with XRF CT for 3-D element mapping.

2.4.2. Theoretically supported data evaluation for XAS

Further development and adaptation of density functional theory or any other competitive approaches in view to overcome the restrictions of current algorithms:
In order to incorporate the effects important for treating the near edge region of the absorption spectra of 1 s ionizations in a reliable manner (e.g. existing ab-initio multi-scattering codes such as FEFF).
In order to harmonize deviations between the absorption spectra and the DOS (density of states) as performed by further developed Robert D. Cowan codes [92]such as the multiplet algorithms by Frank de Groot (The CTM4XAS programme for EELS and XAS spectral shape analysis of transition metal L edges [93], including crystal field effects and so on for 2p and higher ionizations of selected elements to provide access to all elements andeven prediction capabilities instead of the empirical procedures involving parameter variations.

2.4.3. Validation of the theoretical data evaluation

Validation of further developed software codes by independent XAFS data from international SR facilities. Optimization of computational time (e.g. parallel processing techniques) and computational resources (e.g. memory). Access to powerful computing cluster facilities and support to developing countries.

2.4.4. Traceability

Improved traceability of analytical methods with respect to ISO17025 accreditation and quality control procedures expected to be needed in the near future for many relevant international funding applications involving characterization techniques and analytical methodologies. (e.g. surface contamination as mass deposition per unit area traced back to the SI units kg and m)

2.4.5. ISO17025

Support of IAEA NSIL with respect to projects in member state institutions on either improved traceability or ISO17025 accreditation could be provided by means of round Robin

tests involving either calibration samples provided by IAEA or accredited methodologies provided by NSIL in its laboratories.

2.5. Support needs

2.5.1. Support for travel for synchrotron experiments

Training of young researchers and PhD grant programs in the field of SR applied to material science is an important issue for future application. Countries without own synchrotron radiation facility would need financial support for travel and subsistence to access SR facilities not only in Europe but also worldwide.

2.5.2. Synchrotron schools including hands-on training

Training activities in form of SR schools devoted to material science have been performed in several countries and basically at any facility worldwide. These schools are excellent tools to foster international collaboration, to exchange ideas and knowledge. Training on data processing including on software such as PyMCA, GeoPIXE and FEFF, etc. for EXAFS/XANES data mining should be included and supported in training schools with special focus on researchers from developing member states.

2.5.3. Experience in equivalent laboratory techniques for preliminary characterization

Due to the limited access to SR infrastructures efficient preliminary training could be carried out on laboratory sources providing equivalent experimental techniques such as μCT, μXRF, PIXE, μCT, FTIR, Raman, UV/visible spectroscopy. Also speciation capabilities by means of adequate sample pre-treatment and preparation techniques of species selected on ultra-thin membranes in conjunction with elemental analysis techniques such as TXRF modules distributed with the IAEA support can substantially help to prepare and validate SR activities as a valuable complementary methodology [31]. Some of those techniques are already available through the NSIL IAEA and the ICTP laboratories.

3. RECOMMENDATIONS

The two groups of participants have made the following recommendations:

From the Cultural Heritage/Forensics Working Group

- Member States are encouraged to use the existing frameworks of (a) national funding, (b) national and regional IAEA TC funding instruments to support this field of research;
- Regional cooperation should be fostered, including through bilateral agreements and regional initiatives such as the EC Joint Programming Initiative in Cultural Heritage.
- Software freeware development and databases of reference materials should also be supported;

From the Materials Science Working Group

- There is a clear expression of training needs for young especially for countries without Synchrotron radiation sources or without coverage of EU access programs. Further on, opportunities for training fellows from South American region at US synchrotron radiation facilities should be established.
- Research in material science especially in emerging fields of industrial applications (such as energy storage and conversion, effective & advanced materials, and materials under extreme conditions) has major impact on the social economic situation of the member states. Complementary SR based methodologies can substantially contribute to both the R&D as well as the quality control of these materials allowing for an efficient transition in these industrial and social priorities.
- Member states should be encouraged to exchange ideas and knowledge through the official collaborations (which will enable e.g. joint access to SR facilities) moderated by the IAEA.
- Member states should provide more collaborative centres (e.g. ELETTRA, ICTP). These centers will increase the visibility of IAEA actions and will have a positive feedback on future Coordinated Research Projects (CRP).

TABLE 2. SYCHROTRON RADIATION IN MATERIAL SCIENCE BY MEMBER STATES

Country	Field of SR applications	SR techniques utilized/complementary techniques	Facility	SR Instrumentation development current status and specificities	Results obtained on Materials Analyzed	Challenges for the analysis and methodologies to be developed
Austria	Material science	GIXRF+XRR,	no Austrian SR facility	experiments at Hasylab, ANKA, bending magnet, energy 2-17, SDD	depth profile in ultra-shallow junctions, total implanted dose in the ultra-shallow junctions, thin layer thickness and density and composition in high k thin film samples	reduce ambiguity of results combining with other methods like SIMS
China	Materials, cultural heritage Li ion battery, ceramics piece, catalysis, jade, porous polymer, alloy, carbon, CNT film, etc.	XRD, XAFS, SAXS, X ray phase imaging, X ray absorption, CT X ray fluorescence CT	SSRF	BM, 4-30keV, focused beam, Wiggler (XAFS), 4-25keV, focused beam, wiggler (imaging), 8-72.5 keV, unfocused beam	Dynamic stress, Process, Crystal structure, Morphology, Element status, Interface of films	In-situ process, fast process, improve the contrast, imaging for different crystal phases, high resolution Phase retrieval, dynamic CT, CT for part of the sample, dynamic SAXS

Country	Application area	Technique	Facility	Instrumentation details	Capabilities	Future needs
Germany	Metrology, Nanotechnology: Nanoelectronics, Nanoparticles, and materials for energy storage and conversion, Geological, environmental Sciences	X ray spectrometry: total-reflection X ray fluorescence (XRF), grazing incidence XRF, reference-free XRF analysis, XRR, NEXAFS / XANES, EXAFS, XES	PTB lab at BESSY	Well-defined monochromatizedundulator and bending magnet radiation (known higher-order and stray light contributions), calibrated energy-dispersive detectors, calibrated photodiodes, calibrated WDS, uncertainty reduction of selected atomic fundamental parameters	Elemental composition, mass depositions, elemental depth profile, speciation, coordination	Organic nanoscaled materials, complex nanostructured materials involving multi-elemental and spatially varying matrixes, surface contamination on curved samples (Avogadro project) Efficient higher energy and spatial (or depth) resolving techniques based on adaption of new instrumentations (e.g. 2D energy-dispersive detectors), Need for theoretical modelling software packages with true predictive capabilities (e.g. for XAFS and XES)
	Biomedical, Environmental and Materials Science	IR/THZ micro-spectrometry	Metrology Light Source (MLS)	FTIR and THz beam lines, spectrometers and detectors, near field IR microscope providing 20 nm resolution	Chemical analysis, speciation, chemical binding states	Organic and inorganic nanoscaled, environmental and biomedical materials
India	Materials science	Reflectivity, PES	Indus I	Bending magnet, TGM, HSA with MCP, Photodiode	Soft X ray ML optics, Porosity in thin films, resonant photo emission and band structure in Inter-metallic compounds	

Country	Applications	Techniques	Source	Instrumentation	Science cases	Comments
India	Material science, forensics, cultural heritage, biomedical, nano particles, nano structures; glasses, wood rocks, instruments; ancient artefacts	ADXRD, EDXRD EDEXAFS, XRF, Lithography; IR spectroscopy	Indus-2	DCM, Bent Crystal Si(111) polychromator; Ionization chamber, Scintillation counter, Image Plate, HPGe detector	Crystal Structure of metallic alloy and annealing studies in soft amorphous Alloy, macro and micro strain in nanocrystals, structure and coordination of Cu(II) complexes, trace amount of Th in reactor material, calibration of detector using XRF from lunar simulant, fabrication of MEMS structure, refractive X ray lenses, ferrofluidic micro channel	Low and high temperature facility, high pressure setup
Italy		XRF, EXAFS, Xanes,,X ray microscopes, X ray imaging / phase imaging techniques; IR spectroscopy	ELETTRA	bending magnets (typically from some keV to 35 keV) focused beam ~ μm^2, large fan beam (20 cm x 5mm), scanning xrf instrumentation, multi element detectors for imaging and spectroscopy	elemental composition, combined X ray microscopy and elemental mapping, 3-d phase reconstructions, revealing morphology	elemental composition, combined X ray microscopy and elemental mapping, 3-d phase reconstructions; quantitative reconstruction algorithm, phase retrieval, porosity, Need for theoretical modelling software packages with true predictive capabilities (e.g. for XAFS and XES)

Country	Technique	Facility / Instrument	Instruments	Application	Challenges / Needs
Italy	XRD, SAXS, PEEM, XPS, Arpes, LEEM, XMCD-PEEM Dichroism, IVUS, IR/THZ micro-spectrometry	ELETTRA	wiggler and undulatorbeamlines, Pilatus 1 M and Pilatus 100 K hybrid pixel detectors, Picasso Si strip detector in single photon counting mode, cross delay line MCP detectors for electron detection, SDDs, Diamond detectors; zone plates, refractive optics, CCD detectors, 700-4000 cm^{-1}; Confocal microscope	catalysts, interlayer relaxation at metal-oxide interfaces, Graphene, Nanostructures and organic films, Magnetism and highly correlated systems, Atomic and Molecular Physics, speciation, chemical binding states	imaging detectors for electrons with high dynamic range, smaller foci for zone plates, fast multi element energy dispersive detectors
	XRF, phase imaging, SEM, STM	Elettra ICTP, portable instruments	μ-focus X ray tubes, μ-focus CT, scanning xrf, portable xrf; CCD detectors	elemental composition, 3-d reconstructions, revealing morphology	Need for theoretical modelling software packages with true predictive capabilities (e.g. for XAFS and XES)
Lebanon	ToF-SIMS; Molecular imaging, LE-PIXE, PIGE and RBS	ToF-SIMS (Bi cluster source-20/30keV) and 1.7MV accelerator	LE-PIXE and use of PIGE for thin films (several nm)	Elemental, chemical and molecular characterization, active ingredient mapping and quantification in solid drugs, excipient solid form and interactions, banknote paper and painting characterization, degradation of polymers under gamma irradiation, thermal diffusion and interdiffusion and mixing of polymers	Metastability of some ejected molecules and ions. Molecular depth profile in organic matrix, need of direct ToF in parallel with electrostatic reflector MCP detectors

Country	Applications	Techniques	Source		Research topics	Developments needed
Ukraine	reactor material science, forensics, cultural heritage, nuclear medicine Zr, Nb, U, actinide, faince, porcelain, paintings	XRF, Ion beam analytical techniques (RBS, PIXE, PIGE, ERDA, μPIXE)	Focused ionbeam at 2 μm, monochromatic X ray source based on proton accelerator		Elemental composition of actinide for environmental monitoring	new XRF technique for sensitive detection of actinide, design of the multipurpose X ray micro probe facility based on proton accelerator
USA	Batteries, hydrogen storage materials, photovoltaic, catalysis, metalloroteins, solid-state physics	X ray Raman Scattering, X ray Emission, Resonant inelastic X ray Scattering (RIXS), X ray Absorption with a high resolution fluorescence detection	Stanford Synchrotron Radiation Light Source	Wiggler insertion device, 6keV peak performance, energy range 4-18 keV, 3 multi-crystal high energy resolution Johann-type spectrometers for low-q and high-q X ray Raman spectroscopy and XES/RIXS	Local electronic structure, oxidation state, bond length on Li carbon batteries, Li air batteries, carbon based hydrogen storage materials, LiHB4 based H storing materials, asphaltenes	In situ X ray Raman spectroscopy of Li in low concentration samples (<5%). Analysis of samples with a very high sensitivity to radiation damage, higher flux is always welcome, focused incident beam (~um regime) to allow standing wave based X ray Raman as well as efficient studies on high pressure (>GPa) cells

Serbia					
Material Science, Multi-component IV-VI and II-VI solid solutions/mixed crystals, II-VI diluted magnetic oxides	XRF, XRD Raman/IR spectroscopy; Theoretical calculations (FEFF9.0, WIEN2k)	no Serbian SR facility but portable instruments and computational infrastructure based in Belgrade	Computer cluster	Local electronic/magnetic structure, local atomic environments; nearest neighbor distances, nearest neighbor preferences; coordination numbers, bond relaxation, disorder parameters, local/long-range ordering; DOS, electronic configuration, valence state, the site symmetry; Mechanisms of impurity atoms accommodation, lattice distortions	Fully quantitative theoretical model of XANES
Material Science, Multi-component IV-VI and II-VI solid solutions/mixed crystals, II-VI diluted magnetic oxides	XANES, EXAFS, XMCD	DESY, ELETTRA	Bending magnet, Electromagnetic Elliptical Wiggler; focused beam 5x0.8mm; Broad energy range: 5 eV-80keV; Detectors: 7 cell SDD, 7 pixel HPGe, 7 pixel Si(Li); Ionization chambers; UHV chamber equipped with evaporators and Auger analysis	Local electronic/magnetic structure, local atomic environments; nearest neighbour distances, nearest neighbour preferences; coordination numbers, bond relaxation, disorder parameters, local/long-range ordering; DOS, electronic configuration, valence state, the site symmetry; Mechanisms of impurity atoms accommodation, lattice distortions	Fully quantitative theoretical model of XANES

REFERENCES

[1]   ADAMS, F., ADRIAENS, A., AERTS, A., DE RAEDT, I., JANSSENS, K., SCHALM, O., Micro and surface analysis in art and archaeology, J. Anal. Atom. Spectrom. **12** 3 (1997) 257–265.

[2]   BERTRAND, L., "Synchrotron imaging for archaeology, art history, conservation and paleontology", Physical techniques in the study of art, archaeology and cultural heritage Vol. 2 (CREAGH, D. C. BRADLEY, D. A., Ed.), Elsevier Science, Amsterdam (2007) 97–114.

[3]   BERTRAND, L., COTTE, M., STAMPANONI, M., THOURY, M., MARONE, F., SCHÖDER, S., "Development and trends in synchrotron studies of ancient and historical materials", Phys. Rep. (2011) 60 pp. Invited.

[4]   BERTRAND, L., ROBINET, L., THOURY, M., JANSSENS, K., COHEN, S. X., SCHÖDER, S., Cultural heritage and archaeology materials studied by synchrotron spectroscopy and imaging, Appl. Phys. A **106** 2 (2011) 377-396.

[5]   BRADLEY, D. CREAGH, D., Eds, Physical Techniques in the Study of Art, Archaeology and Cultural Heritage, Vol. 1, Elsevier, Amsterdam, 2006.

[6]   COTTE, M., CHECROUN, E., MAZEL, V., SOLÉ, V. A., RICHARDIN, P., TANIGUCHI, Y., WALTER, P., SUSINI, J., Combination of FTIR and X rays synchrotron-based micro-imaging techniques for the study of ancient paintings. A practical point of view, e-Preserv. Sci. **6** (2009) 1–9.

[7]   COTTE, M., DUMAS, P., TANIGUCHI, Y., CHECROUN, E., WALTER, P., SUSINI, J., Recent applications and current trends in Cultural Heritage Science using synchrotron-based Fourier transform infrared micro-spectroscopy, C. R. Physique **10** 7 (2009) 590–600.

[8]   COTTE, M., SUSINI, J., DIK, J., JANSSENS, K., Synchrotron-based X ray absorption spectroscopy for art conservation: looking back and looking forward, Acc. Chem. Res. **43** 6 (2010) 705–714.

[9]   CREAGH, D. C. OTIENO-ALEGO, V., The use of radiation for the study of material of cultural heritage significance, Nucl. Instrum. Methods B **213** (2004) 670–676.

[10]   DE NOLF, W., DIK, J., VANDERSNICKT, G., WALLERT, A., JANSSENS, K., High Energy X ray Powder Diffraction for the imaging of (hidden) paintings, J. Anal. Atom. Spectrom. **26** (2011) 910–916.

[11]   HARBOTTLE, G., GORDON, B. M., JONES, K. W., Use of synchrotron radiation in archaeometry, Nucl. Instrum. Methods B **14** 1 (1986) 116–122.

[12]   JANSSENS, K., DIK, J., COTTE, M., SUSINI, J., Photon-based techniques for nondestructive sub-surface analysis of painted cultural heritage artifacts, Acc. Chem. Res. **43** 6 (2010) 814–825.

[13]   JANSSENS, K., VITTIGLIO, G., DERAEDT, I., AERTS, A., VEKEMANS, B., VINCZE, L., WEI, F., DERYCK, I., SCHALM, O., ADAMS, F., RINDBY, A., KNÖCHEL, A., SIMIONOVICI, A., SNIGIREV, A., Use of microscopic XRF for non-destructive analysis in art and archaeometry, X ray Spectrom. **29** 1 (2000) 73–91.

[14]   KANNGIEßER, W., MALZER W., MANTOUVALOU, I., SOKARAS, D., KARYDAS, A.G. , A Deep View in Cultural Heritage - Confocal Micro X ray Spectroscopy for Depth Resolved Elemental Analysis, Appl. Phys. A. **106** 2 (2011) 325-338.

[15]   KEMPSON, I. M., PAUL KIRKBRIDE, K., SKINNER, W. M., COUMBAROS, J., Applications of synchrotron radiation in forensic trace evidence analysis, Talanta **67** 2 (2005) 286–303.

[16]   LOMBI, E., SCHECKEL, K. G., KEMPSON, I. M., In situ analysis of metal(loid)s in plants: state of the art and artefacts. Environ. Exp. Bot. **72** (2011) 3-17.

[17] MARTIN, M. C., SCHADE, U., LERCH, P., DUMAS, P., "Recent applications and current trends in analytical chemistry using synchrotron-based Fourier-transform infrared microspectroscopy", Trends Anal. Chem. **29** 6 (2010) 453–463.

[18] NAKAI, I., "Synchrotron radiation X ray fluorescence analysis of cultural properties", Spectrometric examination in conservation, Internat. Symp. of the conservation and restoration of cultural property, Tokyo, Japan, 1994, Tokyo national research institute of cultural properties, (1996) 125-135.

[19] PANTOS, E., "Synchrotron radiation in archaeological and cultural heritage science", in X rays for Archaeology, (UDA, M., DEMORTIER, G., NAKAI, I., Eds), Springer, Dordrecht, NL (2005) 199–208.

[20] SALVADÓ, N., BUTÍ, S., TOBIN, M. J., PANTOS, E., PRAG, J. N. W., PRADELL, T., Advantages of the use of SR-FT-IR microspectroscopy: applications to cultural heritage, Anal. Chem. **77** 11 (2005) 3444–3451.

[21] WESS, T. J., DRAKOPOULOS, M., SNIGIREV, A., WOUTERS, J., PARIS, O., FRATZL, P., COLLINS, M., HILLER, J., NIELSEN, K., The use of small-angle X ray diffraction studies for the analysis of structural features in archaeological samples, Archaeometry **43** 1 (2001) 117–129.

[22] KEMPSON, I.M., KIRKBRIDE, K.P., SKINNER, W.M. COUMBAROS, J., Applications of synchrotron radiation in forensic trace evidence analysis, Talanta **67** 2 (2005) 286-303.

[23] RYAN, C.G., SIDDONS, D.P., KIRKHAM, R., DUNN, P.A., KUCZEWSKI, A., MOORHEAD, G., DE GERONIMO, G., PATERSON, D.J., DE JONGE, M.D., HOUGH, R.M., LINTERN, M.J., HOWARD, D.L., KAPPEN, P. CLEVERLEY, J., The new Maia detector system: Methods for high definition trace element imaging of natural material, (Proc. 20th Internat. Congress on X ray Optics and Microanalysis) 1221 American Institute of Physics, Karlsruhe (2010) 9-17.

[24] KEMPSON, I.M. HENRY, D.A., Determination of arsenic poisoning and metabolism in hair by synchrotron radiation: The case of phar lap, Angew. Chem. Int. Edit. **49** 25 (2010) 4237-40.

[25] LAU, D., KAPPEN, P., STROHSCHNIEDER, M., BRACK, N., PIGRAM, P.J., Characterization of green copper phase pigments in Egyptian artifacts with X ray absorption spectroscopy and principal components analysis, Spectrochimica Acta B **63** (2008) 1283.

[26] KEMPSON, I.M., HENRY, D. FRANCIS, J., Characterizing arsenic in preserved hair for assessing exposure potential and discriminating poisoning, J. Synchrotron Radiat. **16** (2009) 422-7.

[27] KEMPSON, I.M., SKINNER, W.M. KIRKBRIDE, K.P., Advanced analysis of metal distributions in human hair, Environ. Sci. Technol. **40** (2006) 3423-8.

[28] CHEN, T.Y., CHEN, Y.T., WANG, C.L., KEMPSON, I.M., LEE, W.K., CHU, Y.S., HWU, Y. MARGARITONDO, G., Full-field microimaging with 8 keV X rays achieves a spatial resolutions better than 20 nm, Opt. Express **19** 21 (2011) 19919-24.

[29] VAN DER SNICKT, G., DIK, J., COTTE, M., JANSSENS, K., JAROSZEWICZ, J., DE NOLF, W., GROENEWEGEN, J., VAN DER LOEFF, L., Characterization of a Degraded Cadmium Yellow (CdS) Pigment in an Oil Painting by Means of Synchrotron Radiation Based X ray Techniques, Anal. Chem. **81** (2009) 2600-2610.

[30] SCHALM, O., PROOST, K., DE VIS, K., CAGNO, S., JANSSENS, K., MEES, F., JACOBS, P., CAEN, J., Manganese staining of archaeological glass: the characterization of Mn-rich inclusions in leached layers and a hypothesis of its formation, Archaeometry **53** (2011) 103-122.

[31] ROUCHON, V., DURANTON, M., BURGAUD, C., PELLIZZI, E., LAVEDRINE, B., JANSSENS, K., DE NOLF, W., NUYTS, G., VANMEERT, F., HELLEMANS, K.,

Room-temperature study of iron gall ink impregnated paper degradation under various oxygen and humidity conditions: Time-dependent monitoring and XANES measurements, Anal. Chem. **83** (2011) 2589-97.

[32]   DIK, J., JANSSENS, K., VAN DER SNICKT, G., VAN DER LOEFF, L., RICKERS, K., COTTE, M., Visualization of a lost painting by Vincent van Gogh using synchrotron radiation based X ray fluorescence elemental mapping, Anal. Chem. **80** (2008) 6436-6442.

[33]   JANSSENS, K., PROOST, K., FALKENBERG, G., Confocal microscopic X ray fluorescence at the HASYLAB microfocus beamline: characteristics and possibilities, Spectrochim. Acta B **59** (2004) 1637-1645.

[34]   ALFELD, M., JANSSENS, K., SASOV, A., LIU, X., KOSTENKO, A., RICKERS-APPEL, K., FALKENBERG, G., The use of full-field XRF for simultaneous elemental mapping, X ray optics and microanalysis, Proceedings, 1221 (2010) 111-118.

[35]   VAN DER SNICKT, G., DE NOLF, W., VEKEMANS, B., JANSSENS, K., mu-XRF/mu-RS vs. SR mu-XRD for pigment identification in illuminated manuscripts, Appl. Phys. A-Mater. **92** (2008) 59-68.

[36]   DE NOLF, W., JANSSENS, K., Micro X ray diffraction and fluorescence tomography for the study of multi-layered automotive paints, Surf. Interface Anal. **42** (2010) 411-418.

[37]   COTTE, M., SUSINI, J., DIK, J., JANSSENS, K., Synchrotron-based X ray absorption spectroscopy for art conservation: Looking back and looking forward, Accounts Chem. Res. **43** (2010) 705-714.

[38]   MONICO, L., VAN DER SNICKT, G., JANSSENS, K., DE NOLF, W., MILIANI, C., VERBEECK, J., TIAN, H., TAN, H.Y., DIK, J., RADEPONT, M., COTTE, M., Degradation process of lead chromate in paintings by Vincent van Gogh studied by means of synchrotron X ray spectromicroscopy and related methods. 1. Artificially aged model samples, Anal. Chem. **83** (2011) 1214-1223.

[39]   MONICO, L., VAN DER SNICKT, G., JANSSENS, K., DE NOLF, W., MILIANI, C., DIK, J., RADEPONT, M., HENDRIKS, E., GELDOF, M., COTTE, M., Degradation process of lead chromate in paintings by Vincent van Gogh studied by means of synchrotron X ray spectromicroscopy and related methods. 2. Original paint layer samples, Anal. Chem. **83** (2011) 1224-1231.

[40]   VAN DER SNICKT, G., DIK, J., COTTE, M., JANSSENS, K., JAROSZEWICZ, J., DE NOLF, W., GROENEWEGEN, J., VAN DER LOEFF, L., Characterization of a degraded cadmium yellow (CdS) pigment in an oil painting by means of synchrotron radiation based X ray techniques, Anal. Chem. **81** (2009) 2600-2610.

[41]   RADEPONT, M., DE NOLF, W., JANSSENS, K., VAN DER SNICKT, G., COQUINOT, Y., KLAASSEN, L., COTTE, M., The use of microscopic X ray diffraction for the study of HgS and its degradation products corderoite ([small alpha]-Hg3S2Cl2), kenhsuite ([gamma]-Hg3S2Cl2) and calomel (Hg2Cl2) in historical paintings, J. Anal. Atom. Spectrom. **26** (2011) 959-968.

[42]   CAGNO, S., NUYTS, G., BUGANI, S., DE VIS, K., SCHALM, O., CAEN, J., HELFEN, L., COTTE, M., REISCHIG P., JANSSENS, K., Evaluation of manganese-bodies removal in historical stained glass windows via SR-m-XANES/XRF and SR-m-CT, J. Anal. Atom. Spectrom. **26** (2011) 2442-2451.

[43]   BUGANI, S., MODUGNO, F., LUCEJKO, J.J., GIACHI, G., CAGNO, S., CLOETENS, P., JANSSENS, K., MORSELLI, L. Study on the impregnation of archaeological waterlogged wood with consolidation treatments using synchrotron radiation microtomography, Anal. Bioanal. Chem. **395** (2009) 1977-1985.

[44]   BUGANI, S., CAMAITI, M., MORSELLI, L., VAN DE CASTEELE, E., JANSSENS, K., Investigating morphological changes in treated vs. untreated stone building materials by X ray micro-CT, Anal. Bioanal. Chem. **391** (2008) 1343-1350.

[45]   JANSSENS, K., DIK, J., COTTE, M., SUSINI, J. Photon-Based Techniques for Nondestructive Subsurface Analysis of Painted Cultural Heritage Artifacts, Accounts Chem. Res. **43** (2010) 814-825.

[46]   ROUCHON, V., PELLIZZI, E., JANSSENS, K. FTIR techniques applied to the detection of gelatine in paper artifacts: from macroscopic to microscopic approach, Appl. Phys. A-Mater. **100** (2010) 663-669.

[47]   ROUCHON, V., PELLIZZI, E., DURANTON, M., VANMEERT F., JANSSENS, K. Combining XANES, ICP-AES, and SEM/EDS for the study of phytate chelating treatments used on iron gall ink damaged manuscripts, DOI: 10.1039/c1ja10185d

[48]   COTTE, M., SUSINI, J., DIK, J., JANSSENS, K., Synchrotron-based X ray absorption spectroscopy for art conservation: looking back and looking forwards, Accounts Chem. Res. **43** 6 (2010) 705-714.

[49]   DE ANDRADE, V., SUSINI, J., SALOMÉ, M., BERALDIN, O., RIGAULT, C., HEYMES, T., LEWIN, E., VIDAL, O., Submicrometer hyperspectral X ray imaging of heterogeneous rocks and geomaterials: Applications at the Fe K-Edge, Anal. Chem. **83** 11 (2011) 4220-4227.

[50]   SOLE, V. A., PAPILLON, E., COTTE, M., WALTER, P., SUSINI, J., A multiplatform code for the analysis of energy-dispersive X ray fluorescence spectra, Spectrochim. Acta B **62** 1 (2007) 63-68.

[51]   COTTE, M., WELCOMME, E., SOLÉ, V. A., SALOMÉ, M., MENU, M., WALTER, P., SUSINI, J., Synchrotron-based X ray spectromicroscopy used for the study of an atypical micrometric pigment in 16th century paintings, Anal. Chem. **79** (2007) 6988-6994.

[52]   COTTE, M., SUSINI, J., SOLÉ, V. A., TANIGUCHI, Y., CHILLIDA, J., CHECROUM, E., WALTER, P., Applications of synchrotron-based micro-imaging techniques to the chemical analysis of ancient paintings, J. Anal. Atom. Spectrom. **23** (2008) 820-828.

[53]   COTTE, M., SUSINI, J., METRICH, N., MOSCATO, A., GRATZIU, C., BERTAGNINI, A., PAGANO, M., Blackening of Pompeian cinnabar paintings: X ray microspectroscopy analysis, Anal. Chem. **78** 21 (2006) 7484-7492.

[54]   COTTE, M., CHECROUN, E., SUSINI, J., WALTER, P., Micro-analytical study of interactions between oil and lead compounds in paintings, Appl. Phys. A-Mater. **89** 4 (2007) 841-848.

[55]   LAHLIL, S., COTTE, M., BIRON, I., SZLACHETKO, J., MENGUY, N., SUSINI, J., Synthesizing lead antimonate in ancient and modern opaque glass, J. Anal. Atom. Spectrom. **26** 5(2011) 1040-1050.

[56]   ARLETTI, R., VEZZALINI, G., QUARTIERI, S., FERRARI, D., MERLINI, M., COTTE, M., Polychrome glass from Etruscan sites: First non-destructive characterization with synchrotron µXRF, µXANES and XRPD, Appl. Phys. A-Mater. 92(2008) 127-135.

[57]   CAGNO, S., NUYTS, G., BUGANI, S., DE VIS, K., SCHALM, O., CAEN, J., HELFEN, L., COTTE, M., REISCHIG, P., JANSSENS, K., Evaluation of manganese-bodies removal in historical stained glass windows via SR-µ-XANES/XRF and SR-µ-CT, J. Anal. Atom. Spectrom. **26** 12 (2011) 2442-2451.

[58]   BURGER, E., BOURGARIT, D., WATTIAUX, A., FIALIN, M., The reconstruction of the first copper-smelting processes in Europe during the 4th and the 3rd millennium BC: where does the oxygen come from? Appl. Phys. A-Mater. **100** 3(2010) 713-724.

[59]   MONNIER, J., NEFF, D., RÉGUER, S., DILLMANN, P., BELLOT-GURLET, L., LEROY, E., FOY, E., LEGRAND, L., GUILLOT, I., A corrosion study of the ferrous medieval reinforcement of the Amiens cathedral. Phase characterisation and localisation by various microprobes techniques, Corros. Sci. **52** 3(2010) 695-710.

[60]   CHADEFAUX, C., VIGNAUD, C., CHALMIN, E., ROBLES-CAMACHO, J., J., A.-C., JOHNSON, E., REICHE, I., Colour origin and heat evidence of paleontological bones: case study of blue and grey bones from San Josecito Cave, Mexico, Am. Mineral. **94** (2009) 27-33.

[61]   MURPHY, B. M., COTTE, M., MUELLER, M., BALLA, M., GUNNEWEG, J., Degradation of parchment and ink of the Dead Sea scrolls investigated using synchrotron based X ray and infrared microscopy, Brill (2010) 77-97.

[62]   SANDSTRÖM, M., JALILEHVAND, F., DAMIAN, E., FORS, Y., GELIUS, U., JONES, M., SALOMÉ, M., Sulfur accumulation in the timbers of King Henry VIII's warship Mary Rose: A pathway in the sulfur cycle of conservation concern, Proceedings of the National Academy of Sciences of the USA **102** (2005) 14165-14170.

[63]   MAZEL, V., RICHARDIN, P., DEBOIS, D., TOUBOUL, D., COTTE, M., BRUNELLE, A., WALTER, P., LAPRÉVOTE, O., Identification of ritual blood in African artifacts using TOF-SIMS and synchrotron radiation microspectroscopies, Anal. Chem. **79** (2007) 9253-9260.

[64]   COTTE, M., DUMAS, P., TANIGUCHI, Y., CHECROUN, E., WALTER, P., SUSINI, J., Recent applications and current trends in Cultural Heritage Science using synchrotron-based Fourier transform infrared micro-spectroscopy, Cr. Phys. **10** 7 (2009) 590-600.

[65]   ECHARD, J. P., COTTE, M., DOORYHÉE, E., BERTRAND, L., Insights into the varnishes of historical musical instruments using synchrotron micro-analytical methods, Appl. Phys. A-Mater. **92** (2008) 77-81.

[66]   COTTE, M., CHECROUN, E., MAZEL, V., SOLÉ, V. A., RICHARDIN, P., TANIGUCHI, Y., WALTER, P., SUSINI, J., Combination of FTIR and X rays synchrotron-based micro-imaging techniques for the study of ancient paintings. A practical point of view, e-Preserv. Sci. **6** (2009) 1-9.

[67]   ROBINET, L., SPRING, M., PAGÈS-CAMAGNA, S., VANTELON, D., and TRCERA, N., Anal. Chem. **83** (2011) 5145

[68]   BERTRAND, L., ROBINET, L., COHEN, S. X., SANDT, C., LE HÔ, A.-S., SOULIER, B., LATTUATI-DERIEUX, A., and ECHARD, J.-P., Anal. Bioanal. Chem. 399 (2011) 3025. ECHARD, J.-P., BERTRAND, L., VON BOHLEN, A., LE HÔ, A.-S., PARIS, C., BELLOT-GURLET, L., SOULIER, B., LATTUATI-DERIEUX, A., THAO, S., ROBINET, L., LAVÉDRINE, B., and VAIEDELICH, S., Angew. Chem. Int. Ed. **49** (2010) 197.

[69]   THOURY, M., ECHARD, J.-P., RÉFRÉGIERS, M., BERRIE, B., NEVIN, A., JAMME, F., and BERTRAND, L., Anal.Chem. **83** (2011) 1737.

[70]   LEROY, S., SIMON, R., BERTRAND, L., WILLIAMS, A., FOY, E., and DILLMANN, P., J. Anal. Atom. Spectrom. **26** (2011) 1078.

[71]   DIAS, M. I. – Principal Investigator of the FCT (Fundação Para a Ciência e Tecnologia) project PTDC/HAH/69506/2006. "Dating, authenticity, materials, pigments. A laboratory study on Portuguese Faience and Chinese Porcelain produced for the Portuguese market (XVI to XVIII centuries)" (2006-2010).

[72]   DIAS, M.I., PRUDÊNCIO, M.I. Neutron activation analysis of archaeological materials: an overview of the ITN NAA Laboratory, Portugal. Archaeometry **49** 2 (2007) 381-391.

[73]   FIGUEIREDO, M.O., SILVA, T.P., VEIGA, J.P., PRUDÊNCIO, M.I., DIAS, M.I., MATOS, M.A., PAIS, A.M. Blue pigments in XVI-XVII century glazes: a comparative study between Portuguese faiences and contemporary Chinese porcelains manufactured for the Portuguese market, 2nd Latin-American Symposium on Physical and Chemical Methods in Archaeology, Art and Cultural Heritage Conservation (LASMAC 2009).

Selected Papers Archaeological and Arts Issues in Materials Science (RuvalcabaSil, J.L., et al. Eds) Univ. Nac. Autónoma de México (2010) 84-88.

[74]   FIGUEIREDO, M.O., SILVA, T.P., VEIGA, J.P., DIAS, M.I., "Speciation state of cobalt in blue glazes: a XAFS study on XVI century Chinese blue-and-white porcelains", Proc. Spring Meeting European Materials Research Society (EMRS), Strasbourg, France, 2009 (abstract).

[75]   DIAS, M.I., PRUDÊNCIO, M.I., On the Importance of Using Sc to Normalize Geochemical Data Previous to Multivariate Analyses Applied to Archaeometric Pottery Studies, Microchem. J. **88** (2008), 136–14.

[76]   BURBIDGE, C.I., RODRIGUES, A.L., DIAS, M.I., PRUDÊNCIO, M.I., CARDOSO, G.O. Optimisation of preparation and measurement protocols for luminescence dating of small samples from a suite of porcelains and faiences. Mediterranean Archaeology and Archaeometry **10** (2010) 53-60.

[77]   FABRY, L., PAHLKE, S., BECKHOFF, B., "Total-Reflection X ray Fluorescence Analysis (TXRF)', in Surface and Thin-Film Analysis 2nd edn (G. Friedbacher et al. Eds), Wiley (2011) 265-292.

[78]   STRELI, C., WOBRAUSCHEK, P., FABRY, L., PAHLKE, S., COMIN, F., BARETT, R., PIANETTA, P., LÜNING, K., BECKHOFF, B.,'Total-reflection X ray fluorescence (TXRF) wafer analysis', in Handbook of Practical X ray Fluorescence Analysis (B. Beckhoff, B. Kanngießer, N. Langhoff, R. Wedell, H. Wolff, Eds.), Springer (2006) 498-553.

[79]   RADISAVLJEVIĆ, I., NOVAKOVIĆ, N., ROMČEVIĆ, N., MANASIJEVIĆ, M., MAHNKE, H.-E., IVANOVIĆ, N., XAFS studies of ytterbium doped lead-telluride, J. Alloys Compd. **501** (2010) 159-163.

[80]   RADISAVLJEVIĆ, I., NOVAKOVIĆ, N., ROMČEVIĆ, N., MANASIJEVIĆ, M., MAHNKE, H.-E., IVANOVIĆ, N., "Quaternary Fe-based Wide-gap Diluted Magnetic Semiconductors: Structural Investigations", HASYLAB Annual Report (2011).

[81]   RADISAVLJEVIĆ, I., NOVAKOVIĆ, N., IVANOVIĆ, N., ROMČEVIĆ, N., MAHNKE, H.-E., "Structural investigations of quaternary Fe-based ZnTeSe semiconductors", 17th International Microscopy Congress, Rio de Janeiro, Brazil (2010) CD-ROM.

[82]   RADISAVLJEVIĆ, I., NOVAKOVIĆ, N., MAHNKE, H.-E., ROMČEVIĆ, N., PASKAŠ-MAMULA, B., MANASIJEVIĆ, M., IVANOVIĆ, N., "Determination of iron charge state in quaternary diluted magnetic semiconductors", XVIII Symposium on Condensed Matter Physics, Belgrade, Serbia, 2011 (abstract).

[83]   FOTTINGER K, VAN BOKHOVEN J.A, NACHTEGAAL M, RUPPRECHTER G, Dynamic Structure of a Working Methanol Steam Reforming Catalyst: In Situ Quick-EXAFS on Pd/ZnO Nanoparticles, J. Phys. Chem. Lett. **2** (2011) 428.

[84]   ANSPOKS A., KUZMIN, A., Interpretation of the Ni K-edge EXAFS in nanocrystalline nickel oxide using molecular dynamics simulations, J. Non-Cryst. Solids **357** (2011) 2604.

[85]   MAKOVEC, D., KODRE, A., ARCON, I., DROFENIK, M., The structure of compositionally constrained zinc-ferrite spinel nanoparticles, J. Nanoparticle Res. **13** (2011) 1781.

[86]   ZALDEN, P., BICHARA, C., VAN EIJK, J., BRAUN, C., BENSCH, W., WUTTIG, M., Atomic structure of amorphous and crystallized Ge15Sb85, J. Appl. Phys. **107** (2010) 4312.

[87]   RÁTKAI, L., GONCALVES, A.P., DELAIZIR, G., GODART, C., KABAN, I., BEUNEU, B., JÓVÁRI, P., "Cu and Te coordination environment in Cu-doped Ge-Te glasses", Solid State Commun. **151** (2011) 1524.

[88]   BECKHOFF B., Reference-free X-ray spectrometry based on metrology using synchrotron radiation, J. Anal. At. Spectrom. (2008) **23**, 845-853

[89]   HÖNICKE P., BECKHOFF B., KOLBE M., GIUBERTONI D., VAN DEN BERG J., PEPPONI G., Depth profile characterization of ultra shallow junction implants, Analytical and Bioanalytical Chemistry, **396** (2010), Issue 8, 2825-2832

[90]   EISENHAUER D., POLLAKOWSKI B., BAUMANN J., PREIDEL V., AMKREUTZ D., RECH B., BACK F., RUDIGIER-VOIGT E., BECKHOFF B., KANNGIEBER B., BECKER C., Grazing incidence X-ray fluorescence analysis of buried interfaces in periodically structured crystalline silicon thin-film solar cells, physica status solidi (a), . **212** (2015), Issue 3, 529–534

[91]   HÖNICKE P., DETLEFS B., MÜLLER M., DARLATT E., NOLOT E., RAMPEIX H., BECKHOFF B., Reference-free, depth-dependent characterization of nanolayers and gradient systems with advanced grazing incidence X-ray fluorescence analysis, physica status solidi (a), **212** (2015), Issue 3, 523–528,

[92]   COWAN R.D., The Theory of Atomic Structure and Spectra, Robert D., Los Alamos Series in Basic and Applied Sciences, **3**, (1981)

[93]   STAVITSKI E. , DE GROOT F.M.F., Micron 41, (2010), 687

34

PAPERS PRESENTED AT THE TECHNICAL MEETING

SYNCHROTRON RADIATION BASED IMAGING AND SPECTROSCOPY OF PIGMENTS, PAINT SAMPLES AND PAINTINGS

K. JANSSENS, L. MONICO, M. RADEPONT, M. ALFELD, J. DIK* and M. COTTE**
Department of Chemistry, University of Antwerp,
Antwerp, Belgium
*Faculty of Materials Science, Delft University of Technology,
 Delft, Netherlands
**Beamline ID21, European Synchrotron Radiation Facility
Grenoble, France

Abstract

The mission of cultural heritage institutions is to preserve and protect artifacts from the distant or more recent past. In order to fulfill this mission in a professional manner, detailed knowledge on alteration phenomena of various kinds that gradually and unobtrusively are taking place at or below the surface of these objects is required. In order to be able to investigate the nature of these chemical transformations that sometimes lead to the formation of microscopically thin alteration layers, the use of state-of-the-art micro analytical methods is required. Next to being able to provide information on the composition of various materials at or just below the surface, these methods also must be able to deliver highly specific information on the nature of the chemical compounds that are locally encountered. In this respect, our recent experience shows that the use of a combination of synchrotron X-ray based spectroscopic and imaging methods such as X-ray fluorescence analysis, X-ray absorption spectroscopy and X-ray diffraction can reveal significantly new information of certain alteration processes that have remained enigmatic for a long time. Concrete examples to be discussed is the darkening of originally yellow lead chromate paint layers, as encountered in paintings of V. Van Gogh and the blackening of red cinnabar-based paint layers in works of Rubens.

Since many decades, X-ray radiography (XRR) is a standard method employed in many cultural heritage institutions and musea to non-destructively inspect paintings. XRR can reveal hidden/overpainted layers in such artifacts, provided the absorption contrast is sufficiently large. By employing element-specific X-ray fluorescence and/or crystal-phase specific X-ray diffraction contrast instead of the X-ray absorption contrast, the information that can be recorded about hidden layers in a painting can be significantly enhanced. The possibilities and limitations of using macroscopic XRF and XRF/XRD scanning for investigation of paintings by artists such as Vincent van Gogh and Rembrandt van Rijn will be discussed.

1. INTRODUCTION

The mission of cultural heritage institutions is to preserve and protect artefacts from the distant or more recent past. In order to fulfill this mission in a professional manner, detailed knowledge on alteration phenomena of various kinds that gradually and unobtrusively are taking place at or below the surface of these objects is required [1]. In order to be able to investigate the nature of these chemical transformations that sometimes lead to the formation of microscopically thin alteration layers, the use of state-of-the-art micro analytical methods is required [2]. Next to being able to provide information on the composition of various materials at or just below the surface, these methods also must be able to deliver highly specific information on the nature of the chemical compounds that are locally encountered.

In this respect, our recent experience shows that the use of a combination of synchrotron X ray based spectroscopic and imaging methods such as X ray fluorescence analysis, X ray absorption spectroscopy and X ray diffraction can reveal significantly new information of certain alteration processes that have remained enigmatic for a long time. Concrete examples to be discussed in the first part of this paper include the brightening of cadmium yellow in painting by J. Ensor and V. Van Gogh [3], the darkening of originally yellow lead chromate paint layers, as encountered in paintings of V. Van Gogh and P. Gauguin [4, 5] and the blackening of red cinnabar-based paint layers in works of Rubens [6].

Since many decades, X ray radiography (XRR) is a standard method employed in many cultural heritage institutions and musea to non-destructively inspect paintings. XRR can reveal hidden/overpainted layers in such artefacts, provided the absorption contrast is sufficiently large. By employing element-specific X ray fluorescence [7, 8] and/or crystal-phase specific X ray diffraction contrast [8] instead of the X ray absorption contrast, the information that can be recorded about hidden layers in a painting can be significantly enhanced. Accordingly, in the second part of this paper, the possibilities and limitations of using macroscopic XRF and XRF/XRD scanning for investigation of paintings by artists such as Vincent van Gogh and Rembrandt van Rijn will be discussed.

2. THE COMBINED USE OF X RAY FLUORESCENCE, X RAY DIFFRACTION AND X RAY ABSORBTION SPECTROSCOPY FOR INVESTIGATION OF DEGRADATION PHENOMENA OF PAINTERS' PIGMENTS

Recently, we had devoted attention to three degradation phenomena of painters' pigments in which chemical transformation involving a change in valence state of the metal or of a chemical element in the counter ion cause the pigment to change colour [2]. When this takes place on a scale that the colour change becomes visible on the macroscopic scale, the colour balance of a painting may be significantly altered and as a result of that, its artistic value and appreciation. It this therefore very relevant from an art conservation point of view to gain increased insight into the nature of such transformation, with the ultimate goal of being able to design better museum conditions in which the affected work of art may be maintained with minimal progress of the alteration or even to design procedures that counteract/reserve these processes.

2.1. The whitening of cadmium yellow in canvasses by J. Ensor

Cadmium sulphide exists in two crystalline and one amorphous form. The hexagonal form (α-CdS) is found in nature as the mineral *greenockite* while the cubic form (β-CdS) is called *hawleyite*; greenockite is frequently used as yellow pigment in modern paints. Manufacturers started to make intense use of this pigment from the moment that cadmium became commercially available as a base material (around the 1840's). This popularity was mainly due to the pigment's high tinting and covering power, bright yellow colour, wide applicability (artists' paint, metallurgy, ceramics, medical use, etc.) and suitability for mass production. In addition, at the beginning of the 20th century, CdS was thought to be highly stable in oil paint and water colours, and this in contradiction with chrome yellow ($PbCrO_4$), the only bright yellow alternative available for painting at that time. Consequently, prominent 19th-20th C painters such as Claude Monet, Vincent Van Gogh and Pablo Picasso frequently employed CdS, as was amply documented by earlier analytical research. Yet, in spite of its excellent reputation with regards to permanency, fading of the yellow colour of CdS and loss of adhesion of the oil paint has been reported.

On several paintings of James Ensor (1860-1949), an avant-garde painter, a gradual fading of originally bright yellow CdS areas is observed. This phenomenon is associated with the formation of small white-coloured globules on top of the original paint surface. Figure 1 shows Ensor's painting "Still life with Cabbage" from which small amounts of yellow paint and the whitish material were examined at the ESRF. Microscopic X ray Absorption Near Edge Spectroscopy (μ-XANES) experiments at ID21 was used to demonstrate that sulphur, originally present in sulphidic form (S^{2-}) is oxidized during the transformation to the sulphate form (S^{6+}). The presence of cadmium sulphate ($CdSO_4.2H_2O$) and ammonium cadmium

sulphate $[(NH_4)_2Cd(SO_4)_2]$ at the surface was confirmed by microscopic X ray diffraction measurements (ID18F), where the latter salt is suspected to result from a secondary reaction of cadmium sulphate with ammonia. The Cd itself remains in its original oxidation state (Cd^{2+}). S-chemical state maps recorded from cross-sections reveal that during the last 100 years, the oxidation front has penetrated into the yellow paint up to ca. 1-2 µm.

The superficial deterioration was exclusively detected in areas where the paint was directly exposed to a combination of light and humidity, allowing the following photo-induced reaction to take place: $CdS + 2O_2 + H_2O \rightarrow CdSO_4.H_2O$

The formation of the globules can be attributed to a process of recurring moistening and drying out of the paint surface that induces the repeated dissolution and (re)precipitation at and near the surface of the highly hygroscopic cadmium-sulphate; fluctuating climatic conditions in the museum gallery are likely to drive this process.

In order to prevent further progression of the oxidation process and loss of colour-vividness, the amount of UV radiation reaching the painting surface must be limited while care must be taken to stabilise the relative humidity level of the surrounding atmosphere.
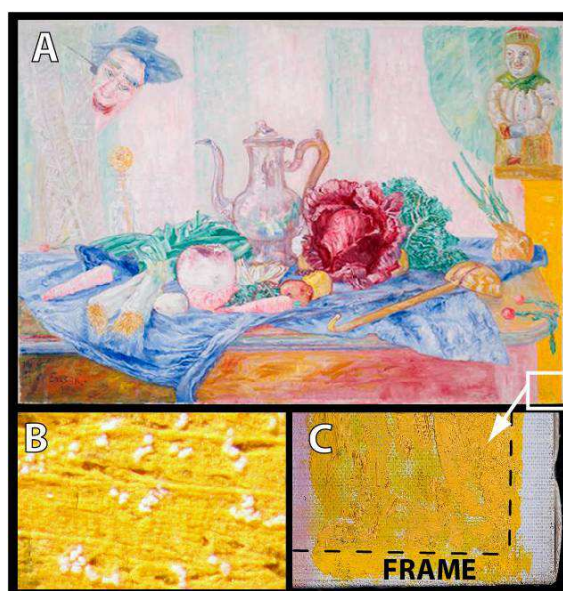
FIG. 1. (A) Optical photograph of the oil painting 'Still life with Cabbage' by James Ensor (ca.1921, KM 105.303); (B) detail of the exposed, yellow paint surface (X40) showing white globules; (C) Detail of the right-lower corner of the painting: the yellow paint covered by the frame retains its vivid yellow colour while the paint in the exposed areas has become dull due to the formation of the white globules. From [3].

2.2. The darkening of chromium yellow in paintings of V. Van Gogh [4, 5].

The alteration of chrome yellow ($PbCrO_4$, $PbCrO_4·xPbSO_4$ or $PbCrO_4·xPbO$), a bright yellow pigment used in both industrial and artistic paints, is a well-known phenomenon which has been studied continuously since its invention in the first decades of the 19th C. Chrome yellow, is often used by artists of the end of 19th C, particularly by V. van Gogh (1853-1890).

FIG. 2. (A) Optical micrograph of a cross section of partially degraded yellow paint.. White rectangle: area where S-chemical state maps (B-D) were obtained. (B) RG composite of C and D (red: sulphides: green; sulphates) (C) sulphide distribution (D) sulphate distribution. Map size = 184 x 50 µm²; step size = 1 x 1 µm². From [3].

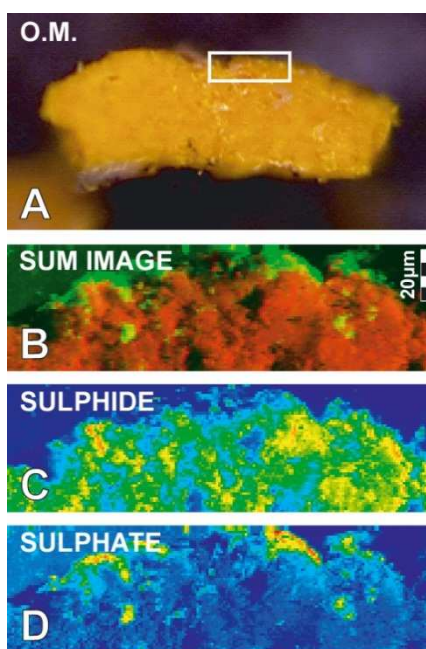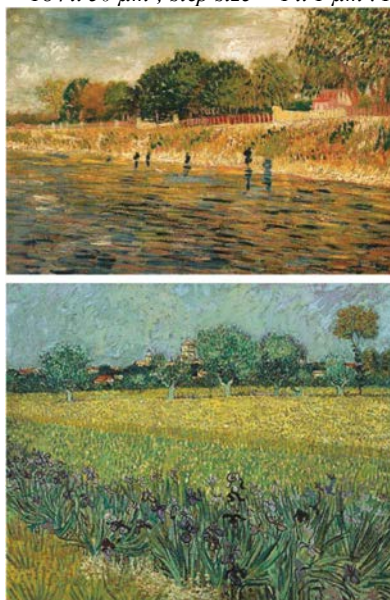FIG. 3. Photographs of (top) Bank of the Seine (F 293 s 77 v/1962), mid May to mid July 1887, oil on canvas (32 x 46 cm), and (bottom) View of Arles with Irises (F 409 s 37 v/1962), May 1888, oil on canvas (54 x 65 cm), by Vincent van Gogh, Van Gogh Museum (Vincent van Gogh foundation), Amsterdam [5].

In general, on many of these paintings, more than one century after their creation, the areas painted with chrome yellow now appear darkened, likely due to a degradation of the pigment itself. Among these paintings the most famous are the different versions of Sunflowers by V. van Gogh.

In a study conducted on artificially aged model samples of lead chromate by means of SR µ-XANES, SR µ-XRF and Electron Energy Loss Spectrometry (EELS) [4], we recently were able to establish for the first time that darkening of chromate yellow is caused by reduction of $PbCrO_4$ to $Cr_2O_3 \cdot 2H_2O$ (viridian green), likely accompanied by the presence of another Cr (III) compound, such as either $Cr_2(SO_4)_3 \cdot H_2O$ or $(CH_3CO_2)_7Cr_3(OH)_2$ [chromium(III) acetate hydroxide]. This Cr(III) species was especially formed in a thin

superficial layer of ca 1-2 μm thickness. In the two paintings shown in Fig. 3, but in the meantime also in other paintings of Van Gogh and P. Gauguin, the same phenomenon has been encountered. As an example, Fig. 4 shows the Cr(III) and Cr(VI) distributions obtained by μ-XANES spectrometry from a cross-sectioned sample of "View of Arles with Irises" (F409, see Fig. 3, top panel).

2.3. The blackening of vermillion red in panels of P. P. Rubens

Since Antiquity, the red pigment mercury sulfide (α-HgS), called cinnabar in its natural form or vermilion red when synthetic, was very often used in frescoes and paintings, even if it was known to suffer occasionally from degradation. The paint hereby acquires a black or silver-grey aspect. The chemical characterization of these alteration products is rather challenging, mainly because of the micrometric size and heterogeneity of the surface layers that develop and that are responsible for the colour change. Methods such as electron microscopy, synchrotron-based microscopic X ray fluorescence, microscopic X ray absorption near edge spectroscopy, Raman microscopy and secondary ion microscopy have been previously employed to identify the (Hg- and S-) compounds present and to study their co-localization.
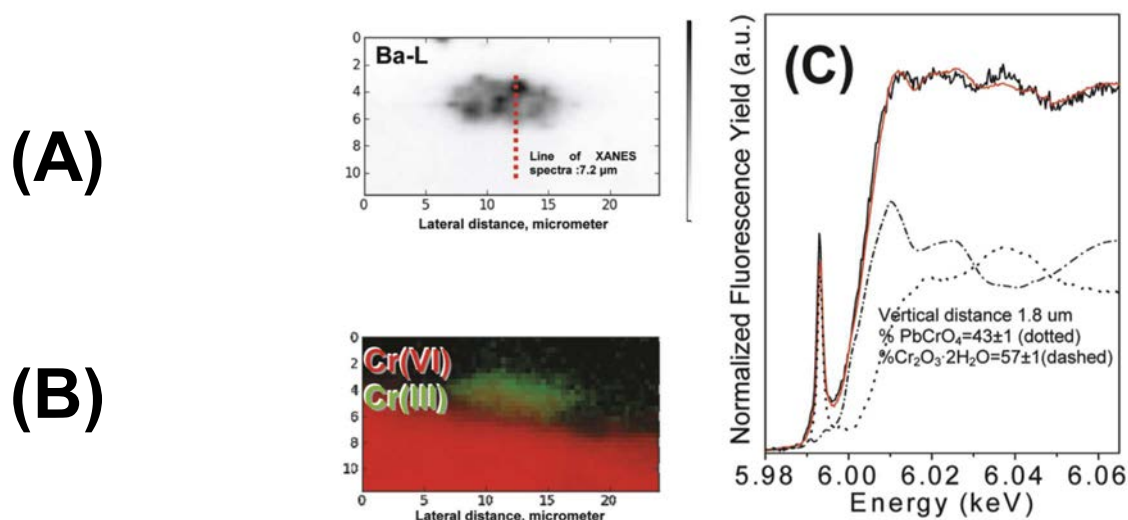
FIG. 4. Panels (A): Ba distribution and (B): RG composite images of Cr(VI) and Cr(III) maps (bottom) obtained by μ-XRF of paint sample F409. Map size: 11.6x24 μm2; pixel size: 0.4 × 0.4 μm2; dwell time: 0.3 s. Panel (C): Computation on one of the μ-XANES spectra at the Cr K-edge (recorded at vertical distance = 1.2 μm). (red) fit of the experimental data (black) by combination of PbCrO4 (dotted) and Cr2O3·2H2O (dashed) and relative result obtained. From [5].

Next to these, also microscopic X ray diffraction (XRD) (either by making use of laboratory X ray sources or when used at a synchrotron facility) allows the identification of the crystal phases that are present in degraded HgS paint layers. We have recently employed these various forms of μ-XRD to analyze degraded red paint in different paintings and compare the results with other X ray based methods. Whereas the elemental analyses of the degradation products revealed, next to mercury and sulfur, the presence of chlorine, X ray diffraction allowed the identification, next to α-HgS, of the Hg and S-containing compound calomel (Hg_2Cl_2) but also of the Hg, S and Cl-containing minerals corderoite (α-$Hg_3S_2Cl_2$) and kenhsuite (γ-$Hg_3S_2Cl_2$). These observations are consistent with X ray absorption spectroscopy measurements performed at the S- and Cl-edges. XRF mapping (see Fig. 5), moreover suggest that a multi-step reaction mechanism is taking place, in which gradually HgS is first converted into $Hg_3S_2Cl_2$ after which this compound gradually loses its S-

component so that is becomes converted into Hg_2Cl_2. This is evidenced by the formation of thin, subsequent layers of resp. α- and γ-$Hg_3S_2Cl_2$ at the surface of the α-HgS, that are themselves covered by Hg_2Cl_2.

3. ADVANCED IN XRF-BASED MACROSCOPIC IMAGING OF PAINTINGS FROM XVI-XX CENTURY

To inspect painted works of art for *pentimenti*, i.e. alterations of (details of) the composition intended by the artists and/or for revealing (more clearly) previous restoration treatments, painting conservators routinely make use of either of the following imaging methods: X ray radiography (XRR) or Infra-red reflectography (IRR). Both methods are for example able to reveal hidden layers and/or underdrawings in paintings but also suffer from a number of limitations. For example, XRR will only reveal in a clear fashion those parts of hidden compositions that were executed with pigments containing strongly absorbing materials such as lead white. IRR on the other hand is very suitable for visualizing underdrawings in carbon black but far less informative when other materials were used [1].
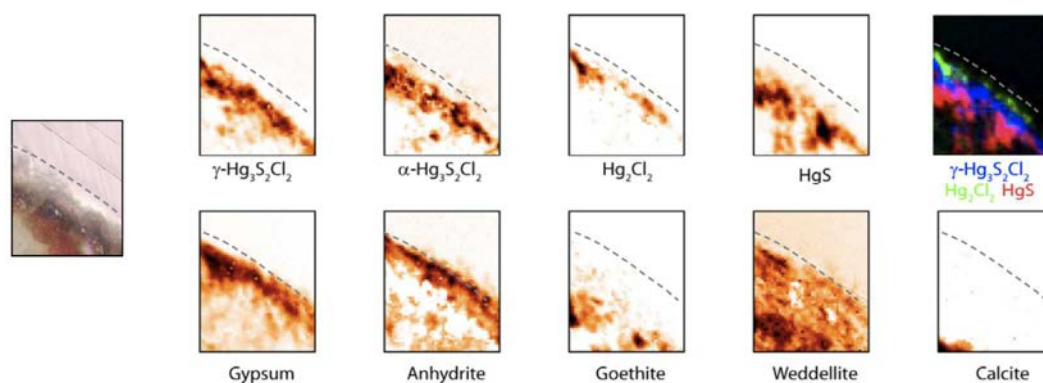
FIG. 5. Diffraction maps from a degraded vermillion sample obtained from a monastery wall painting, showing the lateral distribution of various mercury sulfochlorides, chlorides and sulfides (upper row), next to that of other Ca and Fe-phases. Map size: 280x300 μm². Dotted line indicates sample surface. From [6].

Recently we have proposed the method of scanning macro-XRF as a new way of obtaining in a completely non-destructive manner, image information from paintings on compositions that may be present below their surface and on their restoration history. This method is the equivalent of the more established method of μ-XRF, except for that fact that larger X ray beams (typically of 0.5-1 mm diameter for MA-XRF as opposed to 1-20 μm for μ-XRF), larger step sizes (also in the 0.1-1 mm range) and larger scan-areas (from 10x20 cm up to 2x3 m) are employed. Next to employing this innovative method to examine a number of paintings attributed to V. Van Gogh (20th C.), Ph.-O Runge (18th C.) and Rembrandt (17th C.), we have also designed and constructed a mobile MA-XRF scanner that is able to scan paintings in the galleries or musea where they are normally on display. With this device, in the mean time, paintings attributed to H. Memling (15th. C), Caravaggio (17th C.), Goya (18th C.) and Van Gogh (19th C.) have been examined.

3.1. Examination of a painting attributed to Ph.-O. Runge using a SR-based MA-XRF scanning setup

Philipp Otto Runge is regarded as one of the foremost painters of German Romanticism, second only to Caspar David Friedrich. The painting "Pauline im weissen Kleid vor sommerlicher Bauernlandschaft" has been attributed to Runge in the 1980's. However, this attribution is not generally accepted. In a previous investigation by X ray radiography the

presence of modifications around the shoulder and head of the depicted woman was revealed, yet no details of the initial state could be visualized. The painting (Fig. 6) was brought to DESY, Hamburg for a more detailed investigation by MA-XRF in the hope to reveal additional compositional elements for or against the attribution of the painting to Philipp Otto Runge [9].

The painting was investigated at Beamline L of the Hamburger Synchrotron Strahlungslabor (HASYLAB) at the Deutsches Elektronen Synchrotron (DESY) in Hamburg, Germany. The painting was mounted on a motor stage and moved through a collimated primary beam of 35.2 keV with a beam size of 500 (h) x 300 (v) μm^2. The fluorescence radiation emitted by the painting was recorded with four energy dispersive silicon drift detectors. All elemental distribution images presented in Fig. 7 were acquired with a lateral resolution of 1 mm and a dwell time of 1s per pixel. So the total scanning time amounted to 42 hours for an area of 50 x 30 cm^2.

FIG. 6. "Pauline im weissen Kleid Kleid vor sommerlicher Bauernlandschaft", Philipp Otto Runge, 1804 (?), oil on canvas, 105,7 x 85,2 cm^2, private collection, Germany): photograph (left), X ray radiograph (middle) and (right) photograph taken while the painting was in the MA-XRF scanner at BL L, DESY, Hamburg. From [9].
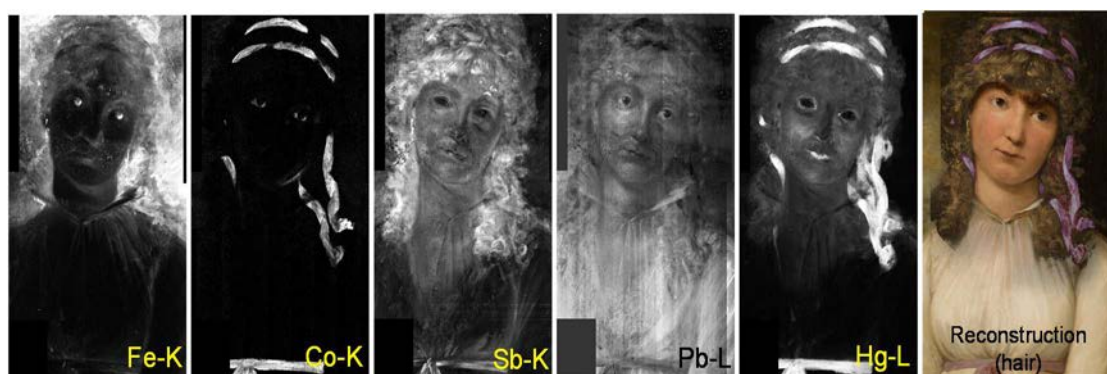
FIG. 7. Selected elemental distribution images obtained from the Runge painting, visualizing the distribution of different pigments (Fe: hematite, Co: smalt, Sb: Naples yellow, Pb: lead white, Hg: vermillion red) and the resulting reconstruction of the original portrait. From [9].

In the resulting elemental maps (Fig. 7), Fe is correlated to earth pigments, which have in general a brownish, reddish colour. Co results from the distribution of the pigment Cobalt Blue (a Co-containing K-rich glass), while Sb is emitted from the pigment Naples Yellow

[Pb(SbO$_3$)$_2$/Pb$_3$(Sb$_3$O$_4$)$_2$]. The distribution of Pb (mainly) shows the usage of Lead White (basic PbCO$_3$) in the painting and Hg is present in the red pigment Vermillion (HgS). Several modifications are visible in these images. From the Co, Sb and Hg images the original hair style can be deduced, of which a reconstruction is shown in the rightmost image. The Sb image also indicates that the eyes were originally not looking to the right in the pose of a modest Victorian young lady, but straight at the observer. Furthermore the original portrait featured a different design/shape of the front of the lady's dress, as can be seen in the Pb image and in the XRR.
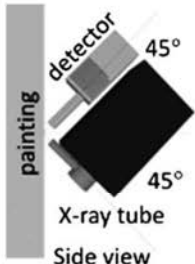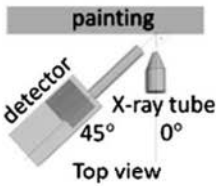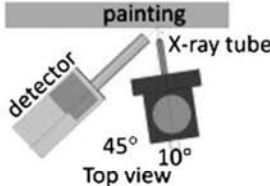
3.2. A mobile scanner MA-XRF scanner and its use for examination of a painting by F. Goya

The applicability of SR-based MA-XRF is limited by the fact that access to synchrotron beam lines is scarce and therefore only available for recording large-scale elemental distributions of selected paintings. Furthermore, the necessity to transport these paintings to a synchrotron facility and the associated risks (theft, damage, and storage in non-optimal climatic conditions) and costs (specialized art transport and insurance) presents other hurdles. Finally, the size of the painting is also a limiting factor; unless special adjustments are made to beam line hutches and scanning stages, in practice, only paintings with dimensions up to ca. 1.5 - 2 m can be examined using synchrotron beams. An alternative manner of performing MA-XRF is to employ a mobile set-up, based on an X ray tube as X ray source rather than a synchrotron [8].

In Table 1, an overview of the characteristics of different versions of a mobile MA-XRF instrument is presented. In the most recent version of the MA-XRF scanner, a four-channel DXP-XMAP multi-channel analyzer connected to 4 Vortex EX detectors, each with 50 mm^2 active area is used for data-acquisition. X rays are produced by either an X-Beam Powerflux X ray tube (XOS, NY, USA) with Mo-anode equipped with a dedicated polycapillary lens or an 10 W MOXTEK 50 kV ''Magnum'' X ray tube (Moxtek, UT, USA) with Rh target. The horizontal and vertical stages currently have a travel range of 60 x 60 cm travel range respectively (Micro-controle spectra-physics S.A, Evry, France) to allow for scanning of a larger area. With this device, it is possible to perform relatively fast (i.e., a fraction of a second dwell time per measurement point) MA-XRF scans.

An example is shown in Fig. 8 where the results of SR-based scanning of the painting "Patch of Grass" (V. Van Gogh) is compared to the equivalent result obtained with the mobile MA-XRF scanner.

TABLE 1. CHARACTERISTICS OF A MOBILE MA-XRF INSTRUMENT

Instrument	A	B	C
Beam-sample/detector-sample geometry[a]			
X-Ray tube	Kevex Microfocus PXS4-613	MOXTEK 50 kV "Magnum"	XOS X-beam Powerflux
Anode	Mo	Rh	Mo
Detector electronics	Inspector CSERF (Canberra)	DXP-XMAP (XIA)	DXP-XMAP (XIA)
Travel range of motors/cm²	10 × 10	60 × 25 (hor. × vert.)	60 × 25 (hor. × vert.)
Number of detectors	1	4	4

[a] For the multi-detector Instruments B and C only the detector in the horizontal plane is shown.
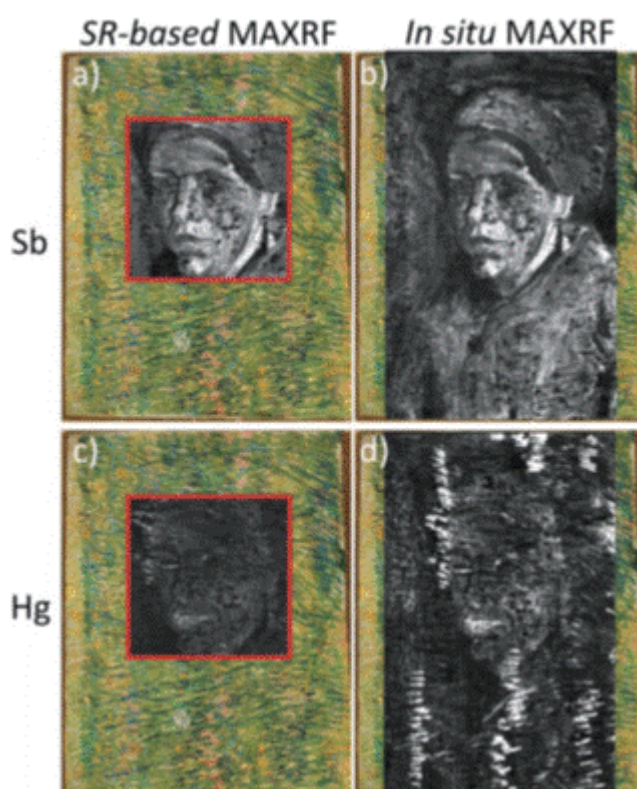
FIG. 8. Elemental maps, obtained on Vincent van Gogh's ''Patch of Grass'', showing the hidden portrait of a woman. (a) and (b) show the Sb distribution, while (c) and (d) show the Hg distribution. (a) and (c) were acquired with MA-XRF at a synchrotron source, while (b) and (d) are results of in situ measurements by means of the mobile scanner. (a) and (c) were acquired with a step size of 0.5 mm and 2 s dwell time in two days, while (b) and (d) were acquired with a step size of 1 mm and a dwell time of 5.1 s in six days.

An area of 25 x 40 cm² was scanned using a step size of 1 mm and a dwell time of 5.1 s per point. A relatively long dwell time was employed in order to obtain a quasi-noise free Sb-K image. The *in situ* scanning therefore took a total of six days. Since the measurement of the painting at the Hamburg synchrotron was done at a higher lateral resolution than *in situ*, the irradiation time per square centimetre was comparable (510 s cm⁻² in the museum, in contrast to 800 s cm⁻² at the synchrotron) in both situations. As observed before, a large number of chemical elements were found to be present in the painting, resulting from van

Gogh's practice to use a wide range of pigments, either pure or in mixtures. In Fig. 8 only the maps of the two elements, Sb and Hg,that reveal information about the hidden face are presented. One can observe that in the images obtained at the SR facility (Fig. 8) a higher level of details is visible and that the images feature a better internal contrast. Both these aspects can be attributed (in part) to the use of a step size of 0.5 mm at the SR facility instead of 1 mm *in situ*. However, also in the images acquired by means of mobile scanner, it is possible to get a sufficiently clear impression of the hidden portrait.

In Fig. 9 the result of employing this scanner for examination of a portrait by the Spanish painter F. de Goya is shown. Combination of the MA-XRF elemental distributions of predominantly Pb, Hg, Fe and Sb allows deducing that below the surface of the standing portrait of a Spanish senior magistrate, *don Ramón Satué*, a much more elaborate depiction of a high-ranking officer of the order of the Orden Real de España is present, sitting in an armchair [10]. The military person depicted wears an insignia with a characteristic 5-pointed star of which parts are visible in the Hg-L and Pb-L X ray maps.
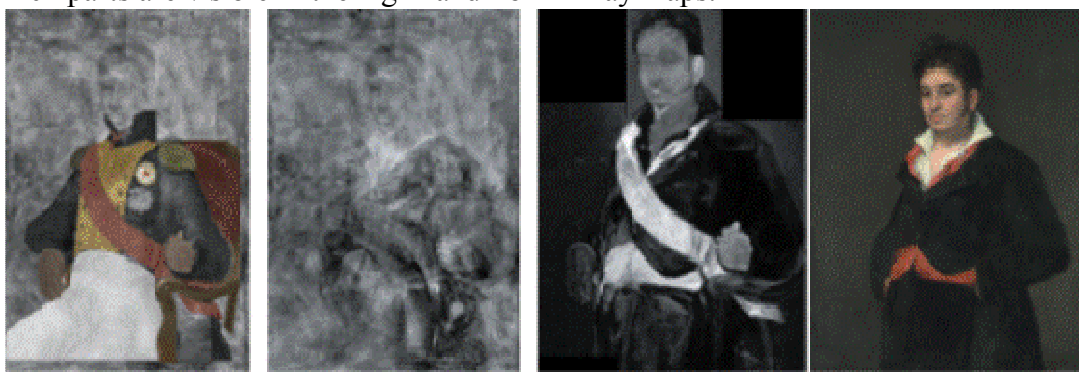
FIG. 9. (from left to right) (a) Photograph of "Portrait of Don Ramón Satué", F. De Goya, 1823, canvas, 107 by 83.5 cm, Rijksmuseum, Amsterdam, NL, (b) reconstructed version of the original portrait present below the surface, (c) X ray radiograph and (d) corresponding Hg-L X ray map obtained by MA-XRF.

4. CONCLUSIONS

Both innovative spectroscopic and imaging SR-based techniques (and for some methods also the table-top equivalents that make use of X ray tubes as source of X rays) are able to reveal significantly new information that is useful to explore, document and study in greater detail either the past or the future of important works of art. Using (sub)microscopic versions of X ray spectroscopy techniques such as XAS, XRF and XRD, it is possible to obtain insights into alteration phenomena that cause painters pigments to change colour and to pinpoint the causes of these chemical transformations. Using innovative imaging methods based on the use of the abore-mentioned methods in scanning mode, exciting new views inside paintings, deep under the actual surface can be obtained that reveal information on pentimenti or on previous restorations of painted works of art.

REFERENCES

[1] JANSSENS, J., DIK, M., COTTE, J., SUSINI, Photon-based techniques for nondestructive subsurface analysis of painted cultural heritage artifacts, Accounts Chem. Res. **43** (2010) 814-825.
[2] COTTE, M., SUSINI, J., DIK, J., JANSSENS, K., Synchrotron-based X ray absorption spectroscopy for art conservation: Looking back and looking forward, Accounts Chem. Res. **43** (2010) 705-714.

[3] VAN DER SNICKT, G., DIK, J., COTTE, M., JANSSENS, K., JAROSZEWICZ, J., DE NOLF, W., GROENEWEGEN, J., VAN DER LOEFF, L., Characterization of a Degraded Cadmium Yellow (CdS) Pigment in an Oil Painting by Means of Synchrotron Radiation Based X ray Techniques, Anal. Chem. **81** (2009) 2600-2610.

[4] MONICO, L., VAN DER SNICKT, G., JANSSENS, K., DE NOLF, W., MILIANI, C., VERBEECK, J., TIAN, H., TAN, H.Y., DIK, J., RADEPONT, M., COTTE, M., Degradation process of lead chromate in paintings by Vincent van Gogh studied by means of synchrotron X ray spectromicroscopy and related methods. 1. Artificially aged model samples, Anal. Chem. **83** (2011) 1214-1223.

[5] MONICO, L., VAN DER SNICKT, G., JANSSENS, K., DE NOLF, W., MILIANI, C., DIK, J., RADEPONT, M., HENDRIKS, E., GELDOF, M., COTTE, M., Degradation process of lead chromate in paintings by Vincent van Gogh studied by means of synchrotron X ray spectromicroscopy and related methods. 2. Original paint layer samples, Anal. Chem. **83** (2011) 1224-1231.

[6] RADEPONT, M., DE NOLF, W., JANSSENS, K., VAN DER SNICKT, G., COQUINOT, Y., KLAASSEN, L., COTTE, M., The use of microscopic X ray diffraction for the study of HgS and its degradation products corderoite ([small alpha]-Hg3S2Cl2), kenhsuite ([gamma]-Hg3S2Cl2) and calomel (Hg2Cl2) in historical paintings, J. Anal. Atom. Spectrom. **26** (2011) 959-968.

[7] DIK, J., JANSSENS, K., VAN DER SNICKT, G., VAN DER LOEFF, L., RICKERS, K., COTTE, M., Visualization of a lost painting by Vincent van Gogh using synchrotron radiation based X ray fluorescence elemental mapping, Anal. Chem. **80** (2008) 6436-6442.

[8] ALFELD, M., JANSSENS, K., DIK, J., DE NOLF, W., VAN DER SNICKT, G., Optimization of mobile scanning macro-XRF systems for the in situ investigation of historical paintings, J. Anal. Atom. Spectrom. DOI: 10.1039/c0ja00257g.

[9] ALFELD, M., JANSSENS, K., APPEL, K., THIJSSE, B., BLAAS, J., J. DIK, J., A portrait by Philip Otto Runge - Visualizing modifications to the painting using synchrotron-based X ray Fluorescence Elemental Scanning, Zeitschrift für Kunsttechnologie und Konservierung, **25** (2011) 157-163.

[10] BULL, D., KREKELER, A., ALFELD, M., DIK, J., JANSSENS, K., An intrusive portrait by Goya, The Burlington Magazine **1303** (2011) 668-673.

METHODOLOGICAL DEVELOPMENTS AND SUPPORT FOR SYNCHROTRON INVESTIGATION IN CULTURAL HERITAGE AND ARCHAEOLOGY

L. BERTRAND
IPANEMA, Synchrotron SOLEIL
Saint-Aubin, France
Email: loic.bertrand@synchrotron-soleil.fr

Abstract

Over the past ten years, the study of ancient materials from archaeology, cultural heritage and palaeontology has strongly developed at synchrotron sources. In the cultural heritage and archaeology fields, main use of synchrotron-based techniques relates to the identification of raw materials, the diffusion of archaeological artefacts, the identification of manufacturing techniques, alteration behaviours of materials in depositional and museum contexts, and finally stabilisation, consolidation and restoration techniques. The trend observed resulted in specific initiatives at several synchrotron facilities such as SRS (Daresbury, UK), LURE / SOLEIL (resp. Orsay / Saint-Aubin, France), the ESRF (Grenoble, France), CHESS (Ithaca, NY, USA), etc. We will discuss here the on-going setting-up of the new European research platform at the SOLEIL synchrotron source, IPANEMA, devoted to ancient and historical materials. The new building currently under construction, adjoining the SOLEIL synchrotron, is due to open in 2013 to European and extra-European users. The activities of the facility are centred on two fields: increased medium-term support to researchers and interdisciplinary research in methodology. Recent projects carried out or supported by IPANEMA will be reviewed with the aim to clarify and discuss future developments expected and foreseen. National and international partnerships such as the PATRIMA Labex and the CHARISMA FP7 European Commission Infrastructure programme also allow for stronger interactions between museums and archaeological laboratories, conservation science, laboratories and conservation studios, and large-scale analytical facilities.

1. INTRODUCTION

In recent years many spectacular synchrotron experiments were performed in the field of ancient and historical materials, resulting in more than 600 publications between 1986 and 2011, with a strong increase over the past ten years. This number doubled over the past 5 years. Cultural heritage and Archaeology account for typically 2 thirds of these publications over the whole period.

This contribution aims at presenting a short history of the use of synchrotron techniques for Cultural heritage and Archaeology, and at discussing the current use of synchrotron techniques in the field. Past and current initiatives carried out at several synchrotron facilities to support Cultural heritage research are presented and discussed. A particular focus is given to the on-going development of the IPANEMA platform at the SOLEIL synchrotron facility, and to European support provided through several initiatives, including the CHARISMA European Commission research infrastructure activity. This article is seen as a complement to recent reviews written in the context of IPANEMA [1,2]. The reader is invited to refer to these reviews as well as to additional articles reviewing the use of synchrotron radiation (SR) based techniques for specific categories of historical materials [1,3–13].

2. USE OF SYNCHROTRON TECHNIQUES TO STUDY CULTURAL HERITAGE AND ARCHAEOLOGICAL MATERIALS

2.1. A short history of the use of synchrotron techniques for Cultural heritage and Archaeology

The first reported reference dealing with the potentials of synchrotron techniques for Cultural heritage and Archaeology dates back to 1986 when Garman Harbottle (Chemistry Dpt, Brookhaven National Lab., NY, USA) published his article "Use of synchrotron radiation in archaeometry" in the journal Nuclear instruments and methods B, particularly focusing on the potentials of synchrotron X ray fluorescence (XRF) in the archaeological field. Synchrotron XRF was foreseen as a promising complement to Particle Induced X ray Emission (PIXE). G. Harbottle identified with great precision the main capabilities of synchrotron techniques: (1) "rapid, multielement bulk analysis of large numbers of (…) homogeneous samples of archaeological materials (…) ceramics and obsidian" for "provenance investigations and ceramic surveys", (2) "in the museum and in some archaeological work, bulk analyses (…) for identification of particular materials, or for tracing the progress of ancient technology", (3) "spatially-detailed analyses (…) in museum research": "the study of inclusions in alloys, the elucidation of construction methods of precious metal objects and the analysis of paintings", (4) examination of "whole paintings and other museum objects by a raster microprobe scan combined with the pixel-by-pixel recording of emitted X ray spectra: the reconstruction of individual element distributions could then be carried out in the computer", (5) "ultrasensitive analyses", (6) chemical speciation: "use of X ray beams to study the chemical states of elements present at the surface": "archaeometric studies of pigment composition, food, and blood residues, primitive dyes and inks, and other, perhaps unidentifiable organic remains", and (7) "absorption and fluorescence tomography". G. Harbottle concluded that "the NSLS X ray beams will, because of their unique intensity, polarization, and wavelength selection capability find ready application to both point and bulk analysis of archaeological and art-historical specimens.

Investigations utilizing this radiation source will greatly contribute to our understanding of the development of ancient technology and trade routes, and the technical and aesthetically-creative processes of artists of all periods of human history" [3]. Most of these suggestions revealed true since his seminal article.

Then head of the X ray microprobe D15 at the LURE facility (Orsay, France), Pierre Chevallier has been another very influential scientist in the use of synchrotron techniques for ancient materials synchrotron. Just three years after G. Harbottle statement, P. Chevallier and colleagues published the first work reporting the use of synchrotron techniques for archaeological materials: a synchrotron XRF based study of Gaulish coinage using their major elemental content [14,15]. Chemical speciation of archaeological systems, using X ray absorption spectroscopy (XAS), appeared shortly after this period. In 1995, Paul Schofield, from the London Natural History Museum, studied the influence of iron and manganese oxidation state on the colour of Fe- and Mn-doped glass intended to mimic mediaeval glass from Northern Europe. He studied the L3 absorption edges of Fe and Mn at beamline 5U.1, SRS, Daresbury, UK [16], concluding on the strong impact of $[Fe^{3+}]/\Sigma[Fe]$ on the glass colour. A few years later, a new important step took place at beamline D15 at the LURE with both the first use of synchrotron X ray diffraction (XRD) and of an X ray microbeam to study

heritage artefacts. Using a Bragg-Fresnel multilayer lens (BFML), P. Chevallier was able to obtain a microbeam of a few square micrometres that Ph. Dillmann used to study isolated micro-inclusions from archaeological iron ingots [17,18]. This setup was very strongly used in the following years and, despite its closure in 2003, the LURE D15 beamline remains in total one of the most used ever in the field (Fig. 1).

Almost ten years later in 2003, first synchrotron analyses of ancient materials outside the X ray range were reported in the infrared domain. We studied archaeological Human hairs from two Egyptian mummies using synchrotron FT-IR (Fourier-transform infrared) spectroscopy at beamline SA5 (responsible: P. Dumas) of the Super-Aco ring at LURE [19]. Synchrotron FT-IR was in particular used to characterize the long-term chemical alteration of keratin fibres in their archaeological setting at the few square micrometre resolution limited by the diffraction limit. The same year, De Ryck et al. reported attempts to use synchrotron FT-IR on inorganic materials (corrosion layer at the surface of bronze fibula), however pointing out difficult data collection in reflection mode [20]. The same year, Gerlach et al. performed phase-contrast synchrotron X ray microtomography at the ELETTRA medical beamline SYRMEP to study the diffusion of a consolidating solution — the widely used ethyl methacrylate co-polymer Paraloid B72 — in an archaeological glass fragment from Germany subjected to successive immersions in the consolidant [21,22].

Although these steps prefigured the research to be carried out in the following years, these first fifteen years of research led to a limited output, with only 26 publications in the whole 1986–1999 period. A limited number of beamlines scientists initiated this effort, counterbalanced by an equally limited number of archaeometrists and conservation scientists. This prompted Mark Pollard to write subsequently that: "the relative lack of success until ≈2000 is a clear indication of the lack of communication between the two fields and shows that, despite the best endeavours of both sides, without the genuine dialogue provided by good science in partnership with meaningful questions, little of value is achieved. Now (in 2007) that this communication has begun, we can anticipate a fruitful period of the application of SR
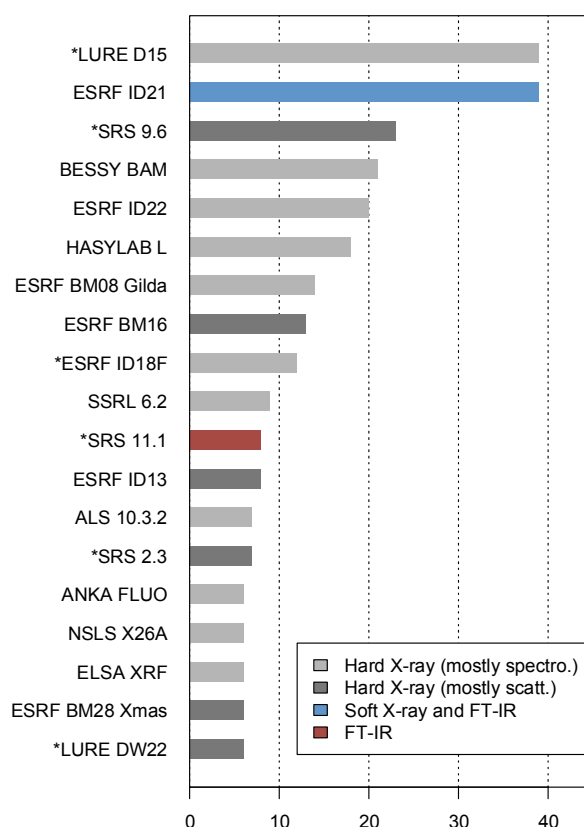
FIG. 1. Synchrotron beamlines used for Archaeology and Cultural heritage with more than 5 resulting publications, based on a review of the literature known to the author in the 1986–2010 period. The six beamlines marked with a star (*) are now shut down.

techniques in archaeology. The interesting question is how could this process have been sped up?" [23]. Indeed, first long-term projects in the field involving synchrotron radiation measurements started from the late 90's onwards with major contributions from Hans Mommsen, Philippe Dillmann, Philippe Walter, Izumi Nakai, Koen Janssens and Maria-Ondina Figueiredo among other researchers.

More recently, in 2008, XRF macro-scanning was used to map the distribution of pigments from their elemental distribution over whole paintings [24]. Finally, the first synchrotron ultraviolet/visible luminescence spectroscopy and imaging applications to Heritage materials were tested and implemented very recently at the DISCO beamline of the SOLEIL synchrotron (responsible: M. Réfrégiers), in the context of IPANEMA.

Luminescence data was collected with a resolution down to fractions of a micrometre on historical cross-sections both in micro-spectroscopy and full-field multispectral imaging modes [25]. The past ten years led to a quasi-exponential increase in the results published over the past ten years. As pointed out by M. Pollard, this period seems to correspond to the establishment of a better dialogue between conservation scientists, technical art historians, archaeometrists and synchrotron scientists. Now that feasibility and interest have been demonstrated, one can expect that the next period will witness a more regular and stable use of synchrotron techniques for the field around focused long-term research topics. SR techniques could well be considered as a 'normal' tool for the field complementing portable and laboratory-based instrumentation.

2.2. Current use of synchrotron techniques

2.2.1 Main techniques reported

The distribution of the main beamlines used for Cultural heritage and Archaeology clearly outlines the main methods of interest (in the past…) for the user community. Among the beamlines from which, to our best knowledge, more than 5 publications resulted in the 1986–2010 period, the great majority are in the medium/hard X ray range (Fig. 1). The only two exceptions are ID21 at the ESRF (tender X rays and infrared) and SRS 11.1 (infrared). Among the 16 identified hard X ray beamlines, 6 are X ray diffraction/scattering beamlines, while the remaining are X ray fluorescence/absorption spectroscopy beamlines. Indeed the use of other techniques, such as X ray tomography and (scanning) transmission X ray microscopy for instance is thus far very limited in the field. One should also point out the fact that most of the corresponding facilities are located in Europe with the five main synchrotrons acting (or having acted) in the field being ESRF, the LURE, SRS, BESSY and HASYLAB (Fig. 2). In terms of beamlines, the three main exceptions are in the USA: beamlines 6.2 at the Stanford Synchrotron Radiation Light source (Stanford, CA), 10.3.2 at the Advanced Light Source (Berkeley, CA) and X26A at the National Synchrotron Light Source (Brookhaven, Upton, NY). One third of the historically very active beamlines were shut down with the LURE and SRS closures in 2003 and 2008 respectively, as well as more recently that of ID18F at the ESRF (March 2011).

2.2.2 Study of heritage microsamples

From the mid-IR (over 4000 cm^{-1}) to the hard X rays (below 50-60 keV), the depth of penetration of photons inside materials is limited to typically below the millimetre range. For this reason, unless in very specific cases (precious metals, 'thoroughly' cleaned artefacts, gems, study of external alteration layers), most of the SR-based characterization methods involve sampling. These methods are therefore identified as 'invasive' meaning that samples will have to be taken from the objects, although mainly 'non-destructive' as characterization leads to no or limited alteration at the point of analysis. The key objective of 'non-destructiveness' is therefore not to hamper subsequent characterization by complementary instrumental means. However, photon capability, in the medium/hard X ray range, to penetrate deeper than the strict surface of microsamples (typ. in the 10 μm – 1 mm range) provides 'sub-surface' sensitivity and lower the need for tedious sample surface preparation. The most widely employed methods thus far for art and archaeological samples remain X ray fluorescence, X ray absorption and X ray diffraction to perform elemental determination, chemical speciation and phase identification [1]. These characterisations are mainly made using microfocused beams to collect data locally, typically with a 1–20 μm spatial resolution, at the exception of X ray diffraction / scattering where collection of accurate data in the reciprocal space is often regarded as more important than spatial resolution. In addition, FT-IR micro-spectroscopy has been widely used in the field particularly taking advantage of the high signal-to-noise ratio when using the brilliant synchrotron beam at high spatial resolution. However, the advent of focal plane array detectors is offering more capabilities in conservation laboratories and they are often now identified as a sufficient alternative to map compounds with significantly distinct spectral features. Although particularly promising, methods in the soft X ray range (such as scanning transmission X ray microscopy – STXM) are still of very limited use for the field, probably due to the fact that equivalent methods do not exist at the laboratory, also to the comparably difficult sample preparation, and to the limited field of view leading to difficulties in understanding systems that are very

heterogeneous at the micrometre length scale. Synchrotron UV/visible micro-spectroscopy and imaging capabilities are currently being tested on several types of heritage cross-sections for identification and characterization of organic materials such as binders and resins and of semiconductor-type pigments [25].
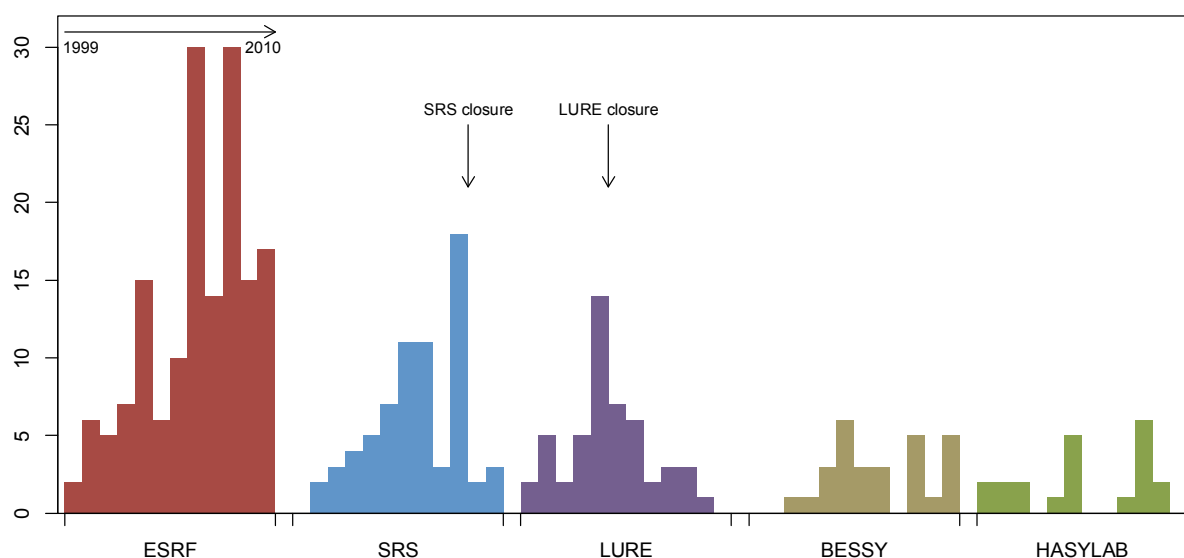

FIG. 2. Evolution in the yearly output from the 5 main synchrotron facilities used for Archaeology and Cultural heritage based on a review of the literature in the 1999–2010 period. Each group of bars corresponds to the years from 1999 to 2010. In total, these 5 facilities account for 76% of the total number of publications in the field during this period. Note the impact of the LURE and SRS closures.

2.2.3 Study of heritage artefacts

Due to the limited penetration of photons within materials except in the lowest and highest regions of the energy accessible at the synchrotron source, a rather restricted set of techniques are applicable to whole artefacts. Non-invasive subsurface study of entire heritage artefacts is limited, as the first few (tens of) micrometres of objects are frequently too much influenced by dust and alteration to provide useful information without accurate depiction of the depth stratigraphy that can be attained by invasive techniques. Of course, one should also mention that transporting and taking care of entire objects, particularly sensitive heritage ones, at synchrotron centres is neither a straightforward nor usual practice. In the hard X ray range, over 60 keV, where typically more than a centimetre of materials can be crossed, very few elements significant for Cultural heritage studies (Z>70) still have (K) absorption edges leading to characteristic absorption. The latter include some rare earth elements, precious metals (Pt, Au) and heavy metals (Hg, Pb). For this reason, the chemical speciation capability of SR-based non-invasive techniques is very limited, and in practical terms not exploited. However, over the past few years, a great interest was shown for XRF macro-scanning involving the use of comparably large X ray beams to scan across entire paintings [24,26]. Potentials of hard energy X ray powder diffraction (HE-XRPD) and texture analysis were also discussed [27, 28]. Here, the use of hard X rays is of interest to lower the dose deposited into the object and therefore decrease the risk of radiation damage and, in HE-XRPD, to collect data through objects and, in the case of paintings, the widely-used lead white paints. Many developments are expected in the use of synchrotron X ray microtomography and laminography techniques for conservation science, archaeometry and technical art history. The technique is expected to be particularly useful to study heterogeneous materials at the mesoscale such as stone, wood, but also paper and paint fragments in complement to

laboratory CT techniques. In-situ CT measurements could be of interest to study the diffusion of consolidating agents in artefacts although water hydrolysis induced by absorption of the synchrotron beam may lead to perturbed measurements unless working at high energies. Finally, far-infrared techniques setups in the terahertz range are under study at several laboratories [29] and report of feasibility assessment using synchrotron radiation sources is expected.

2.2.4   *Sample preparation, reference materials and data processing*

Sample preparation is a major bottleneck for the characterisation of Cultural Heritage materials and several initiatives are under way to organise round robin comparison of sample preparation techniques in realistic conditions, including through the CHARISMA network in Europe. Reference materials are also lacking for the field and require intercomparison efforts. Finally, the other bottleneck lies in the data processing side. In particular, software allowing for data fusion in order to obtain better segmentation and clustering of multispectral data are neither fully available nor employed regularly on synchrotron data collected on Cultural Heritage and Archaeological materials

3.   PAST SUPPORT INITIATIVES AND DEVELOPMENTS OF THE IPANEMA PLATFORM

3.1. Support projects at synchrotron facilities for the field

Two main structured interfaces were set up at synchrotron facilities to support research in Cultural heritage and Archaeology. The first important structured development is the Heritage science unit at the CCLRC and SRS synchrotron (Daresbury, UK), launched by Emmanuel Pantos and co-workers, that was particularly active during the 2003-2008 period at SRS with more than 45 publications in the field at the facility after the year 2002, reflecting the impact of E. Pantos' initiative. E. Pantos initiated specific support to research projects and organized training sessions. These developments were more or less frozen with the closure of the SRS and the opening of the new Diamond Light Source in Didcot, although the "Synchrotrons, Archaeology and Art" meeting was organized at DLS in September 12-13th, 2006 and a dedicated research platform announced in February 2009. At LURE (Orsay, France), a very large amount of work was conducted at beamlines D15, DW22 and D43. The shutdown of the LURE in 2003 and the definition of the new beamlines at the SOLEIL synchrotron led to the launch by Ph. Walter (C2RMF, Paris, France) and M. Anne (Lab. de cristallographie, Grenoble, France) of the CNRS reflection group "SOLEIL and Heritage". At the same period of time, SOLEIL launched its Heritage and Archaeology liaison office (HALO) that was formally announced in 2004 at the C2RMF, Louvre [30,31]. The initiative further developed as the IPANEMA platform (see section 3.3).

Although without a definite structure as in SRS or SOLEIL, other synchrotron facilities have played or today play a prominent role in the field of Cultural heritage and Archaeology, based on the involvement of individual researchers at the corresponding facilities. The ESRF is the most active facility in the field with a tradition of researchers and post-docs including K. Janssens, M. Cotte, E. Chalmin, etc. at the former ID18F and ID21 beamlines, and researchers at the French and Italian Collaborative Research Group beamlines (E. Dooryhée, J.-L. Hodeau, P. Martinetto, F. d'Acapito). The BESSY BAMline (Bundesanstalt für Materialforschung und -prüfung) developed many projects with I. Reiche's

activity in particular. In the US, researchers at SSRL and CHESS also initiated specific activities.

3.2.Synthesis of users' requests and design of the IPANEMA platform

During the period 2007–2008, the setting-up of the IPANEMA platform at SOLEIL was based on advice from four thematic working groups (Archaeometry / Archaeology, Conservation science / Art history, Palaeontology, Palaeo-environments) that met three times and gathered 100 European scientists in total. In May 2009, a workshop was organized at SOLEIL entitled "IPANEMA'09, a beamline for ancient materials at SOLEIL" and, in January 2011, a second workshop "IPANEMA'11, synchrotron radiation for ancient materials" was held at the SOLEIL facility. IPANEMA is now developing with advice from an International Science Advisory Committee. Some of the main points of discussion within these various bodies are outlined below:

(1)   Many users expressed their concern regarding the focus of synchrotron sources on case studies of illustrous heritage artefacts, that can lead to high-impact publications in physics journals, but may not correspond to the main scientific priorities from the users' discipline point of view, an may be seen as a 'vanity'. IPANEMA is therefore seen as an opportunity to foster interactions between the various categories of users and synchrotron facilities, in order to better take into account real research needs in conservation, archaeology and palaeontology. Inclusion of the relevant expertise within synchrotron peer-review committees is therefore a priority;

(2)   Many topics in ancient materials research require a corpus-based approach where series of artefacts need to be compared by applying a similar analytical procedure. Allocation of sufficient beamtime proved difficult in the past due to the oversubscription of multi-purpose beamlines at synchrotron facilities. Corpus-based projects will be the core focus of IPANEMA based on projects where a user from an external laboratory would be hosted physically during medium to long-term periods (stays of 6 month up to max. 3 years). However, regular (short) projects also need specific support;

(3)   Such longer-term projects are time-consuming and IPANEMA comprizes the setting-up of a new beamline, PUMA, at SOLEIL, in order to double the amount of beamtime granted to the user community from 4% (current situation) to 8% in the future of the SOLEIL beamtime. Aside this specific beamline, support concerns many techniques available at synchrotron facilities — more than 50% of SOLEIL beamlines are expected to be impacted by experiments in the field.

(4)   Regarding new users, first access to beamtime was seen as a key step. For instance, an easier access to preliminary tests at synchrotron beamlines may greatly help.

(5)   Sample preparation and data processing were identified as essential limiting steps that may also hamper efficient use of beamtime and of the data collected respectively. For this reason, the optimisation of sample preparation procedures should therefore be considered as a key priority. Both aspects could benefit from specific internal research developments. The interest of setting-up of databases for reference data was also underlined by many users;

(6)   Efficient support should necessarily be coupled to a methodological research activity, around two main directions: instrumentation and data processing;

(7)   The training of young scientists and dissemination / awareness of end-users (palaeontologists, conservators, curators, archaeologists, etc.) are priorities that should be encouraged;

(8)   Finally, given the limited extent of the addressed research community, the project should be developed with European if not international dimension.

3.3. Current status of the IPANEMA platform at SOLEIL

The IPANEMA platform, currently in construction at the SOLEIL site, is described in detail elsewhere [32]. In short, the European research platform for ancient materials (in French, "Institut Photonique d'Analyse Non-Destructive Européen des Matériaux Anciens"), supports four fields of application of synchrotron techniques: Archaeology, Cultural heritage, palaeontology and palaeo-environments, based on two areas of methodological research: photon-based imaging/spectroscopy, and data processing/analysis of ancient and historical materials. The implementation of IPANEMA relies on four main components: a dedicated team, a new building at the SOLEIL site, the new PUMA beamline optimized for ancient materials, and adapted procedures such as access modalities for corpuses and collections of objects at SOLEIL. At the date of the publication of this article, the team is installed in temporary premises at the SOLEIL site including a temporary preparation room. The new building of the platform is in construction and PUMA is in its conceptual review design phase. Since 2007, IPANEMA has developed research on ancient and historical materials through its two main modalities: (a) support to synchrotron projects, (b) dedicated methodological research activities.

3.4.International support initiatives

The European intergovernmental framework COST has been very instrumental in launching a reflection in the field within its COST G7 action "Artwork conservation by laser", and even more COST G8 "Non-destructive Analysis and Testing of Museum Objects". COST also supports the European training cycle New lights on ancient materials devoted to the synchrotron study of ancient materials, organized at SOLEIL since 2004:

- New lights on ancient materials 2004, Synchrotron analysis of museum objects, 14–18 December 2004;
- New lights on ancient materials 2007, Synchrotron methods for the understanding of the long-term ageing, alteration and conservation of Cultural heritage materials, 12–17 March 2007;
- New lights on ancient materials 2010, Synchrotron advanced X ray studies and related sample preparation of ancient sediments, wood, bones, clays and ceramics, 27 May–2 June 2010.

In October 2007, the ESRF also hosted a specialized course for Cultural heritage, as a side event of the HERCULES European course for users of Large-scale facilities.

The European Commission included support to synchrotron access specifically for Cultural heritage within its CHARISMA research infrastructure project (2009–2013, a continuation of the past Labstech in 1999-2002 and Eu-ARTECH in 2004–2009). Synchrotron SOLEIL / IPANEMA and the ion beam accelerator AGLAE jointly make the French platform of the CHARISMA European project.

Synchrotron users from the art and Archaeology communities regularly meet since 2000 at the "Synchrotron radiation in Art and Archaeology" (SR2A) conferences:
- at SSRL, SLAC, California, USA, 18 October 2000;
- at the ESRF and CNRS, Grenoble, France, 9–11 February 2005;
- at BESSY, Berlin, Germany, 27–29 September 2006;
- in Barcelona, Spain, 22–24 October 2008;
- at the Van Gogh museum in Amsterdam, The Netherlands, 8–9 November 2010;
- The next editions are scheduled at the Metropolitan museum of Art in New York, USA (June 2012), and in Paris, France (2014).

We therefore see that a range of instruments was progressively put in place to support Cultural heritage and Archaeology at synchrotrons. Current efforts to better support core topics as seen from users point of view and to widen the number of scientists in the field aware of the capabilities of synchrotron techniques are expected to increase the scientific output of this research, and to help bridging remaining gaps. Methodological development in instrumentation and data processing also appear promising for the field, and novel approaches developed for this field of research are expected to benefit as well to research communities with similar analytical constraints such as environmental sciences, Earth sciences, forensics and medicine.

ACKNOLEDGEMENTS

REFERENCES

[1]   BERTRAND, L., ROBINET, L., THOURY, M., JANSSENS, K., COHEN, S.X., SCHÖDER, S., Cultural heritage and archaeology materials studied by synchrotron spectroscopy and imaging, Appl. Phys. A-Mater **106** (2011) 377-396.

[2] BERTRAND, L., COTTE, M., STAMPANONI, M., THOURY, M., MARONE, F., SCHÖDER, S., Development and trends in synchrotron studies of ancient and historical materials. Submitted.

[3] HARBOTTLE, G., GORDON, B.M., JONES, K.W., Use of synchrotron radiation in archaeometry, Nucl. Instrum. Meth. B **14** 1 (1986) 116–122.

[4] MOMMSEN, H., DITTMANN, H., HEIN, A., ROSENBERG, A., X ray fluorescence analysis induced by synchrotron radiation (SYXRF) and first archaeometric applications, Optical Technologies in the Humanities (DIRKSEN, D., VON BALLY, D.G., Eds) Selected Contributions to the Int. Conf. on New Technologies in the Humanities and 4th Int. Conf. on Optics Within Life Sciences OWLS IV, 1996, Münster, Germany, Jul 1996, Springer, 1996.

[5] JANSSENS, K., VITTIGLIO, G., DERAEDT, I., AERTS, A., VEKEMANS, B., VINCZE, L., WEI, F., DERYCK, I., SCHALM, O., ADAMS, F., RINDBY, A., KNÖCHEL, A., SIMIONOVICI, A., SNIGIREV, A., Use of microscopic XRF for non-destructive analysis in art and archaeometry, X ray Spectrom. **29** 1 (2000) 73–91.

[6] PANTOS, E., SMITH, A.D., KIRKMAN, I.W., PRADELL, T., SALVADÓ, N., MOLERA, J., VENDRELL, M., GLIOZZO, E., MEMMI-TURBANTI, I., BURGIO, L., MARTIN, G., KOCKELMANN, W., PRAG, A.J.N.W., Synchrotron radiation and neutrons in archaeological and cultural heritage science, Physics methods in archaeometry, (MARTINI, M., MILAZZO, M., PIACENTINI, M., Eds) Proc. of the International School of Physics Enrico Fermi, Varenna, Italy, Società Italiana di Fisica (2004) 299-308.

[7] SALVADÓ, N., BUTÍ, S., TOBIN, M.J., PANTOS, E., PRAG, A.J.N.W., PRADELL, T., Advantages of the use of SR-FT-IR microspectroscopy: applications to cultural heritage, Anal. Chem. **77** 11 (2005) 3444–3451.

[8] CREAGH, D., Synchrotron radiation and its use in art, archaeometry, and cultural heritage studies, Physical Techniques in the Study of Art (BRADLEY, D., CREAGH, D., Eds) Archaeology and Cultural Heritage, Vol. 1, Elsevier (2006) 1–95.

[9] BERTRAND, L., Synchrotron imaging for archaeology, art history, conservation and paleontology, Physical techniques in the study of art, archaeology and cultural heritage, (CREAGH, D.C., BRADLEY, D.A., Eds) Vol. 2, Elsevier Science (2007) 97–114.

[10] COTTE, M., CHECROUN, E., MAZEL, V., SOLÉ, V.A., RICHARDIN, P., TANIGUCHI, Y., WALTER, P., SUSINI, J., Combination of FTIR and X rays synchrotron-based micro-imaging techniques for the study of ancient paintings. a practical point of view, e-Preserv. Sci. **6** (2009) 1–9.

[11] COTTE, M., DUMAS, P., TANIGUCHI, Y., CHECROUN, E., WALTER, P., SUSINI, J., Recent applications and current trends in Cultural Heritage Science using synchrotron-based Fourier transform infrared micro-spectroscopy. C. R. Physique **10** 7 (2009) 590–600.

[12] COTTE, M., SUSINI, J., DIK, J., JANSSENS, K., Synchrotron-based X ray absorption spectroscopy for art conservation: looking back and looking forward. Acc. Chem. Res. **43** 6 (2010) 705– 714.

[13] JANSSENS, K., DIK, J., COTTE, M., SUSINI, J., Photon-based techniques for nondestructive subsurface analysis of painted cultural heritage artifacts, Acc. Chem. Res. **43** 6 (2010) 814–825.

[14] BRISSAUD, I., CHEVALLIER, P., DARDENNE, C., DESCHAMPS, N., FRONTIER, J.P., GRUEL, K., TACCOEN, A., TARRATS, A., WANG, J.X., Analysis of Gaulish coins by proton induced X ray emission, synchrotron radiation X ray fluorescence and neutron activation analysis Nucl. Instrum. Meth. B **49** 1–4 (1990) 305–308.

[15] BRISSAUD, I., WANG, J.X., CHEVALLIER, P., Synchrotron radiation induced X ray fluorescence at LURE, J. Radioanal. Nucl. Chem. **131** 2 (1989) 399– 413.

[16] SCHOFIELD, P.F., CRESSEY, G., WREN HOWARD, W., HENDERSON, C.M.B., Origin of colour in iron and manganese containing glasses investigated by synchrotron radiation, Glass Technol. **36** 3 (1995) 89–94.

[17] DILLMANN, P., POPULUS, P., CHEVALLIER, P., ELKAIM, E., FLUZIN, P., BÉRANGER, G., FIRSOV, A., Microdiffraction of the synchrotron radiation. Identification of non metallic phases in iron and steel, CR Acad. Sci. II-B **324** (1997) 763–772.

[18] DILLMANN, P., POPULUS, P., CHEVALLIER, P., FLUZIN, P., BÉRANGER, G. FIRSOV, A., Microdiffraction coupled with X ray fluorescence microprobe, application in archaeometry, J. Trace Microprobe Tech. **15** (1997) 251– 262.

[19] BERTRAND, L., DOUCET, J., DUMAS, P., SIMIONOVICI, A., TSOUCARIS, G., WALTER, P., Microbeam synchrotron imaging of hairs from Ancient Egyptian mummies. J. Synchrotron Radiat., **10** (2003) 387–392.

[20] DE RYCK, I., ADRIAENS, A., PANTOS, E., ADAMS, F., A comparison of microbeam techniques for the analysis of corroded ancient bronze objects, Analyst, **128** (2003) 1104–1109.

[21] GERLACH, S., RÖMICH, H., LOPÉZ, E., ZANINI, F., MANCINI, L., RIGON, L., Phase contrast microtomography for archaeological glasses, Non-

58

destructive analysis and testing of museum objects (DENKER, A., ADRIAENS, A., DOWSETT, M., GIUMLIA-MAIR, A., Eds) Fraunhofer IRB Verlag, 2006, 147–151.

[22]   GERLACH, S., RÖMICH, H., LOPÉZ, E., ZANINI, F., MANCINI, L., RIGON, L., Phase contrast microtomography of archaeological glasses, Elettra Res. Highlights, 2003.

[23]   POLLARD, M., BRAY, P., A bicycle made for two? The integration of scientific techniques into archaeological interpretation, Annu. Rev. Anthropol. **36** (2007) 245–259.

[24]   DIK, J., JANSSENS, K., VAN DER SNICKT, G., VAN DER LOEFF, L., RICKERS, K., COTTE, M., Visualization of a Lost Painting by Vincent van Gogh Using Synchrotron Radiation Based X ray Fluorescence Elemental Mapping, Anal. Chem. **80** (2008) 6436–6442.

[25]   THOURY, M., ECHARD, J.-P., RÉFRÉGIERS, M., BERRIE, B., NEVIN, A., JAMME, F., BERTRAND, L., Synchrotron UV-visible multispectral luminescence microimaging of historical samples, Anal. Chem. **83** 5 (2011) 1737–1745.

[26]   ALFELD, M., JANSSENS, K., DIK, J., RICKERS, K., A portrait by Philip Otto Runge? Visualizing modifications to the painting using synchrotron-based scanning X ray fluorescence elemental imaging, Zeitschrift für Kunsttechnologie und Konservierung, **25** (2011) 157-163.

[27]   DE NOLF, W., DIK, J., VANDERSNICKT, G., WALLERT, A., JANSSENS, K., High Energy X ray Powder Diffraction for the imaging of (hidden) paintings, J. Anal. Atom. Spectrom. **26** (2011) 910–916.

[28]   YOUNG, M.L., CASADIO, F., MARVIN, J., CHASE, W.T., DUNAND, D.C., An ancient Chinese bronze fragment re-examined after 50 years: contributions from modern and traditional techniques, Archaeometry, **52** 6 (2010) 1015–1043.

[29]   LABAUNE, J., JACKSON, J.B., PAGÈS-CAMAGNA, S., MENU, M., MOUROU, G.A., Terahertz investigation of Egyptian artifacts (Proc. 35th Int. Conf. on Infrared, Millimeter and THz Waves, 2010) Rome, Italy (2010).

[30]   BERTRAND, L., J. DOUCET, J., Dedicated liaison office for cultural heritage at the SOLEIL synchrotron, Nuovo Cimento C **30** 1 (2007) 35–40.

[31]   BERTRAND, L., VANTELON, D., PANTOS, E., Novel interface for cultural heritage at SOLEIL, Appl. Phys. A **83** 2 (2006) 225–228.

[32]   BERTRAND, L., LANGUILLE, M.-A., COHEN, S.X., ROBINET, L., GERVAIS, C., LEROY, S., BERNARD, D., LE PENNEC, E., JOSSE, W., DOUCET, J., SCHÖDER, S., European research platform IPANEMA at the SOLEIL synchrotron for ancient and historical materials, J. Synchrotron Radiat. **18** 5 (2011) 765– 772.

SYNCHROTRON-BASED X RAY AND FTIR MICRO-SPECTROSCOPY FOR THE CULTURAL HERITAGE SCIENCE AT THE ID21 BEAMLINE, ESRF

M. Cotte·*,***, M. Radepont**·***, E. Pouyet*, M.Salome*, J. Susini*

*European Synchrotron Radiation Facility,
Grenoble Cedex, France
**Department of Chemistry, University of Antwerp,
Antwerp, Belgium.
***Centre de Recherche et de Restauration des Musees de France,
Paris, France
Email: cotte@esrf.fr

Abstract

Synchrotron-based techniques are increasingly used for the study of Cultural Heritage (CH) materials. These analyses rely on light-matter interactions and can be carried out directly onto the artworks. They also benefit from the synchrotron assets and in particular from the gain in terms of lateral resolution when comparing with laboratory equipment. Thanks to the synchrotron beam high brightness and low divergence, X rays can be focused down to less than 1µm, making possible the selective analysis of various compounds in complex structures. The ID21 beamline, at the ESRF, is devoted to such high resolution microscopy, using both X ray and infrared beams. Almost all kinds of CH materials can be studied, from hard matter, such as metals, glasses, pigments, to soft matters such as varnishes, tissues, wood, paper, textile, wax… Usually, samples are prepared as transversal cross-sections in order to highlight the internal structure of the matter (corrosion patina on metals, multilayer structures in paintings…). 2D elemental mapping are generated by micro-X ray fluorescence, with low detection limit. Chemical information can be obtained both by X ray absorption spectroscopy (micro-XANES) and by infrared spectroscopy (micro-FTIR). Studies usually aim at understanding degradation mechanisms (corrosion, colour variation, formation of crust), or at identifying artistic processes (choice of pigments and binders for paintings, optical effects in glasses…). The X ray energy range at ID21 is 2-9keV, giving access to all the K-edges from P to Cu. It covers S and Cl, which are frequently implied in degradation processes, and the 3d transition metals, which enter in the composition of many artworks (being in pigments, inks, glasses or metal). The FTIR-microscope provides complementary molecular information, and is used more particularly for the analysis of organic and hybrid components. The two microscopes are independent and can be operated simultaneously. Various hardware and software developments are done to further improve the instruments' capabilities.

1. INTRODUCTION

Over the last decade, applications of synchrotron-based techniques for the study of ancient and artistic materials have been clearly increasing worldwide. At the European Synchrotron Radiation Facility (ESRF), Grenoble, France, it has been to such an extent that, in 2005, the ESRF management decided to create a dedicated review committee "Environmental and Cultural Heritage matters" (EC) for the beamtime allocation. Whatever the technical and methodological approach, questions commonly tackled by archaeologists can be separated into two main concerns: a better understanding of the past and a clever projection in the future. Regarding the past, analyses intend to reveal as much as possible about the artefact secrets: what are the objects made of? Which are the ingredients used for their fabrication? How were they made (extraction of the materials, purification, synthesis, etc…)? Where do the ingredients and the objects come from? When and by who were they made (with the particular purpose of authentication)? Regarding the future, many researches are done to improve restoration and conservation methods to preserve the objects as long as possible. Furthermore, a deeper knowledge of ancient techniques can sometimes provide new inputs for developments of future technologies.

Much information can be obtained without the use of synchrotron radiation, for example with macroscopic observations (shape of objects, place of its discovery…). Synchrotron radiation will be particularly useful to get insight into the chemical or/and structural compositions of samples. The principal difficulties for such analyses are: first, the

samples are precious, so sampling is usually forbidden or must remain limited in number and size; second, they are often made of complex mixtures, of organic and mineral materials, so a single method is generally not enough to identify all the ingredients; in addition, they are rather heterogeneous at the micrometer scale, which requires discriminative techniques such as high resolution imaging. The main advantages of synchrotron radiation in this field of research are:

- The low invasiveness of the methods which are based on light-matter interactions (from IR to X rays);
- The abundance of information that can be reached (from the atomic to the structural levels),
- The quality of information, thanks to the high beam brightness, which enables to obtain data rapidly and on a limited amount of matter,
- The high spatial resolution offered by the beam spot size, in particular for micro-imaging, which allows a selective analysis.

All these attributes explain the growing interest of users for synchrotron radiation techniques. In this article, we give a specific focus on CH activities at the ID21 beamline, at the ESRF and in particular we discuss the potential of two synchrotron-based micro-analytical techniques: X ray and FTIR absorption micro-spectroscopy. More general reviews can be found elsewhere: [1] for micro-XANES and [2] for micro-FTIR. After a presentation of the beamline instrument, several examples are presented, covering both the "looking back" and "looking forward" objectives. These composite and precious samples are regularly motivating the improvement of techniques to a state-of-the-art level. A few recent software and hardware developments are thus mentioned.

2. ID21 A BEAMLINE DEDICATED TO X RAY AND FTIR SPECTRO-MICROSCOPY

2.1. Global description of the beamline

Figure 1 presents a schematic view of the ID21 beamline. It hosts two synchrotron-based instruments: a Scanning X ray microscope (SXM) and a FTIR microscope, devoted to micro-spectroscopy. The synchrotron sources are different, and the two microscopes can be operated independently and simultaneously. Using versatile sample holders, the same sample can be consecutively analysed on the two instruments.

2.2. The scanning X ray microscope

The ID21 X ray microscopy beamline is designed for micro-spectroscopy in the 2-9keV range. X rays are produced by three different insertion devices: two undulators (U40 and U42), as and a wiggler (W80). The higher-order harmonics are rejected by a fixed-exit two-bounce mirror system working at a glancing angle of ~7mrad. Depending on the beam energy, Si, Rh or Ni mirror coatings can be chosen. This system allows for harmonics rejection at the level of 10^{-4} with a transmission higher than 70%. The X rays energy is selected by a fixed-exit double-crystal monochromator (Kohzu, Japan) employing either Si(111) or Si(220) crystals, or a Ni/B4C multilayer mirror. The monochromatic X ray beam then passes into the SXM.
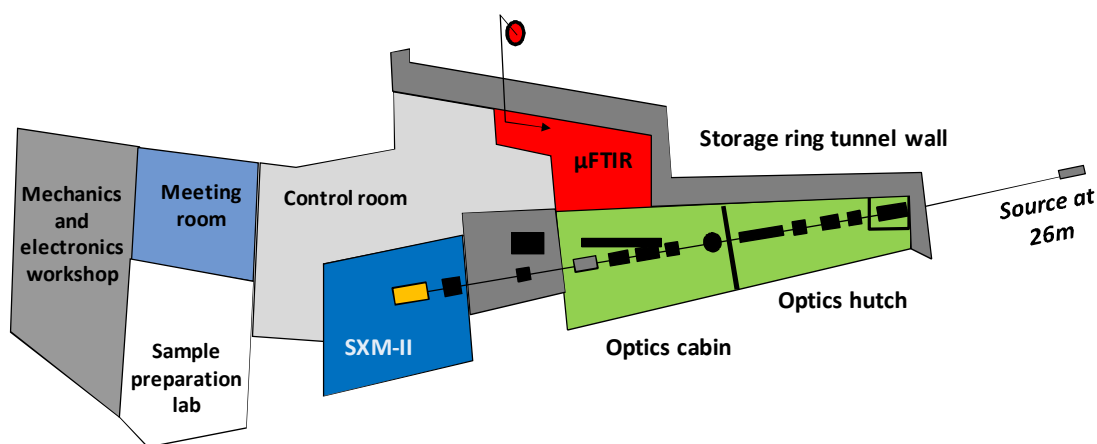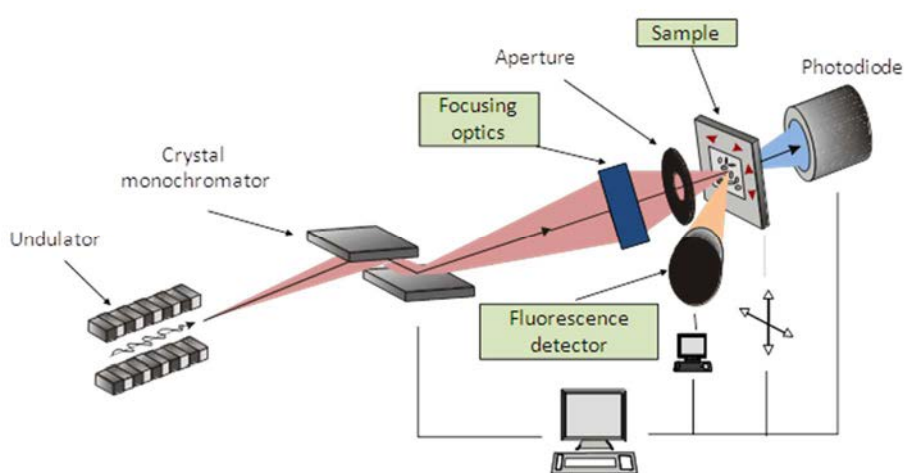
FIG. 1. Overview of the ID21 beamline at the ESRF.

FIG. 2. Optical principle of the SXM at ID21.

Figure 2 summarizes the main elements composing the ID21 SXM. The X ray beam can be focused by means of Fresnel zone plates or a Kirkpatrick–Baez mirror system. The former enables reaching better lateral resolution; the latter is achromatic and provides higher flux. A beam size of 0.3µm (ver.) ×0.7µm (hor.) is commonly achieved with a photon flux of 10^9–10^{10} photons/s depending on the beam energy and the focussing optic used. Alternatively, the beam size can be defined by different pinholes (from 200 to 10µm) for macro-analyses. The sample is raster scanned across the beam focal point to build up two-dimensional elemental or chemical images. The X ray fluorescence (XRF) signal is recorded by a seven-element HpGe (Princeton Gamma-Tech, USA) or a single-element silicon drift diode (SDD) detector (Bruker AXS, Germany), placed at 90° or 60° scattering angles, respectively. Recently, a wavelength dispersive spectrometer has been developed offering access to spectral resolution of a few tens of eV down to a few eV [3]. The microscope can be operated either at atmospheric pressure or under vacuum (10^{-6} mbar).
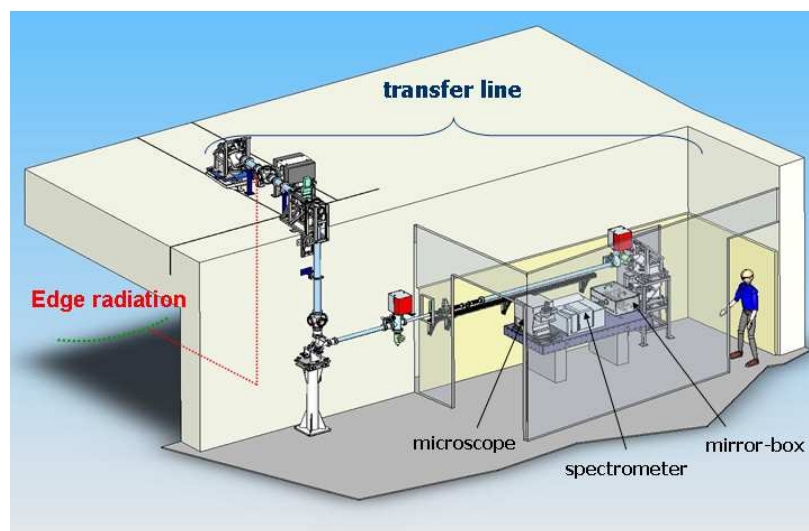
FIG. 3. Schematic layout of the FTIR end-station.

Owing to the wide range of available beam energies and detection modes, the ID21 SXM allows the detection and chemical speciation of almost all elements of the periodic table. In particular, it gives access to the K-edge of all elements from P to Cu. As exemplified in the following examples, this capability explains why the SXM is increasingly requested by the CH community.

2.3. The FTIR microscope

The FTIR end-station exploits the synchrotron infrared emission produced when electrons encounter a rapid change in magnetic field either at the entrance, or at an exit of a bending magnet (named edge-radiation). Comparing with conventional infrared source (e.g. Globar), the synchrotron emission does not provide a much higher photon flux. However, the brightness of synchrotron light, which is defined as the photon flux or power emitted per source area and solid angle, is 2–3 orders of magnitude higher than that of a Globar source. This is particularly important when working with micrometric apertures. In confocal set-up, the lateral resolution is basically limited by diffraction. At ID21, the FTIR spectro-microscope is composed of a Thermo Nicolet Nexus infrared bench associated with an infrared Thermo Continuµm microscope. The beam alignment is achieved by tuning 2 translation and 2 rotation mirrors, in a so-called mirror-box, which enable the perfect position and direction alignment of the beam at the entrance of the spectrometer (Fig.3). Analyses can be performed in transmission, reflection as well as in Attenuated Total Reflectance modes. Spectra are usually collected in the mid-infrared domain (4000 to 700cm^{-1}), as sum of a tens of scans. The beam size is generally reduced from ~10×10µm² down to ~6×6µm², depending on the sample heterogeneity, as well as the energy of the relevant vibration bands.

3. X RAY AND FTIR ABSORBTION MICRO-SPECTROSCOPIES: BASIC PRINCIPLES

3.1. X ray Absorption Near Edge Spectroscopy

X ray absorption spectroscopy techniques are based on the measurement of the variation in the absorption coefficient while scanning the energy of the probing X rays photons in a narrow region around an absorption edge. This variation is physically related to the excitation cross section of the core electrons into unoccupied electronic states or into the

vacuum continuum. The spectral features observed close to the absorption edge, referred to as the X ray absorption near edge structure (XANES), reflect the molecular environment (oxidation state, coordination numbers, site symmetry, and distortion) of a given absorbing atom and provide the basic mechanism for imaging with chemical specificity. Information on different electronic states within systems that have the same elemental composition is therefore possible. In practice, XANES spectra are acquired by following the absorption of X rays by the sample, while tuning the X ray energy around the edge of the element of interest. Measurements can be done in transmission or in fluorescence mode. In the latter case, the detection limit can go down to the ppm level.

3.2.Fourier-Transform InfraRed spectroscopy

The principle of Fourier-Transform Infrared (FT-IR) spectroscopy relies on the excitation of vibrations (length stretching or angle deformation) of molecular groups, by the use of infrared radiations. As Raman spectroscopy, FT-IR spectroscopy is a quite classical method for the characterization of ancient and historical materials [4]. Basically speaking, FTIR spectra are obtained by measuring the infrared signal transmitted or reflected by the sample. A background is also acquired to take into account the spectral and temporal flux variations. A major advantage is the versatility of this technique which can probe almost any kind of materials (metals, glasses, paintings, wood, paper, textile, human remains…), as well as artefacts made of mixtures of such materials. More particularly, it can simultaneously probe organic, inorganic, as well as hybrid materials. For this reason, it is extensively used to study products resulting from controlled or long term reactions of organic binders with mineral pigments, for example in cosmetics [5] or in paintings [6], [7] as well. Combining an FTIR spectrometer with a microscope makes possible the acquisition of 2D chemical maps, which allows not only the identification of ingredients in complex mixtures, but also their localization. Sample preparation can be quite tricky for µFTIR. This aspect is discussed in details for the analysis of artistic materials in a specific paper [8].

4. ANALYSIS OF ARTEFACTS BY X RAY & FTIR MICRO-SPECTROSCOPY, AT ID21

4.1. Revealing ancient artistic and craft practices

In most cases, esthetical values of glasses, ceramics or paintings result from optical effects such as opacity, iridescence, metallic, shine, or colour as well. Such effects can be induced by the presence of opacifying crystals, ionic chromophores, or metallic nanoparticles as well. The oxidation state of elements and more generally their chemical environment is directly correlated to these optical effects. The historical glass and ceramic production methods therefore required adequate control of firing conditions (temperature, atmosphere, and time) as well as the introduction of oxidizing or reducing ingredients. Colouring variations are usually obtained in glass, and in some pigments by modulating the oxidation states of transition elements such as Cr, Mn, Fe, Co, and Cu; these elements have characteristic absorption frequencies in the visible region as a result of d-d electronic transitions. The energy range at ID21 is therefore very well suited to reveal the chemical state of these elements in amorphous glasses, or in pigment micrometric grains. Besides, the FTIR microscope gives essential complementary information regarding organic binders.

4.1.1. Mastering colour and opacification in glasses

A set of experiments carried out in the last three years at ID21 aimed at revealing different opacification processes in three productions of antimony-based glasses: Egyptian glass of the 18th dynasty (1570–1292 BC) (Fig.4A) [9], Roman mosaic tesserae and beads from Aquilea and Rome (2nd c. BC–5th c. AD) [10], and Nevers lampworking glass figures 18th c. AD [11]. Basically, these glasses are made opaque by the presence of calcium antimonate crystals.
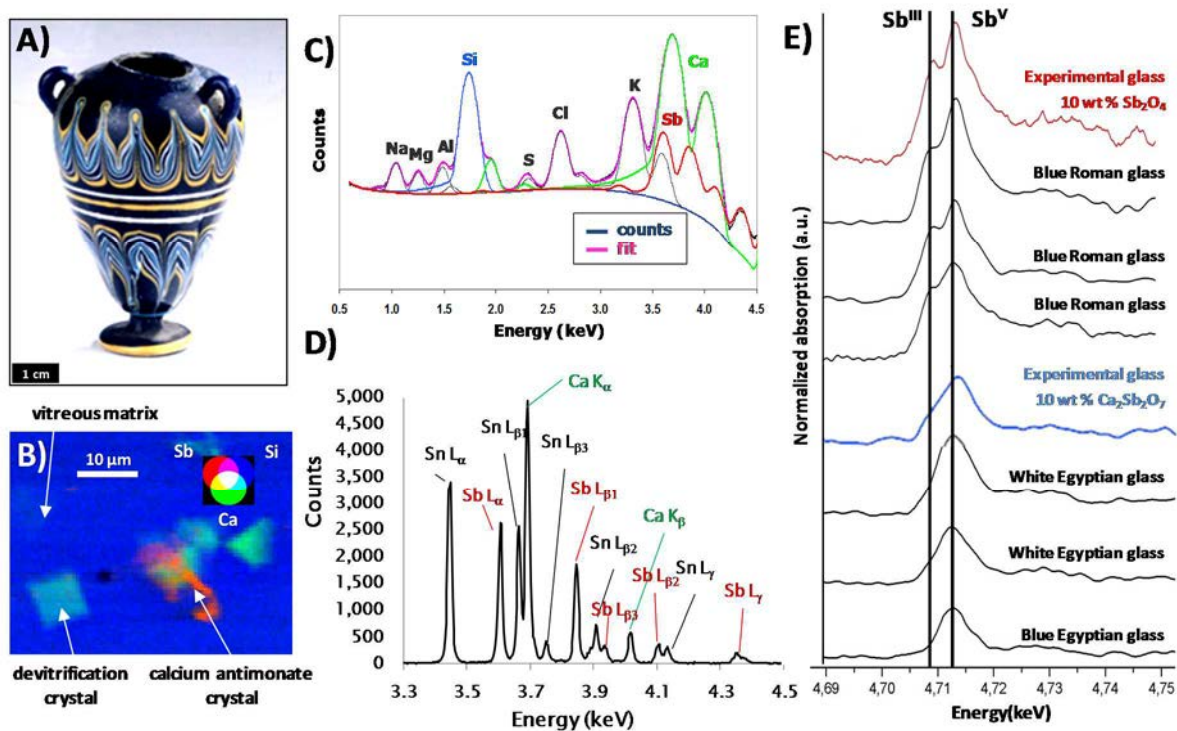

FIG. 4. Determination of the Sb oxidation state in ancient glasses, opacified by the presence of calcium antimonate crystals. A) Opaque coloured glass of the 18th Egyptian dynasty small amphorae (©Bagault C2RMF). B) 46×36μm² XRF maps showing the Sb, Ca and Si elemental distribution, measured with 1.1×0.3μm² X ray microprobe size. C) XRF spectrum fitted with PyMca. D) XRF spectrum on similar sample acquired with the WDS system. E) μXANES spectra of ancient glasses acquired at the Sb L1-edge and reference spectra of glasses synthesized in the laboratory (red and blue). Adapted from [9], [10] with permission from Springer and from [12] with permission from The Royal Society of Chemistry.

These crystals can be synthesized i) *ex-situ*, and introduced into the glass, or ii) *in-situ* by introduction of an antimony oxide and its reaction with the calcium present in the glass. It appeared that the antimony oxidation state keeps a memory of these reactions, and can allow determining how glasses were opacified, centuries ago (Fig.4E).

The use of a microbeam (0.3×1μm²) was essential to selectively probe the matrix, without interference from the antimonate opacifier crystals (Fig.4B). These analyses were made particularly difficult due to the fact that Ca K- and Sb L- XRF emission lines strongly overlap (Fig.4C). This problem is quite recurrent when analyzing artistic materials, which are frequently containing mixtures of low Z and high Z elements. This issue is even more common at ID21 because in the 1-9keV, the M-lines of very heavy elements (such as, e. g. Pb or Hg) interfere with the K-lines of low Z elements. Two parallel strategies have been developed at ID21. One solution relies on PyMca, a software package dedicated to the batch processing of large sets of XRF spectra [13]. XRF are fitted by taking into account the full set of K-, L-, or M- emission lines, and the contributions of the different elements can therefore be separated (Fig.4C). The second solution is based on the development of a Wavelength

Dispersive X ray Spectrometer (WDS), whose spectral resolution of a few tens of eV allows better separation of neighbouring emission lines (Fig.4D). This system is based on a polycapillary optic which collects the XRF and converts it into a quasi parallel beam [3]. The wavelength selection is ensured by a rotating flat crystal. 5 crystals are available at ID21, to cover the full energy range. Applications of this set-up to the study of ancient and artistic materials are presented elsewhere [12].

4.1.2. Pigment: identification and possible heating processes

If most of the experiments dealing with pigments are related to problems of degradation (see below), a few intend at answering questions on pigment identification, as well as origin and processes. In this context, the main assets of the ID21 instruments are the spatial resolution (pigment grains are usually measuring 3-5µm) as well as the chemical sensitivity offered by XAS. As an example, Mn XANES was employed for the characterization of black pigments found in Spanish and French prehistoric caves. Several atypical manganese oxide minerals such as manganite, groutite, todorokite, and birnessite were identified. TEM and XANES analyses revealed that, instead of synthesizing these compounds through heat-induced reactions, natural pigments were favoured. Thus, these raw pigments, rare in nature, are likely to originate from nonlocal geological sites and may have had to be imported from a distant location [14]. Similarly, Mn XANES can give clues about colour origin and heat evidence of palaeontological and archaeological bone and ivory, such as odontolite [15].

A similar approach was used to identify unusual antimony based pigments (stibnite), rendering a metallic aspect in the Isenhein Altarpiece and the Basel's Crucifixion, by Mathias Grünewald, a major painter of the German Renaissance (first part of the 16th century) [16]. It enabled also to identify a less unusual antimony based pigment (Naples Yellow), in the hidden portrait painted by Van Gogh, and rediscovered by macro-XRF at HASYLAB [17].

4.1.3. Painting and varnishes formulation: Identification of organic components

If µXANES is perfectly suited for the study of inorganic materials, µFTIR provides unique information regarding organic ingredients. The ID21 FTIR microscope is increasingly used to determine organic binders in paintings. This question is crucial in art history, because the use of organic binders profoundly modifies the possibilities offered to the painter to apply pigments, mix colours, create transparency, and volume effects… The major example is the discovery of oil in Bamiyan Buddhists paintings, dating from the 5th to the 9th century [18]. Behind the identification of oil, the most interesting information, offered by µFTIR is that oil is present as metallic carboxylates, i.e. product of the reaction of oil with metallic oxides, presumably. In this specific case, all clues converge to the hypothesis that these carboxylates result from a controlled synthesis, rather than long term alteration. Complementary µXRD/µXRF analyses were performed at ID18F, ESRF, for a more precise identification of pigments and inorganic alteration products (Fig. 5).
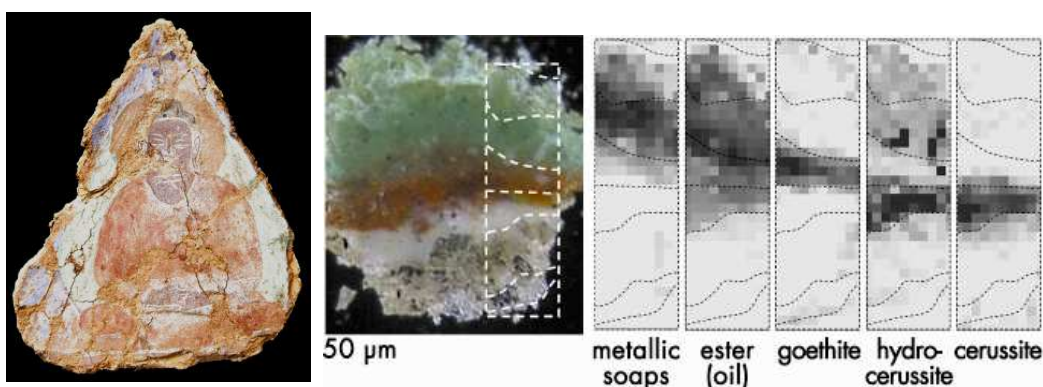
FIG. 5. µFTIR analysis of fragments from Bamiyan Buddhist paintings. Left: A painting from the Foladi cave (© NRICPT). Center: a painting fragment, after compression between two diamond cells. Right: some chemical mappings obtained by µFTIR, showing the identification and localization of iron-based and lead-based pigments, oil as well as metallic soaps.

4.1.4. Identification of blood in African statues patina: when µFTIR is combined to µXANES

This study is a perfect example of a fruitful combination of micro-analytical techniques to extract unequivocal information about the original constituents in unique artefacts. The aim was to identify ingredients (inorganic and organic), spread out on wooden sculptures, during religious and ritual ceremonies. A specific protocol, combining ToF-SIMS (Time of Flight, Secondary Ion Mass Spectroscopy), µFTIR, µXANES, as well as visible and electron microscopy was developed to perform a crossed analysis of tiny patina fragments [19]. These techniques converged to the identification of blood traces, by the presence of proteins (µFTIR), heme groups (ToF-SIMS) as well as iron linked to proteins (Fe K-edge µXANES). Through the study of seven Dogon and Bamana sculptures, it confirms ethnological studies mentioning the use of blood in different religious contexts linked to animal sacrifices.

4.2. Saving Cultural Heritage for future generations

In parallel to the discovery of lost artistic practices, an increasing number of works aims at understanding the evolution of these materials with time. Most of the alteration processes, e.g. metal corrosion, involve modification of the redox states of the original material, while the average elemental composition of the bulk material remains unchanged. Alteration is usually limited to a highly superficial surface gradient, which may have a thickness in the micrometer or even sub micrometer range. Yet, such pure surface changes can have effects on the objects visual appearance. Probing the oxidation of specific elements, and more generally their chemical environments, is therefore of prime importance when studying alteration mechanisms. This field is intensively studied at ID21 for two main reasons. First, because many of these degradations involve 3d transition metals, being in pigments, glasses, inks or metals as well. Second, because the commonest exogenous species responsible for degradation and corrosion are chlorine and SO_2. The ID21 SXM, covering the tender X ray domain 2-9keV with a submicrometric probe, is therefore a key instrument for such studies.

4.2.1. When red turns grey

Cinnabar (HgS) blackening is a dramatic and still incompletely understood phenomenon. The formation of the black phase metacinnabar was for long hypothesized. However, over the ~20 historical and artificially aged model paintings analyzed at ID21, it

has never been observed. Conversely, µXANES at S and Cl revealed two other degradation types: some sulphates (in particular calcium sulphate in Pompeian paintings), and mercury-chalcogen chemicals.

This degradation was observed both on wall paintings (Pompeii [21], Pedralbes, Barcelona [18a]) as well as on panels kept in museum (one painting from Boltraffio at the Louvre museum, Paris, France [20], and one from Rubens, at the Royal Museum of Fine Arts in Antwerp, Belgium[22]). Further analyses are ongoing aiming at a better understanding of the kinetics and thermodynamics factors regulating these processes.

4.2.2. When yellow turns white or brown

Cadmium yellow and chromium yellow are pigments developed in the 19th century which also suffer from some colour instability. µXANES was carried out at Cr, S K-and Cd L-edges in fragments of both original paintings (by J. Ensor for cadmium; and by V. Van Gogh for chromium) as well as artificially aged samples. In cadmium yellow, alteration involved an oxidation of sulphides into sulphates [23] while in chromium yellow, the reduction of Cr(VI) to Cr(III) is observed [24]. In all cases, light is one of the main responsible for alteration.
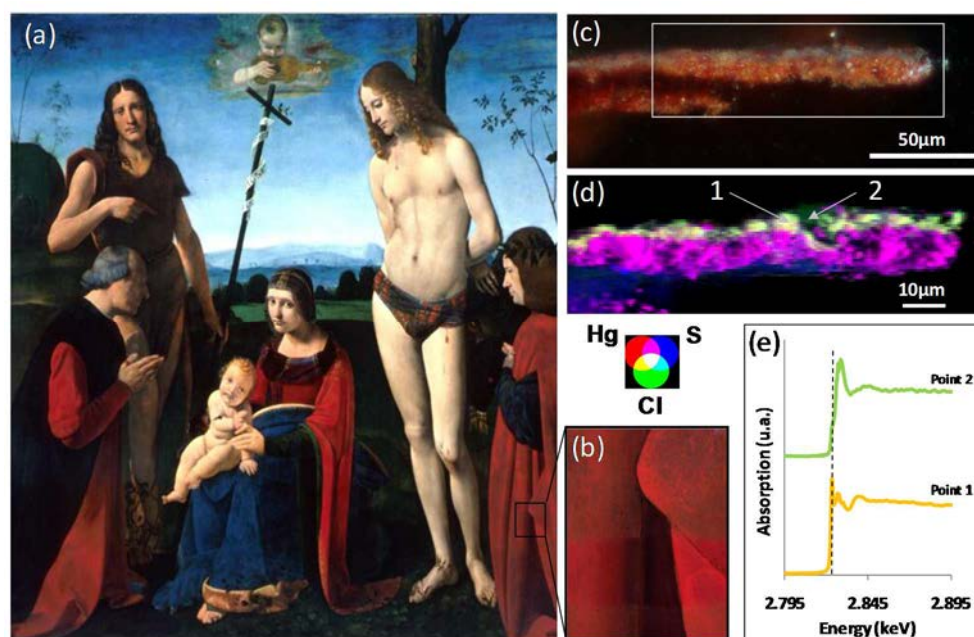

FIG.6. S and Cl µXANES study of cinnabar darkening in Madonna with Child, St. Sebastian, St. John the Baptist and two donors, Boltraffio, between 1467 and 1471, Louvre museum (© C2RMF); the dress of the donor, originally red, shows a severe darkening (a). The painting has been partially cleaned in 1995 (b). Cross-sections of tiny fragments reveal that the grey layer is only superficial (c). XRF mappings show the presence of S and Hg in both red and grey layers, while Cl appears only in the grey layer (d). Cl K-edge µXANES reveals the presence of different chlorinated species, and in particular mercury chloride type compounds, in point 1, resulting from the reaction of chlorine on the original HgS pigment (e) [20].

4.2.3. Beyond pigment discolouration

Most of these analyses focus on colour evolution due to pigment instability. However, the organic binders can also be responsible for some instability. At ID21, different ageing phenomena have been studied, such as the formation of oxalates salts, in particular affecting gilding decoration [25] as well as the formation of lead carboxylates protrusions, kinds of volcanoes that grow and break the painting surface [26].

68

4.2.4. *Beyond paintings*

Paintings are currently the most studied materials at ID21 regarding artefact degradations. However, the versatility of μXANES and μFTIR enables the analysis of many other materials such as metals, glasses, wood in waterlogged shipwreck, or Dead Sea scrolls as well.

5. CONCLUSIONS

The X ray and FTIR spectro-microscopes at ID21 are increasingly used for the study of ancient and artistic materials, both to get new insights on lost artistic practices, as well as to understand degradation mechanisms. The main assets of the instruments are the non-invasiveness, the lateral resolution coupled with 2D mapping possibilities, the chemical sensitivity offered by spectroscopy, and beyond that, the possibility to combine X ray and FTIR micro-analyses. The instruments are continuously developed to provide users with state-of-the-art equipments.

REFERENCES

[1]   COTTE, M., SUSINI, J., DIK, J., JANSSENS, K., Synchrotron-based X ray absorption spectroscopy for art conservation: looking back and looking forwards, Accounts Chem. Res. **43** 6 (2010) 705-714.

[2]   COTTE, M., DUMAS, P., TANIGUCHI, Y., CHECROUN, E., WALTER, P., SUSINI, J., Recent applications and current trends in Cultural Heritage Science using synchrotron-based Fourier transform infrared micro-spectroscopy, Cr. Phys. **10** 7 (2009) 590-600.

[3]   SZLACHETKO, J., COTTE, M., MORSE, J., SALOME, M., JAGODZINSKI, P., DOUSSE, J.C., HOSZOWSKA, J., KAYSER, Y., SUSINI, J., Wavelength-dispersive spectrometer for X ray microfluorescence analysis at the X ray microscopy beamline ID21 (ESRF), J. Synchrotron Radiat. **17** (2010) 400-408.

[4]   PEREZ-ALONSO, M., CASTRO, K., MADARIAGA, J.M., Vibrational spectroscopic techniques for the analysis of artefacts with historical, artistic and archaeological value, Current Anal. Chem. **2** 1 (2006) 89-100.

[5]   COTTE, M., DUMAS, P., RICHARD, G., BRENIAUX, R.; WALTER, P., New insight on ancient cosmetic preparation by synchrotron-based infrared microscopy, Anal. Chim. Acta **553** 1-2 (2005) 105-110.

[6]   SALVADO, N., BUTI, S., TOBIN, M.J., PANTOS, E., PRAG, A.J.N.W., PRADELL, T., Advantages of the use of SR-FT-IR microspectroscopy: Applications to cultural heritage, Anal. Chem. **77** 11 (2005) 3444-3451.

[7]   COTTE, M., CHECROUN, E., SUSINI, J., DUMAS, P., TCHORELOFF, P., BESNARD, M., WALTER, P., Kinetics of oil saponification by lead salts in ancient preparations of pharmaceutical lead plasters and painting lead mediums, Talanta **70** 5 (2006) 1136-1142.

[8] COTTE, M., CHECROUN, E., MAZEL, V., SOLÉ, V. A., RICHARDIN, P., TANIGUCHI, Y., WALTER, P., SUSINI, J., Combination of FTIR and X rays synchrotron-based micro-imaging techniques for the study of ancient paintings. A practical point of view, e-Preserv. Sci., **6** (2009) 1-9.

[9] LAHLIL, S., BIRON, I., COTTE, M., SUSINI, J., MENGUY, N., Synthesis of calcium antimonate nano-crystals by the 18th dynasty Egyptian glassmakers, Appl. Phys. A-Mater. **98** 1 (2010) 1-8.

[10] LAHLIL, S., BIRON, I., COTTE, M., SUSINI, J., New insight on the in situ crystallization of calcium antimonate opacified glass during the Roman period, Appl. Phys. A-Mater. **100** 3 (2010) 683-692.

[11] LAHLIL, S., COTTE, M., BIRON, I., SZLACHETKO, J., MENGUY, N., SUSINI, J., Synthesizing lead antimonate in ancient and modern opaque glass, J. Anal. Atom. Spectrom. **26** 5 (2011) 1040-1050.

[12] COTTE, M., SZLACHETKO, J., LAHLIL, S., SALOMÉ, M., SOLÉ, V. A., BIRON, I., SUSINI, J., Coupling a Wavelength Dispersive Spectrometer with a synchrotron-based X ray microscope: a winning combination for micro-X ray fluorescence and micro-XANES analyses of complex artistic materials, J. Anal. Atom. Spectrom. **26** 5 (2011) 1051-1059.

[13] SOLE, V. A., PAPILLON, E., COTTE, M., WALTER, P., SUSINI, J., A multiplatform code for the analysis of energy-dispersive X ray fluorescence spectra, Spectrochim. Acta B **62** 1 (2007) 63-68.

[14] CHALMIN, E., VIGNAUD, C., SALOMON, H., FARGES, F., SUSINI, J., MENU, M., Minerals discovered in paleolithic black pigments by transmission electron microscopy and micro-X ray absorption near-edge structure, Appl. Phys. A-Mater. **83** (2006) 213-218.

[15] CHADEFAUX, C., VIGNAUD, C., CHALMIN, E., ROBLES-CAMACHO, J., J., A.-C., JOHNSON, E., REICHE, I., Colour origin and heat evidence of paleontological bones: case study of blue and gray bones from San Josecito Cave, Mexico, Am. Mineral. **94** (2009) 27-33.

[16] COTTE, M., WELCOMME, E., SOLÉ, V. A., SALOMÉ, M., MENU, M., WALTER, P., SUSINI, J., Synchrotron-based X ray spectromicroscopy used for the study of an atypical micrometric pigment in 16th century paintings, Anal. Chem. **79** (2007) 6988-6994.

[17] DIK, J., JANSSENS, K., VAN DER SNICKT, G., VAN DER LOEFF, L., RICKERS, K., COTTE, M., Visualization of a lost painting by Vincent van Gogh visualized by synchrotron radiation based X ray fluorescence elemental mapping, Anal. Chem. **80** (2008) 6436-6442.

[18] COTTE, M., SUSINI, J., SOLÉ, V. A., TANIGUCHI, Y., CHILLIDA, J., CHECROUM, E., WALTER, P., Applications of synchrotron-based micro-imaging techniques to the chemical analysis of ancient paintings, J. Anal. Atom. Spectrom. **23** (2008) 820-828, (b) TANIGUCHI, Y., OTAKE, I., COTTE, M., CHECROUN, E. In The painting techniques, materials and conservation of Bamiyan Buddhist mural paintings in Afghanistan, Preprints of the 15th Triennial Meeting of the ICOM Committee for Conservation. New Delhi, 2008, 397-404.

[19] MAZEL, V., RICHARDIN, P., DEBOIS, D., TOUBOUL, D., COTTE, M., BRUNELLE, A., WALTER, P., LAPRÉVOTE, O., Identification of ritual blood in African artifacts using TOF-SIMS and synchrotron radiation microspectroscopies, Anal. Chem. **79** (2007) 9253-9260.

[20] COTTE, M., SUSINI, J., Watching Ancient Paintings through Synchrotron-Based X ray Microscopes, MRS Bull., **34** 6 (2009) 403-405.

70

[21] COTTE, M., SUSINI, J., METRICH, N., MOSCATO, A., GRATZIU, C., BERTAGNINI, A., PAGANO, M., Blackening of Pompeian cinnabar paintings: X ray microspectroscopy analysis, Anal. Chem. **78** 21 (2006) 7484-7492.

[22] RADEPONT, M., DE NOLF, W., JANSSENS, K., VAN DER SNICKT, G., COQUINOT, Y., KLAASSEN, L., COTTE, M., The use of microscopic X ray diffraction for the study of HgS and its degradation products corderoite ([small alpha]-Hg3S2Cl2), kenhsuite ([gamma]-Hg3S2Cl2) and calomel (Hg2Cl2) in historical paintings, J. Anal. Atom. Spectrom. **26** 5 (2011) 959-968.

[23] VAN DER SNICKT, G., DIK, J., COTTE, M., JANSSENS, K., JAROSZEWICZ, J., DE NOLF, W., GROENEWEGEN, J., VAN DER LOEFF, L., Characterization of a degraded cadmium yellow (CdS) pigment in an oil painting by means of synchrotron radiation based X ray techniques, Anal. Chem. **81** (2009) 2600-2610.

[24] (a) MONICO, L., VAN DER SNICKT, G., JANSSENS, K., DE NOLF, W., MILIANI, C., DIK, J., RADEPONT, M., HENDRIKS, E., GELDOF, M., COTTE, M., Degradation process of lead chromate in paintings by Vincent van Gogh studied by means of synchrotron X ray spectromicroscopy and related methods. 2. Original paint layer samples, Anal. Chem. **83** 4 (2011) 1224-1231; (b) MONICO, L., VAN DER SNICKT, G., JANSSENS, K., DE NOLF, W., MILIANI, C., VERBEECK, J., TIAN, H., TAN, H., DIK, J., RADEPONT, M., COTTE, M., Degradation process of lead chromate in paintings by Vincent van Gogh studied by means of synchrotron X ray spectromicroscopy and related methods. 1. Artificially aged model samples, Anal. Chem. **83** 4 (2011) 1214-1223.

[25] LLUVERAS, A., BOULARAND, S., ROQUÉ, J., COTTE, M., GIRÁLDEZ, P., VENDRELL-SAZ, M., Weathering of gilding decorations investigated by SR: Development and distribution of calcium oxalates in the case of Sant Benet de Bages (Barcelona, Spain), Appl. Phys. A-Mater. **90** (2008) 23-33.

[26] COTTE, M., CHECROUN, E, SUSINI, J., WALTER, P., Micro-analytical study of interactions between oil and lead compounds in paintings, Appl. Phys. A-Mater. **89** 4 (2007) 841-848.

MATERIALS, PIGMENTS, DATING, AUTHENTICITY: PORTUGUESE FAIENCE AND CHINESE PORCELAIN PRODUCED FOR THE PORTUGUESE MARKET (XVI TO XVIII CENTURIES).

M. I. DIAS
Instituto Tecnológico e Nuclear
Sacavém, Portugal
Email: isadias@itn.pt

Abstract

A case study concerning an ongoing project of an archaeometric study of ceramic materials from the XVI to the first half of the XVIII century - early Portuguese faience (XVII – 1st half XVIII cent.), and from Chinese porcelain ordered for the Portuguese market (XVI-XVII cent.) is presented. The general aspects to be considered in both cases are related with chronology precision, identification and differentiation of production centers and technologies of ceramic production, and characterization of surface coatings (glazes and pigments). This research project is being carried out on glazed faience and porcelain fragments collected during recent archaeological excavations from Portugal (Lisbon and Coimbra) by applying both laboratory techniques - X ray fluorescence spectrometry and X ray diffraction, instrumental neutron activation analysis - and X ray absorption spectroscopy using synchrotron radiation at the European Synchrotron Radiation Facility in Grenoble/France. The obtained results point to a clear chemical differentiation of Coimbra and Lisbon faience productions, and the definition of two compositional groups for Lisbon. Regarding porcelains, a trend of two large chemical groups is observed, which may reflect the two major porcelain producing regions of China, Jingdezhen (Jiangxi Province) and Zhejiang. After the compositional studies of both paste and surface finishing of faience and porcelains, considering the importance of blue pigments in these XVI-XVII century glazes, the blue chromophore role of cobalt in the glazes was also studied and discussed in relation to the speciation state and coordination environment of this element within the glassy silica-rich matrix of both faience and porcelains. The results obtained of both near-edge and extended fine structure analysis of Co 1s XAFS spectra point to the expected valence state (2+) of cobalt ions hosted as glass-forming components with an average coordination number close to four and a mean Co-O distance of about 2.0 Å. A confirmation of preliminary dating by Art Historians based on stylistic features is attained, taking into account the bulk chemistry of the glazes, particularly the presence or absence of lead and arsenic plus the relative contents of manganese, and iron versus cobalt.

1. INTRODUCTION

Public laboratories and museums worked together in a FCT funded project [1] also involving private collectors. Two main subjects were addressed in this project by applying the same methodological approach to the study of ceramic materials from the XVI to the first half of the XVIII century: (i) to contribute for a better knowledge of early Portuguese faience (XVII – 1st half XVIII cent.); and (ii) to study the Chinese porcelain ordered for the Portuguese market (XVI-XVII cent.). The general aspects to be considered in both cases are related with identification and differentiation of production centers and technologies of ceramic production, characterization of surface coatings (glazes and pigments) and chronology precision/authenticity tests.

Regarding the Portuguese faience (PF) most studies are based on stylistic features [2], therefore it will be very important to clarify some questions that usually come out, namely dating the first PF production and defining the production technology (firing temperature and surface coating technique). Another aspect to be studied is the possibility of establishing chemical and mineralogical patterns for the two important centers of early faience manufacture – Lisbon and Coimbra. The setting up of "signatures" to define each production centre is very important, as it can be usefully applied in future provenance studies of similar ceramics.

Concerning the Chinese porcelain ordered for the Portuguese market (CPOPM), the existing documentary history is reasonably advanced; nevertheless it is necessary to proceed with detailed laboratory analyses so that new relevant aspects can be unraveled like the dating

of the production, the characterization of the techniques of production and the number and/or diversity of producing centers involved in the trade with Portugal. The spreading of Chinese porcelain in Europe is a consequence of the Portuguese naval expansion to the Orient. Returning from the first great trip, Vasco da Gama will have brought exemplars to offer to king D. Manuel who will have become interested in fine porcelains; thereafter, in 1507 the Portuguese Monarch ordered several objects. In this way, the armillary sphere, the royal weapons and religious symbols like the monogram IHS (Iesus Hominum Salvator) encircled by a crown of thorns, were immortalized on the first porcelains manufactured specifically for the Portuguese market and dated about 1520. Between 1540 and 1552 objects with registrations in Portuguese were ordered, and the difficulties felt by Chinese craftsmen in copying alphabetic inscriptions strange for them are perceptible in those pieces. They certify that a clandestine trade proceeded between Portugal and China despite the cut of official relations. To these decorative patterns others were joined like the armory of noble families and emblems of religious Orders dedicated to consolidate the missions of the Portuguese empire in the Orient. This particular anthology of objects, expressing that the Portuguese were pioneers in the commerce of porcelain, is spread all over the world and treasured in national and foreign museums, and private collections [3][4][5][6]. Even if the history of the Chinese porcelain manufactured for the Portuguese market (OCPPM) is reasonably documented, it is necessary to proceed with a detailed laboratory characterization in order that new aspects can be disclosed namely accurate chronology, paste composition and surface coating materials and related techniques.

To attain the objectives of the project the main methodological approaches were instrumental neutron activation analysis (INAA) and X ray fluorescence spectrometry (XRF) for chemical characterization, along with X ray diffraction (XRD) for phase identification, applying these techniques to the study of ceramics, coatings and decorations. An added value was the capability of using non-destructive characterization methodologies based on synchrotron radiation techniques. This approach was used to contribute to ascertain chemical and mineralogical composition of pastes, to outline the technological features and to define the nature of coatings and pigments, as well as to contribute for solve chronological problems. Also luminescence methods were applied aiming to establish authenticity, contributing to well judge genuine and imitative objects, as well as dating accuracy. It was the first time that such detailed studies on chemical and mineralogical composition of pastes, surface coatings and pigments, as well as luminescence dating, have been performed.

Summarizing, the project intended to answer questions related with the History of Art and the worldwide role of Portugal in the production and trade of faience and porcelain from the XVI to the first half of the XVIII century, by using non-destructive and micro-invasive techniques.

2. METHODS

For the study of compositional ceramic body of faience and porcelain (by instrumental neutron activation analyses, X ray diffraction and luminescence), sampling was conducted with a diamond drill with small diameter (2 mm < Ø <5 mm), depending on the thickness of the fragments (Figure 1) in order to avoid any contamination resulting from the composition of the glaze and decoration, as well as from the extraction tool itself.

Chemical analyses were done by instrumental neutron activation analyses (INAA), determining major (a few) and trace elements with very good accuracy and precision. Samples (paste of both faience and porcelain, in this later case, very difficult to individualize

due to very low thickness and high hardness) are ground into a fine powder in an agate mortar and then are dried in an oven at 100 ºC for 24 hours and stored in desiccators until the samples can be weighed for both short and long irradiations (more details can be found in [7]) to measure a total the following elements: Na, K, Mn, Fe, Sc, Cr, Co, Zn, As, Ga, Br, Sb, Rb, Cs, Ba, La, Ce, Nd, Sm, Eu, Tb, Dy, Yb, Lu, Hf, Ta, Th, U. Samples and standards are irradiated together in the core grid of the Portuguese Research Reactor (ITN, Sacavém) for 2 minutes (short irradiation) and seven hours (longer irradiation). So, analyses are done via two irradiations and four gamma counts. The irradiations are carried out in two positions: A short, pneumatic-tube irradiation is 2 minutes long, at a thermal neutron flux of 2.6E12 n/cm/s; the long irradiation is 7 hours long, at a thermal neutron flux of 4.0E12 n/cm2/s, epithermal 3.7E10 n/cm/s and fast flux of 1.6E10 n/cm2/s. The gamma-ray analysis is performed using a Ge γ spectrometer consisting of a 150 cm3 coaxial detector and a low energy photon detector (LEPD), connected through Canberra 2020 amplifiers to Accuspec B (Canberra) multichannel analyser. This system has a FWHM of 1.9 keV at 1.33 MeV (coaxial Ge detector), of 300 eV at 5.9 keV and of 550 eV at 122 keV (LEPD).

X ray diffraction (XRD) measurements were performed by using a Philips X'Pert Pro diffractometer with a PW = 1.5406 Å), with λ3050/6x goniometer and CuKα radiation (available at Chemical and Radiopharmaceutical Sciences Unit). Random powder preparations were used to obtain the diffraction patterns and identification of crystalline phases.

Chemical analyses to determine major and some minor elements contents was performed by X ray Fluorescence (XRF) with an equipment X ray fluorescence spectrometer (XRF-WDS), Philips PW-1400 equipped with a rhodium tube and a LiF200 analytical crystal, and analytical software for the XRF-WDS spectrometer Philips X-40, available at LNEG. Fragments of porcelains and faience were irradiated and fixed-time counting was carried out over the K_α diagnostic peaks of the relevant glaze components, the transition metals (Mn, Fe, Co, Ni, Cu, and Zn) plus K and Sn, as well as arsenic and lead (respectively K_β and L_γ peaks

FIG. 1. Cores from the ceramics paste were obtained using a diamond drill. Several cores needed to be made in order to obtain representative samples, to be grounded, powdered, and then submitted to INAA, XRD and luminescence methods.

due to superposition of K_α and L_α peaks), and measured at the limits of the angular 2θ region of interest (21.50º-134.00º).

Preliminary laboratory tests using X rays based techniques - diffraction (XRD) and fluorescence spectrometry (XRF-WDS) provided a first glance over the bulk phase constitution and the chemical composition of glazes or pigments, contributing to the diagnosis

of fingerprint elements, and also guide the selection of materials to test the Synchrotron Radiation Facility in Grenoble, France. For the study of speciation of the chromophores present in the blue parts of the decorations, Co 1s X ray absorption spectra were collected using the instrumental set-up of beam line BM-29 at the European Synchrotron Radiation Facility (ESRF in Grenoble/France) by directly irradiating the surface of the glazed remains and detecting the fluorescence yield using a germanium detector. The energy was calibrated with a cobalt metal foil. Along with well crystallized cobalt silicate ($Co_2 Si O_4$), a commercial blue pigment based on $Co Al_2 O_4$ (which phase constitution was checked by X ray diffraction) were both irradiated to model cobalt speciation and coordination environment in the glazes [8][9].

The method of absolute dating by luminescence was also applied to the ceramics paste, and developed at Luminescence Dating laboratory at ITN, being the work focused on developing new protocols to optimize the preparation and measurement of samples of small size / quantity, as one can obtain for faience and particularly for porcelain, which is a tough task due to its hardness and markedly reduced thickness. The laboratory preparation of samples followed the specific protocols (cleaning of "impurities" and minerals to obtain specific size of quartz grains, which are subject to the luminescence measurements) in order to assess the equivalent dose, the internal dose and age determination by luminescence (TL - thermoluminescence and OSL - optically stimulated luminescence).

3.   RESULTS AND DISCUSSION

The interpretation of analytical results of PF and CPOPM took into account the typological / stylistic classification as well as the geographical and chronological frameworks, through an interdisciplinary approach. The most characteristic and important Portuguese faience production centers from XVI to XVIII century were Lisbon (Occidental and Oriental), Coimbra and Porto (Vila Nova Gaia). These important centers have been essentially differentiated by stylistic features. Among the most common stylistic groups like "aranhões" (spiders), "rendas" (lace) and "contas" (beans), all from oriental inspiration, there are others, some specifically made for foreign markets like the Portuguese communities in Antwerp and Hamburg. There is a lack of chemically defined reference groups to characterize these primary production sites of Portuguese faience.

Our main purpose is to obtain a more precise understanding of Lisbon and Coimbra faience productions from XVI to 1st half XVIII cent., contributing to the establishment of compositional reference groups of each production, which will contribute for further studies, identifying the provenance of faience that was exported to areas outside of Portugal, such as Holland, Belgium (Antwerp), Germany (namely Hamburg) and Americas (Brasil, Venezuela, United States). A geochemical study of the faience pastes from Lisbon and Coimbra was performed in order to establish geochemical signals characteristics of the respective production, through a multivariate statistical analysis [10][11][12].

The analyzed shards belong to archaeological contexts (dumps, collapsed structures of buildings – in the case of Lisbon assigned to the 1755 Earthquake,) found at archaeological sites from central Lisbon (Rua da Madalena; Rua Manuel Bento Sousa; Rua da Saudade; Praça da Figueira; Pátio do Tronco; Rua Quinteirinho do Mirante; Rua Leite de Vasconcelos; Rua Cruz de Sto. António; Rua das Janelas Verdes), and also at Convento de Sta. Clara-a-Velha, Coimbra (Figure 2).

This study allowed to clearly distinguishing in a geochemical point of view the production of faience of Coimbra from that of Lisbon (Figures 3, 4 and 5). A good chemical identification of Coimbra production has been achieved: higher contents of rare earth Elements (cluster 1, figure 3) particularly light rare earth elements, U and Th, and lower Cerium anomaly (figures 4 and 5), pointing to the use of raw materials resources from the

regional Meso-Cenozoic. Within the Lisbon faience studied, two main chemically differentiated productions were identified during the same chronological period – cluster 2 e 3 (figure 3), may be corresponding to the two main known faience production centers: occidental and oriental Lisbon. Faience with "rendas" (lace), usually assigned to Coimbra production, but also found in Lisbon sites (even with different tones of blue, white, yellow and brown), have a geochemical pattern similar to one of the Lisbon's production – cluster 3 (figure 3). So, chemical composition appears to confirm that this decorative style was also produced in Lisbon, imitating Coimbra production [11][12].

A good chemical identification of Coimbra production has been achieved: higher contents of Rare Earth Elements (cluster 1, figure 3) particularly light rare earth elements, U and Th, and
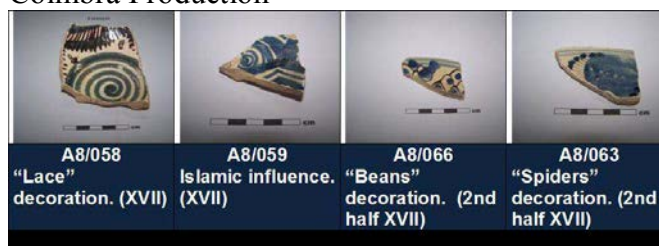

FIG. 2. Faiences assigned to Lisbon and Coimbra productions. The analyzed shards belong to archaeological contexts found at archaeological sites from central Lisbon, and Sta. Clara-a-Velha Convent, Coimbra.
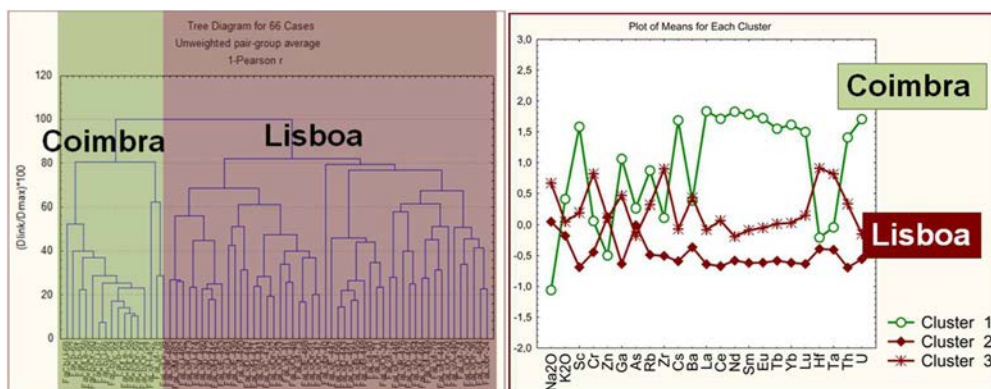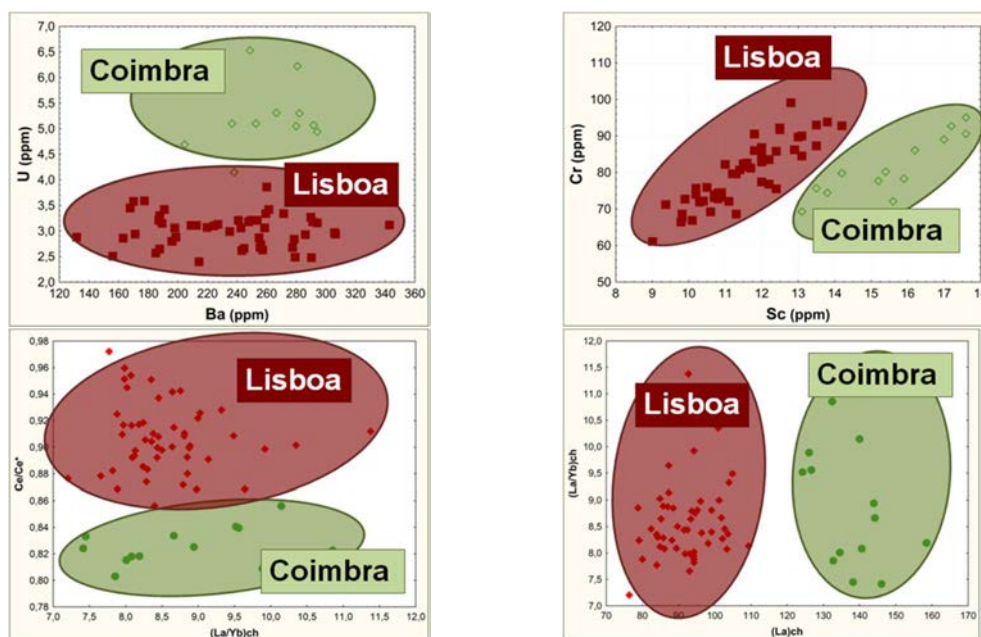
FIG. 3. Multivariate statistical analysis, using as cases the Lisbon and Coimbra faience samples and as variables the chemical elements obtained by INAA (left: cluster analysis, with correlation coefficient of Pearson as distance measure, and the UPGMA - unweighted per group average as amalgamation – linkage – rule; right: plot of means for each cluster using the k-means clustering method)[12]. lower Cerium anomaly (figures 4 and 5), pointing to the use of raw materials resources from the regional Meso-Cenozoic.

Regarding the chemical composition of the porcelain paste obtained by INAA, it is important to emphasize that only in a few we were able to obtain appropriate cores to further analyses. So, in the analyzed ones, the results indicate a greater diversity of backgrounds, although a trend to two large groups is observed, which may also reflect the two major porcelain producing regions of China, Jingdezhen (Jiangxi Province) and Zhejiang. An ongoing task is to analyze porcelains proven to be produced in each of those two major production centers in China, in order to better assess others to their production/provenance.
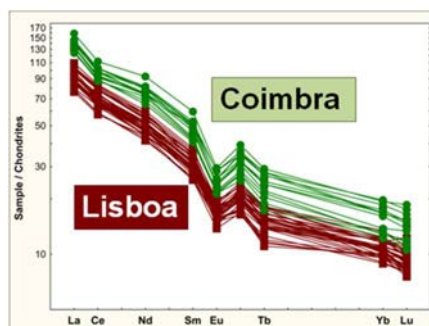

FIG. 4. Geochemical differentiation of the faiences from Coimbra and Lisbon production centres, considering the distribution of Ba and U, Sc and Cr, Ce anomaly and rare earth elements fraccionating (La/Yb)ch, (La/Yb)ch and La(ch) [12].

FIG. 5. Rare earth elements (REE) patterns for the Lisbon and Coimbra faiences (REE normalized to chondrites) [12].

It is also important to highlight that the ceramic producing centers in China can be roughly classified from the North or South, as in a geological point of view, the China of today is composed of two separate land masses geologically different, gathered by the action of the Continental drift, forming a union that is between the Yellow River and Yangtze River. The contrasting geology of the north and south leads to differences in geochemical and mineralogical raw materials available to make pottery, particularly clays [12].

For the mineralogical composition, the results reflect a compositional variability of ceramic materials (Figure 6), where the constant presence of quartz is associated with alkali feldspar and plagioclase, and calcite, in some cases, and mostly, the presence of minerals corresponding to high temperature phases is clearly identified. The main minerals identified were cassiterite, cristobalite, diopside, ghelenite, hematite, mullite (the latter being more present in porcelains then faiences, as expected).

As for the glazes traced by XRD, the main crystalline phases are quartz and cassiterite. A characterization of the surface finishing of PF and CPOPM was achieved, which allow draw conclusions about the "recipe" for pigment and ceramic glaze.
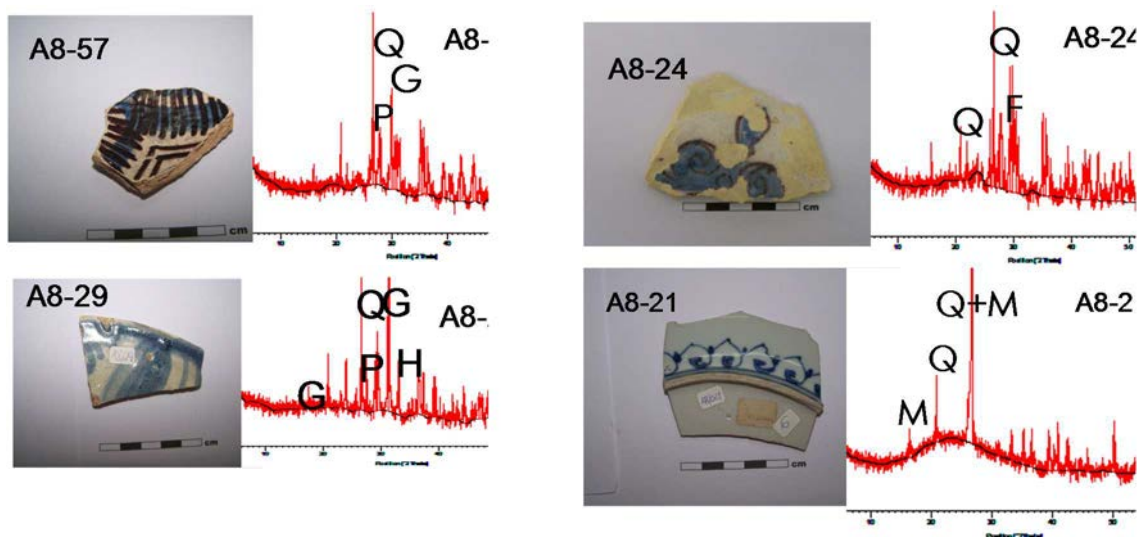

FIG. 6. Mineralogy obtained by XRD of random preparation of powdered samples from faiences and porcelaines: A8-57 (Coimbra faience, Coimbra, Sta. Clara a Velha, lace decoration, 2nd half XVII cent.); A8-24 (Lisbon faience, museum MNAA, "brasões", 2nd half XVII cent.); A8-29 (Lisbon faience, museum MNAA, oriental influence, 2nd quarter XVII cent.); A8-21 (Porcelaine, Lisbon, museum MNAA, 2nf half XVI cent.). Q – Quartz; P – Plagioclase; F – Alkali feldspar; M – Mullite; G – Ghelenite; H – Hematite. [11].

After the compositional studies of both ceramic body and surface finishing of faience and porcelains, considering the importance of blue pigments in these XVI-XVII century glazes, the blue chromophore role of cobalt in the glazes was also studied in selected samples

(Table 1). Regarding the importance in ascertaining authenticity of pieces, particularly the Chinese blue-and-white porcelains, which were traded since the Portuguese maritime contact by the end of the XVI century, and are nowadays spread all over Europe (museums, private collectors), two main methods were experimented in both faience and porcelains: XANES/EXAFS; Luminescence (TL and OSL). It is important to enhance that two main problems are related to this authenticity / dating subject, one is associated with the importance of non-destructive techniques applied to this objects, the other is the difficulty in sampling for analytical techniques (micro-invasive), like luminescence dating due to the thinness/hardness of pieces; therefore XAFS, a non-destructive technique, remains the suitable technique for interpreting the pigment performance contributing to ascertain production periods, bulk chemistry of ancient blue glazes and confirm/validate the cause of colouring through the study of formal valence(s) and coordination(s) of cobalt. In this paper it will be enhanced the XAFS results and their contribution for the authenticity and the cause of colouring, respectively by Mn/Co and Fe/Co ratios, as well as by studying cobalt speciation state in the glazes [8][9]. Cobalt and copper in adequate valence state and suitable coordination environment are the most common pigmenting agents of ancient blue glazes, added separate or together to the siliceous matrix, in a variable proportion according to the desired tonality.

Other studies [13] enhanced the occurred change during the Ming Dynasty (AD 1363-1644) from the use of imported arsenic-rich Persian cobalt-based pigments towards native Chinese blue pigmenting ores - asbolane, a cobalt-containing manganese wad. So, the presence or absence of arsenic plus a combination of Mn/Co and Fe/Co ratios in the glaze constitute a dating criterion. Hence, together with XRF-WDS analyzes, XAFS studies were done [8][9] in order to characterize cobalt speciation plus coordination environment of this element within the glassy silica-rich matrix of both Portuguese faience from the XVII century, and Chinese porcelains imported for the Portuguese market from the XVI century, and they will be summarized in this work.

Chemical results obtained by XRF-WDS show in general low copper content glazes comparatively to cobalt, with the exception of Portuguese faience sample 442. This sample, together with the other analyzed faience fragments, show important differences when comparing with porcelains, i.e. lower Mn content, and lower Fe/Co and Mn/Co ratios, and the lead-richest glazes, as expectable for a Portuguese XVII century production. On the other hand, all porcelain glazes present a Fe/Co ration higher than Mn/Co. Among the porcelains analyzed, samples 94 and 95, from *Mosteiro de Santa Clara a Velha*, Coimbra, are iron richer and also with higher As contents. Thinner porcelains present higher Fe/Co rations when compared with thicker ones (samples 425, 428, 461) [8][9].

As regards to analytical results obtained by synchrotron the Co *K*-edge X ray absorption (XAF) spectrum of the blue glazes display the same general trend for all samples, with a quite intense pre-edge feature centered at ~7709 eV, an edge energy (7718 eV) indicative of a dominant divalent state of the cobalt ions and a poorly defined EXAFS region (Figure 7).
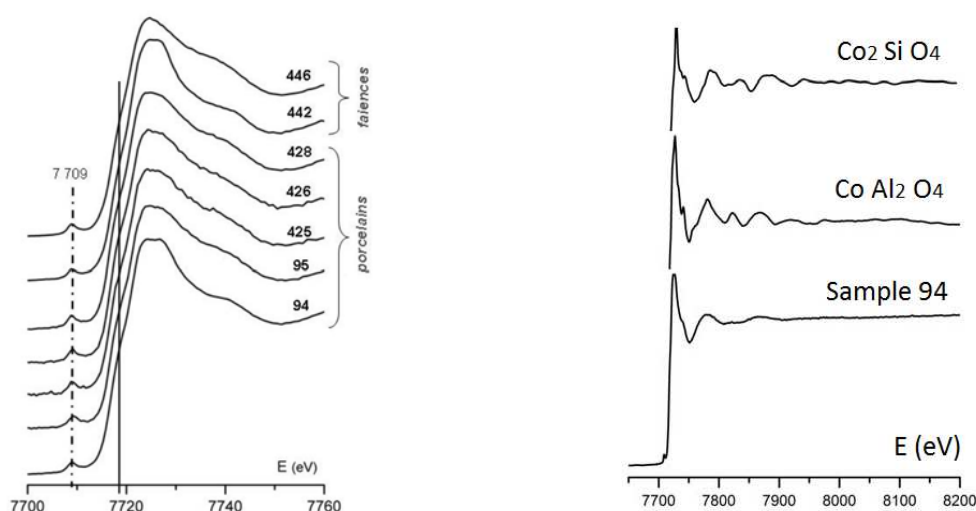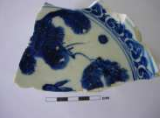
FIG. 7. *Co K-edge XANES spectra obtained from the blue glaze of both porcelain (94, 95, 425, 426, 428) and faience samples (442, 446) and Co K-edge spectra comparison between one porcelain sample (94) and a well crystallized cobalt silicate ($Co_2 Si O_4$) and a commercial blue pigment based on $Co Al_2 O_4$ (from Ref. [8][9]).*

Spectra obtained from model oxides, crystallized cobalt silicate ($Co_2 Si O_4$) and commercial blue pigment based on $Co Al_2 O_4$, and "$Co_2 Sn O_4$" (cerulean blue), display distinct near-edge layout as expected from the presence of exclusively Co^{3+} ions in the last one and Co^{2+} ions with distinct close oxygen coordination environments in the double oxides (tetrahedral coordination in the spinel $Co Al_2 O_4$, octahedral in the silicate $Co_2 Si O_4$, and tetrahedral plus octahedral in the cerulean blue). The diverse obtained edge layouts for these three compounds are clearly enhanced in the first derivatives of Co *1s* XANES spectra collected from those double oxides.

After resolving the pre-edge spectral region (Fityk program [14]), a comparison between the contributing features obtained for the best-fit in model compounds with porcelain 94 enhances that: (i) slightly differences occur in energy position and intensity within models with a dominant contribution centered at 7 709 eV (due to Co^{2+} bordered by two minor contributions when these ions are present in tetrahedral coordination), and a single contribution at higher energy for octahedral coordination, or two significant contributions if Co^{3+} ions; (ii) the comparison between models and porcelain highlight the prevailing tetrahedral environment for most cobalt ions within the glaze, around the $3d^7$ transition metal ion Co^{2+} in the Chinese glazes, in accordance with data extracted from EXAFS spectra comprising a mean coordination number 4.4 ± 0.6 Å and Co-O distances close to 2.0 Å (fitting convergence attained with $Co Al_2 O_4$ spectrum) (Figure 8); similar trend of Co-O distances in the spinel oxide and in the Chinese blue glazed porcelain; divergent trend for the silicate comparison where crystal structure present the oxygen octahedral around Co^{2+} ions sharing edges, hence Co-Co close distances occur) [8][9].

TABLE 1. CHINESE BLUE-AND-WHITE PORCELAINS AND PORTUGUESE FAIENCES

Photo	Sample Ref., type	Site and date of excavation	Dating problematic
	17, Chinese Porcelain	National Museum of Ancient Art (*MNAA*), Lisbon, Portugal	Chinese; 16th century (2nd half?) Very thin shards Not sampling suitable for Luminescence dating

|			
	20, Chinese porcelain	National Museum of Ancient Art, Lisbon, Portugal	Chinese "Wanli" piece; Kraak. 1573-1619 ? Very thin shards Not sampling suitable for Luminescence dating
	94 and 95, Chinese porcelain	*Monastery of Santa Clara-a-Velha,* Coimbra, Portugal (<2003)	Chinese; 16th century (2nd half?) Very thin shards Not sampling suitable for Luminescence dating
	425, Chinese porcelain	*Rua da Madalena,* Lisbon, Portugal (2007)	Chinese "Wanli" piece; 1573-1619 ? Very thin shards Not sampling suitable for Luminescence dating
	426 and 428, Chinese porcelain	*Calçada do Lavra,* Lisbon, Portugal (2004)	Chinese; 16th century; 2nd half ? Very thin shards Not sampling suitable for Luminescence dating
	435 and 436 Chinese porcelain	*Rua do Instituto Bacteriológico* Lisbon, Portugal (2004)	Chinese; 16th century (2nd half? 3rd quarter) Very thin shards Not sampling suitable for Luminescence dating
	461, Chinese porcelain	*Rua de O Século,* Lisbon, Portugal (2005)	Chinese; 16th century (half). Imported from Persia? Zhengde? Jiajing?
	27, Portuguese faience	*Unknown MNAA collection* Lisbon, Portugal	Oriental influence. 17th century (2nd quarter?) Very thin shards Not sampling suitable for Luminescence dating
	36, Portuguese faience	*Unknown MNAA collection* Lisbon, Portugal	17th century (2nd quarter?)
	77, Portuguese faience	National Museum of Ancient Art (*MNAA*), Lisbon, Portugal	Lisbon – Monte Sinai production (17th ? Early 18th ?)
	442, Portuguese faience	*Rua da Madalena*, Lisbon, Portugal (2007)	17th cent., 1st half (15-50?) Similar faience pieces were found in Hamburg, Germany
	446, Portuguese faience	*Rua da Madalena*, Lisbon (2007)	17th cent., 1st half (20-50?); "camellia" decoration; imitation of "Kraak" porcelain

3.
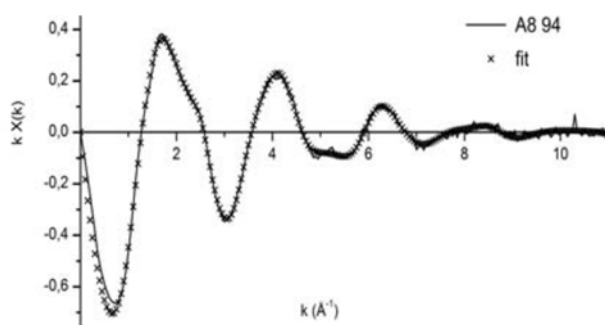
FIG. 8. Porcelain and theoretically calculated spectra of $Co\ Al_2\ O_4$ *by using best-fit approach (from Ref. [8]).*

The luminescence dating applied to faience and porcelains was a challenge, especially because of the thinness and hardness of most of ceramics, particularly porcelains, as well as trying to develop a micro-invasive protocol and with accurate results. Main experiments developed to evaluate protocols for preparation and luminescence measurement of small samples (<100 mg) from those high fired ceramics have included: additive TL of untreated material; multiple stimulation (Predose TL, OSL, TL) of hydrofluoric washed fragments; Simplified Predose and SAR OSL of silicate powders from hydrochloric and fluorosilicic acid treatment. Main obtained results of this ongoing task, point to the fact that the 110 °C TL signal in the Simplified Predose technique minimised required sample size, but growth with cumulative predose was sub-linear. For exponential extrapolations 11/26 faience samples yielded results within 1σ of typological expectations, but substantial scatter was interpreted as relating to radiation quenching effects. Extrapolation errors were investigated by deactivating samples and regenerating their predose responses. Also the laboratory treatment of smaples for luminescence measurements were experimented in different conditions, namely acid treatment of cores drilled from sherds, which enabled preparation of mineral and grain-size fractions while avoiding crushing effects, and damage to or contamination by the glaze and decoration. Results of luminescence measurements indicate that future work should focus on the use of open detection filter combinations to increase signal levels, to enable quenching corrections in predose measurements and the use of high temperature TL signals [15].

4.   CONCLUSIONS

A good chemical based identification of Portuguese faience has been achieved with the analyzed specimens, allowing a clear chemical differentiation of Coimbra and Lisbon faience productions, as well as, the definition of two compositional groups for Lisbon production. This geochemical approach prove former assumptions based on the appearance of the faiences from Lisbon and Coimbra. Chemical analyses of pastes confirmed the production of faience with "rendas" (laces) in Lisbon, usually only assigned to Coimbra. No special correlation between stylistic / decoration and compositional group was found. The chemical homogeneity found for each compositional group may reflect the use of standardize raw materials and probably also recipes for faience production of the studied period. Regarding compositional features of porcelains, a general trend of two large groups is observed, which may reflect the two major porcelain producing regions of China, Jingdezhen (Jiangxi Province) and Zhejiang.

Mineralogical composition of ceramic body reveals the constant presence of quartz, associated with alkali feldspar and plagioclase, and calcite, in some cases, and mostly, the presence of minerals corresponding to high temperature phases is also clearly identified. The main minerals identified were cassiterite, cristobalite, diopside, ghelenite, hematite, mullite (the latter more present in porcelains). The main crystalline phases of glazes traced by XRD are quartz and cassiterite.

Blue glazes owe its colouring mainly to cobalt added to the siliceous matrix. Once the speciation sate of this metallic element embedded in the glass controls the final colouring effect, X ray absorption spectroscopy using synchrotron radiation was particularly suitable to interpret the pigmenting performance through non-invasive assays. Cobalt should then have a dominant role of chromophore and a minor network-former character in the glaze of ancient Chinese porcelains with tetrahedral Co^{2+} ions being responsible for the blue colouring [16], although the higher than 4 coordination value could account for a network-modifying situation of non-colouring pseudo-octahedral Co^{2+} ions filling higher coordination sites available within the tetrahedral silica-rich glassy matrix. Therefore XAFS results confirm that cobalt plays the dual role of chromophore and network-former in the blue glaze of ancient Chinese porcelains.

Differences found in the pre-edge layouts of model oxides XANES spectra are explained by the local symmetry of cobalt ions: Co^{2+} with a regular tetrahedral coordination environment and site symmetry $\bar{4}\,3\,m$ in the spinel-type double oxides (Co Al$_2$ O$_4$) and Co2 Sn O4 and single oxide Co$_3$ O$_4$, and non-colouring octahedral Co^{2+} coordination with two different site symmetries ($\bar{1}$ and m) in the olivine-type crystal structure (Co$_2$ Si O$_4$). Additional details observed in the XANES spectrum of spinel-type single oxide stem from Co^{3+} ions in octahedral coordination [8][9].

Simultaneously, the bulk chemistry of a Chinese glaze – namely, the presence of lead and the absence of arsenic, plus higher iron/cobalt than manganese/cobalt ratios and high cobalt/copper ratio, as determined through non-invasive X ray spectrometry assays – may be confirmative of preliminary dating by Art Historians based on stylistic features, corroborating the advanced manufacture dating predictable for the studied blue-and-white Chinese porcelains (late 16th to early 17th century). On the other hand, cobalt/copper ratios variations point to diverse recipes/manufacture procedures, as well as two diverse Mn/Co and Fe/Co ratios, suggesting two distinctive provenances for blue pigments manufacture. Some samples have high copper content and the systematic presence of lead and arsenic, suggesting the use of cobaltite as Co-carrier. Indeed lead was used in Portuguese ceramic glazed production along the XVI-XVII centuries, but it was not used to produce the blue Chinese glazed porcelain, contributing to better differentiate the Chinese porcelain ordered for the Portuguese market from the Portuguese production. In contrast, it is known [13] that a shift has occurred during the early Ming Dinasty from imported arsenic-rich Persian cobalt-based pigments towards native Chinese blue pigment ores – asbolane (cobalt-manganese wad). Contrary to the blue glazes from European ancient ceramics, the Chinese blue glazes do not contain lead and/or arsenic, indicating that cobaltite was not used as raw material, but most probably a native cobalt ore.

Regarding luminescence measurements, they indicate that future work should focus on the use of open detection filter combinations to increase signal levels, to enable quenching corrections in predose measurements and the use of high temperature TL signals, in order to obtain better signal, thus accurate ages.

REFERENCES

[1] DIAS, M. I. – Principal Investigator of the FCT (Fundação Para a Ciência e Tecnologia) project PTDC/HAH/69506/2006. "Dating, authenticity, materials, pigments. A laboratory study on Portuguese Faience and Chinese Porcelain produced for the Portuguese market (XVI to XVIII centuries)" (2006-2010).

[2] MONTEIRO, J.P., PAIS, A.N. Faiança portuguesa da Fundação Carmona e Costa. Assírio Alvim. Lisboa (2003) 118 pp.

[3] HARRISON-HALL, J. Ming ceramics in The British Museum, London (2001) 640 pp.

[4] KRAHL, R. Chinese Ceramics in the Topkapi Saray Museum, Istanbul (AYERS, J., Ed.) London V.II (1986) 529-817

[5] PINTO DE MATOS, M.A. Chinese Porcelain in Portuguese Written Sources. Oriental Art, **V**. XLVIII nº 5, 36-40. (2002/03)

[6] PINTO DE MATOS, M.A. Porcelana Chinesa na Colecção Calouste Gulbenkian, Lisboa (2003), 223 pp.

[7] DIAS, M.I., PRUDÊNCIO, M.I. Neutron activation analysis of archaeological materials: an overview of the ITN NAA Laboratory, Portugal. Archaeometry, vol **49,** 2, (2007), p.381-391.

[8] FIGUEIREDO, M.O., SILVA, T.P., VEIGA, J.P., PRUDÊNCIO, M.I., DIAS, M.I., MATOS, M.A., PAIS, A.M. Blue pigments in XVI-XVII century glazes: a comparative study between Portuguese faiences and contemporary Chinese porcelains manufactured for the Portuguese market, 2nd Latin-American Symposium on Physical and Chemical Methods in Archaeology, Art and Cultural Heritage Conservation (LASMAC 2009). Selected Papers Archaeological and Arts Issues in Materials Science (RUVALCABA, J.L., et al., Eds) Univ. Nac. Autónoma de México (2010) 84-88.

[9] FIGUEIREDO, M.O., SILVA, T.P., VEIGA, J.P., DIAS, M.I., Speciation state of cobalt in blue glazes: a XAFS study on XVI century Chinese blue-and-white porcelains", European Materials Research Society (EMRS), Spring Meeting, Strasbourg/France, June 8-12, (2009) (abstract).

[10] DIAS, M.I., PRUDÊNCIO, M.I., On the importance of using Sc to normalize geochemical data previous to multivariate analyses applied to archaeometric pottery studies, Microchem. J. **88** (2008) 136–141.

[11] DIAS, M.I., PAIS, A.M., RODRIGUES, A.L., MARQUES, R., PRUDÊNCIO, M.I. Chemical characterization of Portuguese faience from 16th-18th century: a preliminary neutron activation study. 10th European Meeting on Ancient Ceramics, EMAC '09, London, UK (2009) (abstract).

[12] DIAS, M.I., Datação, autenticidade, materiais, pigmentos. Estudos laboratoriais sobre Faiança Portuguesa e Porcelana Chinesa produzida para o mercado Português (séculos XVII a XVIIIIII). Congresso Internacional "A Herança de Santos Simões - Novas Perspectivas para o Estudo da Azulejaria e Cerâmica", Universidade de Lisboa (2010) 94.

[13] CHENG, H. S., B. ZHANG, D. ZHU, F. J. YANG, X. M. SUN, M. S. GUO. Some new results of PIXE study on Chinese ancient porcelain. Nucl. Instrum. Meth. B **240** (2005) 527-531.

[14] http://www.unipress.waw.pl/fityk

[15] BURBIDGE, C.I., RODRIGUES, A.L., DIAS, M.I., PRUDÊNCIO, M.I., CARDOSO, G.O., Optimisation of preparation and measurement protocols for luminescence dating of small samples from a suite of porcelains and faiences. Mediterranean Archaeology and Archaeometry **10** (2010) 53-60.

[16] FERNANDEZ, A.L., PABLO, L. DE, Formation and the colour development in cobalt spinel pigments, Pigm. Resin Technol. **31** (2002) 350-356.

CHARACTERIZATION OF THE ANCIENT DECORATIVE MIRRORS FROM THE GRAND PALACE BANGKOK BY SR-BASED TECHNIQUES

W. KLYSUBUN, P. KLYSUBUN, P. SONGSIRIRITTHIGUL
Synchrotron Light Research Institute,
Thailand
Email: wantana@slri.or.th

W. KLYSUBUN
Thailand Center of Excellence in Physics,
CHE, Ministry of Education,
Thailand

Abstract

Restored in 1831 during the reign of King RAMA III (1824-1851), the whole Temple of the Emerald Buddha was redecorated with fine patterns of very thin colored mirrors or glass mosaics. The mirrors (known in Thai as Krajok Kreab) have unique appearances; they resemble natural gems more than ordinary mirrors and so easy to cut into small sharp pieces. Unfortunately, this fine art of mirror decoration has disappeared for almost 150 years as the original mirror manufacturing process of the royal craftsmen was forgotten over time. Inspired by the exquisite art works, we aim to characterize chemical and physical properties of the ancient mirrors collected from the Temple of the Emerald Buddha. Te ultimate goal is to obtain relevant knowledge necessary for synthesizing new mirrors that are equivalent to the original ones for restoration refinement. The mirror samples studied were red and blue. Each piece consists of thin layer of colored glass with smoothed surface and coating on the back side with some metallic substance. We performed synchrotron XRF, SEM-EDX and PIXE experiments to quantify chemical compositions and traced transition metals in the glass matrix. High quantity of lead was detected in the glass materials among small fractions of sodium, aluminum, potassium and calcium. Manganese, iron, copper and zinc were found in both red and blue glasses whereas only cobalt was present in the blue ones. To obtain information on the chemical states of copper and cobalt, which play important roles in glass coloration, X ray absorption near edge structure (XANES) spectroscopy were carried out. XANES data reveal Cu^{+1} state in both the red and blue glasses while Co^{2+} state in the blue ones. It can be concluded that in the red glass the monovalent copper manifests red whereas in the blue glass the divalent cobalt dominates the monovalent copper, resulting in the blue color.

1. INTRODUCTION

The Temple of the Emerald Buddha is located in the precinct of the Grand Palace. It consists of the ordination hall enshrining the Emerald Buddha, several other halls, pagoda and belfry built since 1782 in the first reign of King Rama of Chakri dynasty. During the third reign (1824-1851), King Rama III had the whole temple restored, additional halls and towers constructed to celebrate the fifty-year anniversary of the Rattanakosin capital (the former name of Bangkok). The major architectural change was the old patterns of gold on red lacquer on the entire walls of the Emerald Buddha chapel being replaced by the golden stucco decorated with fine patterns of very thin mirrors or glass mosaics in a variety of colors, i.e. red, blue, amber, green and silver [1-2]. These mirrors were beautifully fabricated by the royal craftsmen with special features; they were very thin, easy to be cut in to sharp pieces for fine decoration, and importantly resemble natural gems more than mirrors. Figure 1 shows photographs of the exterior of the ordination hall entirely decorated with mirrors and characteristic patterns of mirror arts on royal objects in the Grand Palace. These ancient mirrors are also known in Thai as Kreab mirrors.
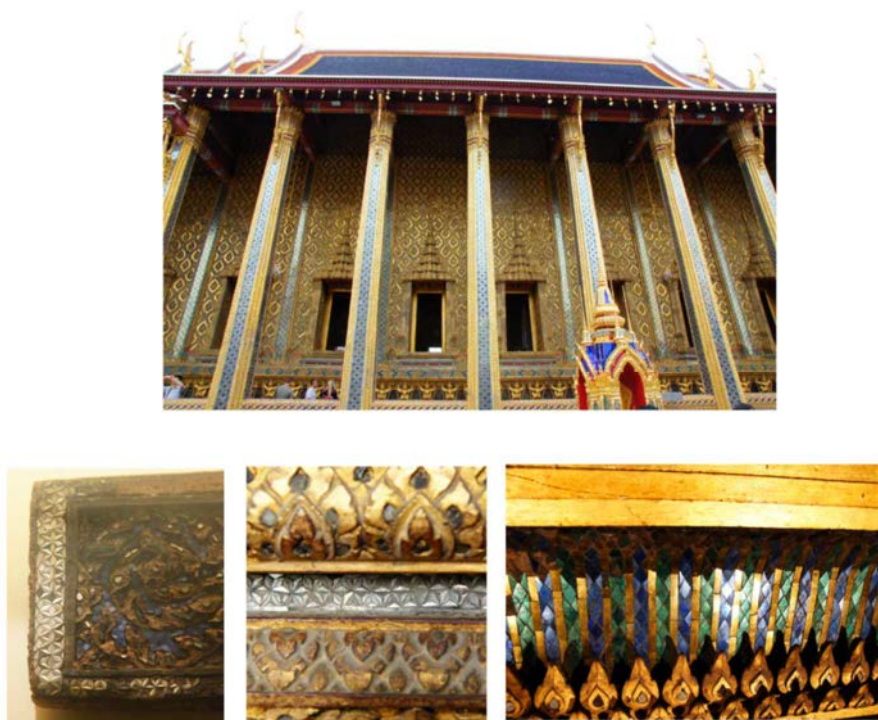
FIG. 1. Photographs of the ordination hall enshrining the Emerald Buddha (upper panel), mirror decorations on wood panels of royal thrones (lower panel, left and middle) and mirror decorations on the base of King Rama I, II and III statuses (lower panel, right).

Although there are documents written in the past to describe the fabrication of Kreab mirrors [3], there has been no success in reproduction of the mirrors for almost 150 years. The reasons may be incomplete description or old writing language, both of which become harder to understand with time. This craftwork is now entirely absent. The last restoration of the temple in 1982 had to be carried out with modern mirrors to replace enormous areas of decayed mirror decoration. However, the elegance of the original arts is nonreplicable by the modern mirrors that are thicker, have unsatisfied sharp colours and show reflection of viewers.

Inspired by the preciousness of the lost art, we studied ancient mirrors from the Temple of the Emerald Buddha in order to understand their physical, optical and chemical properties using a number of characterization methods with advanced tools and technologies. They included a scanning electron microscope coupled with an energy dispersive X ray analyzer (SEM-EDX), proton induced X ray emission (PIXE) technique, synchrotron X ray fluorescence (XRF) analysis and X ray absorption near edge structure (XANES) spectroscopy. The first three techniques are well known and widely used, for many decades, in archaeological science research for quantitative analyses of elemental compositions of ancient objects [4]. On the other hand, XANES spectroscopy, which is a powerful tool for chemical and structural determinations in material science research, has just been applied on ancient artefacts only for sixteen years. Recently studies show that XANES analysis can elucidate colouring mechanisms and opacification in ancient glass objects, such as Thai glass beads [5], Egyptian glassware [6] and Italian glasses [7-8].
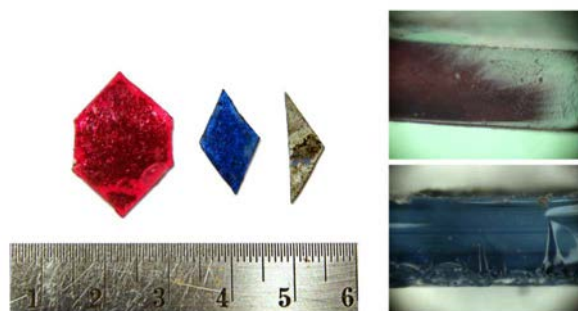
FIG. 2. Photograph of red and blue mirrors on the front side, the back side and their cross-sections.

In this study we focused on the red and blue mirrors to determine main chemical components and traced elements in the glass matrix and to study the cause of colours. Our findings will lead us to the ultimate goal of being able to synthesize the new Kreab mirrors with similar properties to those of the original ones. This will benefit future restoration of the Temple of the Emerald Buddha and the Grand Palace, the place of which the most excellent arts in Thai culture exist, symbolizing the splendour, peace and sovereignty of the nation.

2.   SAMPLES OF ANCIENT MIRRORS

Five samples of red coloured ancient mirrors and four samples of the blue ones were provided by the Bureau of the Royal Household to be investigated in this study. The red samples were used to decorate a pillar of the ordination hall of the Emerald Buddha while the blue ones were used to decorate the platform of the commemorative statuses of King Rama I, II and III in the royal pantheon. Figure 2 shows a photograph of red and blue mirrors and in the right panel depicts their cross-sections viewed by an optical microscope. Each mirror consists of thin glass layer with a thickness ranging from 0.44 mm to 0.85 mm and some metallic coat on the back side. The refractive index (R.I.) of each mirror sample was measured by a refractometer (Chlight CL-181) and given in Table 1.

3.   EXPERIMENTS

3.1. SEM-EDX and PIXE techniques

TABLE 1. THICKNESS AND REFRACTIVE INDICES OF THE ANCIENT MIRRORS

Sample	Colour	Shape	Thickness (mm)	R.I.
1 HR	Red	Hexagon	0.57	1.646
2 HR	Red	Hexagon	0.50	ND
3 HR	Red	Hexagon	0.58	1.645
4 HR	Red	Hexagon	0.44	1.660
5 HR	Red	Hexagon	0.80	1.620
DB	Blue	Diamond	0.50	1.560

12	DB	Blue	Diamond	0.71	1.575
11	TB	Blue	Triangle	0.85	1.575
12	TB	Blue	Triangle	0.50	1.535

SEM-EDX is widely used to identify elements in materials and able to determine relative quantities of the elements. The elemental quantification is based on intensity of X ray fluorescent (XRF) signals emitted from the elements present in a sample that is excited by a focused electron beam of high energy.

The measured XRF intensity is proportional to the elemental concentration, thus the element can be quantified in its elemental form (%wt) or oxide form (oxide %wt). We employed an SEM (Hitashi S-3400N)-EDX (Horiba EMAX), setting a high voltage at 20 kV and a working distance at 10 mm, to explore elements in samples HR5 and DB1. The electron beam was focused on three different spots with a 100x magnification for collecting the XRF spectra, each of which using 30 seconds of integration time. Note that transition metal elements with concentration lower than 0.3 %wt could not be detected by this instrument.

Similar in principle, PIXE technique uses a positive-charged ion beam to induce XRF emission from the elements in the sample. We utilized a PIXE station at the Ion Beam Technology Research Unit, Chiangmai University. The ion beam was generated by a 1.7 MV tandem accelerator with the beam diameter of 1mm at the sample position. The XRF spectra were recorded, using a Si(Li) detector (Canberra), on three different spots for samples HR5 and DB1. The integration time was 3 minutes per spectrum. Because of thick beryllium window of the detector, we could not observed XRF signal from any element that is lighter than aluminium.

3.2. Synchrotron XRF and XANES spectroscopy

Synchrotron XRF and XANES measurements were performed at the beamline BL8 [9] of Synchrotron Light Research Institute, Thailand. The beamline is equipped with a Ge220 double crystal monochromator for scanning photon energies from 3381 eV to 10000 eV. XRF spectra were collected for all of the samples using a 13-element germanium detector (Canberra). The X ray excitation energy was 9970 eV and the integration time was 100 seconds per spectrum.

Copper and cobalt K-edge XANES spectra were recorded in fluorescence yield mode, using the same detector, for samples HR5 and DB1. The fluorescence yield mode is suitable for our samples because the concentrations of copper and cobalt are very low in these samples. Photon energy calibration was performed using a copper foil and a cobalt foil with the known absorption edge positions of 8979 eV and 7709 eV, respectively. The photon energy calibration was accurate within ± 0.1 eV. For each spectrum, the photon energy was scanned from -30 eV to 80 eV, relative to the edge positions of copper and cobalt foils, with an increment of 0.3 eV. Oxides of copper and ones of cobalt were measured in transmission mode for spectral comparisons.

4. RESULTS AND DISCUSSION

4.1. Glass compositions and traced elements

Experimental results from PIXE and SEM were combined to obtain the elemental compositions in the samples HR5 and DB1 quantitatively. They were given in Table 2 as percentages of the common oxides. HR5, which is the red glass, contains about 50% of lead oxide (PbO) while there is 25% of PbO in the DB1 blue sample. Lead was then deliberately used by the Thai royal glasshouse. In glass technology, lead is commonly added to lower a working temperature and viscosity of the glass, making the molten vitreous batch more fluid than that of the ordinary soda glass [10]. Lead also increases the refractive index of the glass. This agrees with our finding that the refractive indices of the red glass samples are higher than those of the blue ones. In addition, lead possibly causes the ancient glass to look like gems. Soda (Na_2O), alumina (Al_2O_3), potash (K_2O) and lime (CaO) are also present in all samples; they are commonly used as flux and stabilizer. Traced transition metal elements found in the red and blue samples are manganese, iron, copper and zinc. Note that cobalt was detected only in the blue glass. The concentration of these metal oxides ranges from 0.04 to 0.86 %wt.

Figure 3 shows consistence in tendency of the metal oxide contents, from five samples of the red glass and four samples of the blue glass, determined by synchrotron XRF. We note that elemental concentration of copper is about 0.19 %wt or 0.22 oxide %wt in the red glasses. It is 4 times higher than that in the blue samples. On the other hand, cobalt and iron dominate in the blue glass.

4.2. Chemical states of copper and cobalt

Gold has been well known for glassmakers as one of colouring agents for dark red colour of gemstone ruby. However, many previous studies, using XANES techniques, reported that copper was an important colorant element found in ancient red ruby glasses either when it was in chemical form of Cu^{+1} ion [5,8,11] or metallic copper Cu^0 nanoparticles. In addition, Cu^{+2} ion can cause blue colour in glass [12]. Thus, the colour in glass is related to the oxidation states (OS) of the transition metals.

Cu K-edge XANES spectra of HR5 and DB1 are presented in Fig. 4, compared with those of copper foil (OS:0), Cu_2O (OS:+1) and CuO (OS:+2). The positions of absorption edge (a), small edge peak (b) and broad crest (c) seen in HR5 and DB1 spectra are lined up with those of Cu_2O. Thus it can be concluded that copper atoms in both red and blue glasses are Cu^{+1} ions. Although the copper oxidation states are the same in our samples and Cu_2O, the electronic states are different. Therefore, the broader hump following the sharp crest in Cu_2O spectrum is hardly observed in glass. This implies that silicon atoms may affect chemical binding between copper and oxygen atoms and that scattering effects from higher coordination shell are weak. The K-edge energy of copper equals to the energy difference between the electronic $1s$ level and the final $4p$ state. The dipole transition between $1s$ and $4p$ states gives rise to a small edge peak (b) observed at 8982.7 eV, 8983.4 eV and 8983.6 eV for Cu^{+1} ions in Cu_2O, sample DB1 and HR5, respectively. The K-edge position (a) is shifted to higher energy with the increase of oxidation state of copper ion. A shift of 1.0 eV is seen between the edges of Cu^0 and Cu^{+1} and a shift of 2.5 eV between the edges of Cu^{+1} and Cu^{+2}.

TABLE 2. ELEMENTAL COMPOSITION OF HR5 AND DB1 MEASURED IN PERCENTAGES OF THEIR OXIDE WEIGHTS

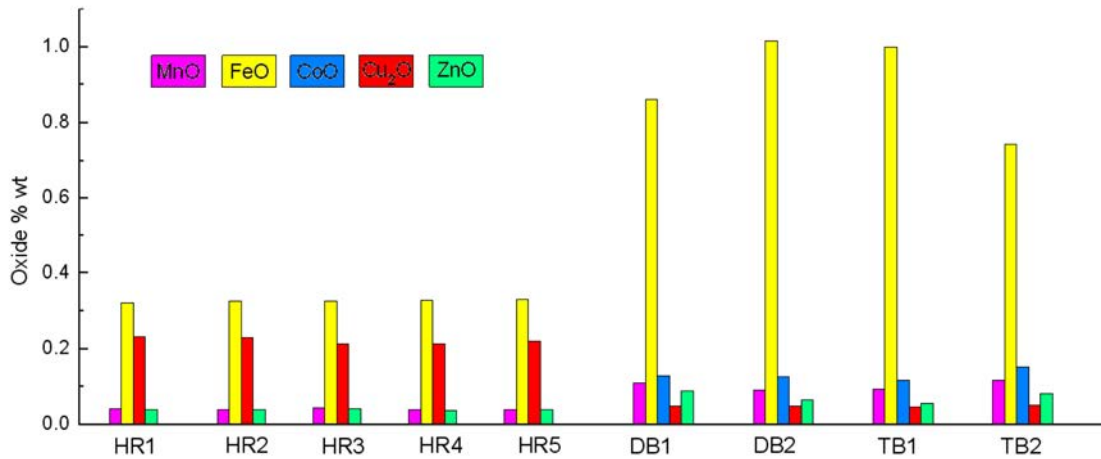| Sample	Na_2O	Al_2O_3	SiO_2	Cl	K_2O	CaO	MnO	FeO	CoO	Cu_2O	ZnO	PbO
HR5	2.54	2.49	43.01	1.12	1.06	2.11	0.04	0.33	<<	0.22	0.04	47.03
DB1	5.10	2.57	56.85	0.51	1.59	6.18	0.11	0.86	0.13	0.05	0.09	25.95

FIG. 3. Comparison on metal oxide contents in red and blue mirrors.

The Co *K*-edge XANES spectrum of DB1 is shown in Fig. 5, compared with those of Co foil, CoO and Co_3O_4. The edge (a) and the edge crest (b) of DB1 are seen nearly at the same photon energies of those in CoO. Thus the cobalt in DB1 is identified as Co^{+2} ions. Note that there is a small pre-edge peak (a′) observed at 7709 eV in all spectra, expect in Co foil. It corresponds to electronic quadrupole transition from 1*s* level to 3*d* state of cobalt. In CoO, each Co^{+2} ion bonds with 6 oxygen atoms in an octahedral arrangement in the first coordination shell, while in Co_3O_4 there is 2/3 of Co ions (Co^{+2}) occupying the distorted octahedral sites and 1/3 of Co ions (Co^{+3}) occupying the tetrahedral sites. The absorption shapes of CoO and Co_3O_4 seen above the edge region obviously differ from that of Co^{+2} ions in our glass. In contrary, Trutia suggested in his study of the crystal field optical spectra that cobalt incorporated in the vitreous matrix as tetrahedral complexes surrounded by four oxygen ions in the first coordination shell, yielding the colour of blue in glass materials [13].
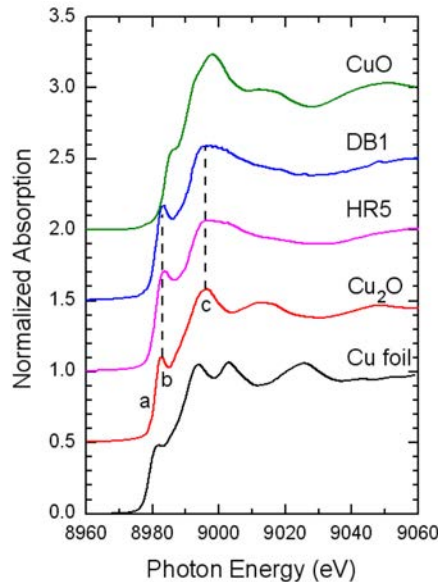

FIG. 4. Normalized Cu K-edge XANES spectra of red glass HR5, blue glass DB1 and copper standards. For clarity, an upper spectrum is vertically shifted by 0.5 relative to a lower one.
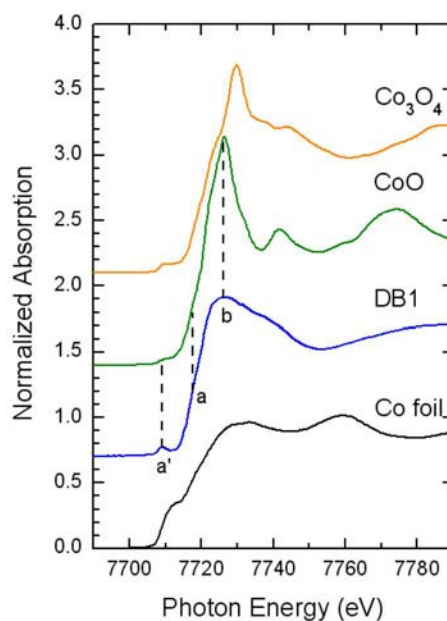
90

FIG. 5. Normalized Co K-edge XANES spectra of blue glass DB1 and cobalt standards. For clarity, an upper spectrum is vertically shifted by 0.7 relative to a lower one.

5.   CONCLUSIONS

Nine samples of ancient Thai glass mosaics or mirrors of red and blue colours from the Temple of the Emerald Buddha were classified as alkali-lead glasses. The lead content is higher in the red glass than the blue one. This suggests that they were fabricated using different recipes. The higher refractive indices of the red glass specimens are attributed to higher lead concentrations. Based on our chemical analysis by SEM-EDX and PIXE, the glass formulas $43SiO_2.47PbO.3(Na_2O.Al_2O_3).2CaO.K2O.(0.3FeO)$ and $57SiO_2.26PbO.5Na_2O.3Al_2O_3.6CaO.2K_2O.(0.9FeO)$ are desired to prepare batch for synthesizing red and blue glasses, respectively. The colorant element for red is copper where Cu_2O can be added at 0.22 %wt. One for blue is cobalt where CoO can be added at 0.13%wt.

XANES spectroscopy identifies copper and cobalt species in these glass samples. In both colours, copper are only in +1 oxidation state; there are no fingerprint of copper in nanometre-scaled metal cluster. Cobalt was detected only in +2 oxidation state responsible for the blue colour. Iron, manganese and zinc present in our samples will be studied by XANES in the near future as we expect that they play mutual roles in glass coloration due to the consistent difference in their concentrations between the red and blue glass samples.

Since glass structure (SiO_2) is non-periodic, thus chemical bonding of the traced transition ions in oxygen-silicon network is complex. To study average local atomic structure, extended X ray absorption fine structure spectroscopy will be desired.

REFERENCES

[1] DISKUL, S., History of the Temple of the Emerald Buddha, Bureau of the Royal Household, Bangkok, 1982, 43 pp.

[2] KRAIRIKSH, P., The Grand Palace and The Temple of the Emerald Buddha: A Handbook for Guides, Bureau of the Royal Household, Bangkok (1988) 52 pp.

[3] Documents on glass making, ancient black Thai book, National Library of Thailand.

[4] UDA, M., DEMORTIER, G., NAKAI, I., X rays for Archaeology, Springer, Dordrecht (2005) 308 pp.

[5] KLYSUBUN W., THONGKAM, Y., PONGKRAPAN, S., WON-IN, K., T-THIENPRASERT, J., DARARUTANA, P., XAS study on Copper Red in Ancient Glass Beads of Thailand, Anal. Bioanal. Chem. **399** (2011) 3033.

[6] LAHLIL, S., BIRON, I., COTTE, M., SUSINI, J., MENGUY, N., Synthesis of Calcium Antimonate nano-crystals by the 18th Dynasty Egyptian Glassmakers, Appl. Phys. A **98** (2009) 1.

[7] QUARTIERI, S., RICCARDI, M.P., MESSIGA, B., BOSCHERINI, F., The ancient Glass Production of the Medieval Val Gargassa Glasshouse: Fe and Mn XANES Study, J. Non-cryst. Solids **351** (2005) 3013.

[8] ARLETTI, R., QUARTIERI, S., VEZZALINI, G., SABATINO, G., TRISCARI, M., MASTELLONI, M.A., Archaeometric Analyses of Glass Cakes and Vitreous Mosaic Tesserae from Messina (Sicily, Italy) **354** (2008) 4962.

[9] KLYSUBUN, W., SOMBUNCHOO, P., WONGPRACHANUKUL, N., TARAWARAKARN, P., KLINKHIEO, S., CHAIPRAPA, J., SONGSIRIRITTHIGUL, P., Commission and Performance of X ray Absorption Spectroscopy Beamline at the Siam Photon Laboratory, Nucl. Instrum. Meth. A **582** (2007) 87.

[10] SHELBY, J.E., Introduction to Glass Science and Technology, Royal Society of Chemistry (2005) 291 pp.

[11] FARGES, F., ETCHEVERRY, M-P., SCHEIDEGGER, A., GROLIMUND, D., Speciation and Weathering of copper in "Copper Red Ruby" medieval Flashed Glasses from the Tours Cathedral (XIII Century), Appl. Geochem. 21 (2006) 1715.

[12] VEIGA, J. P., FIGUEIREDO, M.O., Copper blue in ancient glass bead: a XANES study, Appl. Phys. A **83** (2006) 547.

[13] TRUTIA, A.T.H., J. Optoelectron. Adv. Mater. **7** (2005) 2677.

SYNCHROTRON XRF AND XAS ANALYSIS OF HAIR FOR TOXICOLOGICAL AND PHARMACOKINETIC STUDIES: APPLICATIONS AND ARTEFACTS

I. M. KEMPSON
Ian Wark Research Institute
University of South Australia
Mawson Lakes, Australia
Email: Ivan.Kempson@unisa.edu.au

Assoc. Professor
Institute of Physics, Academia Sinica,
Nankang, 11529, Taiwan
Email: IKempson@phys.sinica.edu.tw

Abstract

Synchrotron X ray Fluorescence (XRF) and X ray Absorption Spectroscopy (XAS) are well suited for studying elemental distributions and speciation in biological samples. In regard to forensic-based hair analysis, XRF is excellent for investigating acute exposures to metals and metalloids. Additionally, XAS offers unique potential in identifying changes in speciation, relating pharmacokinetic profiles along individual hair strands with metabolism. Imaging with XRF microprobes has largely been inhibited by immense time constraints for imaging large areas or with high resolution. The advent of the new Maia detector technology available at the Australian Synchrotron however has revolutionized the ability to conduct thorough, robust research and investigations into fields of forensics and cultural heritage with ultra-fast mapping. A comparison of old and new detector technology is given leading into examples of pharmacokinetic profiles in hair and a case study of the proposed poisoning of the famous race horse, Phar Lap.

1. INTRODUCTION

Synchrotron radiation sources provide beneficial properties for the study of trace evidence in forensics [1] and cultural heritage. For instance, in the study of glass [2], gunshot residues, pigments and biological matrices [3]. In forensic analysis this has often utilized infrared technologies which are robustly utilized in the forensic arena. However, other modalities such as X ray fluorescence (XRF), X ray Absorption Spectroscopy (XAS) and tomography offer unique potential for non-destructive analysis of composition, chemistry and structure.

The properties of synchrotron light sources provide unique ability for XRF imaging at high resolution and sensitivity, and the energy tunability gives powerful chemical speciation through XAS. These two experimental approaches coupled together offer opportunities in imaging elemental species (typically from about K upwards) in biology in so far as divulging elemental distribution, associations and metabolic processes at sub cellular spatial scales. This has broad application in many aspects of research, here it is discussed in the context of characterizing elemental distributions in hair.

The advantages of synchrotron XRF and in particular the immense capability of new detector technology is given with examples of imaging hair under the context of toxicological investigation. The power demonstrated is extendable to a multitude of research/investigative fields. Application of XRF analysis of hair for toxicology is given with the case study of the famous race horse, Phar Lap. The potential in chemical speciation for identifying metabolites is also discussed.

The beneficial aspects of synchrotron based XRF include:

- High resolution due to highly collimated monochromatic intense beams and advances in X ray optics. Sub 20nm can now be achieved [4];
- High sensitivity down to sub femto-gram quantities;
- Very rapid acquisition potential due to the high intensity of incident beams compared to conventional X ray tube technology;

- Coupling with chemical speciation by way of XAS on the same beamline;
- Polarized light leading to reduced scattering and background in spectra;
- Energy tunability to omit excitation of overlapping peaks (e.g. Pb-L$_{III}$ and As-K$_\alpha$).

Many of the problems applying XRF mapping stem from immense amounts of time to image a reasonable area with reasonable resolution. Large areas can easily blow out to needing many hours, days or even months to conduct what an investigator would consider ideal parameters. This has been severely limiting for both the forensic and cultural heritage contexts by making fundamental studies and practical application/investigation prohibitive due to time feasibility. Any imaging of dimensions over approximately 2mm^2 or so is typically not feasible when weighing the beam access time/expense with the research outcome. This severe limitation is primarily due to detector technology being far inferior to the synchrotron microprobe setup and could be considered as the weakest link in synchrotron XRF microprobes.

2.   ULTRAFAST DETECTION FOR XRF MAPPING

The time of acquisition has recently been revolutionized with the advent of new detectors such as the Maia detector [5]. This detector enables on-the-fly rastering of a sample giving almost zero overheads (in a time respect) and down to 50 μsec per pixel. Such ability will open up many avenues for mapping heterogeneous elemental distributions at high resolution over large areas for many fields of research (e.g. see [6]). Currently the set-up at the Australian Synchrotron is able to image areas up to 100x100mm with scan rates on the order of 2 lineal millimetres per second with 5 μm resolution, providing incredible potential for imaging larger samples such as paintings or artefacts. This has multiple advantages:

Much larger areas can be analyzed with comparable resolution compared to conventional detector systems;

A much greater number of samples can be analyzed for statistical confidence and interpretation (critical for forensic investigation);

Much faster analysis implies much lower probability of beam induced damage to the sample;

Significantly less probability of beam induced data artefacts regard to elemental chemistry (e.g. XAS) due to photo-redox processes;

Realistic potential for significant development of microXRF tomography [7].

A comparison of XRF mapping with a conventional detector set-up is compared to the Maia detector at the Australian Synchrotron in the following section.

3.   HAIR ANALYSIS

The concept behind hair analysis is that endogenous trace-level components of blood supply become incorporated into the growing hair cells in the hair bulb. As the hair grows, each segment of growth shifts distally outwards producing a potential time-line of history of the individual's blood concentrations. What the hair may represent can be wide ranging, such as: daily dietary intake; exposure to pollutants; morbid effects of disease; and pharmacokinetic profiles relating to acute ingestion of xenobiotics. The time frame covered by hair is unique. Based on the growth of hair at a rate of approximately 1cm per month in humans, then hair can represent prior days to many months before sampling. Hair testing for metals and metalloids has been extensively reviewed elsewhere [8, 9].

Hair analysis is rather successfully applied in forensic contexts in regards to monitoring organic compounds, in particular drugs of abuse or performance enhancers. This is primarily due to the ability to confirm ingestion because of monitoring metabolites which can exist in the hair due to endogenous metabolism of the parent compounds. In this sense hair analysis has been demonstrating significant ability and future potential. With regards to inorganic compounds however, little success has been achieved specifically due to the lack of distinction of metabolites and relating the hair concentrations to blood concentrations. There are currently several major difficulties in applying hair analysis for studying chronic and acute exposure:

- External contamination is readily incorporated into hair and difficult (and in many cases probably impossible) to discriminate from endogenous incorporation;
- Hair chemistry and composition is highly variable (e.g. with colour, age, location on body, genetics etc) and as such lead to differences in the accumulation of xenobiotics between individuals;
- Leading from these previous points is that ultimately the relation of hair concentrations to blood concentrations is highly problematic.

4.   STATE-OF-THE-ART ELEMENTAL MAPPING IN HAIR WITH XRF

This section demonstrates the current status of XRF micro and nano-scale imaging. At a resolution scale of a few microns the impact of new detector technology at the Australian Synchrotron is immense (as demonstrated below). For higher resolution (i.e. 100-200 nm) fewer systems are available and also have not been integrated with ultrafast detection systems.
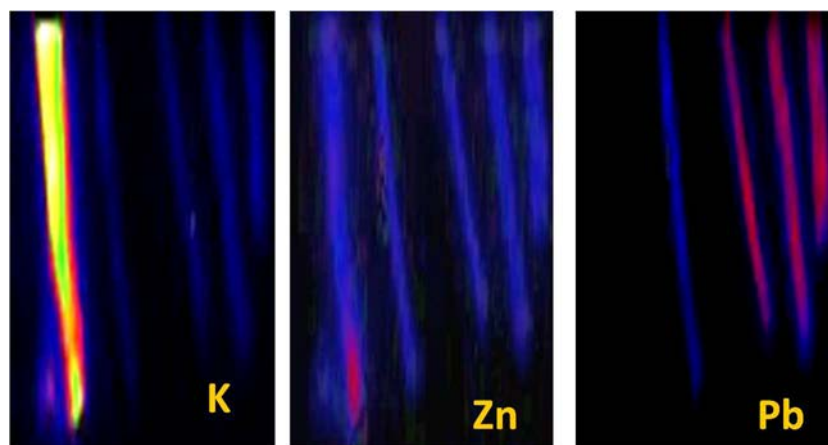

FIG. 1. Segments of an individual hair arranged to show regions sequentially distal from the bulb (left side of each image) to the tip (right side of each image) at approximately 35mm from the bulb. The image is comprised of 33 pixels vertically @ 30 μm steps and 100 pixels horizontally @ 5 μm steps, i.e. 3,300 pixels and a 0.5x1.0 mm FOV. Acquisition took approximately 2 hours. Reprinted from Kempson et al.[10] Copyright (2005), with permission from Elsevier.

Figure 1 shows an XRF map of a hair segmented and arranged into a reasonable field of view produced at the PNC-CAT beamline in the Advanced Photon Source, USA. This sample was obtained from a lead smelter worker and demonstrates the accumulation of lead in the hair moving distally, indicating exogenous accumulation of atmospheric contamination. The image was constructed with a beam focused to approximately 7x7 μm and rastered in 5 μm steps horizontally and 30 μm steps vertically. The hair is clearly imaged but any structure is crudely discernable. The internal distribution has implications in identifying endogenous versus exogenous contributions and can roughly be inferred with modelling of the line profiles [10].
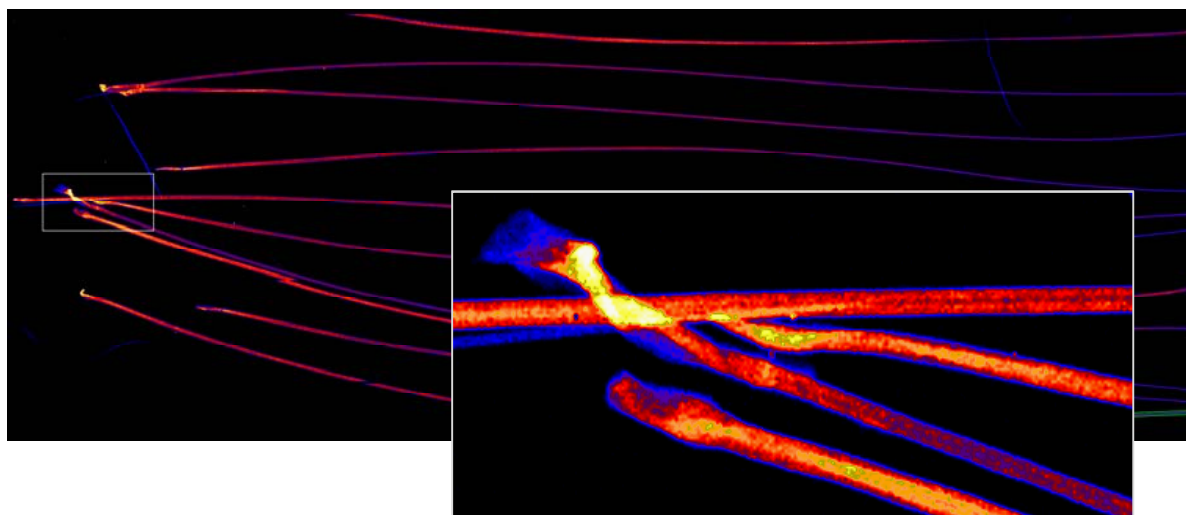
FIG. 2. An XRF image of Zn in plucked mouse whiskers. A much larger number of samples with improved resolution can be imaged with fast imaging detectors, i.e. the Maia detector. The inset image shows a magnified view of the boxed region. The original image was 20x7.25 mm @ 4x4 micron steps (i.e. 5,000 x 1,812 pixels = 9MPixels.) Acquisition took approximately 5 hours.

In comparison, the ultra-fast Maia detector at the Australian Synchrotron acquired in 2010 the image provided in Figure 2. The dimensions, resolution and acquisition time are all significantly improved. The number of pixels in the image produced at the Australian Synchrotron in Figure 2 with the Maia detector contains over 2,700 times the number of pixels compared to that from PNC-CAT at the Advanced Photon Source in a period of time only a factor of 2.5 times greater. By this comparison, it would require 90 days of uninterrupted beamtime on the conventional detector set-up to collect the image produced by the Maia detector. This clearly demonstrates new ability to image fields of view at resolutions not feasible before, thus enabling scientists to dramatically extend applications and improve probing of scientific questions by way of improving statistics and collecting data in satisfactory times.

However, the Maia detector is not yet integrated with the system arrangement for high-resolution imaging (i.e. 10's to 100's nm with zone plate optics focused beams). Currently, imaging such as in Figure 3 is still a laboriously time consuming process (several hours in this case).
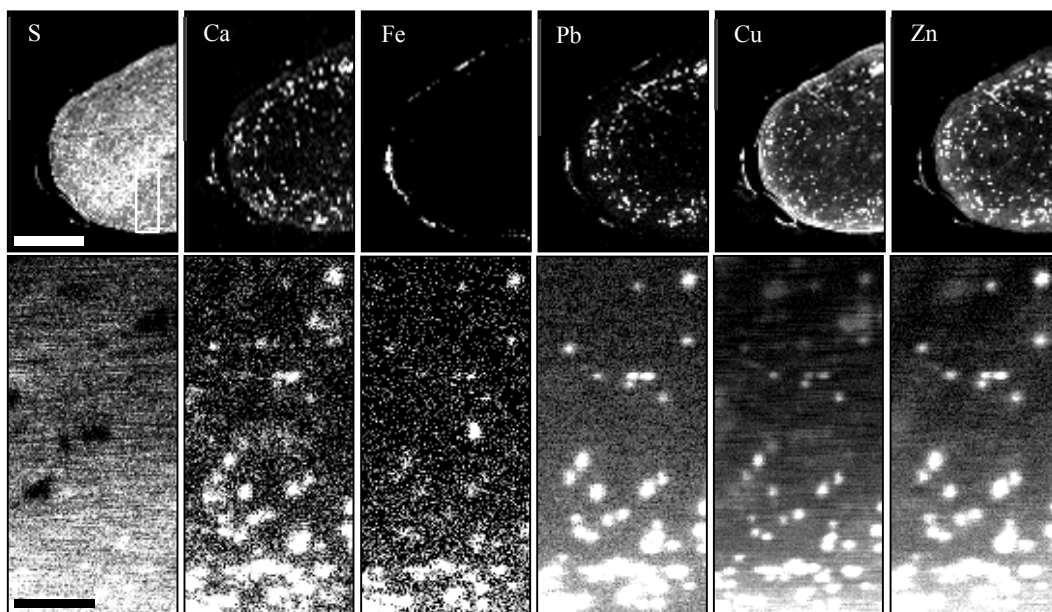
FIG. 3. High resolution XRF images of a hair cross section. The upper images show gross elemental distributions with localized deposits around nuclear remnants and/or melanin granules. The boxed region was re-imaged with smaller step sizes of ~100 nm, shown in the lower images. Bar = 10 μm and 2 μm respectively: Reprinted with permission from Kempson et al.[11]. Copyright 2006 American Chemical Society

This image was produced at the 2ID-D beamline at the APS with a beam focused to approximately 130 nm and shows fine structure in a cross-section of hair obtained from the same individual as the sample shown in Figure 1. With this resolution distinct associations are obvious and it is clear Pb has migrated into the hair. Since the production of this image,improvements have been made in achieving better focusing optics, but so far there is little demonstration in the literature for XRF mapping.

5. USE OF XRF IMAGING OF HAIR FOR TOXICOLOGY AND PHARMACOKINETICS

As seen in the previous section, synchrotron XRF offers a probe perfectly suited to samples on dimensional scales similar to hair. Therefore, there is distinct opportunity in further research into pharmacokinetic profiles represented in individual strands of hair. In this regard, Figure 4 shows an image of Zn and Au in an individual mouse whisker plucked 14 days after intravenous administration of a gold nanoparticle solution. The intense band of gold is very distinct, shows a rapid increase in concentration at the distal edge of the band and a more gradual decrease moving proximally. A plot of the intensity decay of the gold signal on the proximal side has been reproduced in Figure 5. Note that the x-scale has been reversed and changed to a time scale, since the rate of growth is quite well defined, i.e. the distal edge of the gold band should be very close to 14 days old (assuming a constant growth rate).
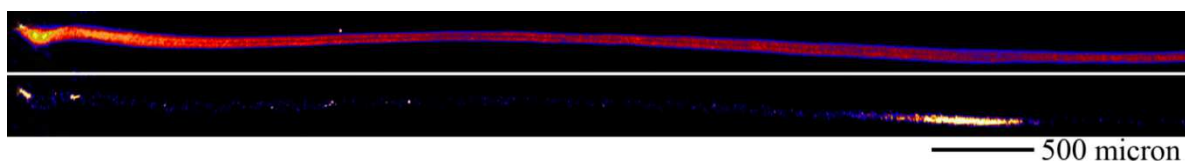

FIG. 4. XRF mapping of an individual hair. The top image shows the whole hair by way of the Zn signal. The bottom image is that of gold 14 days after intravenous injection of gold nanoparticles. The pharmacokinetic decay profile is reproduced as a scatter plot in Figure 5 below.
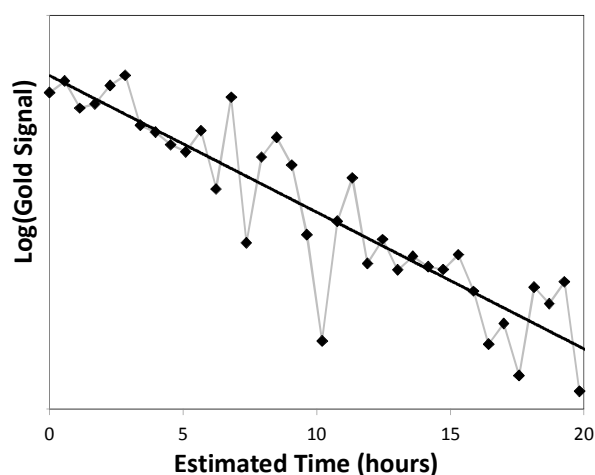
FIG. 5. Pharmacokinetic profile of gold nanoparticle excretion into hair after intravenous administration. Longitudinal intensity data from the decay region of the gold image in Figure 4 was extracted and presented as a scatter plot here. Based on the rate of hair growth, the decay constant indicates a blood half-life of 8.6 hours, consistent with blood concentration profiles.

6.   CASE STUDY – PHAR LAP

Phar Lap was a famous Australian race horse with an incredible racing history in the late 1920's and early 1930's. By many, he has been acclaimed to be the best race horse in history. In 1932 he died in very sudden and suspicious circumstances. Many people attributed his death to murder by intentional arsenic poisoning but the autopsy proved inconclusive. Such was the love for Phar Lap that his skeleton was returned to his birth place in New Zealand, his heart is on display in the National Museum of Australia in Canberra and his hide was mounted and preserved, displayed in pride of place in Museum Victoria, Melbourne. Based on the concept of hair analysis, a small section of hide was removed from Phar Lap's mane to test for any indication of arsenic poisoning. Indeed, XRF mapping of individual hairs showed a distinct band of arsenic in each strand in a location between the hair bulb and the skin level (Figure 6 b,c). The location and distribution are consistent with Phar Lap receiving a large acute exposure to arsenic soon prior to his death. The announcement of this evidence for poisoning resulted in major press coverage, not only in Australia but internationally (Figure 7) and additionally led to a television documentary.

Importantly, the decay in the arsenic profile can test the consistency of the rate of decay with known pharmacokinetics. In the case of the hair analyzed for gold (above), the rate of the hair growth was known. However for samples where the actual rate cannot be deduced it is necessary to estimate the hair growth rate. For horses' mane hair it can be quite variable (see ref. [12]). In Figure 8, the data of the arsenic decay profile from Phar Lap's hair has been plotted along different time scales, to test different possible rates of hair growth. The two extreme cases represent the extreme observations from the literature for horse hair growth rates. An intermediate which could be considered as an estimate of the average is given in between. Based on these 3 growth rates, a half-life calculation indicates a value between 2.3 to 5.8 hours. In pig studies a plasma half-life was found to be less than 5 hours. Thus the arsenic distribution in Phar Lap's hair is consistent with a pharmacokinetic decay profile.
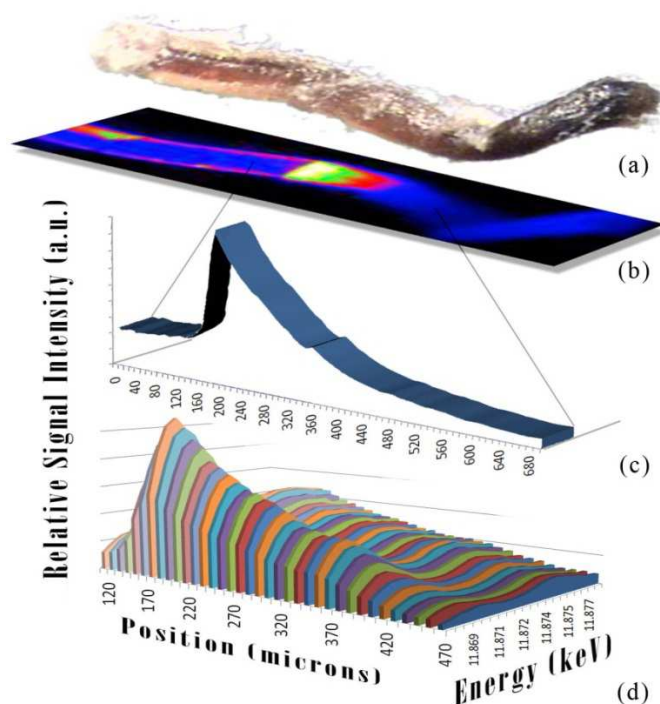
FIG. 6. Analysis of Phar Lap's hair. An optical image shows the root end of one hair with the root sheath intact (a). The hair was analysed with an X ray microprobe at PNC-CAT (Advanced Photon Source) that imaged the internal arsenic distribution (b). The longitudinal pharmacokinetic-like profile reflects the hair growing outwards as the arsenic is metabolized (c), while 2D XANES mapping reveals the variation in arsenic speciation ratios moving longitudinally (d). Reproduced from ref. [12] with permission from John Wiley and Sons.

FIG. 7. Cover articles in popular and scientific media. In Australia, the story of the analysis of hair from Phar Lap was front page news on almost every major newspaper. It's publication in a scientific outlet also attracted international attention (reproduced from ref.[13] with permission from John Wiley and Sons).
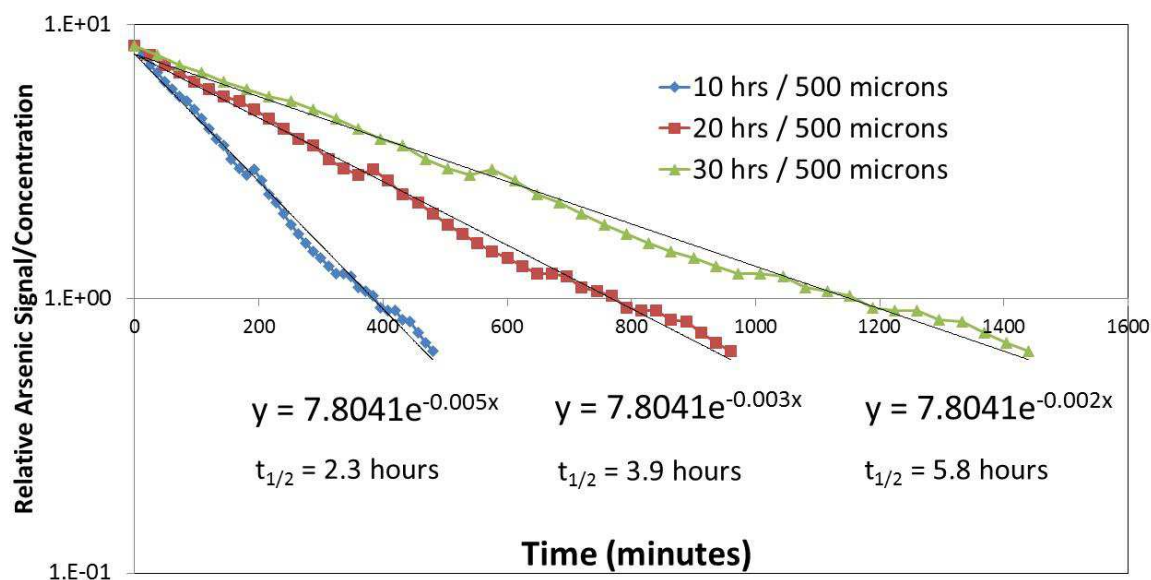
Fig 8. Arsenic decay profiles moving longitudinally along Phar Lap's hair. The same data has been plotted along a time scale assuming 3 different hair growth rates representing the two extreme growth rates observed in horses as well as an intermediate rate. In pigs, the plasma half-life was measured to be <5 hours. The decay in arsenic intensity observed in Phar Lap's hair is consistent with such pharmacokinetics.

6.1. Potential of metabolic profiling based on speciation

As seen in Figure 3 there is significant difficulty in attributing elemental hair concentrations to endogenous consumption since contaminants can easily migrate and associate with internal components of the hair. In this case, there is potential in using the chemical speciation of the elements of interest to infer metabolism and discriminate contamination.

What was further interesting in the case of the Phar Lap study was the longitudinal variation in the ratio of arsenic species moving longitudinally (Figure 6d). The plot shows a dramatic change in the relative intensity of the arsenic species with progression of the time of formation of the hair. It is proposed that this variation is due to metabolic changes in the arsenic while in the blood system and has subsequently affected the speciation of what has been incorporated into the hair. The change with time (length of hair) is consistent with such a process occurring. This appears to indicate a chemical change represented in hair based on metabolism. This is potentially the first indication endogenous consumption of arsenic can be discriminated from exogenous contamination based on metabolic products being reflected as distinct chemical species in hair. Metabolic products are routinely used in hair analysis in investigating drugs of abuse in individuals since many metabolites irrefutably indicate ingestion by the individual. The demonstration of different chemical species varying longitudinally shown here suggest the chemical species could be used for distinction of metabolism. However, at this stage there is little knowledge regarding the speciation of elements in hair, how they vary depending on the chemical form consumed, any differences with contaminating elements and their chemical form, and their longer term stability and variation with hair treatments. As such, significantly more development is needed to understand the elemental incorporation to attribute hair content to blood content.

7.   ARTEFACTS IN XRF AND XAS ANALYSIS

With the use of these techniques there are a few considerations that any experimental plan and interpretation should be mindful of. In particular, the unfortunate effects of the intense X ray beam on samples. In the worst cases, the beam is so intense that the sample may be destroyed or severely damaged. Within a sample and immediately around it, there is typically generation of highly reactive radicals which can have severe impact on the sample chemistry. The radicals undergo redox processes which can completely alter the chemical speciation of elements of interest. Arsenic in biological matrices are particularly susceptible [3, 14]. With regard to XRF mapping, some experimental geometries (in particular when the sample is held at 45 degrees to the incident beam) escapes depths of X rays indicative of different elemental components are highly variable and can distort elemental distributions and associations (for example in Martin et. al.[15]).

8.   GENERAL ACCEPTANCE

In a forensic context there is a distinct difficulty in implementing new technology for administering evidence into a court environment. There is very critical need for data to be accurate and reflective of fact due to the consequences of forensic information to individuals involved in criminal proceedings. Due to the necessity of accuracy in drawing conclusions and accurate representation of all people involved, data from new techniques meets a challenging environment in legal situations. Typically there must be numerous efforts in proving the new technological approach by way of determining all possible ways false negatives and especially false positives can eventuate. As such particularly labourious experiments must be performed to deduce confidence in the findings of the new experimental approach. In this respect, hair analysis requires more fundamental research for toxicology and especially in any effort to infer metabolism based on chemical speciation.

REFERENCES

[1] KEMPSON, I.M., KIRKBRIDE, K.P., SKINNER, W.M. COUMBAROS, J., Applications of synchrotron radiation in forensic trace evidence analysis, Talanta **67** 2 (2005) 286-303.

[2] KEMPSON, I.M., DENMAN, J.A., SKINNER, W. KIRKBRIDE, K.P., Applications of synchrotron X ray sources for forensic characterisation of glass, (Proc. of Australian Institute of Physics 16th National Congress) Australian Institute of Physics, Canberra (2005)

[3] KEMPSON, I.M., HENRY, D. FRANCIS, J., Characterizing arsenic in preserved hair for assessing exposure potential and discriminating poisoning, J. Synchrotron Radiat. **16** (2009) 422-7.

[4] CHEN, T.Y., CHEN, Y.T., WANG, C.L., KEMPSON, I.M., LEE, W.K., CHU, Y.S., HWU, Y. MARGARITONDO, G., Full-field microimaging with 8 keV X rays achieves a spatial resolutions better than 20 nm, Opt. Express **19** 21 (2011) 19919-24.

[5] RYAN, C.G., SIDDONS, D.P., KIRKHAM, R., DUNN, P.A., KUCZEWSKI, A., MOORHEAD, G., DE GERONIMO, G., PATERSON, D.J., DE JONGE, M.D., HOUGH, R.M., LINTERN, M.J., HOWARD, D.L., KAPPEN, P. CLEVERLEY, J., The new Maia detector system: Methods for high definition trace element imaging of natural material, (Proc. of 20th International Congress on X ray Optics and Microanalysis) **1221** American Institute of Physics, Karlsruhe (2010) 9-17.

[6] LOMBI, E., DE JONGE, M.D., DONNER, E., RYAN, C.G. PATERSON, D., Trends in hard X ray fluorescence mapping: Environmental applications in the age of fast detectors, Anal. Bioanal. Chem. **400** 6 (2011) 1637-44.

[7] DE JONGE, M.D., HOLZNER, C., BAINES, S.B., TWINING, B.S., IGNATYEV, K., DIAZ, J., HOWARD, D.L., LEGNINI, D., MICELI, A., MCNULTY, I., JACOBSEN, C.J. VOGT, S., Quantitative 3D elemental microtomography of Cyclotella meneghiniana at 400-nm resolution, Proc. Natl. Acad. Sci. U. S. A. **107** 36 (2010) 15676-80.

[8] KEMPSON, I.M. LOMBI, E., Hair analysis as a biomonitor for toxicology, disease and health status, Chem. Soc. Rev. **40** (2011) 3915-40.

[9] KEMPSON, I.M., SKINNER, W.M. KIRKBRIDE, K.P., The occurrence and incorporation of copper and zinc in hair and their potential role as bioindicators: A review, J. Toxicol. Environ. Health **B 10** 8 (2007) 611-22.

[10] MARTIN, R.R., KEMPSON, I.M., NAFTEL, S.J. SKINNER, W.M., Preliminary synchrotron analysis of lead in hair from a lead smelter worker, Chemosphere 58 (2005) 1385-90.

[11] KEMPSON, I.M., SKINNER, W.M. KIRKBRIDE, K.P., Advanced analysis of metal distributions in human hair, Environ. Sci. Technol. **40** (2006) 3423-8.

[12] KEMPSON, I.M. HENRY, D.A., Determination of arsenic poisoning and metabolism in hair by synchrotron radiation: The case of phar lap, Angew. Chem. Int. Edit. **49** 25 (2010) 4237-40.

[13] KEMPSON, I. HENRY, D., Cover Picture: Determination of Arsenic Poisoning and Metabolism in Hair by Synchrotron Radiation: The Case of Phar Lap Angew. Chem. Int. Edit. **25** (2010) 4145.

[14] SMITH, E., KEMPSON, I., JUHASZ, A., WEBER, J., SKINNER, W.M. GRÄFE, M., Localization and speciation of arsenic and trace elements in rice tissues, Chemosphere **76** (2009) 529-35.

[15] MARTIN, R.R., NAFTEL, S.J., NELSON, A.J., FEILEN, A.B. NARVAEZ, A., Synchrotron X ray fluorescence and trace metals in the cementum rings of human teeth, J. Environ. Monit. **6** (2004) 783-6.

SYNCHROTRON RADIATION INDUCED GRAZING INCIDENCE XRF FOR MATERIAL SCIENCE

Ch. STRELI*, D. INGERLE*, P.WOBRAUSCHEK*, F. MEIRER**, G. PEPPONI**
*TU Wien, Atominstitut, Vienna, Austria
**FBK-irst, Via Sommarive, Povo Italy
Email: Streli@ati.ac.at

Abstract

Grazing Incidence X ray Fluorescence Analysis (GIXRF) is a powerful technique for depth-profiling and characterization of thin layers in depths up to a few hundred nanometers. By measurement of fluorescence signals at various incidence angles GIXRF provides information on depth distribution and total dose of the elements in the layers. The technique is very sensitive even in depths of a few nanometers. Therefore GIXRF is used as a complementary technique to Secondary Ion Mass Spectrometry (SIMS) for the characterization of Ultra Shallow Junctions (USJ). SIMS is widely used for depth-profiling of implants in semiconductors, but is lacking accuracy in the first few nanometers of the substrate. Results from Arsenic USJ are presented. Hf based high k dielectric thin films in the thickness range of 2 and 5 nm deposited on a single crystal Si(100) substrate were analyzed using GIXRF. The angle dependent fluorescence signals of the Si substrate and Hf layers collected, were analyzed using a newly developed software package in which both signals are fitted simultaneously to optimize layer thickness determination by a least squares fit of the measured signals to theoretically based data curves. The analysis showed that a good fit requires not only the surface and interfacial roughness to be considered, but also the density values used in the model, thus leading to the idea of a combined GIXRF and X ray Reflectivity (XRR) measurement. The simultaneous acquisition of the fluorescence signal and the reflected X ray beam, which is a measure of the X ray Reflectivity of the surface, has been experimentally tested. The advantage of this combined approach lies in the complementary information provided by these two techniques. GIXRF is clearly very sensitive to elemental gradients in the surface vicinity, whereas X ray Reflectivity unveils the electronic density gradient, and having a much better signal to noise ratio it can provide more precise information about film thickness. Though both techniques can be performed also at lab scale, using synchrotron radiation as excitation sources offers the advantage of high intensity and controlled divergence conditions. Experimental data from measurements at HASYLAB@DESY, Hamburg, Beamline L are presented.

1. INTRODUCTION

GIXRF is a powerful technique for depth-profiling as well as characterization of thin layers on reflecting surfaces in depths up to a few hundred nanometers. By measurement of fluorescence signals at various incidence angles GIXRF provides information on depth distribution and total dose of the elements in the implanted layers. The technique is very sensitive even in depths of a few nanometers, but does not provide unambiguous depth profile information [1]. Therefore it needs a realistic input depth profile for fitting [2], which can be obtained by simulation of the manufacturing process or by other analytical techniques [3].

In XRF the intensity of the wave field is generally assumed to be locally constant *in vacuo* and to be exponentially decreasing in solids. However, in GIXRF the primary beam appears as an evanescent wave field or as a standing wave field with locally dependent electric field fluctuations. The intensity of the fluorescence radiation emitted by atoms which are excited by these fields is directly proportional to the wave field intensity. Therefore the fluorescent signal emitted by a sample refers to the varying field intensity of the standing or evanescent wave field within the sample. Moreover it additionally provides information on the elemental composition of the sample. As the distribution of nodes and antinodes of the standing wave field within the sample is a function of the incident angle of the primary radiation the (consequently angle dependent) fluorescence signal can be used for non-destructive depth profiling of implants. The fluorescence intensity dependence on the incidence angle in the grazing incidence region can be calculated.

2. CHARACTERIZATION OF AS IMPLANTS IN SILICON

As mentioned above GIXRF is very sensitive especially in depths of a few nanometers but does not provide an unambiguous depth profile, it needs a realistic input depth profile for

fitting, which can be obtained by SIMS (Secondary Ion Mass Spectrometry). For SIMS on the other hand implants confined in the first few nanometres of a substrate pose a challenge as this technique suffers uncertainties during an initial transient width correspondent to a depth comparable with the dopant distribution. A software package was developed, which uses the SIMS measurement data to calculate a simulated GIXRF curve and fits the calculated to the measured GIXRF curve, resulting in modified parameters for the SIMS profile. This procedure is repeated until simulated and measured GIXRF curve show good agreement. The outcome is a modified depth profile, containing information from SIMS and GIXRF.

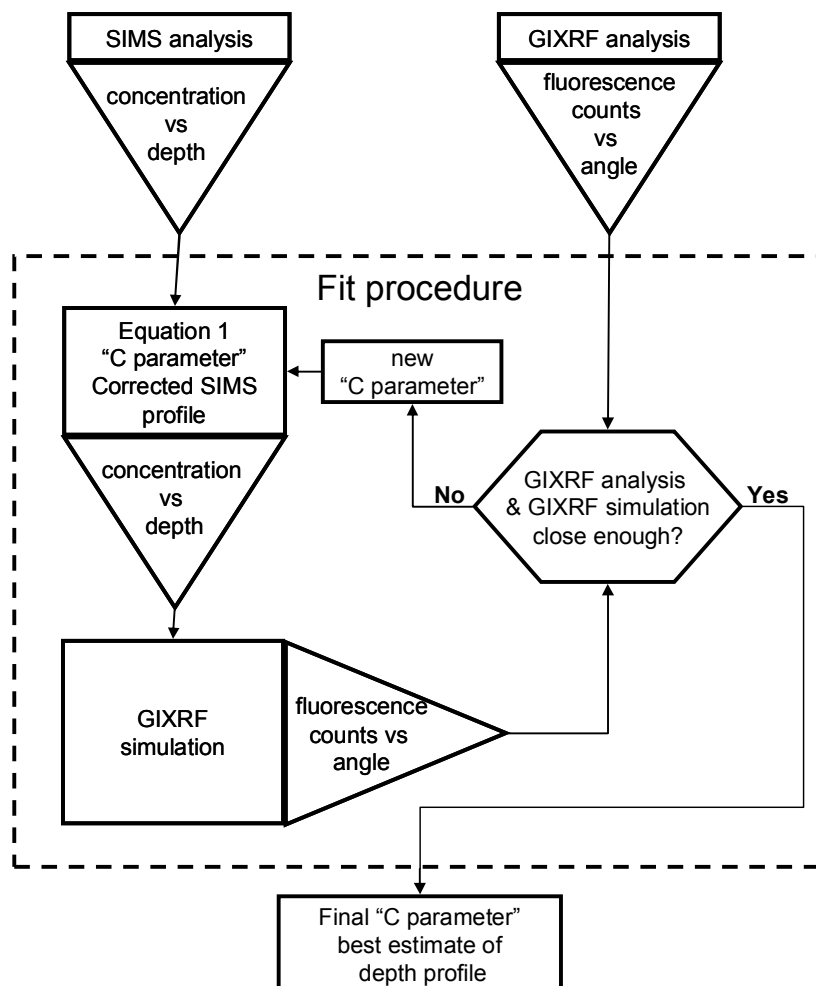In Figure 1 a flow chart depicts the algorithm.

FIG. 1. Flow chart of the fitting procedure

Figures 2 and 3 show measured intensity profiles of Si and As respectively, and a comparison with calculated curves. The curves were calculated and modified for beam divergence using an algorithm developed in Pepponi et al. [3]. By means of the iterative fitting algorithm described above the parameters matching the measured data were determined. The beam divergence was taken into account by convoluting the theoretical data with a Gaussian function. Here, the FWHM value of the Gaussian function was varied until best agreement with the experimental data was reached. The final FWHM value determines the total divergence of the beam being the sum of angular and energy divergence. In the presented case (figure 2) a beam divergence of 0.3mrad was calculated.
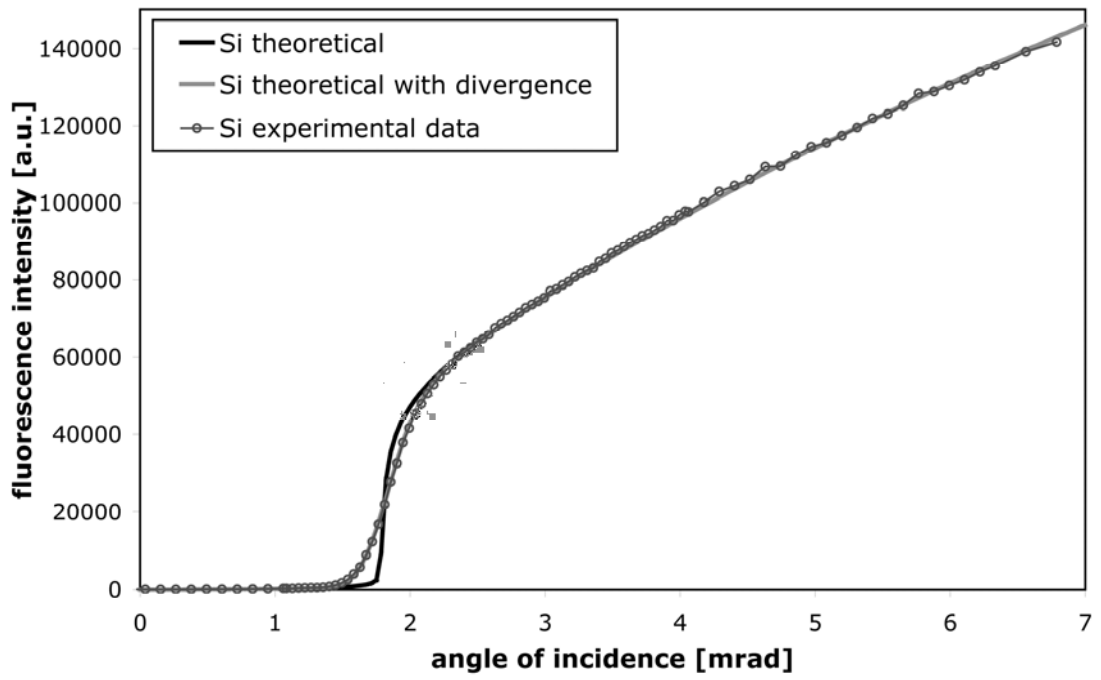
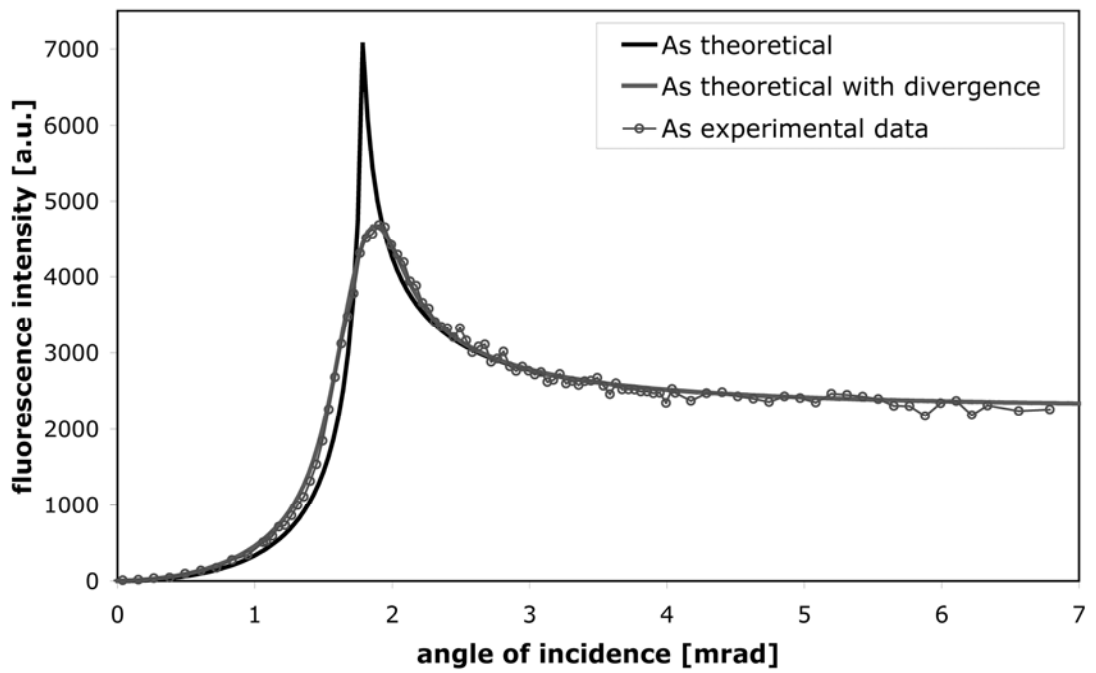*FIG. 2. Si fluorescence data from a Si-wafer with As-implant.*

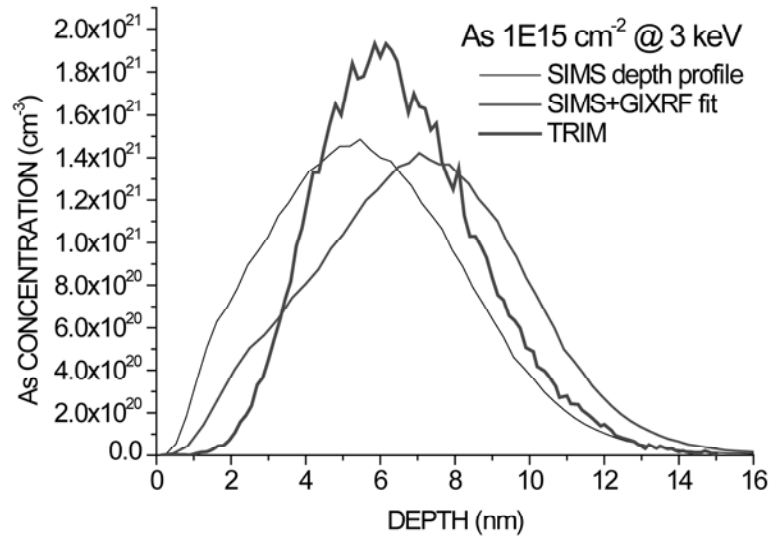*FIG. 3. As fluorescence data from a Si-wafer with As-implant.*

FIG. 4. As fluorescence data from a Si-wafer with As-implant.

Figure 4 shows a SIMS profile, a TRIM simulated profile and the GIXRF profile resulting from the change of the SIMS profile by means of the developed fitting procedure for the GIXRF data. The Figure refers to a 1E15 atoms/cm^2 implant of As atoms at 3keV into Silicon. The GIXRF correction moves the SIMS profile into the depth. This is in agreement with the TRIM simulation.

3. COMBINED APPROACH OF GIXRF+XRR FOR CHARACTERIZATION OF THIN FILMS ON SI WAFER

Motivation: Due to reduction of transistor dimensions to the nm-range, the dielectric constant of SiO_2 is no longer sufficient for reliable and efficient operation. Therefore the semiconductor industry is investigating and evaluating materials with higher dielectric constant (high-K materials) like HfO_2 and has indeed introduced these materials in device manufacture. Fabrication of these materials requires precise control of the film thickness and composition, thus inducing the need for research and development in this area.

GIXRF is a powerful non-destructive technique for depth-profiling and characterization of thin layers in depths up to a few hundred nanometers. GIXRF provides information on depth distribution and total dose of the elements even in depths of a few nanometers. [3-9]

In GIXRF fluorescence signals at various incidence angles of the exciting X ray beam have to be measured. As the penetration of the primary X rays becomes larger as a function of increasing incidence angles, GIXRF provides information on the elements in the layers and substrate material. Typical measurements are performed as automated angle scans across the critical angle of total reflection.

X ray Reflectometry (XRR): XRR is a non-destructive, highly accurate method used to determine thickness and roughness of thin layers, with thicknesses ranging from a few nanometers to some hundred nanometers, as well as the optical properties of the reflecting interfaces. The technique uses the average electron density of a layer and thus cannot provide information on the elementalcomposition. In XRR the specular reflected intensity resulting from an incident X ray beam is measured. Varying the incidence angle shows oscillations in the recorded intensity due to interference effects between reflections from different layer

boundaries, and accordingly the period of these oscillations is directly correlated with the thickness of the layer.

Both techniques use a similar measurement procedure, i.e. increasing the incidence angle and collecting data at various angles. (see Fig. 5) Typically the angular range for GIXRF is smaller than for XRR, but can be extended easily. In both cases part of the produced radiation and thus information is left unused. By combining them the additional information can be used to eliminate the uncertainties of the individual methods.
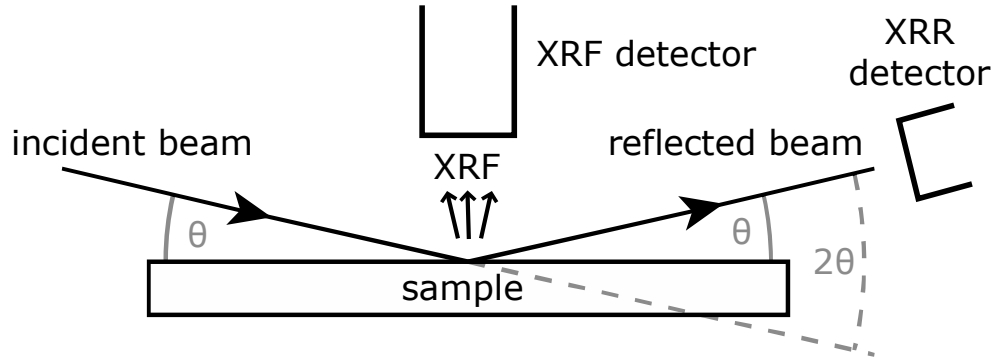

FIG. 5. Setup of combined GIXRF and XRR measurements.

The requirements on the primary beam are similar for both setups: low angular and energy divergence. Typically multilayers or crystals are used in combination with several slits to create a monochromatic and almost parallel beam.
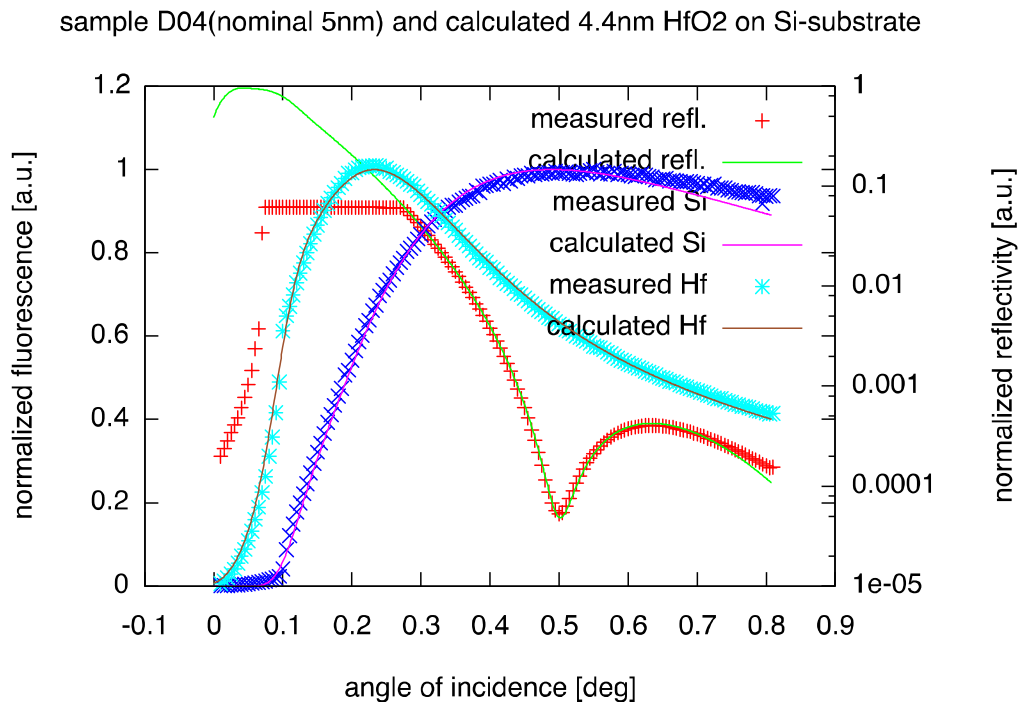

FIG. 6. The use of data from both detectors combines the benefits of both techniques and thus reduces the ambiguities of the fitting-procedure, increasing the confidence in the found solution. The following parameters were used for the calculation: thickness d=4.4nm, density ρ=9.7g/cm³, roughness σ=0.7nm

The evaluation of GIXRF and XRR data involves an iterative process for finding the best fit of measured to calculated data. Calculations are performed with changing parameter sets until the difference (chi-squared) between measured and calculated curves reaches a minimum. Figure 6 shows an example for the result of this procedure.

Each technique used on its own has limitations and ambiguities. Assembling a combined setup is relatively easy and straightforward. The calculations for GIXRF-simulation already include the XRR-calculation. The combination of GIXRF and XRR in one fitting procedure improves the result.

REFERENCES

[1] SCHWENKE, H., KNOTH, J., Depth Profiling in Surfaces Using Total Reflection X ray Fluorescence, Anal. Sci. **11** (1995) 533-537.

[2] WEISBROD, U., GUTSCHKE, R., KNOTH, J., SCHWENKE, H., Total reflection X ray fluorescence spectrometry for quantitative surface and layer analysis, Appl. Phys. A: Mater. Sci. Process. **53** (1991) 449-456.

[3] PEPPONI, G., STRELI C., WOBRAUSCHEK, P., ZOEGER, N, LUENING, K., PIANETTA, P., GIUBERTONI, D., BAROZZI, M., BERSANI, M., Nondestructive dose determination and depth profiling of arsenic ultrashallow junctions with total reflection X ray fluorescence analysis compared to dynamic secondary ion mass spectrometry, Spectrochim. Acta B **59** (2004) 1243-1249.

[4] DE BOER, D.K.G., Glancing-incidence X ray fluorescence of layered materials, Phys. Rev. B: Condens. Matter **44** (1991) 498.

[5] SCHWENKE, H., KNOTH, J., FABRY, L., PAHLKE, S., SCHOLZ, R., FREY, L., Measurement of Shallow Arsenic Impurity Profiles in Semiconductor Silicon Using Time-of-Flight Secondary Ion Mass Spectrometry and Total Reflection X ray Fluorescence Spectrometry, J. Electrochem. Soc. **144** (1997) 3979-3983.

[6] STOEV, K.N., SAKURAI, K., Review on grazing incidence X ray spectrometry and reflectometry, Spectrochim. Acta B **54** (1999) 41-82.

[7] KREGSAMER, P., STRELI, C., WOBRAUSCHEK, P., GATTERBAUER, H., PIANETTTA, P., PALMETSHOFER, L., BREHM, L.L., Synchrotron radiation-excited glancing incidence xrf for depth profile and thin-film analysis of light elements, X ray Spectrom. **28** (1999) 292-296.

[8] WOBRAUSCHEK, W., Total reflection X ray fluorescence analysis - a review, X ray Spectrometry **36** (2007) 289-300.

[9] STRELI, C., WOBRAUSCHEK, P., FABRY, L., PAHLKE, S., COMIN, F., BARRETT, R., PIANETTA, P., LÜNING, K., BECKHOFF, B., Total-Reflection X ray Fluorescence (TXRF) Wafer Analysis, Handbook of Practical X ray Fluorescence Analysis (BECKHOFF, B., KANNGIESSER, B., LANGHOFF, N., WEDELL, R., WOLFF, H., Eds) Springer Verlag, Heidelberg (2006) 498 - 554.

3D STRUCTURE INVESTIGATION OF COLLOIDAL CRYSTAL ARRAYS USING SYNCHROTRON RADIATION X RAY IMAGING

Y.N. FU, H.L. XIE, B. DENG, G.H. DU, T.Q. XIAO
Shanghai Synchrotron Radiation Facility, Shanghai Institute of Applied Physics, Chinese Academy of Science,
Shanghai, People's Republic of China
Email: fuyanan@sinap.ac.cn

Abstract

The colloidal crystal arrays composed of polystyrene (PS) spheres were assembled by gravity sedimentation and membrane filtration method. Computed tomography (CT) together with X ray phase contrast imaging (PCI) technology based on synchrotron radiation (SR) was used to nondestructively characterize the structure of the arrays which had rarely been observed in three dimensions (3D). The imaging parameters were studied based on the image quality to choose the X ray energy of 12keV and the object-to-detector distance of 2cm. The image of every slice in the PS array was reconstructed by conventional filtered back projection algorithm so as to acquire the sphere stacking mode and the 3D volume rendering was obtained from the slice images. By comparing the different parts of slices of the array assembled with sedimentation in a gravitational field, it is seen that the interspaces among the PS spheres upper are larger than the ones below.

1. INTRODUCTION

Colloidal crystal arrays are two-dimensionally (2D) or three-dimensionally (3D) periodic lattices with some arrangement mode of monodisperse colloidal spheres. The colloidal crystal with long-range ordered structure taking on many important and special physical characters has attracted great attention for application in various technical fields [1], such as, photonic band gap crystals [2] and nanosphere lithography [3]. There also has been great interest in the preparation of ordered macroporous materials with the colloidal crystals as templates, used in the fields of catalyst [4], photovoltaic solar cells [5], separation technology [6] and absorption [7].Colloidal crystal arrays have been fabricated by several self-assembled approaches such as gravity sedimentation [8,9], vertical deposition [10,11], solvent evaporation [12,13], physical confinement [14], membrane filtration [15], and the LB method [16]. The majority of these studies were focused on polystyrene (PS) latex particles and silica spheres.

The colloidal crystal prepared by self-assembly method always has defects, such as vacancy, anti-site, and crack in large area. In order to control the structure of colloidal crystal array, including the arrangement mode and defects, and fabricate samples with large area, characterization of the 3D structure and study the self-assembly mechanism are necessary. Kumacheva [17] reveal that the oscillatory shear effect could improve the ordering degree of colloidal crystal assembled by gravity sedimentation, which usually make difficulty in controlling the surface structure and the number of layer of the array. And the arrangement structures induced by this method are multi-crystal, including fcc、bcc、rhcp and disorder stack. Vertical deposition method has attracted much attention due to the controllable number of layer and the short preparing period. Theory [18] and model [19] study both certify the fcc packing structure is usually acquired by this method. For characterizing the 3D structure, Sato [20] fabricated colloidal crystal comprising of fluorescence colloidal spheres with drawing vertical deposition and observed the surface morphology of several single layers along substrate by using fluorescence microscope, certifying the uniform structure in successive 10 layers. Solvent evaporation is generally adopted to prepare 2D colloidal crystal. We brought forward an in-situ solvent evaporation self-assembly method [21] to obtain PS colloidal crystal on the substrate, and discussed its self-assembly process and mechanism by researching the surface morphology from SEM and presented a hypothesis for the process.

But the common characterization methods, such as SEM, optical microscope, spectrophotometer, etc, generally have limitations in showing the 3D sample structure with defects information, meanwhile, not bringing destroy and impact to the samples. Therefore, a lossless and in-situ characterization method is required for learning the 3D structure and self-assembly mechanism of colloidal crystal array. Hard X ray from synchrotron radiation (SR) can penetrate thick samples, so make it possible to image its interior structure in-situ and non-destructively. Moreover, the developed phase contrast imaging (PCI) method based on the better interference quality of SR source could achieve better image contrast due to the sensitivity of light element to the wave phase, solving that the traditional absorption contrast brings low contrast for samples consisted of light element, such as, PS. Combining the PCI and computed tomography (CT) could show the 3D array structure of PS colloidal crystal.

In this paper, the PS colloidal crystal arrays were prepared by gravity sedimentation and membrane filtration, and their 3D structures were in-situ characterized by SR X ray phase contrast CT technology. The proper imaging parameters, X ray energy and object-to-detector distance, were discussed. The projection image, reconstructed slice, and 3D rendering of the self-assembled colloidal crystal array were shown and investigated.

2. EXPERIMENTAL

2.1. Fabrication of PS colloidal crystals

PS sphere emulsion purchased from Baseline Chromtech Research Center was adopted as the raw material with the PS sphere content of 2.5 % w/v and the diameter of 11μm. Before the self-assembly preparation, the emulsion was ultrasonically treated for 2 min to obtain uniform dispersion. For the restrictive field of view for CT experiment, polypropylene capillary with inner diameter less than 700 μm was prepared and the width of substrate is also restricted within this size. For gravity sedimentation method, 2 drops of the dispersion was added into the cleaned capillary, and settled overnight at room temperature to complete the PS spheres sedimentation under gravity and the evaporation of the agent. For membrane filtration, 3 drops of the emulsion were successively dropped on a porous polytetrafluoroethene film substrate and then left to dry the agent.

2.2. SR X ray phase contrast CT

The X ray phase contrast CT experiment was performed at X ray imaging and biomedical application beamline (BL13W1) of Shanghai Synchrotron Radiation Facility (SSRF). The schematic outline of the setup was shown in Fig. 1. The monochromatic X ray with energy of 8-72.5 keV was obtained from SR white beam through Si (111) double-crystal monochromator. The X ray sensitive detector with 2048 pixels×2048 pixels CCD was used to record the X ray transmitting from the fixed colloidal crystal sample which rotated for 180 °. The number of projection images was 900, and two background images were captured between every 10 ° rotation.
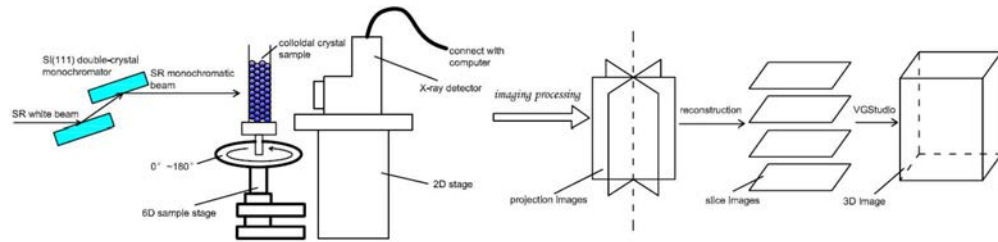
FIG. 1. Schematic outline of SR X ray phase contrast CT.

2.3. Image processing

The background and dark images were used to rectify the projection images, from which the slice images were reconstructed with thickness of 0.37 µm by filtered back projection (FBP) algorithm. Then the slice images were displayed as a 3D image using the software VGStudio.

3. RESULTS AND DISCUSSION

3.1. SR phase contrast imaging

In order to find the proper imaging parameters for SR phase contrast imaging, part of the PS colloidal crystals in capillary were imaged at different X ray energies and for the corresponding exposure time, shown as Fig. 2, which hasn't been rectified by background images. Fig. 2 (a) was snapped at 9 keV for 8s, displaying a little blurred and costing a relatively long exposure time. When the SR X ray energy was raised to 12 keV (Fig. 2 (b)), the image became clearer. As the colloidal crystal was imaged at 15 keV for 4s (Fig. 2 (c)), the contrast between the PS spheres and the background became worse.

Figure 3 reveals the phase contrast images of the PS colloidal crystals at the X ray energy of 12 keV with different object-to-detector distances, respectively, 0 cm, 2 cm, 3 cm, and 4 cm. When the distance is 0 cm (Fig. 3 (a)), the attenuation only contains absorption showing little contrast due to the low density PS sample. As the object-to-detector distance rose, the PS sphere array can be distinguished from the background, as seen in Fig. 3 (b)-(d), in which the phase shift information between the X ray wave and the PS sphere sample was exhibited so as to enhance the image contrast. But the edge enhancement is excessive for the image with the distance of d=3 cm and d=4 cm, compared with Fig. 3 (b).
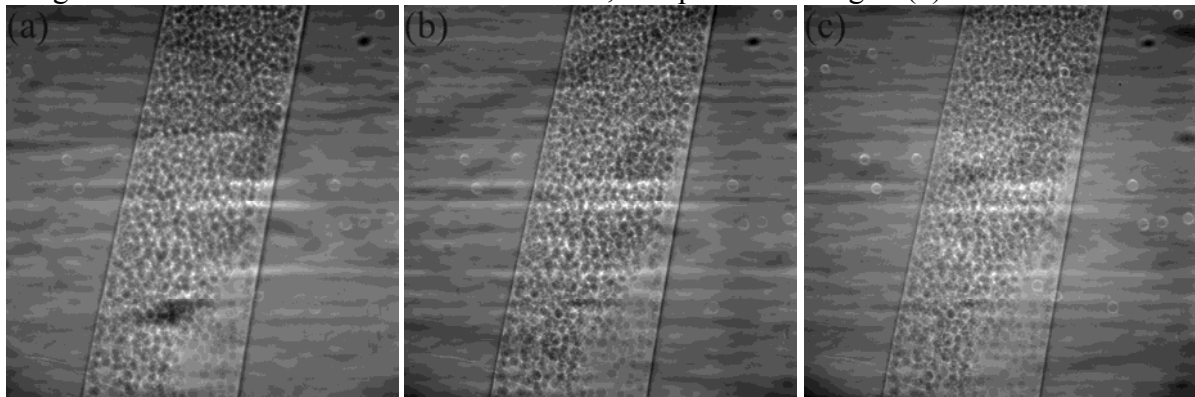

FIG. 2. SR images of PS colloidal crystals at different energies (E) and for the corresponding exposure time (t). (a) E=9 keV, t=8 s; (b) E=12 keV, t=6 s; (c) E=15 keV, t=4 s.
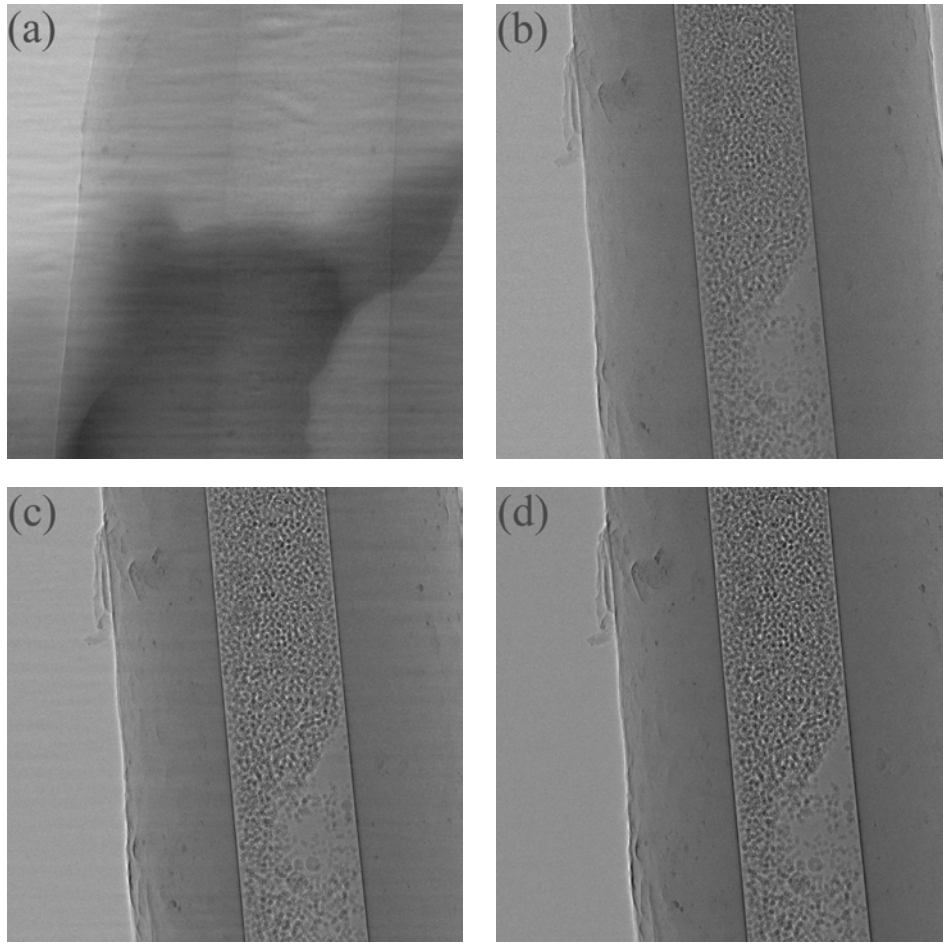
FIG. 3. SR images of PS colloidal crystals at 12keV with different object-to-detector distances (d). (a) d=0 cm; (b) d=2 cm; (c) d=3 cm; (d) d=4 cm. The exposure time is 4 s.

3.2. SR phase contrast CT

Fig. 4 shows the images of PS colloidal crystal fabricated by gravity sedimentation. From the projection image (Fig. 4 (a)) of the top part of the sample, we can see the overlapped PS spheres with some interspaces exhibit a wormlike transmission image. The upper segment of the array has lower stacking density than that below. However, the distinct arrangement mode for different locations can only be identified by numbers of slice images. Corresponding to the two positions shown in Fig. 4 (a), two reconstructed CT slices are given in Fig. (b) and (c), respectively, relevant to the 910 and 1410 layer of the CCD array. The PS spheres in a capillary are discernible with clear edges, through which of several sequential slices the 3D arrangement structure of the colloidal crystal can be confirmed. Due to a quicker sedimentation process in this self-assembly method, the spheres didn't achieve a close-packing structure in the whole sample, only with part of square and hexagonal stacking. Figure 4 (d) presents a 3D volume rendering segment corresponding to the marked part between the two lines in FIG. 4 (a).
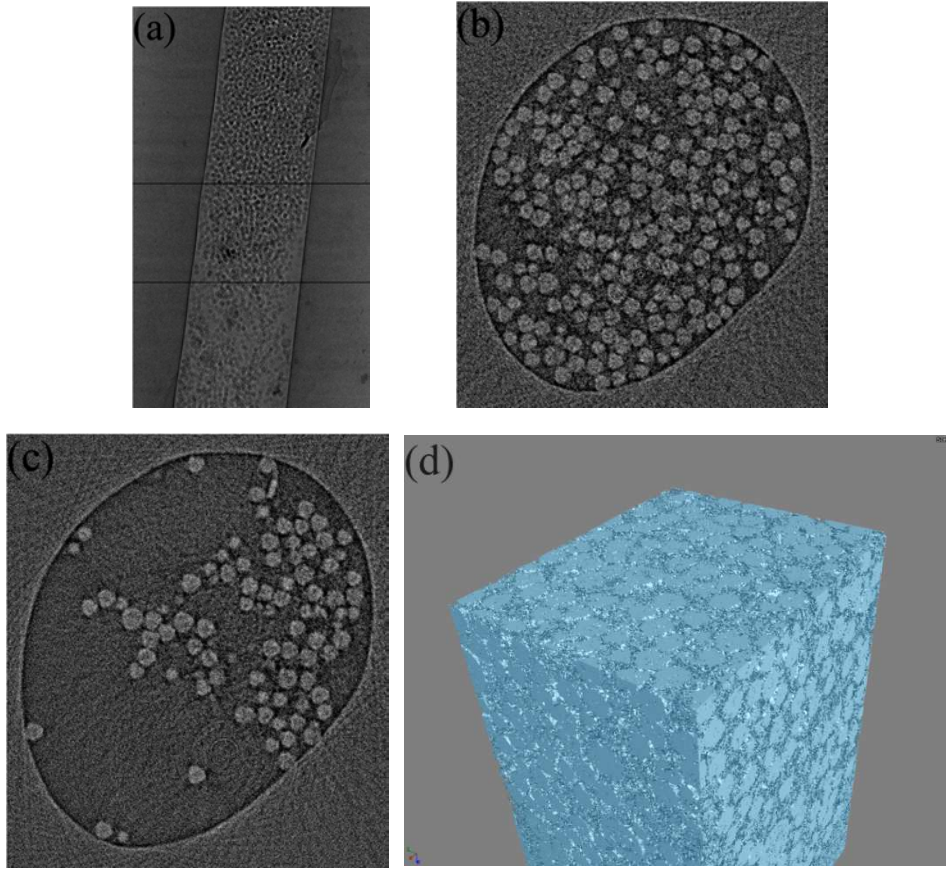
FIG. 4. Images of PS colloidal crystal fabricated by gravity sedimentation: (a) SR projection image; (b) (c) slice image corresponding the position of the two lines in (a); (d) 3D volume rendering segment in the marked part between the two lines in (a).

For the membrane filtration method to assemble a PS colloidal crystal, the SR phase contrast CT results are shown in Fig. 5. Figure 5 (a) was snapped with SR X ray spreading vertically to the substrate, and the PS spheres array take on multi-crystal structure of close-packing square and hexagonal arrangement along the substrate direction with 1-3 layers.
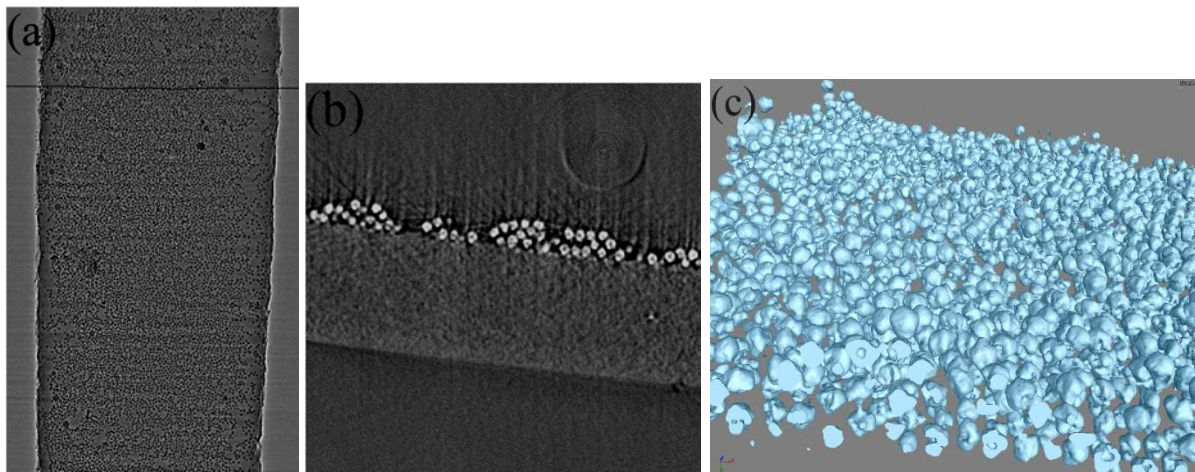

FIG. 5 Images of PS colloidal crystal fabricated by membrane filtration: (a) SR projection image; (b) (c) slice image corresponding to the position of line in (a); (d) 3D volume rendering of the PS colloidal crystal without the substrate.

Fig. 5 (b) is the slice image corresponding to the position of line in (a). We can see the islands of ordered PS sphere distinguished from each other. Figure 5 (c) gives the 3D display of the slices after removing the substrate from the image.

4. CONCLUSIONS

The colloidal crystal arrays composed of PS spheres were fabricated by self-assembly process. The 3D structures of the arrays were non-destructively researched by combing X ray PCI with CT technology based on SR. The imaging parameters were studied based on the image quality to choose the X ray energy of 12keV and the object-to-detector distance of 2cm. The slice image and 3D volume rendering were achieved from the projection images of the PS colloidal crystal by gravity sedimentation and membrane filtration method. Due to a quicker assembly process of sedimentation in field of gravity, the spheres didn't achieve a close-packing structure in the whole sample. For membrane filtration, the reconstructed 3D partly-ordered structure with 1-3 layer spheres was seen directly.

REFERENCES

[1] XIA, Y.N., GATES, B., YIN, Y.D., LU Y., Monodispersed colloidal spheres: old materials with new applications, Adv. Mater. **12** (2000) 693.
[2] LÓPEZ, C., Materials aspects of photonic crystals, Adv. Mater. **15** (2003) 1679.
[3] HULTEEN, J.C., TREICHEL, D.A., SMITH, M.T., DUVAL, M.L., JENSEN, T.R., DUYNE, R.P.V., Nanosphere lithography: size-tunable silver nanoparticle and surface cluster arrays, Phys. Chem. B **103** (1999) 3854.
[4] ZHONG, Z.Y., YIN, Y.D., GATES, B., XIA, Y.N., Preparation of mesoscale hollow spheres of TiO_2 and SnO_2 by templating against crystalline arrays of polystyrene beads, Adv. Mater. **12** (2000) 206.
[5] YI, D.K., KIM, D.Y., Polymer nanosphere lithography: fabrication of an ordered trigonal polymeric nanostructure, Chem. Commun. **8** (2003) 982.
[6] KULINOWSKI, K.M., JIANG, P., VASWANI, H., COLVIN, V.L., Porous metals from colloidal templates, Adv. Mater. **12** (2000) 833.
[7] WATERHOUSE, G.I.N., WATERLAND, M.R., Opal and inverse opal photonic crystals: fabrication and characterization, Polyhedron **26** (2007) 356.
[8] MAYORAL, R., REQUENA, J., MOYA, J.S., LÓPEZ, C., CINTAS, A., MIGUEZ, H., MESEGUER, F., VÁZQUEZ, L., HOLGADO, M., BLANCO, A., 3D Long-range ordering in a SiO2 submicrometer-sphere sintered superstructure, Adv. Mater. **9** (1997) 257.
[9] MIGUEZ, H., MESEGUER, F., LÓPEZ, C., BLANCO, A., MOYA, J.S., REQUENA, J., MIFSUD, A., FORNES, V., Control of the photonic crystal properties of fcc-packed submicrometer SiO_2 spheres by sintering, Adv. Mater. **10** (1998) 480.
[10] YE, Y.H., LEBLANC, F., HACHE, A., TRUONG, V.V., Self-assembling three-dimensional colloidal photonic crystal structure with high crystalline quality, Appl. Phys. Lett. **78** (2001) 52.
[11] JIANG, P., BERTONE, J.F., HWANG, K.S., COLVIN, V.L., Single-crystal colloidal multilayers of controlled thickness, Chem. Mater. **11** (1999) 2132.
[12] DENKOV, N.D., VELEV, O.D., KRALCHEVSKY, P.A., IVANOV, I.B., YOSHIMURA, J.H., NAGAYAMAT, K., Mechanism of formation of two-dimensional crystals from latex particles on substrates, Langmuir **8** (1992) 3183.
[13] LIU, Y.F., WANG, S.P., LEE, J.W., KOTOV, N.A., A floating self-assembly route to

colloidal crystal templates for 3D cell scaffolds, Chem. Mater. **17** (2005) 4918.

[14] PARK, S.H., XIA, Y., Assembly of mesoscale particles over large areas and its application in fabricating tunable optical filters, Langmuir **15** (1999) 266.

[15] DENG, J.G., TAO, X.M., LI, P., XUE, P., ZHANG, Y.H., SUN, X.H., KWAN, K.C., A simple self-assembly method for colloidal photonic crystals with a large area, J. Colloid Interface Sci. **286** (2005) 573.

[16] RECULUSA, S., RAVAINE, S., Colloidal photonic crystals obtained by the Langmuir–Blodgett technique, Appl. Surf. Sci. **246** (2005) 409.

[17] VICKREVA, O., KALININA, O., KUMACHEVA, E., Colloid crystal growth under oscillatory shear, Adv. Mater. **12** (2000) 110.

[18] ZHONG, Y.C., ZHU, S.A., SU, H.M., WANG, H.Z., CHEN, J.M., ZENG, Z.H., CHEN, Y.L., Photonic crystal with diamondlike structure fabricated by holographic lithography, Appl. Phys. Lett. **87** (2005) 06110301.

[19] NORRIS, D.J., ARLINGHAUS, E.G., MENG, L., HEINY, R., SCRIVEN, L.E., Opaline photonic crystals: how does self-assembly work? Adv. Mater. **16** (2004) 1393.

[20] GU, Z.Z., FUJISHIMA, A., SATO, O., Fabrication of high-quality opal films with controllable thickness, Chemistry of Materials, **14** (2002) 760.

[21] FU, Y.N., JIN, Z.G., LIU, G.Q., YIN, Y.X., Self-assembly of polystyrene sphere colloidal crystals by in situ solvent evaporation method, Synthetic Metals, **159** (2009) 1744.

CHARACTERIZATION OF NANOELECTRONICS AND PHOTOVOLTAICS BY GRAZING INCIDENCE X RAY SPECTROMETRY

B. BECKHOFF
Physikalisch-Technische Bundesanstalt, X ray Spectrometry
Berlin, Germany
Email: Burkhard.Beckhoff@PTB.de

Abstract

Information on the elemental composition and binding states of advanced materials can be effectively revealed by X ray Spectrometry (XRS) which is a wide spread non-destructive analytical technique. Reference-free quantification in X ray spectrometry is based on the knowledge of both the instrumental and fundamental atomic parameters. In different configurations, both matrix and trace constituents of a sample or layer thicknesses can be determined, providing lateral or even depth-profiling elemental and species information. The photon energy and the angle of incidence of the exciting radiation determines the probing depth of XRS analysis ranging from a few up to several hundreds of nanometers, thus allowing to probe buried interfaces that can crucially determine the properties of advanced materials.

1. INTRODUCTION

Information on the elemental composition and binding states of advanced materials can be effectively revealed by X ray Spectrometry (XRS) which is a wide spread non-destructive analytical technique. Reference-free quantification in X ray spectrometry is based on the knowledge of both the instrumental and fundamental atomic parameters [1,2]. In different configurations, both matrix and trace constituents of a sample or layer thicknesses can be determined, providing lateral or even depth-profiling elemental information. With respect to very flat samples, such as semiconductor wafers, the photon energy and the angle of incidence of the exciting radiation determines the probing depth of XRS analysis. In total-reflection geometry, i.e. having an angle of incidence smaller than the critical angle of total external reflection, only surface contamination and the surface-near layer of a few nm contributes to the fluorescence spectra. Allowing the angle of incidence to be varied, the probing depth ranges from a few up to several hundreds of nm.

The development of XRS at Physikalisch-Technische Bundesanstalt (PTB), Germany's National Metrology Institute, is dedicated to high-end investigations in the R&D of semiconductor samples requiring reference-free methods, in particular for advanced materials where not enough appropriate reference materials are available. Grazing incidence investigations demonstrated the capability for elemental depth profiling in nanolayers. Reference-free XRS has the potential to contribute to the thickness and composition analysis of novel materials such as high k nanolayers and nearly vertical sidewalls of semiconductor test structures [3]. This technique is also able to contribute to the elemental depth-profiling of ultra-shallow junctions (USJ) [4], i.e. near-surface implantation profiles in different semiconductor wafers, or of matrix element gradients in CIGS based photovoltaics [5]. XRS can be combined with X ray Absorption Fine Structure (XAFS) spectroscopy [6], revealing information on the depth profile of the chemical binding state in deeply buried nanolayers [7] or interfaces with varying chemical state or coordination.

2. X RAY SPECTROMETRY PRINCIPLES AND INSTRUMENTATION

The basic principle of X ray Spectrometry (XRS) is to excite an inner-shell electron by an incident photon, thereby emitting a fluorescence photon. The energy of the emitted photon is specific to each transition of an outer-shell electron filling the inner-shell vacancy. Thus,

the fluorescence radiation emitted is characteristic for the element allowing for its identification. The concentration or mass deposition of an element can be derived from the intensity of its fluorescence radiation. X ray Fluorescence (XRF) analysis has become a well-established non-destructive and multi-elemental analytical technique in various fields of applications ranging, e.g., from materials science and semiconductor characterisation to geology and environmental issues. The quantification [8] of XRF is, in general, based on the use of appropriate reference materials that are as similar as possible to the sample to be analysed, as the interplay of many often unknown instrumental and fundamental atomic parameters determines the measured fluorescence count-rates in a complex manner. However, the continuing development of analytical methods by PTB aims at reference-free XRS [1,2], which is enabled by using well-known X ray sources, detectors and experimental arrangements. Two of PTB's well-characterised beamlines at BESSY II, the plane grating monochromator (PGM) for undulator radiation and the four-crystal monochromator (FCM) for bending magnet radiation, serve as excitation sources for reference-free XRS. Employing calibrated photodiodes in conjunction with monochromatised SR of preselectable intensity, the absolute counting efficiency and response behaviour of the energy-dispersive detectors employed, such as Si(Li) detectors or Silicon Drift Detectors (SDDs), can be determined. With respect to the XRS beam geometry, special attention is paid when defining the angles of incidence and observation as well as the solid angle of detection.
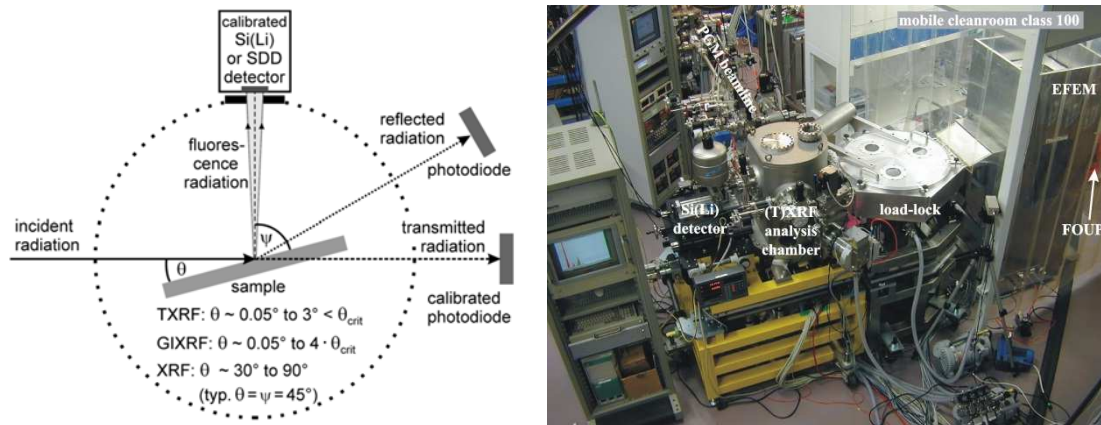

FIG. 1. Reference-free XRS arrangements using monochromatised SR as the incident radiation. A known diaphragm placed in front of the energy-dispersive Si(Li) or SDD detector at a given distance with respect to the sample defines the effective solid angle of detection. The angle of incidence θ is selected in line with the probing depth of interest, θ_{crit} designating the critical angle of external total reflection at a flat sample surface. The observation angle ψ may range from 30° to 90°. To the right the entire UHV arrangement for XRS investigations at 200 mm and 300 mm Si wafers is shown including an EFEM for contamination-free transport.

The methodological XRS development at PTB is dedicated to high-end R&D investigations of semiconductor samples requiring reference-free methods, e.g. for novel materials lacking appropriate reference materials. The use of SR has led to the advanced non-destructive analysis and speciation of both wafer surface contamination and nanolayered materials by reference-free XRS. Figure 1 shows the basic arrangements in reference-free XRS: Total-reflection XRF (TXRF) at very shallow angles of incidence, Grazing-Incidence XRF (GIXRF) at intermediate angles of incidence, and conventional XRF at high angles of incidence. Calibrated photodiodes are used to record the radiant power of the incident, transmitted or reflected beam, thus, providing the instrumental data needed for reference-free quantification in addition to calibrated diaphragms and energy-dispersive detectors. In total-reflection and grazing-incidence applications, the beam profile of the excitation radiation has to be known to determine the effective solid angle of detection [1]. The relative uncertainty of the experimental data in total is about 3 % [1,9]. Besides the instruments' contributions, the relative uncertainties of the XRF analytical results are affected by the atomic fundamental

parameters, some of which only have estimated uncertainties. There are several databases containing atomic fundamental parameters such as transition and Coster-Kronig probabilities, fluorescence yields as well as photoionisation and scattering cross sections. Also dedicated experiments have been aiming at the determination of improved values for reference-free XRS applications. Employing thin foils, the K-shell fluorescence yield of B, C, and Al could be determined at PTB [10,2] by recording fluorescence radiation together with transmission measurements at both the excitation and fluorescence energies. Using the same approach, cross sections of resonant Raman scattering below K edges were derived for Mg, Al, Si [9,11], Ni, and V.
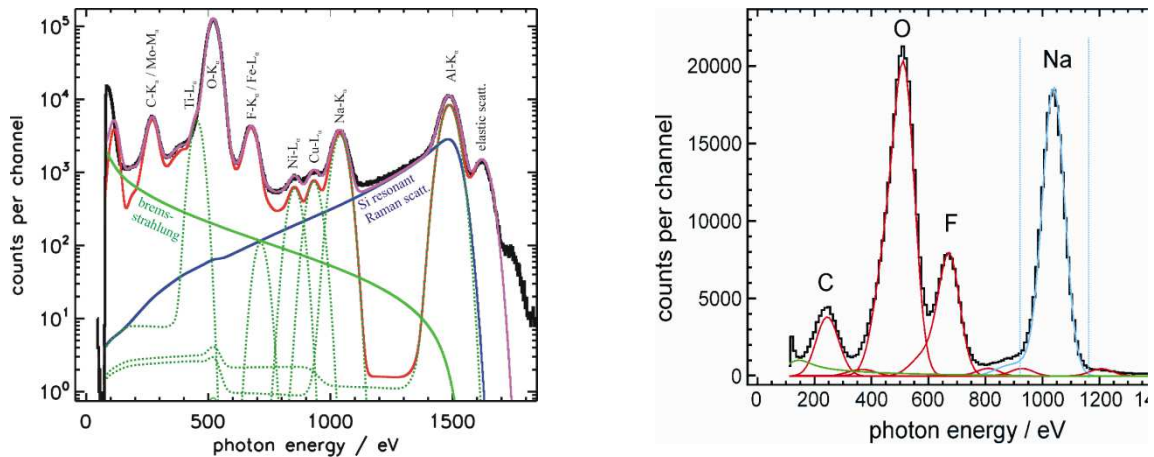

FIG. 2. TXRF spectrum of a spin-coated 200 mm wafer containing 10^{12} cm^{-2} of various transition metals and 10^{13} cm^{-2} of the light elements Na and Al. The spectrum is deconvoluted by means of detector response functions at the energies of fluorescence lines (dotted lines). The background includes bremsstrahlung and resonant Raman scattering contributions. To the right the TXRF spectrum of a Na containing droplet deposition on a Si wafer demonstrates the impact of response tailing on the detection limits of neighbouring elements.

Reference-free XRS can contribute to the assessment of not only surface contamination [1], but also the thickness and composition of micro- and nanolayers [12,13] as well as the composition of bulk specimens, e.g. for space applications [14]. PTB can handle 200 mm and 300 mm silicon wafers as well as smaller semiconductor wafers for industrial applications [15,16]. The instrumentation for large Si wafers is equipped with an Equipment Front End Module (EFEM) [1]. The use of undulator radiation is advantageous for contamination control on semiconductor surfaces as it provides high photon fluxes of polarised radiation for the efficient excitation of light elements in TXRF analysis ensuring corresponding detection limits in the femtogram range [1]. Figure 2 shows a TXRF spectrum recorded from a contaminated Si wafer surface. The fluorescence intensities deduced are used to calculate the respective elemental mass depositions taking into account the incident radiant power, the efficiency of the SDD detector employed, and the effective solid angle of detection without using any reference sample.

Varying the angle of incidence of the exciting radiation with respect to the surface of a flat sample, the X ray standing wave field can also probe sub-surface regions depending on the incident photon energy and angle. Due to the higher information depths of photons as opposed to electrons, elemental depth profiling by GIXRF allows for the analysis of buried nanolayers and interfaces from a few to several hundreds of nanometers below the surface. Reference-free GIXRF can also contribute to the analysis of nearly vertical sidewalls of semiconductor test structures [3] and of ultra-shallow junctions, i.e. near-surface implantation profiles in wafers. Furthermore, information can be revealed by GIXRF about buried

nanolayers with varying chemical states when combined with Near-Edge X ray Absorption Fine Structure (NEXAFS) [7]. High energy resolution in XRS offers two complementary methods for probing transitions between either two different occupied bound states or an occupied bound state and an unoccupied bound or continuum state: X ray emission and absorption spectroscopy, XES and XAFS respectively. Due to the tunability of SR, NEXAFS can be combined with a TXRF analysis to contribute to the speciation of contamination by light or organic compounds [1]. Micro- and nanoparticles deposited on wafer surfaces can be likewise speciated [17]. Even nanolayers mainly composed of light elements have been investigated by TXRF-NEXAFS [18,19].

Crystal spectrometers [20] can be employed in the hard X ray range to determine relevant atomic data such as transition probabilities when a sufficiently high energy resolution is needed. In the soft X ray range, the need for high resolution detection systems is even more pronounced due to the lower absolute differences in characteristic energies. In contrast to Wavelength-Dispersive Systems (WDS), the most interesting features of superconducting energy-dispersive X ray detectors are the broader energetic range that can be detected simultaneously and the higher solid angle of detection. However, most superconducting energy-dispersive X ray detectors show relevant drawbacks with respect to practical applications in XRS such as line splitting, additional lines associated with contact and substrate events [2] and unstable energy scales, restricting them to only very few promising XRS applications (such as XAFS applications) in which a low intensity line, being energetically close to a high intensity line of a relevant matrix element, is of interest. In view of these relevant restrictions, PTB built a WDS based on a spherical grating and a CCD camera. This WDS system has been calibrated and the first XRS experiments were initiated. Its resolving power reaches about 500. The WDS has been used to determine transition [21] and Coster-Kronig probabilities as well as sub-shell fluorescence yields of transition metals, thus contributing to the main advantage of reference-free X ray spectrometry, which is its straightforward applicability to probing novel materials for which no appropriate reference materials exist. In addition, the WDS was employed in complementary XES and XAFS investigations [7] on the speciation of different Ti compounds performed in both the soft and hard X ray ranges.

In order to fulfil the requirements for the characterisation of nanoscaled advanced materials by synchrotron radiation based XRS a dedicated instrumentation has been built by PTB the commissioning of which is going to start. Figure 3 shows the principle arrangement and its sample manipulator.
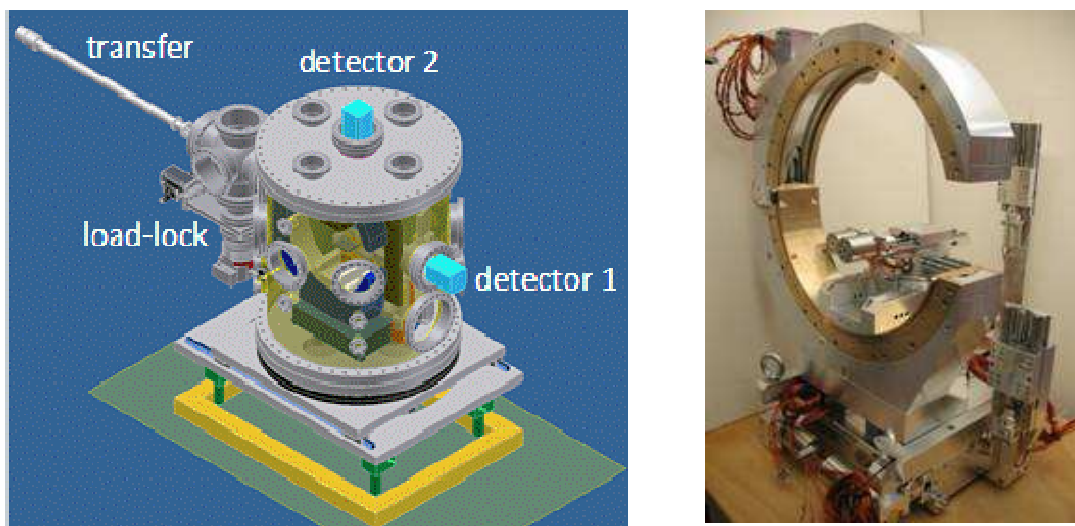
FIG.3. Novel PTB instrumentation for material analysis of nanoscaled samples by means XRS and XAFS at grazing incidence and varying polarisation. Engineering scheme of the entire arrangement as to be operative by March 2011 to the left and picture of the UHV manipulator for 5 mm to 100 mm large sample to the right.

3.   CHARACTERIZATION OF NANOSCALED ADVANCED MATERIALS

The reliable characterisation of nanoscaled advanced materials with respect to the spatial distribution of elemental composition, species and morphology requires for many analytical methodologies calibration sample or reference materials the matrix of which is to be as similar as possible to the specific sample of interest. While several tens of novel nanoscaled material systems are showing up every month the number of available nanoscaled reference materials is rather restricted as shown in a corresponding list at www.nano-refmat.bam.de/en/. The qualification of characterisation methodologies for the reliable calibration of nanoscaled samples originating from either R&D or production processes require the traceability of these methods. In the case of synchrotron radiation based XRS the traceability is based upon source and detector radiometry as well as knowledge on atomic fundamental parameters such as photoelectric and scattering cross sections, fluorescence yields, and transition and Coster-Kronig probabilities.

Fig.4 indicates the possibilities to adapt the probing sensitivity and depth to nanoscaled samples by means of different configurations of synchrotron radiation based XRS. Selected examples of different fields of application will be described in the following to demonstrate the potential to substantially contribute to the analysis and characterisation of nanoscaled materials with respect to elemental composition, speciation, coordination and depth profiling.

The tremendous progress of silicon ULSI technology (ultra large scale integrated circuits) has mainly been made possible by the on-going downsizing of their components such as MOSFETs. This reduction is realized by a downscaling of typical parameters such as gate width and length. However, as these parameters and thus the distance between source and drain decrease, their influence on the distribution of the electrostatic potential under the gate electrode increases. As a result, short-channel effects occur and the threshold voltage of the device rolls off. This can only be avoided if the junction depth of the source and drain diffusion is also scaled down.
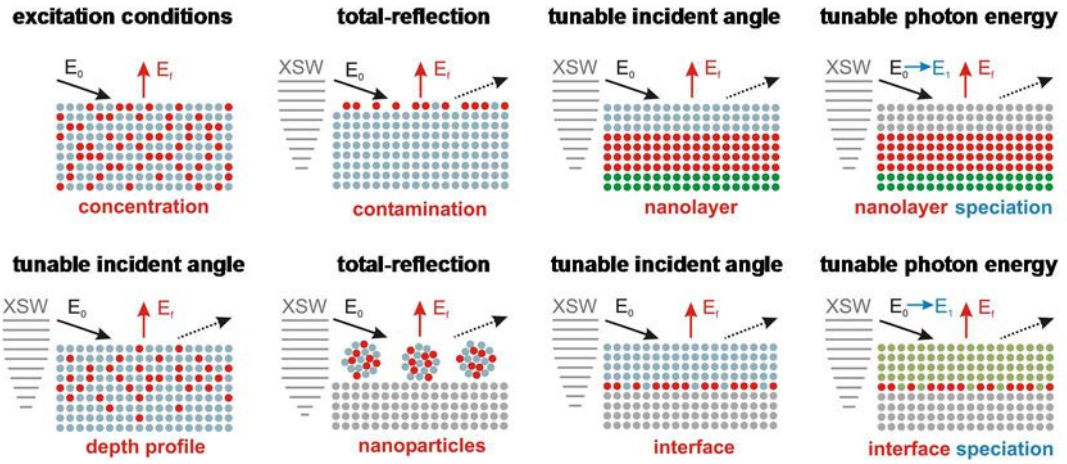
FIG. 4. Tunability of the analytical sensitivity, penetration and information depth by means of appropriate operational parameters of XRS to meet the specific requirements of different nanoscaled sample systems. E_0 indicates the photon energy of excitation radiation, E_f the photon energy of fluorescence radiation and E_1 a photon energy above the adsorption edge of an element of interest. XSW designates the X ray Standing Wave field.

Therefore so-called ultra-shallow junctions (USJ) were introduced for the realization of junction depths in the 20-nm regime and below. Such USJs can be formed by ultra-low energy (ULE) ion implantation of boron, arsenic, and other elements into the silicon followed by a low thermal budget annealing such as a rapid thermal process, e.g., spike or laser annealing to remove lattice damage and electrically activate dopant atoms. These ultra-shallow dopant distributions represent a challenge for secondary ion mass spectrometry (SIMS), the well-established depth profiling technique and method of choice for implantation and diffusion profiles. Uncertainties in the profile as well as the dose determination are mainly caused by transient effects, leading to the so-called transient width corresponding to the depth from 1 to 3 nm to be sputtered before the erosion becomes stationary.

In order to assess and to improve SIMS quantification of USJ a characterization approach using synchrotron radiation-induced GIXRF was developed at PTB in the soft X ray range[4, 22,23]. GIXRF is very sensitive to near-surface layers because in-depth changes of the underlying X ray standing wave (XSW) field intensity are dependent on the angle of incidence θ between wafer surface and the exciting X ray beam. The GIXRF quantification of the elemental depth profile $P_{Imp}(t)$ is based on ab-initio calculations, using the simulated XSW field intensity, all relevant atomic fundamental parameters involved, and an assumed dopant profile. The shape of the assumed profile serves as the fitting parameter and is varied to fit the calculated curves to the measured ones. The physical model used for the description of an implant-induced GIXRF signal is the following: The angle-dependent count rate of the detected boron Kα or the arsenic Lα fluorescence radiation $F_{Imp}(\theta)$ is determined by a geometrical-experimental factor G and the depth integration of the product of an assumed implant profile $P_{Imp}(t)$, the depth-dependent intensity modification of the XSW field $I_{XSW}(t, \theta)$ as well as an absorption correction term for the emitted fluorescence radiation. Fig.5 shows B and As implantation profiles as revealed by GIXRF and SIMS for different implantation energies. Fig. 6 demonstrates the comparability of different analytical methodologies and theoretical calculations for the case of a low energy As UJS sample.
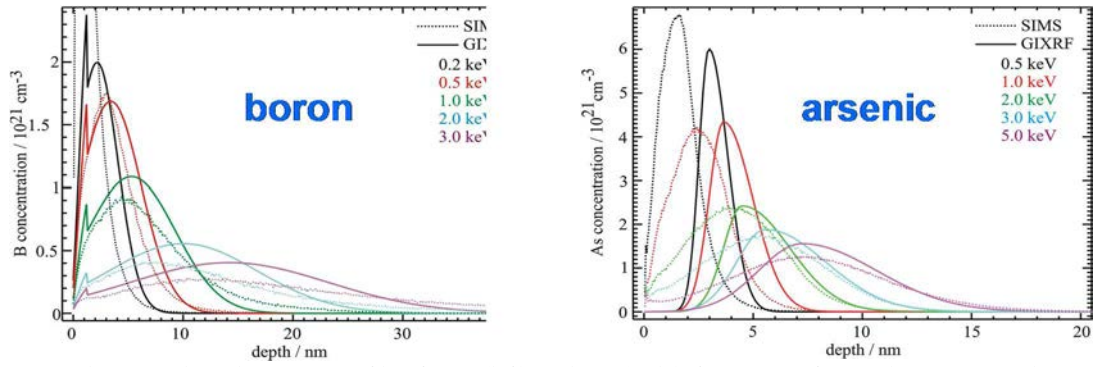
FIG. 5. GIXRF-determined implantation profiles for B (left) and As (right) for USJ wafers with varying implantation energy. Additionally SIMS profiles determined on the same samples are shown (dotted lines). Adapted from [4].
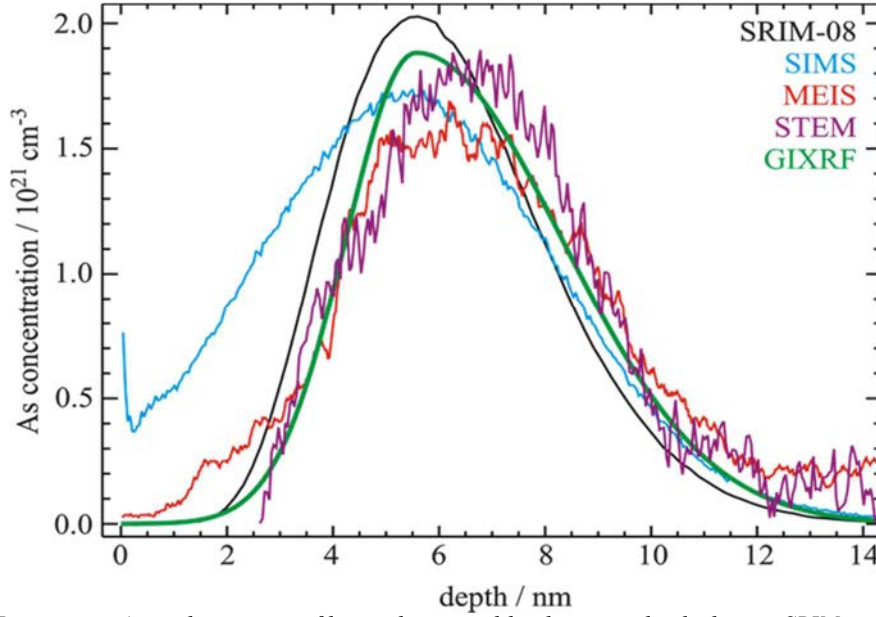

FIG. 6. Low energy As implantation profiles as determined by theroretical calculations SRIM and by SIMS, MEIS, STEM and GIXRF measurements. Adapted from [4].

Interfacial speciation by means of grazing incidence X ray absorption spectrometry addresses characterization needs e.g. in thin film photovoltaic as chemical reactions at the interface and diffusion of impurities into the various layers can modify the electronic properties of the layer stack such as the depth profile of the band structure. Thin-film stacks comprising ZnO and Si films are basic building blocks of various promising thin-film solar cell concepts. In these stacks the electronic quality of the ZnO/Si interfaces critically affects solar cell performance. In case of polycrystalline silicon (poly-Si) films which are formed on ZnO at temperatures above 600 °C the control of the ZnO/Si interface becomes especially crucial. Through the high temperature, chemical reactions at the interface and diffusion of impurities into the various layers may modify the electronic properties of this layer stack that serves as an important ingredient of new types of thin-film solar cells. To study this in detail, a combined TXRF- and GIXRF-NEXAFS approach to characterize the buried ZnO/Si interfaces by means of tunable synchrotron radiation was applied [24]. Fig. 7 shows the corresponding NEXAFS spectra recorded around the Zn-$L_{iii,ii}$ absorption edges just below and above the critical angle of external total-reflection at the a-Si:P/ZnO:O interface for both as deposited and annealed samples. With the help of measured spectra of pure Zn and ZnO specimens the Zn L_{iii} edge energies were derived to be at 1020.5 eV for Zn and 1023.8 eV for ZnO.
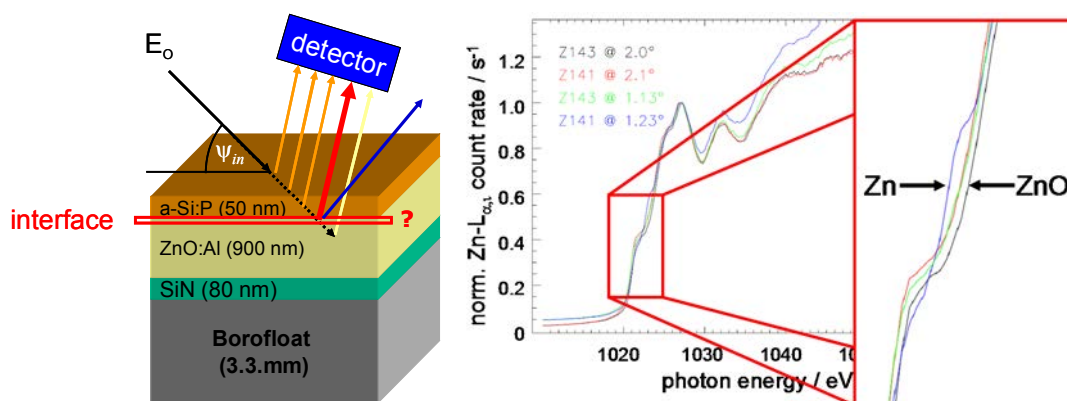
FIG. 7. *Spatial structure of a thin film photovoltaics to the left. TXRF- and GIXRF-NEXAFS spectra from the interfacial layer between a-Si:p and ZnO:Al from the thin silicon photovoltaics to the right. A species depth resolution of only a few nanometers can be associated with TXRF beam conditions. Adapted from [24].*

The formation of a Zn fraction in the ZnO at the ZnO/Si interface would result from a chemical reaction at this interface through annealing. A common assumption is that the oxygen migrates from the zinc to the silicon during annealing, leaving oxygen depleted zinc and forming silicon oxide at the interface.

Reference-free XRS can also reliably derive matrix concentration gradients in thin film solar cells based on chalcopyrites, such as copper indium gallium diselenide (CIGSe). The matrix elemental depth profiles can imply a depth gradient in the band gap and carrier density and thus determines the photovoltaic properties of the solar cell. Reference-free GIXRF is a promising method for non-destructive access to the compositional depth profile of CIGSe absorber layers [5] and high k nanolayers [25-27].

Forward calculations demonstrated that slightly different gradient systems might be distinguished under grazing incidence conditions by angular variations. GIXRF studies have also been performed to probe quantitatively self-assembled monolayers (SAM) [28,29] and nano-scaled structures deposited on a flat sample surfaces [30].

GIXRF-NEXAFS has successfully contributed to the non-destructive speciation of both boron and silicon carbonitride nano-layers [31] as well as buried titanium oxide nano-layers [7]. Currently the X ray absorption fine structure technique is further developed to arrange for a tunable penetration depth while preserving a sufficient information depth when probing deeply buried interfaces of nano-layered systems. The development of this technique involves the application to state-of-the-art thin-layer nanoelectronics deposited on novel substrates [32,33] as well as quantitative fundamental parameter [34] based XRF in comparison to grazing incidence XRF [35] analysis.

4. CONCLUSION

Due to the use of both radiometrically calibrated instrumentation and well-known synchrotron radiation XRS can substantially contribute to the characterisation of elemental mass depositions, depth profiles and compositions of nanoscaled sample systems without the need for any calibration sample or reference materials. In view of the steadily increasing amount and variety of nanoscaled advanced material systems this approach can be expected to substantially contribute to analytical challenges in nanoelectronics, energy storage and conversion.

ACKNOWLEDGMENTS

REFERENCES

[1] BECKHOFF B., FLIEGAUF, R., KOLBE, M., MULLER, M., WESER, J., ULM, G., Reference-free total reflection X ray fluorescence analysis of semiconductor surfaces with synchrotron radiation, Anal. Chem.**79** (2007) 7873-7882.

[2] BECKHOFF B., Reference-free X ray spectrometry based on metrology using synchrotron radiation, J. Anal. At. Spectrom. **23** (2008) 845-853.

[3] HÖNICKE P., BECKHOFF, B., KOLBE, M., LIST, S., CONARD, T., STRUYFF, H., Dept-profile of vertical sidewall nanolayers on structured wafers by grazing incidence X ray fluorescence, Spectrochim. Acta B **63** (2008) 1359-1364.

[4] HÖNICKE P., BECKHOFF, B., KOLBE, M., GIUBERTONI, D., VAN DER BERG, J., PEPPONI, G., Depth profile characterization of ultra shallow junction implants, Anal. Bioanal. Chem. **396** (2010) 2825-2832.

[5] STREECK C., BECKHOFF, B., REINHARDT, F., KOLBE, M., KANNGIESSER, B., KAUFMANN, C.A., SCHOCK, H.W., Elemental depth profiling of Cu(In,Ga)Se$_2$ thin films by reference-free grazing incidence X ray fluorescence analysis, Nucl. Instrum. Meth. B **268** (2010) 277-281.

[6] REINHARDT F., BECKHOFF, B., EBA, H., KANNGIESSER, B., KOLBE, M., MIZUSAWA, M., MUELLER, M., POLLAKOWSKI, B., SAKURAI, K., ULM, G., Evaluation of high-resolution X ray absorption and emission spectroscopy for the chemical speciation of binary Titanium compounds, Anal. Chem. **81** (2009) 1770-1776.

[7] POLLAKOWSKI, B., BECKHOFF, B., REINHARDT, F., BRAUN, S., GAWLITZA, P., Speciation of deeply buried TiO$_x$ nanolayers with grazing-incidence X ray fluorescence combined with a near-edge X ray absorption fine-structure investigation, Phys. Rev. B **77** (2008) 235408.

[8] MANTLER M., et al. Handbook of Practical X ray Fluorescence Analysis, (BECKHOFF, B., KANNGIESSER, B., LANGHOFF, N., WEDELL, R., WOLFF, H. Eds), Springer, (2006), 309.

[9] MÜLLER M., BECKHOFF, B., ULM, G., KANNGIESSER, B., Absolute determination of cross sections for resonant Raman scattering on silicon, Phys. Rev. A **74** (2006) 012702.

[10] BECKHOFF B., ULM, G., Determination of fluorescence yields using monochromatized undulator radiation of high spectral purity and well-known flux, Adv. X ray Anal. **44** (2001) 349-354.

[11] SOKARAS D., MUELLER, M., KOLBE, M., BECKHOFF, B., ZARKADAS, CH., KARYDAS, A.G., Resonant Raman scattering of polarized and unpolarized X ray radiation from Mg, Al and Si, Phys. Rev. A **81** (2010) 012703.

[12] KOLBE M., BECKHOFF, B., KRUMREY, M., ULM, G., Thickness determination for

Cu and Ni nanolayers: Comparison of completely reference-free fundamental parameter-based X ray reflectometry, Spectrochim. Acta B. **60** (2005) 505-510.

[13] BAAKE O., HOFFMANN, P.S., FLEGE, S., ORTNER, H.M., GOTTSCHALK, S., BERKY, W., BALOGH, A.G., ENSINGER, W., BECKHOFF, B., KOLBE, M., GERLACH, M., POLLAKOWSKI, B., WESER, J., ULM, G., HASCHKE, M., BLOKHINA, E., PETER, M., PORTA, D., HECK, Nondestructive characterization of nanoscale layered samples, Anal. Bioanal. Chem. **393** (2008) 623-634.

[14] OWENS A., BECKHOFF, B., FRASER, G., KOLBE, M., KRUMREY, M., MANTERO, A., MANTLER, M., PEACOCK, A., PIA, M.-G., PULLAN, D., SCHNEIDER, U.G., ULM, G., Measuring and interpreting X ray fluorescence from planetary surfaces, Anal. Chem. **80** (2008) 8398-8405.

[15] NUTSCH A., BECKHOFF, B., ALTMANN, R., VAN DEN BERG, J.A., GIUBERTONI, D., HOENICKE, P., BERSANI, M., LEIBOLD, A., MEIRER, F., MUELLER, M., PEPPONI, G., OTTO, M., PETRIK, P., READING, M., PFITZNER, L., RYSSEL, H., Complementary metrology within a European joint laboratory, Solid State Phenom. **145-146** (2009) 97-100.

[16] BECKHOFF B., NUTSCH, A., ALTMANN, R., BORIONETTI, G., PELLO, C., POLIGNANO, M.L., CORDEGONI, D., GRASSO, S., CAZZINI, E., BERSANI, M., LAZZERI, P., GENNARO, S., KOLBE, M., MUELLER, M., KREGSAMER, P., POSCH, F., Highly sensitive detection of inorganic contamination, Solid State Phenom. **145-146** (2009) 101-104.

[17] OSAN J., TÖRÖK, S., BECKHOFF, B., ULM, G., HWANG, H., RO, C.-U., ABETE, C., FUOCO, R., Nitrogen and sulfur compounds in coastal Antarctic fine aerosol particles - an insight using non-destructive X ray microanalytical methods, Atmosph. Environm. **40** (2006) 4691-4702.

[18] HOFFMANN P., BAAKE, O., BECKHOFF, B., ENSINGER, W., FAINER, N., KLEIN, A., KOSINOVA, M., POLLAKOWSKI, B., TRUNOVA, V., ULM, G., WESER, J., Chemical bonding in carbonitride nanolayers, Nucl. Instrum. Meth. A **575** (2007) 78-84.

[19] BAAKE O., HOFFMANN, P.S., KLEIN, A., POLLAKOWSKI, B., BECKHOFF, B., ENSINGER, W., KOSINOVA, M., FAINER, N., SULYAEVA, V.S., TRUNOVA, V., Chemical character of BC_xN_y layers grown by CVD with trimethylamine borane, X ray Spectrom. **38** (2008) 68-73.

[20] LEGALL H., STIEL, H., SCHNUERER, M., PAGELS, M., KANNGIESSER, B., MUELLER, M., BECKHOFF, B., GRIGORIEVA, I., ANTONOV, A., ARKADIEV, V., BJEOUMIKHOV, A., An efficient X ray spectrometer based on thin mosaic crystal films and its application in various fields of X ray spectroscopy, J. Appl. Cryst. **42** (2009) 572-579.

[21] MÜLLER M., BECKHOFF, B., FLIEGAUF, R., KANNGIESSER, B., Nickel L_{III} fluorescence and satellite transition probabilities determined with an alternative methodology for soft-X ray emission spectrometry, Phys. Rev. A **79** (2009) 032503.

[22] PEPPONI G., GIUBERTONI, D., BERSANI, M., MEIRER, F., INGERLE, D., STEINHAUSER, G., STRELI, C., HOENICKE, P., BECKHOFF, B., Grazing incidence X ray fluorescence and secondary ion mass spectrometry combined approach for characterization of ultra shallow arsenic distribution in silicon, J. Vac. Sci. Technol. B **28** (2010) C1C59-64.

[23] GIUBERTONI D., PEPPONI, G., SAHINER, M.A., KELTY, S.P., GENNARO, S., BERSANI, M., KAH, M., KIRKBY, K.J., DOHERTY, R., FOAD, M.A., MEIRER, F., STRELI, C., WOIC, J.C., Deactivation of sub-melt laser annealed arsenic ultra shallow junctions in silicon during subsequent thermal treatment, J. Vac. Sci. Technol. B **28** (2010) C1C84-89.

[24] PAGELS M., REINHARDT, F., POLLAKOSKI, B., ROCZEN, M., BECKER, C., LIPS, K., RECH, B., KANNGIESSER, B., BECKHOFF, B., GIXRF-NEXAFS investigations on buried ZnO/Si interfaces: A first insight in changes of chemical states due to annealing of the specimen, Nucl. Instrum. Meth. B **268** (2010) 370-373.

[25] FLEISCHMANN C., SIONCKE, S., SCHOUTEDEN, K., PAREDIS, K., BECKHOFF, B., MUELLER, M., KOLBE, M., MEURIS, M., VAN HAESENDONCK, C., TEMST, K., VANTOMME, A., Investigations oft he surface composition and atomic structure of ex-situ Sulfur passivated Ge(100), ECS Transactions **25** (2009) 421-432.

[26] SIONCKE S., LIN, H.C., ADELMANN, C., BRAMMERTZ, G., DELABIE, A., CONARD, A., FRANQUET, A., CAYMAX, M., MEURIS, M., STRUYF, H., DE GENDT, S., HEYNS, M., FLEISCHMANN, C., TEMST, K., VANTOMME, A., MUELLER, M., KOLBE, M., BECKHOFF, B., ALD on high mobility channels: engineering the proper gate stack passivation, ECS Transactions **33** (2010) 9-23.

[27] VAN DEN BERG J.A., READING, M.A., PARISINI, A., KOLBE, M., BECKHOFF, B., LADAS, S., FRIED, M., PETRIK, P., BAILEY, P., NOAKES, T., CONARD, T., DE GENDT, S., Ground-based callibration and characterization of the Fermi gamma-ray burst monitor detectors, ECS Transactions **25** (2009) 349-361.

[28] LOMMEL M., REINHARDT, F., HÖNICKE, P., KOLBE, M., MÜLLER, M., BECKHOFF, B., KOLBESEN, B.O., A comparison between self-assembled monolayers on gold and germanium employing grazing incidence X ray absorption spectrometry GIXRF-NEXAFS, ECS Transactions **25** (2009) 433-439.

[29] LOMMEL M., REINHARDT, F., KOLBE, M., BECKHOFF, B., MÜLLER, M., HÖNICKE, P., Characterisation of self-assembled monolayers on germanium surfaces via NEXAFS, ECS Transactions **19** (2009) 227-234.

[30] OSAN J., REINHARDT, F., BECKHOFF, B., PAP, A.E., TÖRÖK, S., Probing patterned wafer structures by means of grazing incidence X ray, ECS Transactions **25** (2009) 441-451.

[31] BAAKE O., HOFFMANN, P.S., KOSINOVA, M.L., KLEIN, A., POLLAKOWSKI, B., BECKHOFF, B., FAINER, N.I., TRUNOVA, V.A., ENSINGER, W., Analytical characterization of BCN films generated by LPCVD with triethylamine borane, Anal. Bioanal. Chem. **398** (2010) 1077-1084.

[32] FLEISCHMANN C., SIONCKE, S., COUET, S., SCHOUTEDEN, K., BECKHOFF, B., MÜLLER, B., HÖNICKE, P., KOLBE, M., VAN HAESENDONCK, C., MEURIS, M., TERNST, K., VANTOMME, A., Towards passivation of Ge(100) surfaces by sulfur adsorption from a $(NH_4)_2S$ solution : a combined NEXAFS, STM and LEED study, J. Electrochem. Soc. **158** (2011) H589-H594.

[33] FLEISCHMANN C., HOUSSA, M., SIONCKE, S., BECKHOFF, B., MÜLLER, M., HÖNICKE, P., MEURIS, M., TERNST, K., VANTOMME, A., Self-affine surface roughness of chemically and thermally cleaned Ge(100) surfaces, J. Electrochem. Soc. **158** (2011) H1090-H1096.

[34] SOKARAS D., KOCHUR, A.G., MÜLLER, M., KOLBE, M., BECKHOFF, B., MANTLER, M., ZARKADAS, CH., ANDRIANIS, M., LAGOYANNIS, A., KARYDAS, A.G., Cascade *L*-shell soft-X ray emission as incident X ray photons are tuned across the $1s$ ionization threshold, Phys. Rev. A **83** (2011) 052511.

[35] UNTERUMSBERGER R., POLLAKOWSKI, B., MÜLLER, M., BECKHOFF, B., Complementary characterization of buried nanolayers by quantitative X ray fluorescence spectrometry under conventional and grazing incidence conditions, Anal. Chem. **83** (2011) **DOI:** 10.1021/ac202074s

IMAGING METHODS TO REVEAL MORPHOLOGIC FEATURES IN MATERIALS

R.H. MENK
Sincrotrone Trieste, Basovizza,
Trieste, Italy
Email: Ralf.Menk@elettra.trieste.it

Abstract

The first century of imaging with X rays was affected by transmission properties of matter putting dose restrictions on certain applications in forensic, material science and cultural heritage and thus limiting the window of visibility. With the advent of phase based X ray imaging techniques in the early 1990's a new dimension in X ray imaging was added. It is anticipated that these techniques certainly have a major impact in near future to reveal morphologic features in materials.

1. INTRODUCTION

X rays offer remarkable analytical capabilities and have been used to reveal morphological features in materials immediately after the discovery by Wilhelm Conrad Roentgen in November 1895 [1] that the intensity of an X ray beam, as measured by the exposure on a film, was related to the relative transmission properties of an object and thus to its linear absorption coefficient μ. Already in February 1896 X ray imaging emerged in diagnostic radiology and material science [2] and still nowadays radiography or CT [3,4] with X rays plays a major role in those fields. Although the window of visibility was constantly enlarged during the last century, the basic principle of image formation remained the absorption of X rays by matter. Optimizing X ray sources, detection devices and image acquisition modalities, the signal to noise ratio (SNR_{out}) in radiographs and CTs have been pushed close to that of Poisson statistics and is subsequently dose limited.

Synchrotron radiation (SR) emerged in the 1980's in the fields of medical imaging research and material science [5-10 and other references] and enabled high-resolution micro tomography, however still based on absorption properties. A new dimension to imaging with X rays was added in the early 1990's utilizing different modalities, which convert phase shifts into measurable intensity variations [11]. Although the base of some of these phase based imaging modalities are tracing back even into the 1960's [12-14] full exploitation started three decades later. In the following the impact of these techniques on cultural heritage (CH), forensics and material science (FS & MS) will be discussed.

2. THEORETICAL PRINCIPLES OF PHASE IMAGING

In order to understand the impact of phase based imaging to reveal morphological features in CH, FS and MS it is useful to discuss its underlying principle of image formation and compare it to that of absorption based imaging. Taking the wave nature of X rays into consideration the propagation of a wave field can be described by the complex index of refraction $n = 1 - \delta - i \cdot \beta$ of a material [15] where $|n-1| \ll 1$ for X rays. The parameters δ and β are called the refractive index decrement and the absorption index, respectively and they correspond to the phase shift and to absorption of the wave. When an X ray wave traverses a sample over a distance z the beam is attenuated by $\mu \cdot z$ and its phase is changed by ϕ given by

$$\mu \cdot z = \left(\frac{4 \cdot \pi}{\lambda}\right) \cdot \int \beta \cdot dz \ and \ \phi = \left(\frac{2 \cdot \pi}{\lambda}\right) \cdot \int \delta \cdot dz = -r_e \cdot \lambda \cdot \int \rho_e(x,y,z) \cdot dz \tag{1}$$

where λ is the wavelength of the X rays, r_e the classical electron radius, ρ_e the electron density and μ is the linear absorption coefficient. If the phase shift depends on the transverse variable $r_\perp$ the wave is refracted by an angle

$$\theta(r_\perp) \approx \frac{\lambda}{2 \cdot \pi} \cdot \nabla_{r_\perp} \cdot \phi(r_\perp)$$

(2)

Applying the Rose criterion [16] in case of absorption imaging utilizing a detection device with matched pixel size and monoenergetic X rays of the energy E_γ it requires an entrance dose $D_{entrance}$ of

$$D_{entrance} = \frac{2 \cdot SNR_{out}^2 \cdot e^{\mu_T \cdot L} \cdot E_\gamma}{w^4 \cdot C_\mu^2 \cdot DQE \cdot \mu_T^2} \cdot \left(\frac{\mu_T}{\rho}\right), C_\mu = \frac{\Delta\mu}{\mu_T} = \frac{(\mu_w - \mu_T)}{\mu_T}$$

(3)

in order to visualize a detail of the size w (density ρ) with a certain SNR_{out} [17]. Here the detail is tough to be embedded in a similar environment of length L defined by its density ρ and its linear absorption coefficient μ_T. Due to the use of monoenergetic X rays equation (3) describes the best case scenario. The DQE is a detector parameter ranging between 0 and 1 that describes how good a certain signal is transmitted through the detection chain [18]. State of the art detectors feature a DQE of about 0.5. Of note is that $(1 - DQE)$ is the useless fraction of dose applied to the sample that does not contribute to the SNR_{out}. C_μ is the object contrast (the normalized difference in the linear absorption coefficients of the detail μ_w and the embedding material μ_T). In the discussed applications C_μ can be very small. Of note is that $D_{entrance}$ scales with the inverse fourth power of the detail size, the inverse square of the contrast and exponential with the sample size L. It is worth to mention that further technical improvements in absorption imaging will yield marginal gains in SNR_{out} for a given $D_{entrance}$ and in fact applications such as absorption-based CT for instance of mummies [19] are already dose limited. In spite of these limitations X ray imaging is still attractive since in principle it allows very fast acquisition (< μs) with high spatial resolution where the length scale extends from some meters to structures on the atomic or molecular level. Therefore a method that overcomes the inherent limitations given by equation (3) is extremely valuable for applications in the discussed fields with X rays.

In the energy regime where the photoelectric effect dominates absorption and above 10 keV δ is $10^3 - 10^4$ times greater than β. For example an organic sample of $L = 50$ μm absorbs at 20 keV X ray energy ($\delta = 3 \cdot 10^{-7}$ and $\beta = 1 \cdot 10^{-10}$) ca. 0.2% of the incident radiation but generates a phase shift of π which can produce complete extinction of the wave in case of interference.

Note, that the phase shift and subsequently the scatter angle (2) is proportional to r_e and hence to the nuclear charge Z_k. This dependency is similar to that of the Compton cross section. The latter, however, is well known to produce little contrast in images when compared to absorption imaging providing much higher contrast since here the cross section is proportional to Z^5. But the expectation of faint images in phase imaging is not justified for three reasons:
- The Compton cross sections is proportional to r_e^2 instead of the much larger factor $r_e\lambda$,
- The phase shift at a given energy is only weakly coupled to absorption through the Kramers - Kronig dispersion relations [20] and

- The interference with the primary wave gives a strong enhancement

In this light phase techniques to overcome dose restrictions are very attractive in CH, FS and MS. However, due to the underlying principle of X ray detection conventional image receptors register only intensities of wave fields and not their phases. Therefore the phase information has to be translated into intensity variations. In the last decade several methods were developed to exploit phase information in this fashion. These methods can be subdivided into four classes:

- monolithic crystal or grating based interferometers, [12-14, 21-24]
- crystal analyzer based imaging methods (ABI)[25-29]
- free propagation based imaging methods (PBI)[30-32]
- a combination of 1 and 2 [33]
- and a combination of 2 and 3 [34]

and they are based on measuring the phase shift ϕ directly, the gradient $\nabla\phi$, or the Laplacian $\nabla^2\phi$ or a combination of $\nabla\phi$ and $\nabla^2\phi$, respectively. Although all four methods can be applied to polychromatic X ray sources the native source is SR, featuring monochromatic and reasonable coherent X ray beams.

In the following only the classes 2 & 3 will be discussed. PBI often also referred as to Phase Contrast or "in line holography" is preferable the discussed research fields because of its simple geometry and relatively simpler technical requirements in operation at least if a detector with sufficiently high *DQE* is utilized. Theoretically, the maximal phase contrast occurs at $Z_{OD} = 1/(2 \cdot \lambda \cdot g)$, where Z_{OD} is the object to detector distance at which the optimal phase contrast can be produced, *g* is the spatial frequency characterizing the object and λ is the X ray wavelength. A problem is that a single PB image features only edge-enhancement and cannot give the whole phase distribution. Many phase retrieval algorithms are proposed and demonstrated for both, plain radiographs [35-37] and PB CT [38].

In ABI, often also referred as to "Schlieren Imaging", "Diffraction Enhanced Imaging (DEI)" [29] or "refraction imaging", absorption, refraction and scattering can be exploited by means of an analyzer crystal placed between the object and the detection device even if interference is not detectable. In this fashion it is possible to convert the angular distribution of refracted beams (equation 2) into intensity variations onto the detector.

Under certain conditions a single image on an arbitrary position of the analyzer's reflectivity curve (RC) is sufficient to extract a phase and an amplitude image [39,40]. If this image is taken on the far slope or on the tail of the RC the direct beam is sufficiently suppressed and only scattered radiation contributes to the image formation. More details of this dark field method can be found in ref [41] and the references therein. From two images taken at the half slopes of the RC an absorption equivalent image and a refraction image, respectively can be extracted (DEI). If three or more images are recorded at different positions of the reflectivity curve, absorption, refraction and scattering effects can be separated [42-47]. The latter are extremely interesting since scattering in the µrad and mrad range correspondent to sub µm length scales and yields information even on the molecular level.

3. PHASE DETECTION TECHNIQUES IN CH, FS AND MS

Both, PBI and ABI are routinely used in MS, CH and FS [49 and the references therein]. To discuss all application beyond the scope here and thus in the following focus will be drawn on some examples in which ABI and PBI has been applied to samples in CH and FS.

Pearls are one of the most sought after gems in the world. They are a mark of distinction, elegance, success, and social standing. Natural pearls contain no nucleus and are extremely expensive. Natural pearls strands will be priced well into $100,000 and beyond. These strands can be found in the mideast (around the Persian Gulf), high-end auction houses, and luxury jewellers. At present pollution and greed have destroyed the ocean's ability to produce pearls and therefore the days of pearl divers who would scour the ocean floors in search of the sea's most valuable treasure are mainly history. Today, all pearls, no matter if fresh water or salt water, are produced through a grafting process made famous by Kokichi Mikimoto (25 January 1858 – 21 September 1954) and perfected by Robert Wan of "Perles de Tahiti" [50]. These pearls are called cultured pearls and subsequently all cultured pearls contain a nucleus. Many Chinese dealers claim to sell natural pearls but refer to cultured pearls. Although this is generally due to translation from Chinese to English, there are more than a few fraudulent dealers coming from China. Therefore it requires a reliable method to distinguish natural pearls from cultured ones. Clearly the need of a seed in cultured pearls gives rise to discrimination but those nuclei might be invisible with normal X ray technology (FIG. 1) and only detectable by destructive methods, which, with respect to the retail price of natural pearls is not a very attractive method or by advanced phase based X ray methods such as ABI. In 2002 antique ear pendants based on pearls that were claimed natural appeared on the German market and raised suspicion to be cultured ones. These were investigated using the ABI system at HASYLAB, which was installed in the frame of the European Phasy project [50]. Utilizing this phase based imaging technology it was possible to reveal the internal morphology of the pearls and to detect the seeds, which have not been visible using X ray absorption previously.
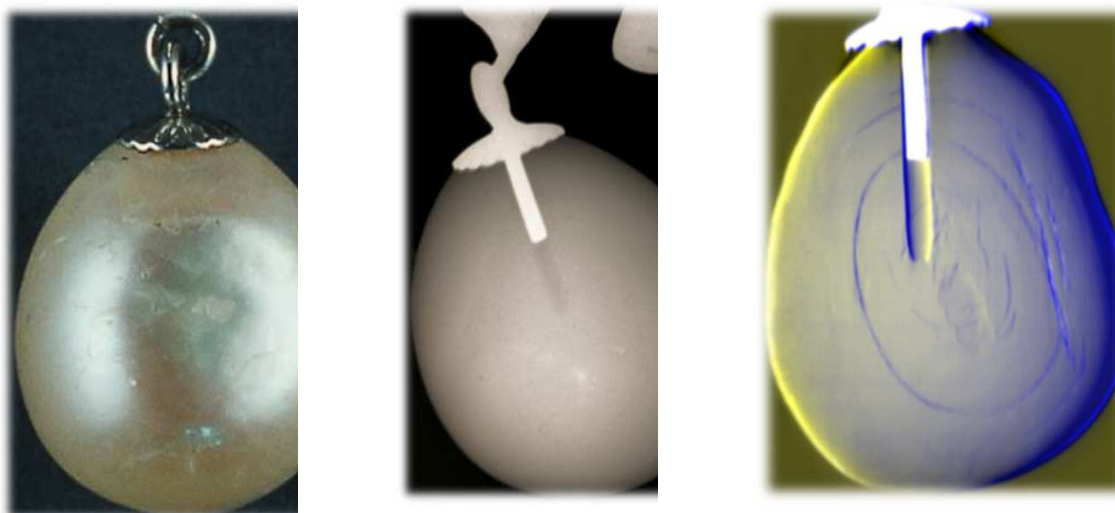

FIG. 1. Left panel: Photography of an antique ear pendant which was claimed to contain a natural pearl. Middle panel: X ray absorption image of the ear pendant and right panel the ABI image recorded at HASYLAB clearly revealing the graft. The ABI image in this case is colour coded in which the absorption properties a displayed as grey value, refraction are the blue channel and scattering are displayed in the red channel.

Once proven that ABI is able to reveal also the subtle differences between nacre and seed, some Keshi pearls that also appeared on the German market at that period have been examined using ABI. Keshi Pearls are natural, irregularly shaped pearls. Since it is impossible

to determine whether an individual Keshi pearl grew serendipitously or as a result of mantle tissue insertion, they are all classified as cultivated/cultured pearls. It is possible to speculate on the likelihood of Keshi pearls from various cultivations based on supply and demand; however there had not been any reliable non-destructive methods to determine if Keshi pearls are natural or cultivated.
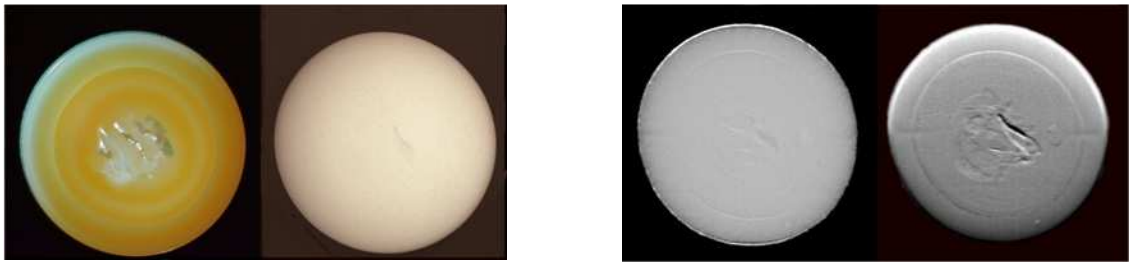

FIG.2. Left panel: Cross section and X ray absorption CT of a cut Keshi pearl. While the seed is clearly visible in the cut pearl it is not in the X ray CT. Right panel: ABI CT of the Keshi pearl showing the reconstructions from the absorption image and the refraction image. Both images reveal the seed, however, the signal to noise ratio in the refraction CT is evidently higher.

ABI was also successfully applied to render partially buried fossils. As an example in Fig.3 a fossil starfish, also known as Furcaster palaeozoicus is depicted which was hold in a 7.5" x 6.0" slab from the Lower Devonian (390 million year old). The artefact was found at the Hunsruck slate of the Rhine region near Bundenbach, Germany. Its arms are 1.2" - 1.6" across, and all-in-all it is a fine example of life in the shallow seas of that time. The central body makes it easy to understand the appellation aster, or star, in Latin. Notice that even the "hydraulic system" by which the starfish moved is preserved in great detail and could be revealed by ABI even in buried layers.
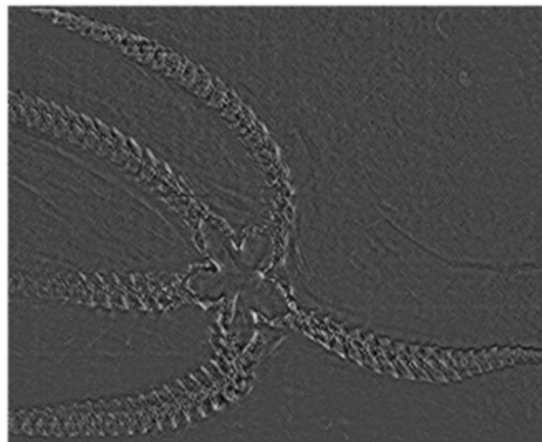

FIG. 3. ABI image of Furcaster palaeozoicus.

Another example of ABI in CH is reported in [52] in which ABI was combined with CT and laminography [53] to visualize thin organic objects in paintings and medieval altarpieces.

Dendrochronological analysis is a well-established wood dating technique that has been demonstrated to be a powerful system in various areas of research [54]. Dendrochronological dating is based on the fact that annual growth rings are influenced by the environmental conditions in which a tree grows. Variables such as rainfall, temperature and humidity result in a pattern in the sequence of ring widths, which is usually similar and distinctive in trees of the same species growing in the same conditions, i.e. the same area. This allows to construct a reference chronology, which is a sequence of ring widths calculated by averaging the values from trees of a known age.

In the field of musical instrument research, dendrochronology has found application in the dating of bowed stringed instruments. The construction of most members of the violin family involves the use of maple (Acer platanoides L.) or sycamore (Acer pseudoplatanus L.) for the back, sides and neck. The front plate is generally assembled with Norway spruce (Picea abies
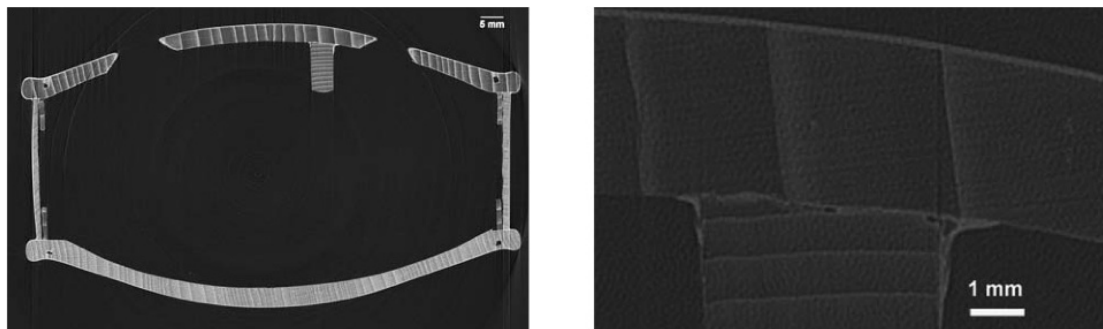

FIG.4. Left panel: Figure 2: Transaxial μCT scan of a student violin taken at SYRMEP. The section has been taken at the middle bout, at the level of the f-holes. Note the bass bar and the linings, which attach the front and back plates to the ribs. Right panel: Detail in full system resolution showing the bass bar and the glue used to attach it to the front plate.

L.), due to the ideal acoustic properties related to the stiffness/weight ratio of the wood from this particular species. Usually only the spruce front plate is used for dendrochronological investigation as neither maple nor sycamore can be used, due mainly to their irreproducible growth characteristics. To date antique bowed string instruments phase contrast X ray CT can valuable non-destructive technique to reveal the subtle differences in the year ring pattern. As an example, an expanded image of the bass bar, parallel to the long axis of the violin and attached to the inner surface of the front plate, shows details of the adhesion with the plate, which cannot be seen with other means (FIG.4).

4. CONCLUSIONS

During the last decade phase based X ray imaging techniques emerged in the field of CH, FS and MS and they are very promising candidates to overcome current dose limitations. Up to now it appears that synchrotron radiation is the native source of X rays for these applications even though they are in principle also applicable to conventional X ray tubes. The real breakthrough of phase based applications can be expected once reasonable priced and suitable compact sources are available [33]. Portable synchrotrons might be a solution here. The final success of phase based imaging in these applications will depend from the technology transfer from the synchrotron work bench towards laboratory environments.

REFERENCES

[1] RÖNTGEN, W.C., Über eine neue Art von Strahlen, Sitzungsberichte der Physikalisch-medizinischen Gesellschaft zu Würzburg **137** (1895).

[2] GOCHT, H., Sekundenaufnahmen mit Röntgenschen Strahlen, Deutsche medizinische Wochenschrift, **22** (1896) 323.

[3] CORMACK, A., J. Appl. Phys. **34** (1963) 2722.

[4] HOUNSFIELD, G.N., Computerized transverse axial scanning (tomography). 1. Description of system, Brit. J. Radiol. **46** 552 (1973) 1016-22.

[5] THOMLINSON, W., Medical applications of synchrotron radiation, Nucl. Instrum. Meth. A **319** (1992) 295–304.

[6] CASTELLI, E., Medical applications planned at Elettra: SYRMEP project Biomedical Applications of Synchrotron Radiation, Proc. Int. School of Physics Enrico Fermi Course CXXVIII (BURATTINI, E., BALERNA, Eds) IOS Press, Amsterdam (1996) 379–394.

[7] CHARVET, A.M., LE BAS, J.F., ELLEAUME, H., SCHULZE, C., SUORTTI, P., SPANNE, P., Medical applications of synchrotron radiation at the ESRF Biomedical Applications of Synchrotron Radiation, Proc. Int. School of Physics Enrico Fermi Course CXXVIII (BURATTINI, E., BALERNA, Eds) IOS Press, Amsterdam (1996) 355–378.

[8] LEWIS, R.A., Medical applications of synchrotron radiation, Phys. Med. Biol. **42** (1997) 1213–1243.

[9] ANDO, M., HYODO, K., NISHIMURA, K., OHTSULA, S., The medical application programme using AR & PF ring at KEK, Phys. Med. **13** (1997) 1–6.

[10] ARFELLI, F., Synchrotron light and imaging systems for medical radiology, Nucl. Instrum. Meth. A **454** (2000) 11–25.

[11] FITZGERALD, R., Phase sensitive X ray imaging, Phys. Today **53** (2000) 23.

[12] BONSE, H., HART, M., Appl. Phys. Lett. **6** (1965) 155.

[13] ANDO, M., HOSOYA, S., in Proc. Interat. Conf. of X ray Optics and Microanalysis, Tokyo (1972) 63.

[14] FÖRSTER, E., GÖTZ, K., ZAUNSEIL, P., Kristall und Technik **15** (1980) 973.

[15] JAMES, R.W., The optical principles of the diffraction of X rays, Chap. 4 Bell & Sons, London (1962).

[16] ROSE, A., in Advances in Electronics (MARTON, L., Ed.) Vol. **1**, New York (1948) 131–166.

[17] MENK, R.H., ARFELLI, F., Biomedical Applications of Particle Detectors, IEEE short course notes, IEEE, NSS/MIC, Rome (2004).

[18] MENK, R.H., THOMLINSON, W., GMÜR, N., ZHONG, Z., CHAPMAN, D., ARFELLI, F., DIX, W.R., GRAEFF, W., LOHMANN, M., ILLING, G., SCHILDWÄCHTER, L., REIME, B., KUPPER, W., HAMM, C., GIACOMINI, J.C., GORDON, H.J., RUBENSTEIN, E., DERVAN, J., BESCH, H.J., WALENTA, A.H., The concept of spatial frequency depending DGE and its application to a comparison of two detectors used in transvenous coronary angiography, Nucl. Instr. and Meth. A **398** (1997) 351-367.

[19] MURPHY, W.A.J., NEDDEN D., GOSTNER, P., KNAPP, R., RECHEIS, W., SEIDLER, H., The iceman: Discovery and imaging. Radiology **226** (2003) 614-629.

[20] TAKEDA, T., Phase contrast and fluorescent X ray imaging for biomedical applications, Nucl. Instrum. Meth. A **548** (2005) 38-46.

[21] KRONIG, R.L., KRAMERS, H.A., Zur Theorie der Absorption und Dispersion in den Röntgenspektren- Zeitschrift für Physik A 48 (1928) 174-179.

[22] MOMOSE, A., Nucl. Instrum. Meth. A **353** (1995) 622.

[23] FUJIMOTO, H., GIOVANNI, M., NAKAYAMA, K., Light bounces in two-beam scanning laser interferometers, Jpn. J. Appl. Phys. 1, regular papers, short notes and review papers **39** 5A (2000) 2870-2875.

[24] TAKEDA, T., MOMOSE, A., HIRANO, K., HARAOKA, S., WATANABE, T., ITAI, Y., Human carcinoma: Early experience with phase-contrast X ray CT with synchrotron radiation – Comparative specimen study with optical microscopy radiology **214** (2000) 298-301.

[25] PFEIFFER F., WEITKAMP, T., BUNK, O., DAVID, C., Nature Physics **2** (2006) 258-261.

[26] SOMENKOV, V.A., TKALICH, A.K., SHIL'SHTEIN, Sov. Phys.-Tech.Phys **36** (1991), 1309.

[27] DAVIS, T.J., GAO, D., GUREYEV, T.E., STEVENSON, A.W., WILKINS, S.W., Phase-contrast imaging of weakly absorbing materials using hard X rays, Nature **373** (1995) 595-598.

[28] GAO, D., TIMOTHY, J.D., WILKINS, S.W., X ray phase-contrast imaging study of voids and fibres in a polymer matrix, Aust. J. Phys. **48** (1995) 103-112.

[29] INGAL, V.N., BELIAECSKAYA, E.A., X ray plane-wave topography observation of the phase contrast from a non-crystalline object, J. Phys. D **28** (1995) 2314.

[30] CHAPMAN, L.D., THOMLINSON, W., JOHNSTON, R.E., WASHBURN, D., PISANO, E., GMÜR, N., ZHONG, Z., MENK, R., ARFELLI, F., SAYERS, D., Phys. Med. Biol. **42** (1997) 2015.

[31] WILKINS, S.W., GUREYEV, T.E., GAO, D., POGANY A., STEVENSON, A.W., Phase-contrast imaging using polychromatic hard X rays, Nature **384** (1996) 335-338.

[32] SNIGIREV A., SNIGIREVA, I., KOHN, V., KUZNETSOV, S., SCHELOKOV, I., On the possibility of X ray phase contrast microimaging by coherent high-energy synchrotron radiation, Rev. Sci. Instrum. **66** (1995) 5486.

[33] CLOETENS, P., BARRETT, R., BARUCHEL, J., GUIGAY, J.-P., SCHLENKER, M., Phase objects in synchrotron radiation hard X ray imaging, J. Phys. D Appl. Phys. **29** (1996) 133.

[34] PFEIFFER, F., WEITKAMP, T., BUNK, O., DAVID, C., Phase retrieval and differential phase-contrast imaging with low-brilliance X ray sources, Nature Physics **2** (2006) 258-261.

[35] COAN, P., PAGOT, E., FIEDLER, S., CLOETENS, P., BARUCHEL, J., BRAVIN, A., Phase contrast imaging combining free propagation and Bragg diffraction, J. Synchrotron Radiat. **12** (2005) 241-245.

[36] FIENUP J.R., Phase retrieval algorithms: a comparison, Appl. Opt. **21** (1982) 2758-2769.

[37] GUREYEV, T.E., Composite techniques for phase retrieval in the Fresnel region, Opt. Commun. **220** (2003) 49-58.

[38] NAKAJIMA, N., Improvement of resolution for phase retrieval by use of a scanning slit, Appl. Opt. **43** (2004) 1710-1718.

[39] BRONNIKOV, A.V., Theory of quantitative phase-contrast computed tomography, J. Opt. Soc. Am. A **19** (2002) 472-480.

[40] NESTERETS, Y.I., GUREYEV, T.E., PAGANIN, D., PAVLOV, K.M., WILKINS, S.W., Quantitative diffraction-enhanced X ray imaging of weak objects, J. Phys. D Appl. Phys. **37** (2004) 1262.

[41] PAGANIN, D., GUREYEV, T.E., PAVLOV, K.M., LEWIS, R.A., KITCHEN, M., Phase retrieval using coherent imaging systems with linear transfer functions, Opt. Commun. **234** (2004) 87-105.

[42] ANDO, M., HASHIMOTO, E., HASHIZUME, H., HYODO, K., INOUE, H., KUNISADA, T., MAKSIMENKO, A., MORI, K., RUEBNSTEIN, E., ROBERSON, J., SHIMAO, D., SUGIYAMA, H., TAKEDA, K., TOYOFUKU, F., UENO, E., UMETANI, K., WADA, H., PATTANASIRIWISAWA, W., Clinical step onward with X ray dark-field imaging and perspective view of medical applications of synchrotron radiation in Japan, Nucl. Instrum. Meth. A **548** (2005) 1-16.

[43] ARFELLI, F., MENK, R.H., BESCH, H.J., RIGON, L., PLOTHOW-BESCH, H., Contrast improvement with diffraction enhanced imaging for scattering materials, Proc. 2002 IEEE Int. Symp. Biomedical Imaging (2002) 133.

[44] RIGON, L., BESCH, H.-J., ARFELLI, F., MENK, R.-H., HEITNER, G., PLOTHOW-BESCH, H., A new DEI algorithm capable of investigating sub-pixel structures, J. Phys. D: Appl. Phys. **36** (2003) A107–A112.

[45] PAGOT, E., CLOETENS, P., FIEDLER, S., BRAVIN, A., COAN, P., BARUCHEL, J., HARTWIG, J., THOMLINSON, W., A method to extract quantitative information in analyzer-based X ray phase contrast imaging, App. Physics Lett. **82** 20 (2003) 3421-3423.

[46] WERNICK, M.N., WIRJADI, O., CHAPMAN, D., OLTULU, O., ZHONG, Z., YONGYI, Y., Preliminary investigation of a multiple-image radiography method, Proc. of 2002 IEEE ISBI (2002) 129.

[47] WERNICK, M.N., WIRJADI, O., CHAPMAN, D., ZHONG, Z., GALATSANOS, N.P., YONGYI, Y., BRANKOV, J.G., OLTULU, O., ANASTASIO, M.A., MUEHLEMAN, C., Multiple-image radiography, Phys. Med. Biol. **48** (2003) 3875.

[48] OLTULU, O., ZHONG, Z., HASNAH, M., WERNICK, M.N., CHAPMAN, D., Extraction of extinction, refraction and absorption properties in diffraction enhanced imaging, J. Phys. D Appl. Phys. **36** (2003) 2152.

[49] BARUCHEL, J., BUFFIERE, J.-Y., MAIRE, E., X ray tomography in material science, Hermes Science (2000) 204 pp.

[50] http://www.perlesdetahiti.net/site/en/home.html

[51] http://cordis.europa.eu/search/index.cfm?fuseaction=proj.document&PJ_RCN=5216783

[52] KRUG, K., PORRA, L., COAN, P., WALLERT, A., DIK, J., COERDT, A., BRAVIN, A., ELYYAN, M., REISCHIG, P., HELFEN, L., BAUMBACH, T., Relics in medieval altarpieces? Combining X ray tomographic, laminographic and phase-contrast imaging to visualize thin organic objects in paintings, J. Synchrotron Radiat. **15** (2008) 55-61.

[53] HELFEN, L., BAUMBACH, T., PERNOT, P., CLOETENS, P., STANZICK, H., SCHLADITZ, K., BANHART, J., Investigation of pore initiation in metal foams by synchrotron-radiation tomography, Appl. Phys. Lett **86** (2005) 071915.

[54] RIGON, L., VALLAZZA, E., ARFELLI, F., LONGO, R., DREOSSI, D., BERGMASCHI, A., SCHMITT, B., CHEN, R., ASSUNTA COVA, M., PERABO, R., FIORAVANTI, M., MANCINI, L., MENK, R.H., SODINI, N., TROMBA, G., ZANINI, F., Synchrotron-radiation microtomography for the non-destructive structural evaluation of bowed stringed instruments, e-Preserv. Sci. **7** (2010) 71-77.

INDUS SYNCHROTRON SOURCE AND MATERIALS SCIENCE RESEARCH

S.K. DEB
Indus Synchrotrons Utilization Division, Raja Ramanna Centre for Advanced Technology
Indore, India
Email: skdeb@rrcat.gov.in

Abstract

Indus Synchrotron Radiation complex at Raja Ramanna Centre for Advanced Technology at Indore, India houses two synchrotron radiation sources: Indus-1 and Indus-2 respectively. Indus-1 is a 450 MeV source emitting in VUV and soft X ray region and operating at 100 mA since 1990 and Indus-2, designed for 2.5 GeV, 300 mA and is currently operating at 2 GeV and 100 mA. Indus-1 has five operational beamlines while Indus-2 has six beamlines installed and operational. Two more beamlines namely 'Grazing Incidence X ray Scattering (GIXS)' and 'Protein crystallography' beamlines are at advanced stage of installation. Several materials research related problems have been investigated using the reflectivity and photo-electron spectroscopy beamlines at Indus-1 and also the beamlines at Indus-2. Here we will report a few of our studies like, probing porosity at buried interfaces in B_4C-on-Fe bilayers using soft X ray reflectivity beamline, valance electronic structure of $CeAg_2Ge_2$ intermetallic compounds by resonant photoemission studies using the angle integrated PES beamline and also electronic band structure mapping along Γ-Z direction on $CeAg_2Ge_2$ single crystal using the angle resolved PES beamline. The Indus-2 beamlines are being used by users from Universities, IIT's and other National laboratories and we will report results of few works carried out using some of the beamlines of Indus-2.

1. INTRODUCTION

Synchrotron Radiation (SR) is emitted by charged particles travelling in curved trajectories at relativistic speed. This radiation is emitted in a direction tangential to the electron trajectory with high degree of collimation. The intensity and wavelength region of emitted radiation can be modified in modern day SR sources by inclusion of 'insertion devices' which can be 'undulator' or 'wiggler'. The SR has emerged as a highly important tool for basic and applied research in physics, chemistry, biology and industry, because of its unique characteristics, namely the broad spectral range from IR to hard X rays, small beam size and small divergence resulting in high brightness. In addition it also possesses pulsed nature with short pulse duration and high degree of polarization. More than 80 SR sources are currently operating across the world and apart from basic and applied research it is also being used as an important analytical tool in the field of materials science, energy research, biological and environmental sciences, microelectronics etc. The non-destructive character of this technique enables in-depth element specific compositional and chemical state analysis resulting in its application in novel materials research, forensic science and research related to cultural heritage.

2. INDUS SYNCHROTRON SOURCES

In India two dedicated synchrotron sources Indus-1 and Indus-2 have been built at the Raja Ramanna Centre for Advanced Technology, Indore. Indus-1 is a 450 MeV source with critical wavelength of 61Å and is a soft X ray/Vacuum ultraviolet (VUV) source with designed current of 100 mA and lifetime of 1.8 hrs. This was commissioned and made available for beamline installation by early 2000[1]. On the other hand Indus-2 is a 2.5 GeV electron energy source with critical wavelength of $\approx$ 2 Å. The designed beam current is 300 mA with a lifetime of $\approx$ 24 hrs [2]. The first light was observed in Dec. 2005 and currently being operated at 2 GeV and 100 mA since 2010 and the beam lifetime at present is $\approx$19 hrs. Five beamlines have been installed and currently operational in Indus-1 and are being used by users from universities and different institutions. A total of 22 "bending magnet (BM)" beamlines and five "Insertion device (ID)" beamlines can be installed in Indus-2 and currently

six BM beamlines have been installed and are operational. All these beamlines in Indus-1 and Indus-2 are continuously being upgraded and are currently being used primarily for materials science research.

3.   INDUS-1

The beamlines currently operational in Indus-1 are shown below in Table-1 with their broad specifications [3]. Two beamlines BL-1 and BL-5 are for carrying out gas phase VUV spectroscopy and the beamlines BL-2, BL-3 and BL-4 are for condensed matter studies. The Angle Integrated (AIPES) [4] and Angle Resolved Photo electron spectroscopy (ARPES) [5] beamlines are for valance band study of solids while the Soft X ray (SX)/VUV beamline is primarily for reflectivity studies from thin films and multilayer films. These three beamlines have been extensively used for condensed matter research.

TABLE 1. BEAMLINES IN INDUS-1 WITH BROAD SPECIFICATIONS

	Beamline	Range	Monochromator	Resolution ($\lambda/\Delta\lambda$)	Experimental station
BL-1	High Resolution VUV	400 - 2500 Å	6.65 m Off-plane Eagle mount	~ 70,000	Absorption cell with High temperature
BL-2	Angle Integrated PES	60 – 1600 Å	2.6 m TGM	~ 600	EA125 Omnicron 180° HSA
BL-3	Angle Resolved PES	40 – 1000 Å	1.4 m TGM	~ 400	AR-65 AR HAS.(±1°)
BL-4	SX-VUV Reflectivity	40 –1000 Å	1.4 m TGM with three gratings	~ 400	Reflectometer, TOF mass spectrometer
BL-5	Photophysics	500 - 2500 Å	1 m Seya-Namoika	~ 1000	Gas absorption cell

3.1. INDUS-1 utilization

We now present a few works carried out using these beamlines which are operational in Indus-1. X ray reflectivity (XRR) is an important non-destructive tool to characterize thin film parameters like the thickness, surface and interface roughness, interface width and also material optical constants. In addition high penetrating power allows one to study buried layers. The technique becomes more powerful with tunability of the SR wavelength which allows measurement of resonant soft X ray reflectivity across the absorption edge of constituent elements. This makes use of the property that the refractive index of the material varies rapidly with photon energy and by varying the incident wavelength across the absorption edge, the electron density contrast can be enhanced which can yield information on several other properties not obtainable otherwise. The soft X ray reflectivity measurements are carried out in the BL-4 beamline which consists of a constant deviation grazing-incidence Torroidal Grating Monochromator (TGM) which disperses and focuses the X ray beam. It covers a range of 40 - 1000 Å (12-300 eV) with three gratings (200, 600 and 1800 lines/mm) which are interchangeable in situ and the spot size on the sample in 1 mm x 1mm. The experimental station is a multipurpose reflectometer with a two axis goniometer and Si and GaAsP photodiode detector [6].

Angle dependent soft X ray reflectivity (XRR) measurements were carried out for energy around the B K-edge at 187.5 eV for B_4C film (60nm) on Fe (18nm) bi-layers deposited on float glass substrate by electron beam evaporation. The reflectivity data has been fitted using simulated profiles using Parrat's formalism [7] and the optical constants δ and β as a function of energy across the edge has been determined. These are shown in figure 1 along with the values calculated from the Henke's values. The β value shows an abrupt jump and δ a dip to a negative value through the edge. Best fit results also indicate ~ 1.3 nm of porous B_4C layer in pure B_4C layer. Hard X ray reflectivity at 8 keV have been measured and its analysis gives an Fe layer of 17.2 nm and B_4C layer of 59.6 nm thickness however using hard X ray it is difficult to obtain good quantitative estimate of porous layer due to poor contrast between dense and porous B_4C. Resonant soft XRR measurements carried out at selected photon energies are shown in figure 2 along with the fitted curves. It can be seen that the reflectivity curves change considerably with change in incident energy [7].
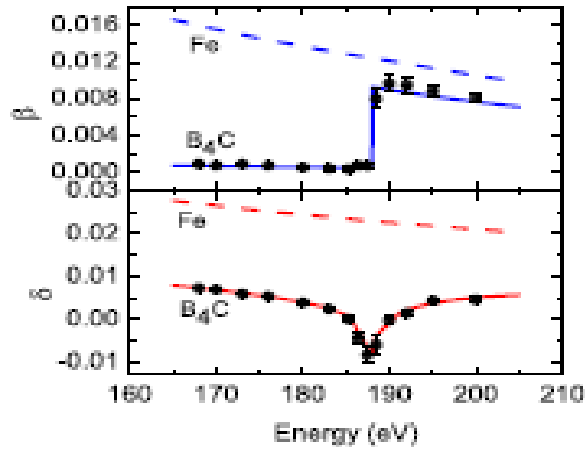

FIG. 1. Optical constants (β, δ) for B_4C and Fe near B K-edge, Measured (●) and values calculated using Henke's value are shown by continuous and dashed line.
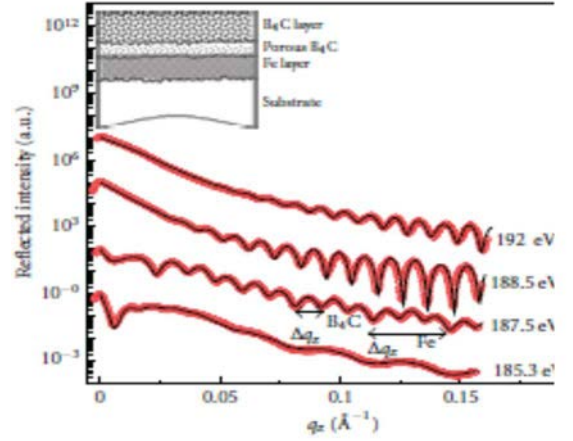
FIG. 2. Soft XRR for B_4C on Fe near B K-edge with experimental and calculated profiles.

The values of δ and β for B_4C at 185.3 eV are close to zero and the layer is transparent to incident X ray and the observed oscillation is due to substrate/Fe and Fe/virtually invisible B_4C layer respectively. At 187.5 eV all the layers can be seen with oscillations due to B_4 C super imposed on Fe layer oscillation. At 188.5 eV the absorportion in B_4C layer is significant so that the Fe layer is invisible and at still higher energy the oscillations become poorer. This full analysis of the resonant reflectivity suggest the presence of a porous B_4C layer of 1.3nm with 95% porosity at the bottom of the higher density top B_4C layer.

We now report the results of a few works carried out in the photoelectron spectroscopy beamlines in Indus-1. The angle integrated PES beamline consists of constant deviation TGM covering an energy range of 7-200eV and an Omnicron (EA125) electron analyzer and the total resolution of the beamline is ~ 300 meV [8]. This beamline was used to study resonant photoemission from $CeAg_2Ge_2$ inter metallic compound near the 4d threshold of Ce. This system crystallizes in body-centered tetragonal lattice and is paramagnetic at room temperature and anti-ferromagnetic below 7K.
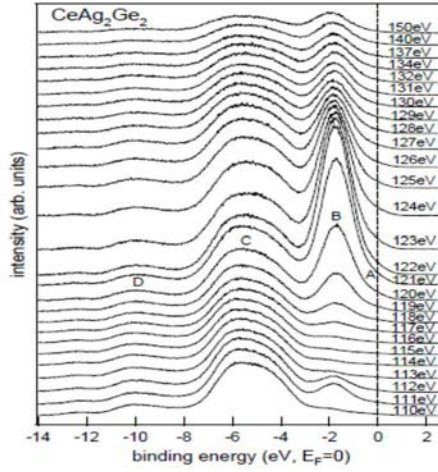
FIG. 3. VB spectra of CeAg₂Ge₂ recorded at different photon energy across the 4d − 4f resonance.
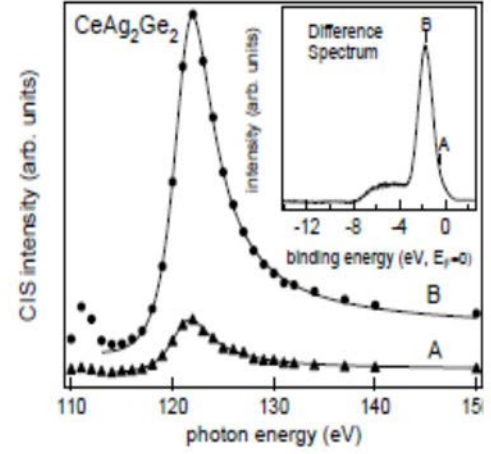
FIG. 4. Resonant feature A and B with photon energy. The solid line shows the fitting with the fano line shape.

CeAg2Ge2 crystals were grown by self/flux method and for PES measurement, they were mechanically polished and cleaned in situ by Ar+ etching and annealing. The valence band (VB) photo emission spectra were recorded using photons of energy 110-150 eV in steps of 1 eV and the position of the fermi energy was determined using signal from a gold foil. The VB spectra with background subtraction using Tougard procedure, is shown in figure 3. The VB shows several features and the features marked by A and B are greatly enhanced above the Ce 4d threshold located around 121eV (figure 4) and is related to the Ce 4f states. The resonance is due to interference effect due to the direct photo emission process $4d^{10}4f^{n} + h\nu \rightarrow 4d^{10}4f^{n-1} + e$ and the photo-ionization of the excited electron into the conduction band followed by auger transition $4d^{10}4f^{n} + h\nu \rightarrow 4d^{9}4f^{n+1} \rightarrow 4d^{10}4f^{n-1} + e$ and one can observe resonance enhancement at 121eV due to $4d_{3/2}$(A) and the other one at 111eV due to $4d_{5/2}$(B) threshold. The resonance profile shows a characteristic shape which can be fitted to a Fane line shape. Electron density of states calculated using a FPLAPW code indicate considerable hybridization of Ce 4f orbital with other states and the resonance feature B is primarily due to hybridized Ce 4f orbital[8].
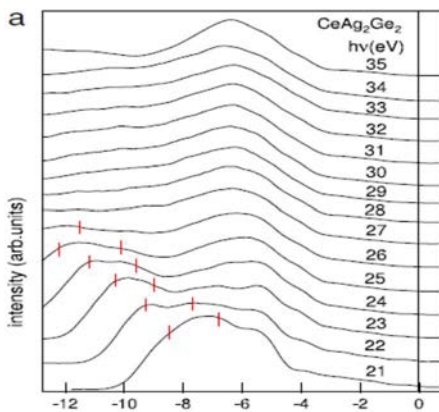

FIG. 5. Normal emission VB spectra of CeAg2Ge2 from the (001) surface (Γ-Z direction) recorded at photon energies from 21 to 35 eV
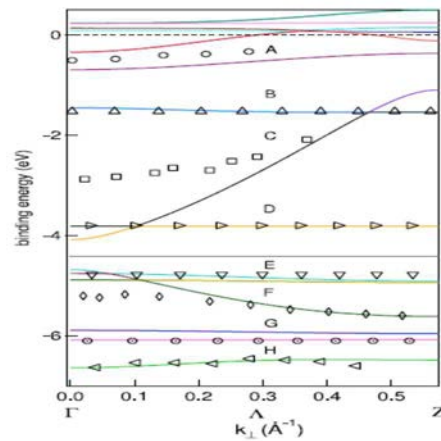
FIG. 6. Expt. band dispersion of CeAg₂Ge₂ along Γ-Z (001) direction compared to the calculated band structure (solid lines).

We have also carried out the electronic band dispersion measurement in single crystals of CeAg₂Ge₂ using Angle resolved PES beamline BL-3 in Indus-1[9]. The crystal was

mechanically polished to mirror finish and mounted in preparation chamber. This beamline is also similar to the BL-4 with an overall resolution $\approx$ 300 meV. The incident photon energy was varied from 21 to 35 eV and photon flux was $\sim 10^{10}$ ph/sec with a beam size of 1.5 x 1mm. The normal emission angle resolved photo emission were recorded from the (001) face using an Omnicron hemispherical analyzer and is shown in figure 5. Apart from the peaks at 6.5 eV and 8.5eV there are two more features which shift to higher binding energy. These originate from $O_{23}VV$ auger process in Ce and their contribution was subtracted to obtain the actual valence band spectra. The valance band has been resolved into eight features whose origin can be understood from the DOS calculation using FPLAPW method. Normal emission spectra give information about the momentum perpendicular to the surface, which is calculated from knowledge of work function and constant positive inner potential. The band structure calculated for each of the eight branches for the first Brillouin Zone i.e. along the Γ-Z direction is shown in figure. The theoretical band structure shows two bands at -0.3 eV and -0.7eV whereas experimentally we observed only one band which may be due to poor experimental resolution. However the overall experimental band structure is in reasonable agreement with the calculated ones.

4.   INDUS-2

In Indus-2 six BM beamlines have been installed and are currently operational. These are listed in Table II with their primary specifications. We now discuss a few works carried out using the Indus-2 beamlines. Indus-2 is operating since beginning of 2010 in round the clock shift at 2 GeV and 100 mA and at present the beam lifetime of $\approx$ 19 hrs. A total of sixteen bending magnet beamlines have been planned and currently six of them are operational and others are at different stages of installation and commissioning and are expected to be operational by 2012. The beamlines which have been commissioned and operational currently are given in the Table 2.

TABLE 2. BEAMLINES INSTALLED AND OPEARTIONAL IN INDUS-2

	Beamline	Range (keV)	Monochromator	Resolution (E/ΔE)	Experimental station
BL-7	Soft/hard X ray Lithography	1.5 -20	Pink X ray beam selected by two mirrors.	-------	Mask and substrate holder with precession scanner
BL-8	EDEXAFS	5 -20	Si(111) bent crystal polychromator	10^4	X ray CCD with high and low temp sample stage
BL-11	EDXRD	5 – 50	_____	100	HPGe detector
BL-12	Angle Resolved XRD	5 – 20	Si(311) Double Crystal Monochromator	10^4	6-circle Huber Goniometer, MAR Image plate
BL-14	XPS	5-20	Si(111) Double crystal Monochromator		Hemispherical Electron Analyzer
BL-16	Micro-probe XRF	5- 25	Si(111) Double crystal Monochromator	10^4	Sample scanning stage with photo-diode detector

4.1. Indus-2 utilization

The dispersive EXAFS is the first bending magnet (BM) beamline to be installed in Indus-2 and is being used by several users. The beamline consists of a 460 mm long Si(111) crystal mounted on an elliptical bender which focuses the X ray beam to a spot size of 200x400 μm[10]. The full EXAFS spectrum in the absorption mode is recorded simultaneously using an X ray CCD and the beamline has an energy resolution of 1eV at 10 KeV. The energy has been calibrated using the absorption edges of different metal foils. This has been used to obtain structural parameters of four metal-organic Cu complexes by recording the EXAFS spectra of the hydroxe-bridge Cu(II) complexes at the Cu K edge[11]. The energy has been calibrated using the Cu K-edge of Cu-foil and L_3 edge of Lu in Lu_2O_3 powder. Normalized μ(E) vs E curves for 1,2,3,4 complexes are used to obtain the EXAFS signal χ(K) which are then Fourier transformed . The Fourier transformed data are then fitted to obtain with the theoretical modal in R-space to obtain the different fitting parameters. The theoretical models for the compounds 1 and 3 have been generated and fitted to EXAFS data band lengths, coordination numbers and thermal disorder. As the crystallographic data for 2 and 4 are not available, the structural parameters were determined by fitting the experimental EXAFS data. The values of the chemical shifts imply that Cu(II) is in the 2+ oxidation state in all the compounds. The experimental EXAFS data and the model fitted curves for the compounds 1 and 3 are shown in figure 7.
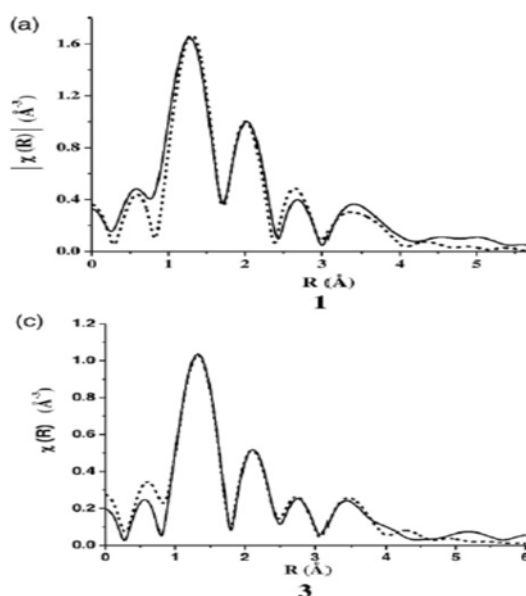

FIG. 7. Fourier transformed EXAFS data for 1 and 3 complexes, Solid lines are experimental data and dashed lines are modeled fit as explained in the text.
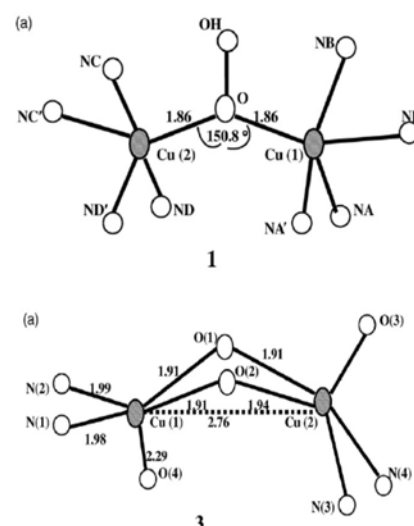
FIG. 8. Coordination geometry about copper(II) in 1 and copper(II) in 3 as deduced from EXAFS Data.

The angle dispersive XRD (ADXRD) beamline has been installed and commissioned on BM port BL-12 and a large number of users have been using this beamline for materials research. The beamline covers an energy range of 5-25 KeV and consists of a premirror, a DCM with a pair of Si(311) crystals and a post mirror. The experimental station consists of a 6-circle Huber diffractometer and MAR image plate. A low temperature stage (3K) and a high-pressure facility will be commissioned soon. Here I report our study on the effect of isochronal annealing on the microstructure and magnetic properties of soft magnetic FeCoNbB amorphous alloys [12]. $Fe_{40.5}Co_{40.5}Nb_7B_{12}$ alloy was prepared by arc melting of Fe,

Co, Nb and B in form of ribbons of thickness ≈ 25 μm. The samples were isochronically annealed for ~1 hr from 300 to 973 K and were studied in the ADXRD beamline of Indus-2 using 15 KeV X ray. As quenched samples show broad diffraction pattern characteristic of amorphous phase and with increasing temperature the system gradually transforms to nano crystalline phase as shown by the diffraction pattern in figure 9.

The sample becomes partially crystalline for temperature >450°c consisting of α and α'-(Fe.Co) nanocrystalline phase dispersed in remaining amorphous matrix. For temp > 700°C the peaks corresponding to the α/α'-(Fe.Co) becomes very sharp, showing no evidence of the remaining amorphous phase. The average grain size of the nano crystalline phases change from 33 nm to fully crystalline beyond 700°C. Further, anomalous XRD at Fe K-edge (7.112 KeV) has been used to distinguish between the ordered ferromagnetic α'-(Fe.Co) alloy from the disordered α-(Fe.Co) alloy. The presence of the (100) superlatice reflection suggests formation of atomically ordered α'-(Fe.Co) nano crystalline phase.
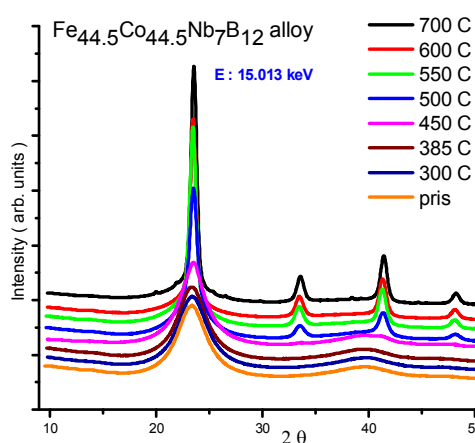

Fig. 9. XRD patterns of the $Fe_{40.5}Co_{40.5}Nb_7B_{12}$ after annealing till the onset of second crystallization stage.
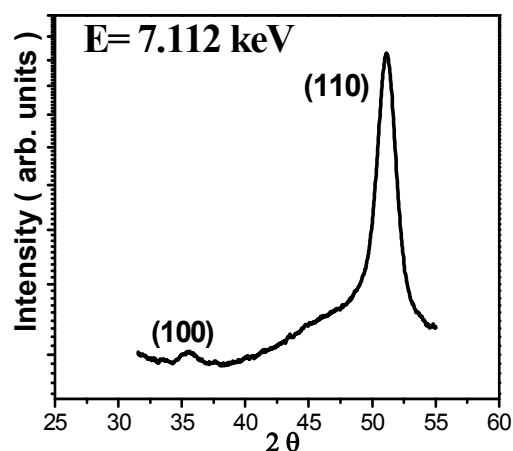
Fig. 10. XRD measurement at Fe K-edge (7.112 keV) shows formation of ordered α'-Fe Co phase by the presence of (100) super lattice reflection

The EDXRD beamline installed in BL-11 BM port is mainly meant for high pressure XRD measurements and is equipped with Ruby fluorescence for pressure calibration. For 2.5 GeV operation it covers an energy upto 45-50 keV and high pressure measurements have been carried out up to ≈ 25 GPa. It is also equipped with a sample heating stage upto 400°C. Of the several studies being carried out, the in-plane and out-of -plane diffraction from thin films are interesting (figure 11).

Co thin film have been deposited on CoO layer and grazing incidence diffraction with **q** vector in and perpendicular to the thin film plane has been carried out to study textured growth of Co film giving rise to structure induced magnetic anisotropy. The other studies carried out are (a) melting of Cd-arachidate LB thin film by carrying out in-plane energy dispersive diffraction due to SR radiation exposure and thermal annealing (b) Co thin film deposited on nano rippled si (100) substrate which show non-isotropic grain orientation along and normal to ripple wave-vector(figure12) [13].

The XRF microprobe beamline has been commissioned and currently being used for carrying out several studies. It covers an energy range of 5-20 KeV and the X ray beam can be focused to a spot size of 6 x 12 μm using a KB mirror, and selective area element-specific fluorescent image can be obtained for spatially inhomogeneous sample.
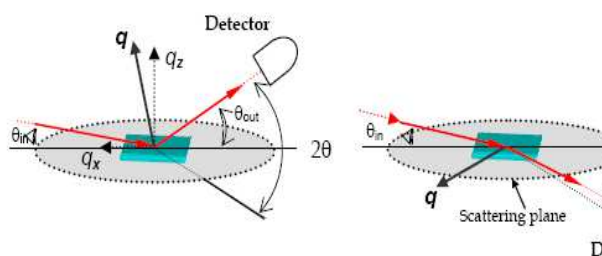
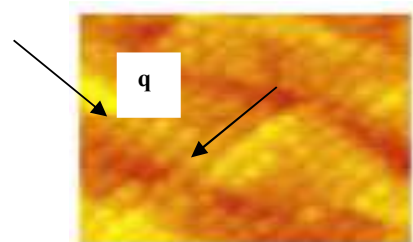FIG. 11. In plane and out of plane diffraction geometry

FIG. 12. q vector parallel and perpendicular to ripple wave vector (K)

It can be used in the macro mode for conventional XRF sample analysis. Recently this beamline together with the ADXRD beamline has been used to study archaeological samples from an ancient fort in northern India-the kalinjar fort. Samples of stone pieces and white wash paints were studied and XRF shows predominantly the presence of Ca and Fe and small percentage of Sr, Rb, Ti, Mn and Zn. The preliminary assignment of XRD data shows presence of TiO_2, $CaCO_3$, Fe_2O_3, SiO_2 and Al_2O_3. Very small percentage of oxides of other heavy metals could not be detected in XRD. Similarly stone sample have also been analyzed by XRF which shows Fe as the most dominant element, followed by Ca, Rb, Sr, Ti, Zn etc. On the other hand XRD analysis shows presence of FeO, Fe_2O_3, $CaCO_3$, SiO_2, Al_2O_3, MgO, TiO_2 etc. Although the XRD shows presence of oxides of Si, Al, Mg etc light elements, their presence in XRF could not be detected since the experiments were carried out in ambient and low energy fluorescent X rays were absorbed. Beamline is currently being modified for conducting experiments in vacuum.
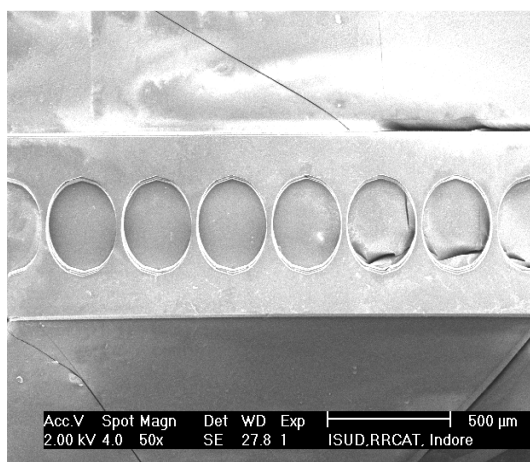

FIG. 13. Compound refractive lens fabricated on PMMA resist designed for 9 keV X ray.
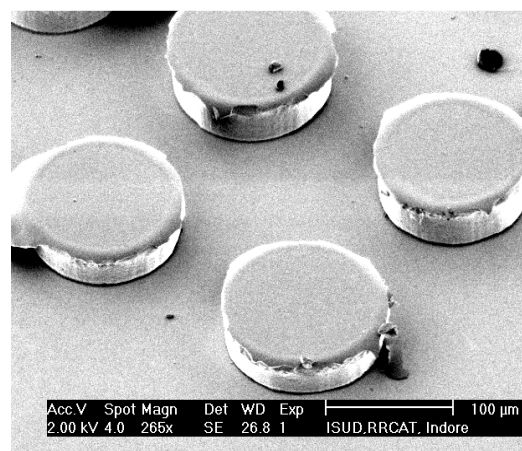

FIG. 14. Micro-pillars fabricated on SU-8 at with 200 μm in diameter, 170 μm deep and 300 μm pitch

The soft and hard X ray lithography beamline has been commissioned in BL-7 which has an energy range of 1.5 keV to 20 keV which can be operated in pink beam mode using two mirrors. The X ray beam is ribbon shaped with 70 mm(H) x 10 mm (V) size. For the fabrication of three dimensional high aspect ratio (few hundred) structures with minimum feature size of few microns, a custom built X ray scanner is installed as an experimental station. As test experiments, the beamline has been used for the fabrication of few micro fluidic devices, compound X ray refractive lens micro pillars and test patterns with minimum feature size of 15 μm and aspect ratio of about 40. The structures are fabricated in photo resists (PMMA and SU8).

5. CONCLUSIONS

Two Synchrotron Radiation sources (Indus-1 and Indus-2) have been designed, built and commissioned at Raja Ramanna Centre for Advanced Technology, Indore. Indus-1 is a 450 MeV source emitting in soft X ray/VUV and five beamlines have been commissioned and operational. Indus-2 is a 2.5 GeV source emitting in the hard X ray region and currently being operated at 2 GeV. Six BM beamlines have been commissioned are being used for carrying out several materials research experiments and more beamlines are expected to be comssioned by mid 2012. We have described a set of representative experiments carried out using these beamlines in Indus-1 and Indus-2. More than fifty papers have been published using Indus-1 in several refereed journals and a few papers have already been published using Indus-2 beamlines.

ACKNOWLEDGMENTS

The author would like to thank Dr G S Lodha and all other members of the Indus Synchrotrons Utilization Division for several discussions and for their input to this article.

REFERENCES

[1] ANGAL-KALININ, D., BANERJI, A., HANNURKAR, P.R., KARMARKAR, M., KOTAIAH, G.S., MHASKAR, S.P., NEMA, P.K., PRABHU, S.S., PRAVIN KUMAR, M., RAMAMURTHI, S.S., SHUKLA, S.K., SINGH, G., SONI, H.C., VAIDYA, B.J., Synchrotron radiation source Indus-1, Curr. Sci. India **82** (2002) 283-290.

[2] SAHNI, V.C., Commissioning of the Indus-2 storage ring, 4th Particle Accelerator Conf. APAC 2007, RRCAT, Indore (2007) 61pp.

[3] NANDEDKAR, R. V., Beamlines on Indian Synchrotron Radiation Source Indus-1, Curr. Sci. India **82** (2002) 291.

[4] CHAUDHARI, S.M., PHASE, D.M., WADIKAR, A.D., RAMESH, G.S., HEGDE, M.S. DASANNACHARYA, B.A., Photoelectron spectroscopy beamline on Indus-1 synchrotron radiation source, Curr. Sci. India **82** (2002) 305-309.

[5] DAS, N.C., JHA, S.N., BHASKARA, RAO, S.V.N., RAJASEKHAR, B.N., BHATTACHARYA, S.S., SIKKA, S.K., JAGANNATH, KORGAONKAR, A.V., BHUSHAN, K.G., YAKHMI, J.V., AND, SAHANI, V.C., Development of angle resolved photoelectron spectroscopy beamline at Indus-1 synchrotron radiation source, Journal of Optics (India) **32** (2003) 27.

[6] NANDEDKAR, R.V., SAWHNEY, K.J.S., LODHA, G.S., VERMA, A., RAGHUVANSHI, V.K., SINHA, A.K., MODI, M.H., AND NAYAK, M. First results on the reflectometry beamline on Indus-1, Curr. Sci. **82** (2002) 298-304.

[7] NAYAK, M., LODHA, G.S., PRASAD, T.T., NAGESWARARAO, P., SINHA, A.K., Probing porosity at buried interfaces using soft X ray resonant reflectivity, J. Appl. Phys. **107** (2010) 023529-023529-5..

[8] BANIK, S., CHAKRABARTI, A., JOSHI, D.A., THAMIZHAVEL, A., PHASE, D.M., DHAR, S.K., DEB, S.K., Electronic structure of CeAg2Ge2 studied by resonant photoemission spectroscopy, Phys. Rev. B **82** (2010) 113107.

[9] BANIK, S., CHAKRABARTI, A., DEB, S.K., JHA, S.N., BHASKARA RAO, S.V.N., JOSHI, D., THAMIZHAVEL, A., DHAR, S.K., Band mapping of CeAg2Ge2 using angle-resolved photoemission spectroscopy, Solid State Commun. **150** (2010) 1936.

[10] BHATTACHARYYA, D., POSWAL, A.K., JHA, S.N., SANGEETA, SABHARWAL, S.C., First results from a dispersive EXAFS beamline developed at INDUS-2 synchrotron source at RRCAT, Indore, India, Nucl. Inst. Meth. A **609** (2009) 286-293.

[11] GAUR, A., SHRIVASTAVA, B.D., GAUR, D.C., PRASAD, J.K., SRIVASTAVA, K, JHA, S.N., BHATTACHARYYA, D., POSWAL, A., DEB, S.K., EXAFS study of binuclear Hydroxo-bridged Copper(II) complexes, J. Coord. Chem. **64** (2011) 1265.

[12] GUPTA, P., et al., (private communication)

[13] SARATHLAL, K.V., DILEEP, K., AJAY G., Growth study of Co thin film on nanorippled Si(100) substrate, Appl. Phys. Lett. **98** (2011) 123111.

LOCAL ATOMIC AND ELECTRONIC STRUCTURES IN COMPLEX SOLID-STATE SYSTEMS

I. RADISAVLJEVIĆ, N. NOVAKOVIĆ, N. ROMČEVIĆ, N. IVANOVIĆ
Vinča Institute of Nuclear Sciences-University of Belgrade
Belgrade, Serbia

H.-E. MAHNKE
Helmholtz-Zentrum Berlin für Materialien und Energie GmbH
Berlin, Germany

Abstract

The paper highlights capabilities of X ray absorption spectroscopy (XAS) for local atomic and electronic structure determination in complex solid-state systems. In particular, it focuses on X ray absorption near edge structure (XANES), extended X ray absorption fine structure (EXAFS) and X ray magnetic circular dichroism (XMCD), and their success in addressing problems of disordered solid solutions; multi-component systems where two or even three ions are competing for the same lattice site; (magnetic) impurity atoms accommodation and lattice relaxation in extreme cases of the limited solubility and mixed valence behaviour.

1. INTRODUCTION

X ray absorption spectroscopy (XAS) is nowadays one of the most powerful experimental tools to study electronic and structural properties of matter, and has found application in many diverse scientific fields. Strong energy and polarizability tuned photon beams with high spectral purity produced in third-generation synchrotron sources coupled with highly efficient energy resolving detectors with excellent statistics, give rise to high-quality experimental spectra. The improvements in experimental design and instrumentation are accompanied with advances in theoretical methods for XAS spectra reproduction.

XAS is particularly suited for studies of local environments in complex systems. It gives a direct experimental access to the effects related to the impurity atoms accommodation, lattice distortions and its relaxation. In this review, after a brief introduction to fundamentals of XAS process and the current trends in its theoretical simulations is given, capabilities of XAS in resolving the structure of complex solid-state systems are illustrated on a number of examples involving multi-component IV-VI and II-VI disordered and diluted systems.

2. XAS FUNDAMENTALS

The fundamental XAS process is the absorption of an X ray photon by matter giving rise to the electronic transition from an initial core state to an unoccupied final-electron state determined by dipole selection rules. The transitions occur at certain energies (the absorption edges) that are characteristic to a particular element and its local environment. The oscillatory structure in the X ray absorption coefficient appearing above the absorption edge, referred to as X ray absorption fine structure (XAFS), is generally divided into two regions: X ray absorption near-edge structure (XANES) located in the energy region above the absorption edge up to 50 eV and the extended X ray absorption fine structure (EXAFS) in the energy region up to 1500 eV (see Fig.1.). The XANES results from the multiple scattering of ejected electrons by neighboring atoms, and is strongly sensitive to the electron density around the atom excited by X rays. The EXAFS is dominated by the single scattering of photoelectrons by the surrounding atoms and contains information on the local structure in terms of number, type and distances of atoms surrounding the absorber. The region immediately below the absorption edge, the pre-edge region (see inset of Fig.1.), also contains valuable bonding

information, such as oxidation state of the absorber and symmetry of its local environment. Another variation to the XAS technique is X ray magnetic circular dichroism (XMCD) which utilizes circularly polarized X rays to probe atomic scale magnetism.
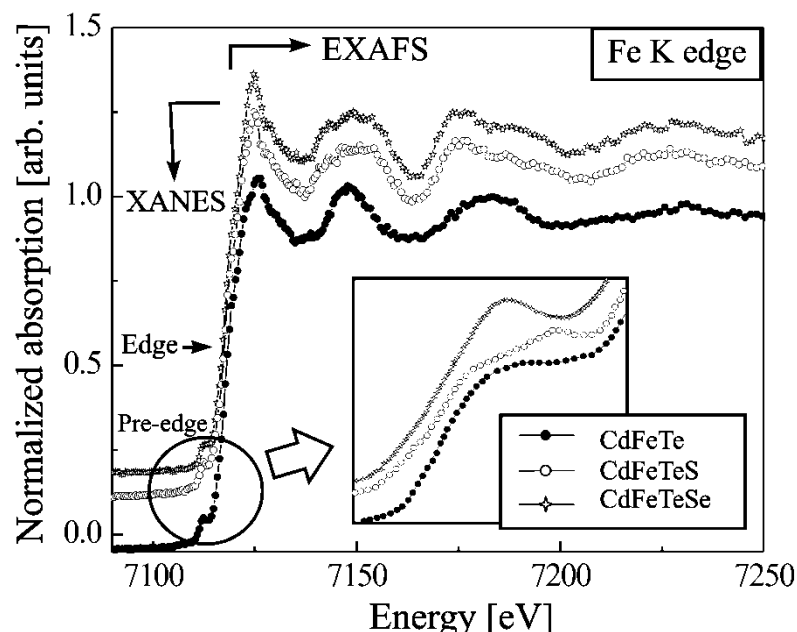

FIG.1. Normalized XAFS spectra of $Cd_{1-x}Fe_xTe_{1-y}(Se,S)_y$ taken at Fe K edge. Inset shows pre-edge structure enlarged.

3. THEORETICAL SIMULATIONS OF XAS

Analysis and interpretation of experimental XAS data is realized through theoretical simulations which enable to extract structural and electronic information of interest. The present developments in theory tend to unify description of XANES and EXAFS using one theoretical approach. However, while the theory of EXAFS is well understood, a fully quantitative treatment of the XANES is still challenging. Complications in the theory of XANES arise from various many-body effects (the photoelectron-core hole interaction, the photoelectron self-energy, multi-electron excitations, local field effects, …). These effects are difficult to account for in one-electron approach, used for calculation of the X ray absorption cross-section in a number of dedicated ab initio codes (FEFF 0, [2], CONTINUUM [3], EXCURV [4], GNXAS [5]), that make use of real space multiple scattering formalism. Another major drawback of these codes is that the XANES is calculated for fixed model structures. The atomic-like multiplet calculations, developed for the systems with localized (3d, 4f) states [6], also have their disadvantages in utilizing a crystal-field parameterization of solid state effects. The other group of theoretical approaches works in reciprocal space and are based on density functional theory (DFT), such as ABINIT [7], QUANTUM-ESPRESSO [8], VASP [9], WIEN2k [10]. Their advantage is in self-consistency which allows more precise treatment of the electronic structure. However, due to translational symmetry required in band-structure calculations, it is not always feasible to account for the core-hole effects. More rigorous calculations of the XANES would comprise going beyond the single-particle description and treatment of the electron–hole interactions within many-body theory. Recent developments in time dependent DFT (TDDFT) based codes and the Bethe–Salpeter formalism promise to significantly improve the treatment of the XANES in the near future.

In the real space multiple scattering formalism, the EXAFS analysis is based on theoretical modelling of the oscillating absorption coefficient, conveniently expressed as a sum of contributions due to all possible scattering paths of the photoelectron [11]:

$$\chi(k) = \sum_j \frac{N_j}{kR_j^2} S_0^2(k) F_j(k) \cdot e^{-2k^2\sigma_j^2} \cdot e^{\frac{-2(R_j-\Delta)}{\lambda}} \cdot \sin\left[2kR_j + \delta_j(k)\right].$$

Here, N_j is the number of atoms in the j-th shell; R_j-the mean distance between the absorbing atom and the j-th shell; $F_j(k)$-the backscattering amplitude of the photoelectron wave from atoms in the j-th shell; $\delta_j(k)$-the photoelectron phase shift; S_0^2- passive electron reduction factor. The photoelectron mean free path λ is a mean distance travelled by the photoelectron without inelastic scattering. The decay of the EXAFS amplitude due to restricted mean free path and finite lifetime of the photoelectron is expressed as $e^{-2(Ri-\Delta)/\lambda}$, where $\Delta \approx R_j$ is a "core radius" of the absorbing atom; σ_j^2 is the mean-squared variation of the distance between the absorbing atom and an atom in the j-the shell. Fine structure associated with different coordination shells oscillate at different frequencies and can be isolated by means of Fourier transform (FT) [12].

4.   XAS APPLICATION TO COMPLEX SOLID-STATE SYSTEMS

In this section capabilities of XAS in addressing problems of impurity atoms accommodation and local structural distortions they cause, will be demonstrated on IV-VI disordered solid solutions and quaternary II-VI mixed crystals, as representatives of complex solid-state systems. In order to extract as much as possible details of the electronic and local structure around impurity atoms, the combined XANES and EXFAS approach is used. Structural parameters, as derived from EXAFS analysis, served to construct theoretical models of XANES spectra, which are then compared with the experimental spectra, and the structural models are refined as needed in order to achieve the best possible matching with experiment. Regardless of the complexity of the system and level of distortion of the impurity local environment, a through XAS analysis by means of IFEFFIT [13] as implemented in ATHENA and ARTEMIS software packages [14], enabled precise determination of the structural and electronic parameters of interest: impurity valence; symmetry of the lattice site it occupies; type, number and distances of the neighbours in some cases extending up to the third coordination shell.

4.1. IV-VIs. Case study: PbTe-based disordered solid solutions

Lead telluride is polar semiconductor with mixed ionic-covalent-metal bond which crystallizes in cubic NaCl type-structure (O_h symmetry). It belongs to a family of narrow band gap IV-VI semiconductors and is characterized by direct energy gap, high efficiency of radiative recombination, large static dielectric constant and small effective mass of charge carriers. Solid solutions it forms by means of conventional crystal growth methods, are often limited to a certain range of concentrations (like, for instance, $Pb_{1-x}Mn_xTe$ which exists for x <0.15). Behaviour of impurity atoms in lead telluride is not always consistent with theoretical predictions. Most of the rare-earths and chalogen elements act as donors. Alkali metals are acceptors, transition metals Cr, Co and Ni are donors, while Mn is neutral impurity. The group III elements (In, Ga), which are expected to act as acceptors, actually act as donors. Moreover, the same impurity, depending on a particular composition of the system, can act both as donor and as acceptor. Also, depending on the type of impurities, doping can lead to appearance of new physical properties, such as ferroelectricity induced by impurity atoms off-centering [15]-[17], and in whose better understanding XAFS played a significant role.
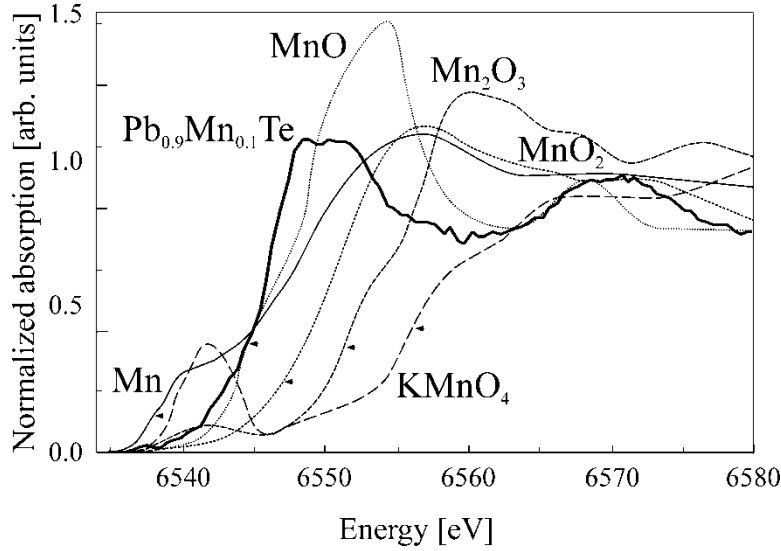
FIG. 2. Determination of the oxidation state of Mn in $Pb_{0.9}Mn_{0.1}Te$ [21] from the comparison of its Mn K edge position to that in metal manganese, MnO, Mn_2O_3, MnO_2 and $KMnO_4$, with Mn valence 0, +2, +3, +4 and +7, respectively [22]. Energies of the corresponding absorption edges are indicated by arrows.

4.1.1. $Pb_{1-x}Mn_xTe$

Manganese is considered electro-neutral impurity in PbTe and, as such, does not form local or quasi-local impurity states near the band gap (E_g), which, however, in $Pb_{1-x}Mn_xTe$ increases with Mn concentration (x). Above the solubility limit (x=0.15) deformation of the cubic NaCl towards the hexagonal NiAs-type structure of MnTe occurs (note that Mn is octahedrally coordinated with Te atoms in both MnTe and $Pb_{1-x}Mn_xTe$), whereas for the concentrations x lower than 0.02 it has no significant influence on the lattice dynamics and dielectric properties of material. However, XAFS studies of $Pb_{1-x}Mn_xTe$ in the concentration range 0.002<x<0.1 [18]-[21] revealed a considerable increase of local structural disorder with increase of Mn concentration. Moreover, for the highest investigated concentration (x=0.1) splitting of the first coordination shell into two well defined sub-shells (first of which corresponds to MnTe and second to PbTe) is observed, revealing that the local NaCl to NiAs transformation starts already at this concentration. The characteristic double peak structure in Mn K edge XANES spectra (see Fig. 2.) further evidences the existence of two different bond lengths Mn forms with Te atoms from its immediate surroundings. In addition, Mn valence is found to be larger than the nominal 2+ [19], [21], which is probably the consequence of considerable charge transfer and its redistribution among the two Mn-Te bonds.

4.1.2. $Pb_{0.9}Mn_{0.1}Te$ (In, Ga)

Group-III impurities (In, Ga) in PbTe-based systems induce a series of effects unusual for narrow band gap semiconductors, such as Fermi level pinning at impurity level, persistent photoconductivity, ferroelectric phase transition, semiconductor-metal phase transition [23]. These effects are closely connected to formation of so called deep defect states (whose position can be tuned by additional doping with transition metals) and mixed-valence phenomenon. In highly polarizable PbTe lattice (i.e. anomalously large dielectric constant) group-III impurities are believed not to be stable in the neutral two-valent state, and exist in mono- and three-valent states instead [23]. In addition, due to large differences of ionic radii and polarizabilities as compared to Pb they interchange, displacement of group-III impurities from the regular lattice sites are readily observed. In highly locally distorted $Pb_{1-x}Mn_xTe$ these

effects are expected to be even more pronounced [18]. Under the high stress and in order to lower the elastic energy of the crystal, the impurity local environment gets reorganized. In $Pb_{0.9}Mn_{0.1}Te(2$ at.% In) [21] reorganization of the indium local environment proceeds towards InTe, where it occupies two inequivalent lattice positions, $In(1)=In^{1+}$ and $In(2)=In^{3+}$ (both being tetrahedral, but involve different In valences). Arguments supporting this assumption are bimodal distribution of distances found around In (whose lengths are close to those expected in InTe) and decrease of coordination number from six in octahedral, toward four in tetrahedral coordination. As a result of two considerably different types of In-Te bonds, a mixed (non-integer) mean valence of In is observed, which opposes the premises of the model given in [23]. On the other side, in $Pb_{0.9}Mn_{0.1}Te(4$ at.% Ga) [21] gallium is found to be substantially off-centered from the regular lattice position. Displacement of Ga atoms might come as a consequence of the competition with Mn for the same lattice site, but could also be related to the theoretical prediction of its energetically more favourable incorporation into interstitial lattice position [24].

4.1.3. PbTe:Ni

Nickel in PbTe [25] preserved the local structure of one of its native tellurides $NiTe_2$ (CdI_2-type structure, with Te forming a hexagonal close packed arrangement and Ni occupying all octahedral sites in alternate layers). From the Ni K edge XANES analysis it was determined that tellurium atoms from the immediate Ni-surrounding form a temperature-stable octahedron whose orientation is adjusted to the PbTe long-range order (see Fig. 3). EXAFS analysis revealed that the second, and even the third coordination shell are also more $NiTe_2$-alike. However, the influence of Ni doping is localized and the long-range order is well preserved, as verified from Te K and Pb L_{III} edges EXAFS data. Lead sub-lattice remains almost unaffected by the presence of Ni at the investigated doping level (10^{19} at/cm^3), and the structural parameters extending up to the third coordination shell (~6 Å) correspond to the NaCl-type structure.
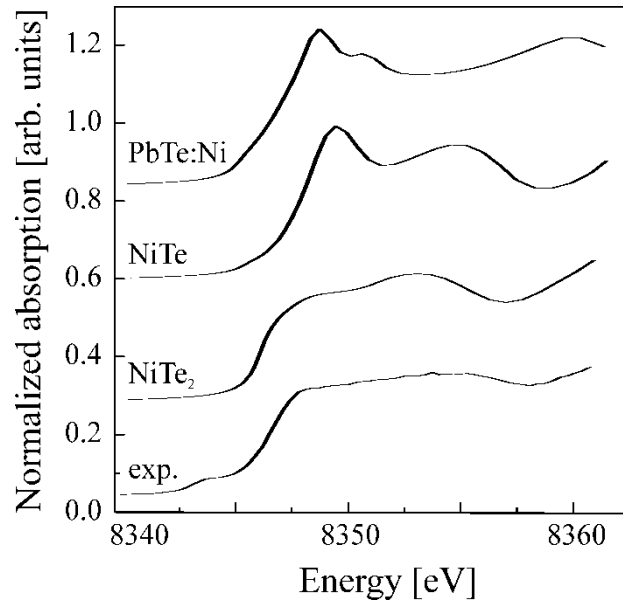

FIG. 3. Normalized PbTe:Ni XANES spectrum taken at Ni K-edge and models used in analysis. There is a large mismatch between experiment and model which assumes Ni atom replacing Pb at the ideal PbTe lattice position. The same is true for the model with Ni atoms in NiTe-like immediate surrounding. The best description of the experimental spectrum is achieved when Te octahedron is rotated from the NiTe₂-position so to match the orientation it has in PbTe.
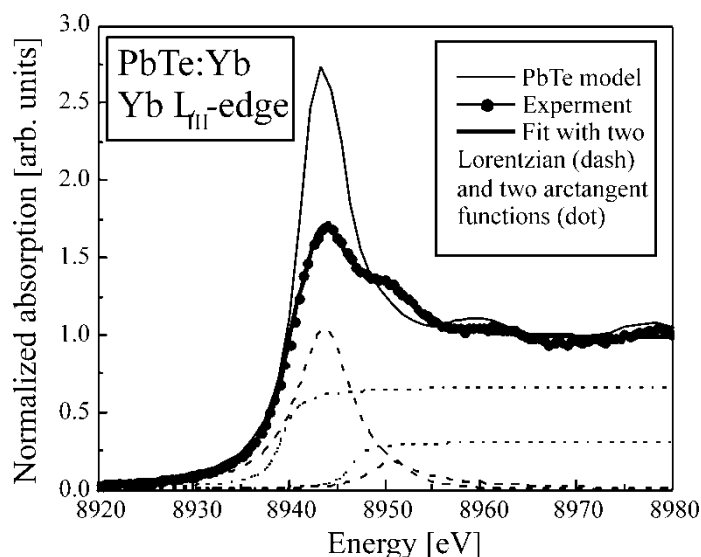
FIG.4. Fit of PbTe:Yb XANES spectrum taken at Yb L_{III}-edge (arctangent functions represent the L_{III}-edge absorption and Lorentzian functions represent the white line). The top curve is the model XANES spectrum of Yb placed at regular PbTe lattice position.

4.1.4. PbTe:Yb

At low doping level (1.3 at.%) ytterbium is incorporated in PbTe as substitutional impurity [26]. The deformation of the host PbTe lattice it causes, is manifested through slight outward relaxation of all the nearest-, and next-nearest neighbour distances. Structural disorder is confined to the first two coordination shells and does not reach the third coordination atoms. However, a large discrepancy was observed in the XANES region of the Yb L_{III}-edge absorption spectra between the experiment, and the model spectrum of Yb placed at regular PbTe lattice position (see Fig. 4.). This discrepancy is explained in terms of mixed valence Yb ground state. Using linear peak fit analyses, it was determined that at 20 K the Yb mean valence is 2.12+ (0.88 Yb^{2+}: 0.12 Yb^{3+}) and that it does not change significantly with temperature. This intermediate valence ground state of Yb is believed to be responsible for the valence instabilities phenomena observed in many rare-earth based compounds, which are subject of investigation by means of even more sophisticated analysis techniques [27].

4.2. II-VIs. Case study: CdTe-based mixed crystals

Wide band gap II-VI semiconductors doped with transition metals, commonly referred to as diluted magnetic semiconductors (DMS) or semimagnetic semiconductors (SMSC), are of scientific interest because of their wide range of optical, magnetic and electronic transport properties. $Cd_{1-x}Mn_xTe$ is one of the first materials from this class to be studied by XAFS. Refinement of its local structure served to establish random cluster model of ternary alloys [28], which was later further developed [29], [30] to include other related materials, especially quaternary systems [31], [32], where the atomic correlations (site occupation and nearest-neighbour preferences) are even more pronounced than in ternary systems [33]-[35].

151

4.2.1. $Cd_{1-x}Fe_xTe_{1-y}(Se,S)_y$

In $Cd_{1-x}Fe_xTe_{1-y}(Se,S)_y$ ($x \leq 0.02$, $y \leq 0.03$) mixed crystals [34], [35], Cd atoms are randomly replaced with Fe and Te with Se (S). The low concentrations of impurity atoms ensure preservation of the monophase zinc-blende structure (T_d symmetry) of the host CdTe. The distribution of Cd and Fe atoms regarding Te sub-lattice is bimodal, meaning that the nearest neighbour Cd-Te and Fe-Te distances are different and independent of both composition (Se/S) and concentration (x). Also, there is a clear preference for Fe distribution around Te in $Cd_{0.98}Fe_{0.02}Te_{0.97}Se_{0.03}$ and around S in $Cd_{0.99}Fe_{0.01}Te_{0.97}S_{0.03}$. The T_d symmetry of the Fe site in $Cd_{0.99}Fe_{0.01}Te_{0.97}S_{0.03}$ is broken due to the presence of two types of anions (Te and S) in nearest Fe-neighbourhood, and therefore its ground state is expected to become magnetically active [36]. However, no magnetic moments associated with Fe ions were observed by X ray magnetic circular dichroism (XMCD) measurements [37].

Pre-edge structure that appears below the main edge (often observed in the XANES spectra of transition metal compounds [38]), is assigned to weak quadrupole transitions from 1s to 3d states, with additional intensity acquired from dipole transitions into 3d-band with 4p character resulting from 4p-3d orbital mixing (note that in T_d symmetry p-d mixing is allowed because of the lack of inversion symmetry). Closer inspection of the pre-edge structure appearing in the investigated systems Fe K edge XANES spectra (see inset of Fig. 1.) revealed the existence of Fe ion in the mixed valence 2+/3+ configuration [39]. In $Cd_{0.97}Fe_{0.03}Te$ and $Cd_{0.98}Fe_{0.02}Te_{0.97}Se_{0.03}$, where Fe shares the same local environment composed of Te atoms only [34], Fe^{2+} component is predominant. The presence of a double peak structure in the pre-edge region of $Cd_{0.99}Fe_{0.01}Te_{0.97}S_{0.03}$ Fe K edge XANES spectrum, is ascribed to the mixture of Fe^{2+}/Fe^{3+} states. Mixed valence of Fe is further confirmed from Fe $L_{2,3}$ edge XMCD measurements [37].

5. OUTLOOK

The X ray absorption spectroscopy (XAS), as advanced analysis technique, has been employed in studies of PbTe-based disordered solid solutions and quaternary CdTe-based mixed crystals. To refine the details of their complex electronic and local structures, combined approach based on XANES and EXAFS was used. In addition, XMCD is used to probe microscopic magnetism in the systems with diluted magnetic ions. It was shown how XAS enabled recognition of a variety of impurity atoms (transition metals, rare earths, group-III elements) incorporation mechanisms, which often involve specific changes of the local conditions in the host lattices, deformation of the impurities local environments and adjustment of their valences.

REFERENCES

[1]   REHR, J.J., ALBERS, R.C., Theoretical approaches to X ray absorption fine structure, Rev. Mod. Phys. **72** (2000) 621-654.

[2] REHR, J. J., KAS, J. J., PRANGE, M. P., SORINI A. P., YOSHINARI, T., FERNANDO, V., Ab initio theory and calculations of X ray spectra, C. R. Phys. **10** (2009) 548–559.

[3] NATOLI, C. R., MISEMER, D. K., DONIACH, S., KUTZLER, F. W., First-principles calculation of X ray absorption-edge structure in molecular clusters, Phys. Rev. A **22** (1980) 19801104–8.

[4] BINSTED, N. (1998) EXCURV98: CCLRC Daresbury Laboratory Computer Program.

[5] FILIPPONI, A., Di CICCO, A., NATOLI, C. R., X ray Absorption Spectroscopy and n-Body Distribution Functions in Condensed Matter. I. Theory and II. Data Analysis and Applications, Phys. Rev. B **42** (1995) 15122–49.

[6] DE GROOT, F., Multiplet effects in X ray absorption, Coord. Chem. Rev. **249** (2005) 31-63.

[7] GONZE, X., AMADON, B., ANGLADE, P.-M., BEUKEN, J.-M., BOTTIN, F., BOULANGER, P., BRUNEVAL, F., CALISTE, D., CARACAS,R., COTE, M., DEUTSCH, T., GENOVESE, L., Abinit: first-principles approach to material and nanosystem properties, Comput. Phys. Commun. **180** (2009) 2582–615.

[8] GIANNOZZI, P., BARONI, S., BONINI, N., CALANDRA, M., CAR., R., CAVAZZONI, C., CERESOLI, D., CHIAROTTI, G.L., COCOCCINI, M., DABO, I., DAL CORSO, A., FABRIS, S., FRATESI, G., DE GIRONCOLI, S., GEBAUER, R., GERSTMANN, U., GOUGOUSSIS, C., KOKALJ, A., LAZZERI, M., MARTIN-SAMOS, L., MARZARI, N., MAURI, F., MAZZARELLO, R., PAOLINI, S., PASQUARELLO, A., PAULATTO, L., SBRACCIA, C., SCANDOLO, C., SCLAUZERO, G., SEITSONEN, A.P., SNOUGNOV, A., UMARI, P., WENTZCOVITCH, R.M., Quantum espresso: a modular and open-source software project for quantum simulations of materials, J. Phys.: Condens. Matter. **21** (2009) 395502-19.

[9] KRESSE, G., FURTHMLLER, J., Efficient iterative schemes for ab initio total-energy calculations using a plane-wave basis set, Phys. Rev. B **54** (1996) 11169-11186.

[10] BLAHA, P., SCHWARZ, K., LUITZ, J., WIEN 2k, Vienna University of Technology, Vienna, 1997. Improved and updated UNIX version of the original copyrighted WIEN code, published by P. Blaha, K. Schwarz, P. Sorantin, S. B. Trickey, Comput. Phys. Commun. 59 (1990) 399.

[11] STERN, E.A., Structural determination by X ray absorption, Contemp. Phys. **19** (1978) 239-310.

[12] KONINGSBERGER, D.C., PRINS, R., X ray absorption: principles and application techniques of EXAFS, SEXAFS and XANES, Wiley, New York (1988).

[13] NEWVILLE, M., IFEFFIT: interactive XAFS analysis and FEFF fitting, J. Synchrotron Radiat. **8** (2001) 322-324.

[14] RAVEL, B., NEWVILLE, M., ATHENA, ARTEMIS, HEPHAESTUS: data analysis for X ray absorption spectroscopy using IFEFFIT, J. Synchrotron Radiat. **12** (2005) 537-541.

[15] LEBEDEV, A., SLUCHINSKAYA, I., EXAFS study of the Influence of Impurities on the phase transition in GeTe, Ferroelectrics **298** (2004) 189-197.

[16] WANG, Z., BUNKER, B.A., X ray-absorption fine structure studies of PbS_xTe_{1-x} alloys: Ferroelectric phase transition induced by off-center ions, Phys. Rev. B **46** (1992) 11277-11283.

[17] RAVEL, B., COCKAYNE, E., NEWVILLE, M., RABE, K.M., Combined EXAFS and first-principles theory study of $Pb_{1-x}Ge_xTe$, Phys. Rev. B **60** (1999) 14632-14642.

[18] RADISAVLJEVIĆ, I., IVANOVIĆ, N., NOVAKOVIĆ, N., ROMČEVIĆ, N., MAHNKE, H.-E., Local structures in $Pb_{1-x}Mn_xTe$ systems, X ray Spectrom. **36** (2007) 150-157.

[19] RADISAVLJEVIĆ, I., IVANOVIĆ, N., NOVAKOVIĆ, N., ROMČEVIĆ, N., MAHNKE, H.-E., Mn K-edge XANES studies of $Pb_{1-x}Mn_xTe$ systems, International Conference on Electronic Materials, Sydney, Australia, 2008 (abstract).

[20] RADISAVLJEVIĆ, I., IVANOVIĆ, N., NOVAKOVIĆ, N., ROMČEVIĆ, N., MAHNKE, H.-E., "XANES studies of imperfections in lead telluride-based multi-component semiconductors", paper presented at Gordon Research Conferences-Defects in Semiconductors, New London, NH (USA), 2008.

[21] RADISAVLJEVIĆ, I., IVANOVIĆ, N., NOVAKOVIĆ, N., ROMČEVIĆ, N., MAHNKE, H.-E., Structural aspects of changes induced in PbTe by doping with Mn, In and Ga, in preparation.

[22] CROFT, M., SILLS, D., GREENBLATT, M., LEE, C., CHEONG, S.-W., RAMANUJACHARY, K.V., TRAN, D., Systematic Mn d-configuration change in the $La_{1-x}Ca_xMnO_3$ system: A Mn K-edge XAS study, Phys. Rev. B **55** (1997) 8726-8732.

[23] VOLKOV, B.A., RABOVA, L.I., KHOKHLOV, D.R., Mixed-valence impurities in lead telluride-based solid solutions, Phys. Usp. **45** (2002) 819-846.

[24] AHMAD, S., HOANG, K., MAHANTI, S.D., Ab-initio study of deep defect states in narrow band-gap semiconductors: Group III impurities in PbTe, Phys. Rev. Lett. **96** (2006) 056403-4.

[25] RADISAVLJEVIĆ, I., IVANOVIĆ, N., NOVAKOVIĆ, N., ROMČEVIĆ, N., MAHNKE, H.-E., XAFS studies of nickel-doped lead telluride, Physica B **404** (2009) 5032–5034.

[26] RADISAVLJEVIĆ, I., NOVAKOVIĆ, N., ROMČEVIĆ, N., MANASIJEVIĆ, M., MAHNKE, H.-E., IVANOVIĆ, N., XAFS studies of ytterbium doped lead-telluride, J. Alloys Compd. **501** (2010) 159-163.

[27] YAMAOKA, H., JARRIGE, I., TSUJII, N., IMAI, M., LIN, J.-F., MATSUNAMI, M., EGUCHI, R., ARITA, M., SHIMADA, K., Electronic structure of $YbGa_{1.15}Si_{0.85}$ and $YbGa_{xGe2-x}$ probed by resonant X ray emission and photoelectron spectroscopies, Phys. Rev. B **83** (2011) 104525-10.

[28] BALZAROTTI, A., MOTTA, N., KISIEL, A., ZIMNAL-STARNAWSKA, M., CZYŻYK, M. T., PODGÓRNY, M., Model of the local structure of random ternary alloys: Experiment versus theory, Phys. Rev. B **31** (1985) 7526-7539.

[29] PONG, W.-F., MAYANOVIC, R. A., BUNKER, B. A., FURDYNA, J. K., DEBSKA, U., Extended X ray-absorption fine-structure studies of $Zn_{1-x}Mn_xSe$ alloy structure, Phys. Rev. B **41** (1990) 8440-8448.

[30] WIEDMANN, M. R., GREGG, J. R., NEWMAN, K. E., Local structure in $Zn_{1-x}Mn_xSe$ alloys, J. Phys.: Condens. Matt. **4** (1992) 1895-1904.

[31] ISLAM, S. M., BUNKER, B. A., Studies of atomic correlations in quaternary semiconductor alloys using the extended X ray absorption fine structure technique, Phys. Lett. A **156** (1991) 247-252.

[32] ROBOUCH, B.V., KISIEL, A., EXAFS data resolved into individual site occupation preferences in quaternary compounds with tetrahedral coordinated structure, J. Alloys Compd. **286** (1999) 80–88.

[33] RADISAVLJEVIĆ, I., NOVAKOVIĆ, N., IVANOVIĆ, N., ROMČEVIĆ, N., MAHNKE, H.-E., Structural investigations of quaternary Fe-based ZnTeSe semiconductors, 17th International Microscopy Congress, Rio de Janeiro, Brazil (2010) CD-ROM.

[34] RADISAVLJEVIĆ, I., NOVAKOVIĆ, N., ROMČEVIĆ, N., MANASIJEVIĆ, M., MAHNKE, H.-E., IVANOVIĆ, N., Quaternary Fe-based Wide-gap Diluted Magnetic Semiconductors: Structural Investigations, HASYLAB Annual Report (2011).

[35] RADISAVLJEVIĆ, I., NOVAKOVIĆ, N., IVANOVIĆ, N., ROMČEVIĆ, N., MAHNKE, H.-E., Structural and electronic properties of quaternary CdTe-based diluted

magnetic semiconductors, Microscopy of Semiconducting Materials XVII, Cambridge, UK, 2011 (abstract).

[36] MYCIELSKI, M., ARCIESZEWSKA, M., DOBROWOLSKI, W., LUSAKOWSKI, A., DYBKO, K., SZYMACZAK, R., SZADKOWSKI, A., Fe-based semimagnetic semiconductors with two anions, Phys. Rev. B **53** (1996) 10732-10739.

[37] RADISAVLJEVIĆ, I. Local structure and electronic properties of transition metal ions (TM=Mn, Fe, Co) in wide gap diluted magnetic semiconductors, ELETTRA experimental report (2011).

[38] DE GROOT, F., VANKÓ, G., GLATZEL, P., The 1s X ray absorption pre-edge structures in transition metal oxides, J. Phys.: Condens. Matter **21** (2009) 104207-7.

[39] RADISAVLJEVIĆ, I., NOVAKOVIĆ, N., MAHNKE, H.-E., ROMČEVIĆ, N., PASKAŠ-MAMULA, B., MANASIJEVIĆ, M., IVANOVIĆ, N., Determination of iron charge state in quaternary diluted magnetic semiconductors, XVIII Symposium on Condensed Matter Physics, Belgrade, Serbia, 2011 (abstract).

ADVANCED MATERIALS INVESTIGATIONS THROUGH HIGH RESOLUTION X RAY SPECTROSCOPY AT STANFORD SYNCHROTRON RADIATION LIGHTSOURCE

D. SOKARAS
Stanford Synchrotron Radiation Lightsource, SLAC National Accelerator Laboratory,
Stanford University, USA
Email: dsokaras@slac.stanford.edu

On behalf of SLAC's Spectroscopy Group (D. Sokaras, D. Nordlund, T.-C. Weng, R. Alonso Mori, U. Bergmann)

Abstract

Reliable characterization of modern technological materials consists the key element for the long- and near-term progress for a wide range of scientific and technological fields. Materials characterization is related both with the chemical and the structural information that in many cases are strictly correlated through the description of the electronic structure. In this view, techniques able to sensitively probe the electronic structure are expected to have a very critical role on the progress of energy related science, physical chemistry, surface science, etc. X rays based spectroscopies implemented under appropriate experimental conditions can undoubtedly provide the required energy and momentum transfer information by exhibiting an adequate resolving power. The high brilliance X ray incident beams that nowadays are provided by wiggler or undulator beamlines at modern synchrotron radiation facilities allow the effective implementation of high-energy resolution X ray spectroscopy.

Here we present a state-of-the-art X ray Raman spectroscopy end-station recently developed, installed, and operated at the Stanford Synchrotron Radiation Lightsource (SSRL). The end-station consists of two multi-crystal Johann type spectrometers arranged on a Rowland circle of 1 m. The first one, positioned at the forward scattering angles (low-**q**), consists of 40 diced and spherically bended Si(110) crystals of 4 inches of diameter providing a large solid angle of detection as well as an overall energy resolution of about 270 meV at 6462.20 eV. The second spectrometer, consisting of 14 spherically bent Si(110) crystal analyzers, is positioned at the backward scattering angles (high-**q**) enabling the study of non-dipole transitions. These features, as exceed the specifications of the currently existing relevant instrumentation, are opening up new perspectives on the systematic implementation of this photon-in/photon-out hard X ray technique on emerging research of multidisciplinary scientific fields such as energy related sciences, material science, physical chemistry, etc.

1. INTRODUCTION

Soft X ray Absorption Spectroscopy (XAS) is an exceptional technique for the structural and chemical characterization of low-Z based systems. Up until today, an enormous amount of studies related to surface science, material science, physical chemistry, and many others, have been reported extensively [1]. Evidently C, O and N are the most studied elements due to their role of enormous importance and their rich chemistry as their electronic structure tends to get sensitively influenced by the local chemical environment. Through the symmetry-allowed core electrons excitation, the respective density of the lower unoccupied electronic states can be probed (i.e. σ^* and π^*) providing detailed information related to the bonds type and length with a sensitivity way below the Angstrom length-scale. Soft XAS can be realized through various detections modes; total electron yield (TEY) and total or partial fluorescence yield (PFY) are the most often employed ones. Although the fluorescence-based modes can result to an information depth of up to several hundreds of nanometers, while the TEY probes the very first few nanometers, soft XAS is in general a surface sensitive technique. Inner-shell electron energy loss spectroscopy (EELS) consists another technique of a very high sensitivity that can provide XAS equivalent information [2,3]. However, the very short elastic and inelastic scattering mean free path of energetic electrons restricts the required thickness of the appropriate samples in the nanometer regime. In both cases (XAS and EELS), the very strong interaction of the observables (soft X rays or electrons) within matter, as well as the required ultra-high vacuum (UHV) analysis environment are posing some significant limitations towards the study of various categories of samples.

It has been extensively demonstrated that X ray Raman Spectroscopy (XRS), consists an alternative hard X ray based technique that can extract soft-XAS alike information [4-13]. The great advantage of this hard X ray photon-in/photon-out technique is that provides soft X ray equivalent information while maintains the benefits of hard X ray spectroscopy, i.e., bulk sensitivity, none UHV limitation (extreme pressure/ temperature environments, flow tubes, furnaces, liquids, in-situ cells, etc...), minimization of radiation damage, etc. The main limitation that hampers the wide applicability of XRS is the very weak Raman cross section (in the order of a few barns) that consequently lead, in most of the cases, to a significantly broader energy resolution when compared to soft X ray based techniques, or EELS, in order for acceptable counting rates to be achieved. For optimizing the detected signal the implementation of hard X ray high energy resolution spectrometers with multiple crystal analyzers has been proposed and adopted [14]. During the last decade, various dedicated instruments based on Bragg-type crystal analyzers have been developed in various 3rd generation synchrotron radiation facilities [14-20]. Until recently, a pioneer 14-crystal analyzer spectrometer was developed and extensively applied for these purposes at Stanford Synchrotron Radiation Lightsource [21-24].

Here, we describe the novel X ray Raman spectroscopy end-station that was recently developed, installed and operated at the beamline 6-2 at Stanford Synchrotron Radiation Lightsource (SSRL) [25]. The experimental setup consist of two multicrystal high energy resolution X ray spectrometers leading to a wide solid angle of detection whereas providing at the same time a soft-XAS equivalent energy resolution. Further on, the spatial arrangement of the instruments enables also the implementation of XRS studies beyond the dipole approximation providing in this way insights to non-dipoled allowed electronic excitations (e.g. monopole, quadruple or octupole transitions). Some representative first applications of this, now on, operational end-station will be briefly presented and discussed.
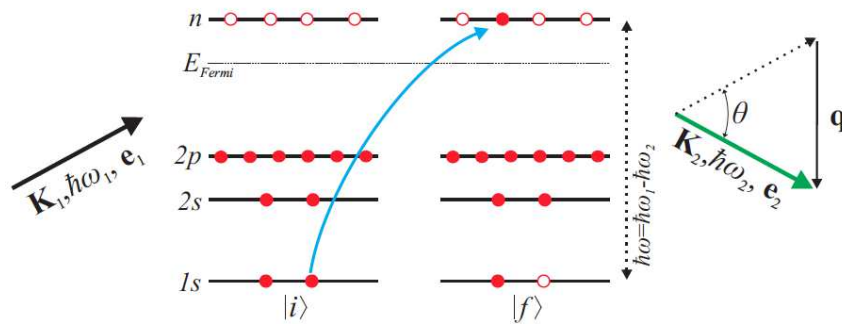

FIG. 1. A schematic representation of the X ray Raman scattering process. An high energy incident photon $\hbar\omega 1$ interacts with an atom being at the ground state ($|i>$) resulting on a core electron excitation ($|f>$) and an inelastically scattered photon, $\hbar\omega 2$. The figure is reproduced from [25].

2. TECHNICAL CONCEPT AND INSTRUMENTATION

The weak X ray Raman cross section demands a high intensity monochromaric X ray source as well as a large acceptance detection system in order for the X ray Raman spectroscopy to be efficiently realized. At the same time, for the spectral features to be resolved comparably to soft XAS, an overall energy resolution down to a few hundreds of meV is necessary. Third generation synchrotron radiation facilities incorporating wiggler or undulator insertion devices (ID), coupled with flat double crystal monochromators and the necessary collimating/focusing X ray optics (e.g. mirrors), consist ideal X ray sources as they provide the required flux (10^{12}-10^{13} photons/s) and monochromaticity (E/ΔE=35000). On the other hand, the divergently scattered X ray photons can be efficiently analyzed with an high

energy resolution by means of Bragg-type cylindrically or spherically bent crystal analyzers positioned over proper geometrical arrangements.

The X ray Raman end-station of SSRL is set at the 56-pole 0.9T Wiggler beamline 6-2 at the Stanford Synchrotron Radiation Lightsource. Beamline 6-2 is equipped with two liquid nitrogen cooled double crystal monochromator options, namely Si(111) (φ=0) and Si(311) (φ=0), while a collimating and a focusing Rh-coated mirror positioned before and after the monochromator, respectively, deliver highly monochromatic X ray photons within the energy range of about 4-18 keV. Under the present SPEAR3 storage ring operational conditions (electron energy of 3 GeV, current 350 mA at top-off mode) and through the Si(311) (Si(111)) monochromator, an incident beam flux of about 4×10^{12} photons/s (2×10^{13} photons/s) at 6.5 keV with an energy resolution of about 180 meV (850 meV) and a size of about \$100x400 μm^2 (vxh) is delivered at the sample position (~28 m from the source).

X ray Raman station consists of two Johann type X ray spectrometers in a Rowland geometry of 1 m of radius and are operating on a fixed Bragg angle. Both spectrometers are based on the multiple spherically bent analyzers concept positioned on intersecting Rowland circles. As the beamline's 6-2 vertical beam size (100μm) is narrower than the horizontal one (400μm), a vertical Rowland circle has been selected. In this way, the beam size contribution to the spectrometers energy resolution is minimized. Accounting the horizontal polarization of the incident beam, the polarization pre-factor of Raman cross section defines the maximum scattering intensity along the vertical plane. However, both spectrometers were selected to set on the storage ring plane instead. This selection, besides facilitating significantly the experiments and the sampling environments from a practical point of view, has also an important influence on the optimization of the energy resolution. More in specific, since for most of the samples a very shallow incident angle is selected, a relatively wide beam footprint is formed on the sample surface along the beam direction. Then, the effective beam size is defined as the projection of the irradiation area along the dispersion plane for each spectrometer. In this view, any spectrometer position away from the storage ring plane would gradually increase the projected beam size and consequently degrade the energy resolution. Detailed calculations based on both spectrometers geometry indicate that the overall loss of intensity due to the beamline's horizontal polarization (~85%) and the selected plane for the spectrometers is about 40%. At the same time an open option still remains the possibility to implement appropriate transmission elements in order to rotate the beam polarization by $\pi/2$.

The first spectrometer consist by 40-crystal analyzers arranged on a 8x5 stacking array that forms a 1m spherical segment and covers a solid angle of about 2.5% of 4π (Fig. 2). The spectrometer incorporates diced Si-110 spherically bent analyzers (NJ-XRS). Each diced crystal constitutes from several thousand spherically bent parquets of about 1x1 mm^2 bonded on a glass substrate and covering an overall active surface of about 75% within the 4 inches of the each crystal's overall diameter. The parquets of a diced crystal exhibit a significantly lower lattice deformation induced by the mechanical stretch applied for bending, when compared to the conventional spherically bent analyzers; in this way, a better performance in terms of energy resolution is expected. SLAC's metrology department examined a few arbitrary selected NJ-XRS diced crystals and confirmed that the optical surface for each 1x1mm^2 parquet maintains a bent curvature of 1 m along their overall surface with an accuracy of a few micrometers.
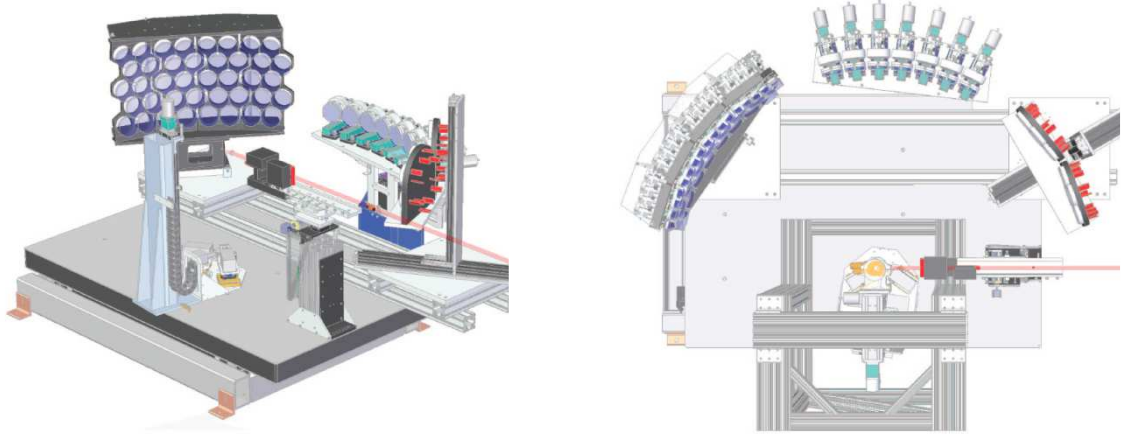
FIG 2. Three dimensional technical drawing of the high resolution X ray spectroscopy end-station at the beamline 6-2 at Stanford Synchrotron Radiation Lightsource (side perspective and top view). Besides the two X ray Raman spectrometers positioned along the forward and the backward scattering angles, the X ray emission/rixs spectrometer of beamline 6-2 is also depicted. The figure is reproduced from [25].

At the same time, the relative position of the parquets on the glass substrate lies on 1 m sphere with an accuracy of a few micrometers. This spectrometer is set along the forward scattering angles regime with its center lying at 40° in order to meet as much a possible the dipole approximation condition and thus to enable soft-XAS equivalent studies. On the other hand, the extended size of the spectrometer (that has an angular opening of about 50°) unavoidably is averaging out the information emitted along a relatively wide range of momentum transfers (for instance, for the Si(440) reflection, the spectrometer surface corresponds to momentum transfers within 0.4-1.7 a.u.). Nevertheless, the possibility to perform **q**-dependent measurements employing individual columns of the spectrometer is also feasible.

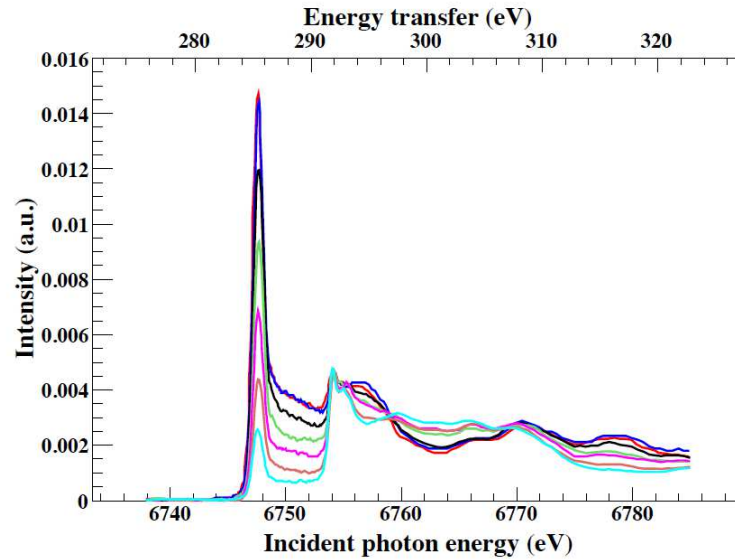*FIG. 3. Angular dependent X ray Raman spectra of the HPOG. When q transfer vector is perpendicular to the c - axis, a maximum π* to σ* ratio is observed (red curve); the ratio is gradually decreasing as the c -axis is changed with steps of 10° degrees. For comparison purposes all spectra are normalized at the sharpest σ* feature. The figure is reproduced from [25].*
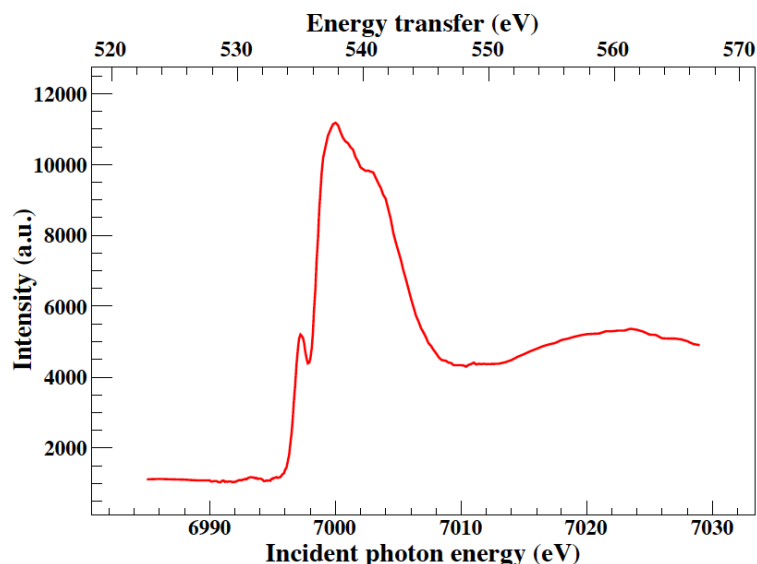
FIG. 4. X ray Raman scattering of Oxygen 1s electrons as measured on liquid water. The figure is reproduced from [25].

The second spectrometer, consisting by 14 crystal analyzers, is dedicated for the high-**q** transfer regime and thus positioned at the backward scattering angles enabling the study of non-dipole transitions. The 14 crystal analyzers are arranged on two 7-crystal arrays as seen on Fig 1. Currently, the spectrometer is using conventional spherically bend Si-110 crystals of 4 inches of diameter. The center of spectrometer is set at 145° and has an angular opening of about 40°; for the case of Si-440 crystal reflection the angular opening corresponds to momentum transfers in the range of 3.0-3.4 a.u. Both XRS spectrometers are designed to operate on a fixed analyzing angle (low-q at 88° and high-q at 87.2^o) as close as possible to 90° in order for the energy resolution to get optimized. The angle of 88° for a 1 m Rowland circle defines the minimum distance between detector and sample to be about 70 mm providing thus the required space to implement a wide variety of sample environments (cryostats, in-situ cells, diamond anvil cells, etc.). As the spectrometers are locked at given analyzing energy, beamline's monochromator is the scanning element enabling to acquire energy transfer measurements for an extended range along the absorption edge of interest (Fig. 4).

This, now on, standard experimental procedure adopted for inelastic X ray scattering measurements assures both a constant solid angle of detection and an overall efficiency of the spectrometer along the whole region of the energy scan. At the same time, in most of the cases any XRS cross section deviations as a function of the incident photon energy can be considered negligible since the relevant dependence is significantly slow; in a different case appropriate corrections for the cross section variation can be applied.

3. FIRST APPLICATIONS

In order to demonstrate some of the capabilities of the experimental station, a few representative examples of applications are presented below. In Fig. 3 a series of carbon 1s XRS spectra from highly oriented pyrolytic graphite (HPOG) sample are shown as obtained through the low-**q** 40 crystal spectrometer. The various spectra correspond to different angles of incidence for the incident beam with steps of 10° degrees. When the **c** –axis of the HPOG is perpendicular to the momentum transfer vector a maximum π* to σ* ratio is observed; on the other hand, as the **c** -axis orientation is changing with respect to the **q** vector this ratio is

gradually decreasing in favour of the σ* transition which dominates when the **c** -axis is approaching the q orientation.
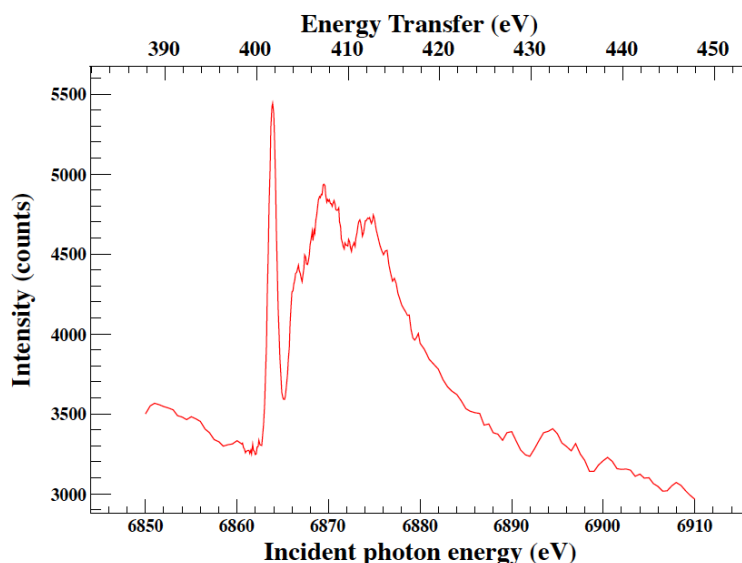

FIG. 5. Raw data of a Nitrogen X ray Raman spectrum measured on liquid dimethylformamide (DMF).

Further on, it's worth noting that the energy resolution permits to resolve in details the spectral features along the complex σ* region, as well as that the required measuring time for each of the spectra that is less than 5 min. In Fig. 4 and Fig. 5 an oxygen and nitrogen 1s spectrum is shown respectively as obtained from liquid phase samples (water and dimethylformamide, respectively).

4.   CONCLUSIONS

We described the X ray Raman spectroscopy end-station that was recently developed, installed, and operated at the Stanford Synchrotron Radiation Lightsource (SSRL). The apparatus consists of two Bragg-type multi-crystal Johann spectrometers arranged on a Rowland circle of 1 m. A large acceptance 40-crystal spectrometer is positioned along the low momentum transfer direction (forward scattering angles) providing in this way soft XAS alike information with a remarkable overall energy resolution of about 270 meV, after employing state-of-the-art diced Si(110) crystal analyzers. Concurrent, a second 14 crystal spectrometer positioned at the high-q regime (backward scattering angles) can provide further insights for electronic transitions beyond the dipole approximation. The large acceptance, as well as the high-energy resolution of this experimental station, overcomes some important limitations that used to hamper the wide applicability of the X ray Raman spectroscopy (i.e. very weak interaction cross sections and low energy resolution compared to the corresponding soft XAS based studies). These capabilities are expected to open up new directions on the applicability of this hard X ray photon-in/photon-out technique on various emerging scientific fields. Studies under extreme conditions (high temperature or/and high-pressure), aqueous or diluted samples as well as in-situ cells with various operational conditions can now on become feasible leading to an improved research related to new generation batteries, photovoltaic, hydrogen storage materials, etc. Further on, the continuous progress on the X ray optics technology as well as the availability of ultra-brilliance X ray sources like modern undulator radiation beamlines at state-of-the-art storage rings will boost further this technique to a wider range of application while may also enable extended X ray absorption fine structure (EXAFS) studies in short acquisition times. Moreover, the combination of such instrumentation with the

recent available X ray free electron laser sources (e.g. LCLS) is expected to provide further opportunities in the field of ultra-fast chemical dynamics.

ACKNOWLEDGMENTS

REFERENCES

[1] STOHR, J., NEXAFS Spectroscopy, Springer Series in Surface Sciences 25, Springer Verlag, Berlin, 1992.

[2] EGERTON, R.F., Electron energy-loss spectroscopy in the TEM, Rep. Prog. Phys. **72** (2009) 016502.

[3] EGERTON, R.F., Electron Energy Loss Spectroscopy in the Electron Microscope, Plenum, New York, 1996.

[4] SUZUKI, T., J. Phys. Soc. Jap. **22** (1967) 1139.

[5] SCHULKE, W., BERTHOLD, A., KAPROLAT, A., GUNTHERODT, H.-J., Evidence for interlayer band shifts upon lithium intercalation in graphite from inelastic X ray scattering, Phys. Rev. Lett. **60** (1988) 2217-2220.

[6] NAGASAWA, H., MOURIKIS, S., SCHULKE, W., J. Phys. Soc. Japan **58**, 710 (1988).

[7] TOHJI, K., UDAGAWA, Y., X ray raman scattering as a substitute for soft-X ray extended X ray-absorption fine structure, Phys. Rev. B **39** 11 (1989) 7590-7594.

[8] WATANABE, N., HAYASHI, H., UDAGAWA, Y., TAKESHITA, K., KAWATA, H., Anisotropy of hexagonal boron nitride core absorption spectra by X ray Raman spectroscopy, Appl. Phys. Lett. **69** (1996) 1370.

[9] MASCIOVECCHIO, C., BERGMANN, U., KRISCH, M., RUOCCO, G., SETTE, F., VERBINI, R., A perfect crystal X ray analyser with meV energy resolution, Nucl. Instr. Meth. B **111** (1996) 181-186.

[10] BERGMANN, U., GLATZEL, P., CRAMER, S.P., Bulk-sensitive XAS characterization of light elements: from X ray Raman scattering to X ray Raman spectroscopy, Microchem. J. **71** (2002) 221-230.

[11] TSE, J.S., SHAW, D.M., KLUG, D.D., PATCHKOVSKII, S., VANKO, G., MONACO, G., KRISCH, M., X ray raman spectroscopic study of water in condensed phases, Phys. Rev. Lett. **100** (2008) 095502.

[12] FISTER, T.T., FONG, D.D., EASTMAN, J.A., IDDIR, H., ZAPOL, P., FUOSS, P.H., BALASUBRAMANIAN, M., GORDON, R.A., BALASUBRAMANIAM, K.R., SALVADOR, P.A., Total-reflection inelastic X ray scattering from a 10-nm thick $La_{0.6}Sr_{0.4}CoO_3$ Thin Film, Phys. Rev. Lett. **106** (2011) 037401.

[13] HUOTARI, S., PYLKKANEN, T., VERBENI, R., MONACO, G., HAMALAINEN, K., Direct tomography with chemical-bond contrast, Nature Mater. **10** (2011) 489-493.

[14] BERGMANN, U., CRAMER, S.P., Proc. SPIE 3448, 198 (1998).

[15] KAO, C.C., HAMALAINEN, K., KRISCH, M., SIDDONS, D.P., OVERSLUIZEN, T., Optical design and performance of the inelastic scattering beamline at the national synchrotron light source, Rev. Sci. Instrum. **66** (1995) 1699.

[16] FISTER, T.T., SEIDLER, G.T., WHARTON, L., BATTLE, A.R., Ellis, T.B., CROSS, J.O., MACRANDER, A.T., ELAM, W.T., TYSON, T.A., QIAN, Q., A multielement spectrometer for efficient measurement of the momentum transfer dependence of inelastic X ray scattering, Rev. Sci. Instrum. **77** (2006) 063901.

[17] VERBENI, R., PYLKKANEN, T., HUOTARI, S., SIMONELLI, L., VANKO, G., MARTEL, K., HENRIQUET, C., MONACO, G., Multiple-element spectrometer for non-resonant inelastic X ray spectroscopy of electronic excitations, J. Synchrotron Rad. **16** (2009) 469-476.

[18] CAI, Y.Q., CHOW, P., CHEN, C.C., ISHII, H., TSANG, K.L., KAO, C.C., LIANG, K.S., CHEN, C.T., AIP Conf. Proc. 705 (2004) 340.

[19] HAZEMANN, J.-L., PROUX, O., NASSIF, V., PALANCHER, H., LAHERA, E., DA SILVA, C., BRAILLARD, A., TESTEMALE, D., DIOT, M.-A., ALLIOT, I., DEL NET, W., MANCEAU, A., GLBART, F., MORAND, M., DERMIGNY, Q., SHUKLA, A., J. Synchrotron Rad. **16** (2009) 283.

[20] HILL, J.P., COBURN, D.S., KIM, Y.-J., GOG, T., CASA, D.M., KODITUWAKKU, C.N., SINN, H., A 2 m inelastic X ray scattering spectrometer at CMC-XOR, advanced photon source, J. Synchrotron Rad. **14** (2007) 361-365.

[21] BERGMANN, U., DI CICCO, A., WERNET, Ph., PRINCIPI, E., GLATZEL, P., NILSSON, A., Nearest-neighbor oxygen distances in liquid water and ice observed by X ray Raman based extended X ray absorption fine structure, J. Chem. Phys. **127** (2007) 174504.

[22] BERGMANN, U., NORDLUND, D., WERNET, Ph., ODELIUS, M., PETTERSSON, L.G.M., NILSSON, A., Isotope effects in liquid water probed by X ray Raman spectroscopy, Phys. Rev. B **76** (2007) 024202.

[23] WALUYO, I., HUANG, C., NORDLUND, D., BERGMANN, U., WEISS, Th.M., PETTERSSON, L.G.M., NILSSON, A., The structure of water in the hydration shell of cations from X ray Raman and small angle X ray scattering measurements, J. Chem. Phys. **134** (2011) 064513.

[24] NILSSON, A., NORDLUND, D., WALUYO, I., HUANG, N., OGASAWARA, H., KAYA, S., BERGMANN, U., NASLUND, L.-A., OSTROM, H., WERNET, PH., ANDERSSON, K.J., SCHIROS, T., PETTERSSON, L.G.M., X ray absoption spectroscopy and X ray Raman scattering of water and ice; an experimental view, J. Electron Spectrosc. Relat. Phenom. **177** (2010) 99-129.

[25] SOKARAS, D., NORDLUND, D., WENG, T.-C., ALONSO MORI, R., VELIKOV, P., WENGER, D., GARACHTCHENKO, A., GEORGE, M., BORZENETS, V., JOHNSON, B., QIAN, Q., RABEDEAU, T., BERGMANN, U., A high resolution and large solid angle x-ray Raman spectroscopy end-station at the Stanford Synchrotron Radiation Lightsource, Review of Scientific Instruments 83, (2012) 043112-1.

DESIGN OF X RAY QUASI-MONOCHROMATIC SOURCE BASED ON ELECTROSTATIC PROTON ACCELERATOR

S.A. VERSHYNSKYI, I.O. BILOSHAPKA, O.M. BUHAY, V.L. DENYSENKO, V.E. STORIZHKO, M.I. ZAHARETS
Institute of Applied Physics of NAS
Sumy, Ukraine

Abstract

The microanalytical facility with a 2 μm resolution station based on an electrostatic accelerator available at the Institute of Applied Physics, is used to construct a high-intensity quasi-monochromatic X ray source. The X rays are produced by a proton beam focused by a doublet of electrostatic quadrupole lenses onto a converter. X ray focusing is performed by polycapillary lenses with a large solid angle and high integral transmission. As preliminary calculations show, 2 MeV proton beams provide the K-line yield similar to that obtained with 30 - 50 keV electron beams but with the bremsstrahlung background reduced by two orders of magnitude. Thus, filters or monochromators are practically unnecessary.

1. INTORDUCTION

The X ray techniques have been extensively used in various areas of science and technology. New synchrotron radiation sources (SRS) of the third generation allow a submicron resolution to be achieved while operating in the X ray range. However, the SRS's are very expensive and bulky, and thus not suitable for extensive use. In view of this circumstance considerable effort is presently being invested in the development of compact laboratory quasi-monochromatic X ray sources.

Among compact X ray sources are: X ray tubes, pyroelectric crystal based X ray generators [1, 2], compact accelerator based sources, radioactive sources, and plasma X ray sources [3, 4, 5, 6]. Using a liquid metal jet as a target it is possible to achieve the maximum beam power density greater by an order of magnitude than in present microfocus X ray tubes and the X ray source brightness of 10^{10} photons/(s·mm^2·mrad^2·0.1%BW) [7].

The pyroelectric crystal based X ray generators and plasma X ray sources generate a time-varying X ray flux, an X ray spectrum being polychromatic. In compact accelerator based sources use is made of transition radiation from cyclic accelerators [8], ion-induced excitation [9], and inverse Compton scattering [10, 11, 12, 13] to generate the X rays.

X ray sources with electron excitation (X ray tubes, sources like MIRRORCLE) are characterized by a high level of bremsstrahlung that may be lowered (using filters or monochromators) at the cost of reduced intensity.

Radiation from generators with a pyroelectric crystal and plasma X ray sources requires monochromatisation, too. Meanwhile proton beams with energy of 2 MeV provide the *K*-line yield similar to that obtained with 30 - 50 keV electron beams (see Table 1) but with the bremsstrahlung background reduced by two orders of magnitude [14]. Thus in [15] a proton beam with energy of 10-38 MeV and a circular spot of about 20 mm^2 generated by a cyclotron was incident onto a fixed water-cooled converter. In [16] a proton beam was focused by a quadruplet of electrostatic quadrupole lenses (EQL) at a Ti converter producing an effective focal spot of about 50×50 micron. Then a zone plate was used to form a 5 μm dia X ray beam with a flux of 5-10 photons/s.
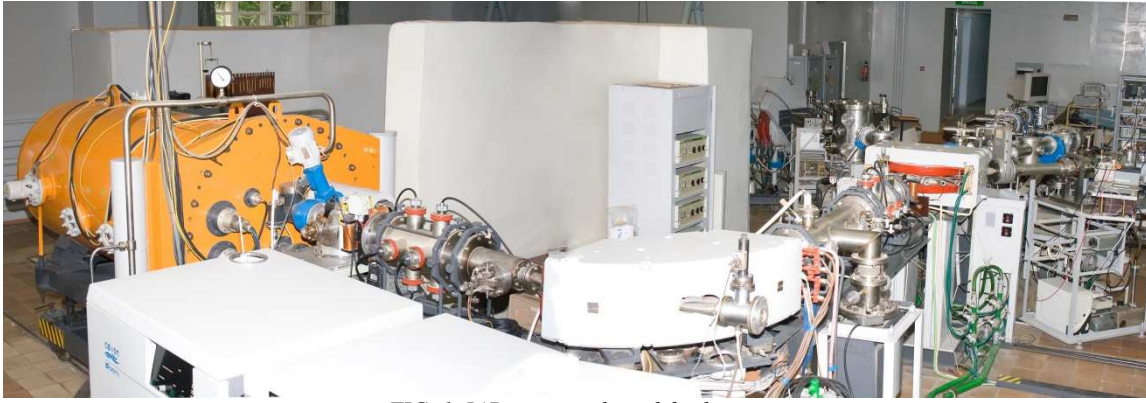
FIG. 1. IAP microanalytical facility

It should be mentioned that in [16] a source operates at 1.8 MeV proton beam energy while at higher energies the background is increased and defined mainly by nuclear reactions. In [15] nuclear reactions strongly interfere with the X ray fluorescence (XRF) measurements.

At the Institute of Applied Physics of NAS of Ukraine (IAP NASU) work is currently under way on production of MeV proton beams of micron diameter. A microanalytical facility of the IAP NASU [17] with a 2 μm nuclear microprobe [18] shown in Fig. 1 permits an X ray source to be constructed with features comparable to [16].

This work describes the first measurements performed with a prototype X ray quasimonochromatic source based on the IAP NASU microanalytical facility [17].

2. CALCULATION OF THE PROTON-INDUCED X RAY YIELD

As is known [19], the yield of X ray photons from the thin target is described by

$$dN = \omega\sigma(E)\frac{dE}{S(E)}N_p\varepsilon\frac{d\Omega}{4\pi}\exp\left(-\mu\frac{\cos\alpha}{\cos\beta}\int_{E_0}^{E}\frac{dE'}{S(E')}\right),\qquad(1)$$

where S(E) is the stopping power of the target material, measured in 10-15 eV·cm2/atom; ω is the fluorescence yield; σ(E) is the ionization cross section for the proton energy E; Np is the number of protons; ε and dΩ are the efficiency and the solid angle of the detector, respectively; μ is the linear attenuation coefficient; α and β are the angles between the normal to the target and the directions of a proton and an X ray photon, respectively; E0 is the proton initial energy.

The yield from a thick target (see Eq. 2) is determined by the integration (1). It should be taken into account that there is certain minimal proton energy EF which is still sufficient for a proton to ionize a target atom.

The photon yield from the thick target is

$$N(E_0) = \frac{\varepsilon\omega I}{4\pi e}\int_{E_0}^{E_F}\frac{\sigma(E)}{S(E)}\exp\left(-\mu\frac{\cos\alpha}{\cos\beta}\int_{E_0}^{E}\frac{dE'}{S(E')}\right)dE \quad \left[\frac{photons}{s\cdot sr}\right],\qquad(2)$$

where e is the electron charge; I is the proton beam current.

Differential ionization cross sections σ calculated within the ECPSSR theory were taken from [20, 21]. The calculated yields for electron and ion excitation of X rays are presented in Table 1.

TABLE 1. COMPARISON OF PHOTON YIELDS FROM ELECTRON AND PROTON BEAMS [9].

Yield, photons/particle/sr	Protons		Electrons	
	1 MeV	2 MeV	30 keV	40 keV
Y(Cu)	$0.10 \cdot 10^{-4}$	$1.66 \cdot 10^{-4}$	$1.26 \cdot 10^{-4}$	$2.6 \cdot 10^{-4}$
Y(Ti)	$0.85 \cdot 10^{-4}$	$8.10 \cdot 10^{-4}$	$3.70 \cdot 10^{-4}$	$5.55 \cdot 10^{-4}$

As can be seen from the above table, a 2 MeV proton accelerator provides a similar yield to that of X ray tubes.

It is seen from Fig. 2 that the calculations performed in this study are in good agreement with the results presented in [15].

The calculations show that in order to construct a laboratory source of quasimonochromatic X rays it will suffice to use an accelerator with beam energies below the threshold of a nuclear reaction with a neutron yield. Calculations of the X ray yield as a function of α and β angles were performed to find the ways for improvement of the source parameters (Fig. 3) using a self-developed computer program.

When a proton beam impinges on a converter at an α angle smaller than 90 degrees, the absorption of the X rays is less because the path of photons in the target material in the β direction is shorter in comparison with that for the normal incidence of the proton beam onto the converter.

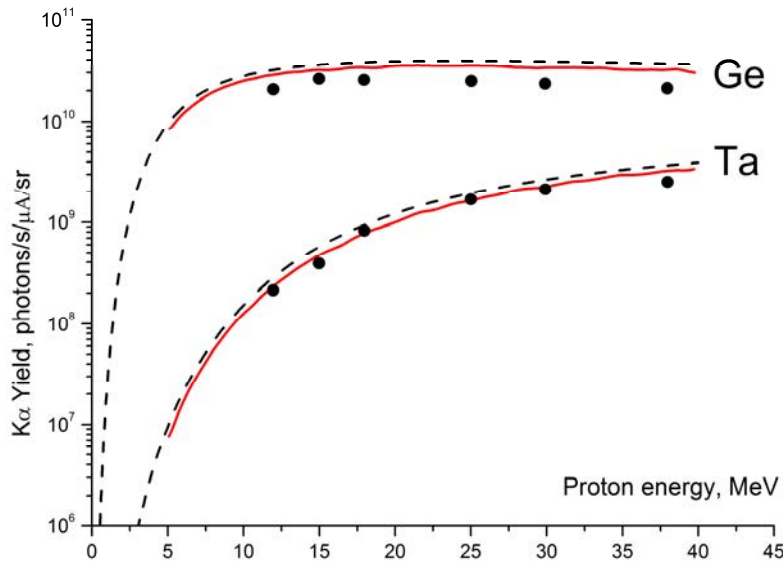*FIG. 2. Experimental (dots, from[15]) and calculated (dashed – this work, red line – from [15]) Kα X ray yields for Ta and Ge as a function of proton energy. The uncertainties on the experimental data are within the dot size.*

From the calculations performed the following conclusion can be derived: for increasing the X ray flux entering the X ray optical system the α angle should be a little smaller than 90 degrees (an angle between the proton beam and converter surface is small) and the β angle should be about 0 degrees (normal to the converter surface).

Note that an effective area of X rays generation seen by the X ray optical system is changed as a function of the α angle (between the normal to the target and the ion beam axis) and the β angle (between the normal to the target and the axis of the X ray optical system).

For effective capture of the X rays by the optical system (in the case of using a polycapillary optics for this purpose the effective focal spot size in the β direction should not exceed a certain value) it is necessary to find a relation between such parameters as α and β, X ray flux from the target and that from the X ray optical system, and the X ray spot size.

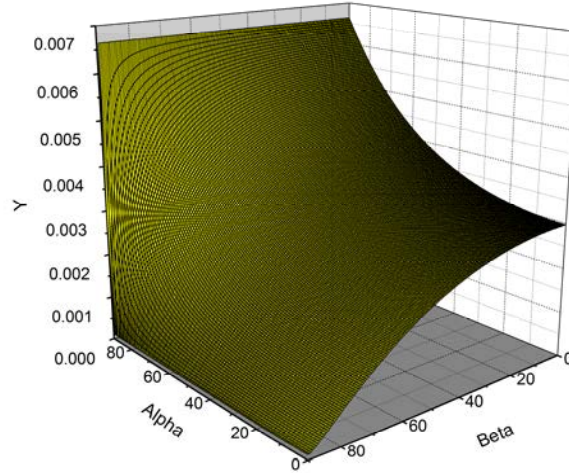*FIG. 3. X ray yield Y as a function of α and β angles. Yield is in photons/(proton·sr); α and β are in degrees.*

Additional research is necessary to select satisfactory values for the above mentioned parameters.

3. DESCRIPTION OF THE SOURCE PROTOTYPE

A prototype X ray quasimonochromatic source based on the IAP NASU microanalytical facility [17] is shown in Fig. 4.

A target unit (Fig. 5) is fixed on a flange of the accelerator ion guide. A beam passes along the axis of the target unit and impinges on the copper water-cooled converter at an angle of 45°. X rays are registered at an angle of 90° to the proton beam direction. The converter can be moved to and fro along the beam axis and turned round (fixation is provided by three hold-down screws and three draw bolts) without disturbing the vacuum. When the converter is rotated through 180 degrees the beam impinges on its other opposite side with a plate made of different material. This allows the X ray energy to be varied without disturbing the vacuum. On the cylinder side an X ray detector or X ray lens (which can be tilted and shifted as a whole along the X and the Y axes) can be mounted. In this case the X ray detector is placed behind the lens.

FIG. 4. Prototype X ray quasimonochromatic source based on the electrostatic accelerator:1 ion-beam accelerator "SOKIL"; 2 doublet of EQL; 3 entrance slit of analyzing magnet with its chamber; 4 analyzing magnet MA-90-500; 5 X ray source target unit.
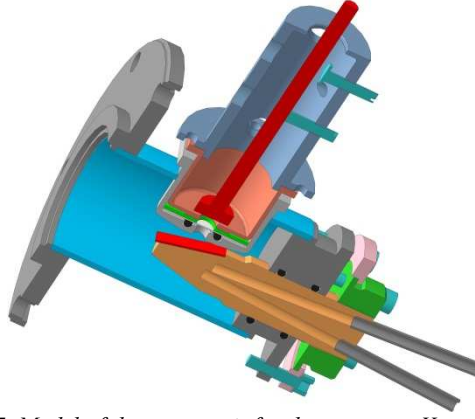
FIG. 5. Model of the target unit for the prototype X ray source.

4. ION OPTICS MODELLING FOR THE X RAY SOURCE

For a focal spot to be reduced the source is equipped with a doublet of two EQL whose focusing properties are independent of the charge-to-mass ratio. This permits all ion species present in the accelerator-produced beam to be involved in X ray generation.

For the ion-beam energy ε_0 from the accelerator of several MeV the dynamics of the beam in electrostatic ion-optical systems is described with sufficient accuracy by non-relativistic equations of motion:

$$x'' = \frac{1}{2[u_0(1+\delta) - u(x,y,z)]}(E_x - x'E_z)(1 + x'^2 + y'^2),$$ (3)

$$y'' = \frac{1}{2[u_0(1+\delta) - u(x,y,z)]}(E_y - y'E_z)(1 + x'^2 + y'^2)$$

with initial conditions

$$x(z_0) = x_0, x'(z_0) = x'_0, y(z_0) = y_0, y'(z_0) = y'_0,$$ (4)

where u_0 is the potential at the high-voltage terminal of the electrostatic accelerator; δ is the relative deviation of the particle energy from the average value $\delta = (\varepsilon - \varepsilon_0)/\varepsilon_0$; $u(x,y,z)$ is the EQL potential; E_x, E_y, E_z are the components of the electric field strength; x, y are the ion displacements in the xoz and yoz planes, respectively; x', y' are the ion trajectories in the xoz and yoz planes, respectively; Z-axis is aligned with the beam axis.

The proton beam space charge has to be taken into account for perveance $Q > 4 \cdot 10^{-7} \frac{A}{V^{3/2}}$ [22]. As the beam current in electrostatic accelerators for energy of several MeV reaches 1 mA, the space charge is not included in equations (3) since perveance $Q \approx 10^{-13} \frac{A}{V^{3/2}}$.

The approximate solution of the Cauchy problem for equations (3) with initial conditions (4) is sought for as a conversion of the initial phase coordinates from the object plane (x_0, x'_0, y_0, y'_0) into the target plane (x_t, y_t)

$$x_t = x_0/D_x(\boldsymbol{\tau}) + C_{px}(\boldsymbol{\tau})x_0'\delta + \sum_{\substack{i,j \\ i+j=3}} \left\langle x/x_0'^i y_0'^j \right\rangle(\boldsymbol{\tau})x_0'^i y_0'^j , \qquad (5)$$

$$y_t = y_0/D_y(\boldsymbol{\tau}) + C_{py}(\boldsymbol{\tau})y_0'\delta + \sum_{\substack{i,j \\ i+j=3}} \left\langle y/x_0'^i y_0'^j \right\rangle(\boldsymbol{\tau})x_0'^i y_0'^j$$

where $D_x(\boldsymbol{\tau})$ and $D_y(\boldsymbol{\tau})$ are the demagnifications along the x and the y axis, respectively; $C_{px}(\boldsymbol{\tau})$ and $C_{py}(\boldsymbol{\tau})$ are the chromatic aberration coefficients; $\left\langle x/x_0'^i y_0'^j \right\rangle(\boldsymbol{\tau})$, $\left\langle y/x_0'^i y_0'^j \right\rangle(\boldsymbol{\tau})$ are the spherical aberration coefficients.

All aberration coefficients in equation (5) depend on the vector $\boldsymbol{\tau} = (a, \lambda, g, L_{eff}, r_a)^T$ defining the ion-optical system parameters, where a is the distance between the object plane and the effective field boundary of the first lens; λ is the distance between the effective field boundaries of the lenses; g is the working distance (drift space between the effective field boundary of the last lens and the image plane); L_{eff} is the effective length of the lenses, and r_a is the lens aperture radius.

To calculate the coefficients of demagnifications and aberrations that specify the ion-optical system parameters a method of matrizants was used [23] which was implemented in the PROBFORM computer program [24].
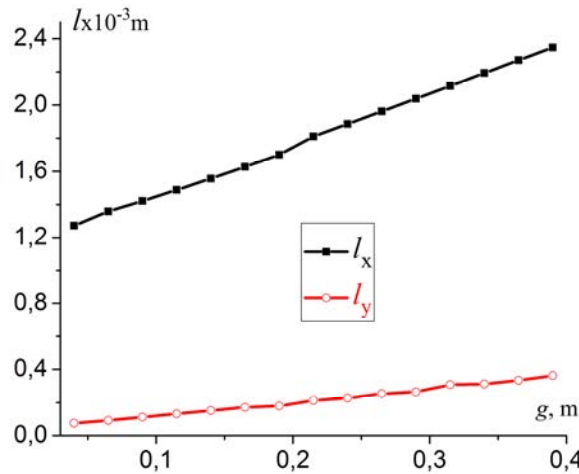

FIG. 6. Ion spot size on the converter along mutually perpendicular X and Y axes (l_x, l_y) as a function of the working distance for the EQL doublet.

When estimating a spot size the quantity of beam particles impinging on the converter area $l_x \times l_y$, should not be less than 80% [25]. Initial parameters of the particles were obtained from the measured emittance of the beam produced by the microanalytical facility [17].

The calculations show (Fig. 6) that in order to obtain smaller ion spot sizes the working distance in the facility should be as small as possible.

Choice of an X ray optical system for the X ray source
For the interaction of X rays with solid the index of refraction n is [26]:
$$n = 1 - \delta - i\beta \qquad (6)$$
$$\delta = \frac{N_a}{2\pi} r_0 \lambda^2 \rho \frac{Z + f'}{A}$$
$$\beta = \lambda\mu/4\pi$$

where N_a is Avogadro's number, r_0 is the classical electron radius, λ is the photon wavelength, ρ is the density of the material; $Z + f'$ is the real part of the atomic scattering factor including the dispersion correction f', A is the atomic mass, μ is the linear coefficient of attenuation.

X ray sources can be divided into three groups [27]:

refractive optics;
diffractive (crystals, zone plates, and gratings) and interference (multilayers) optics;
reflective optics.

The focal length (f) of a refractive lens with the parabolic profile $s^2 = 2Rw$ is given by eq. 8 [28]

$$f = \left(\frac{R}{2}\right)\Big/(n-1)$$

(7)

As δ is of the 10^{-4} order (for X ray quanta energy of 1.24 keV), the real part of the index of refraction is a little less than 1 (eq. 6). It means that a focussing X ray lens must be of concave shape and the focal distance of the lens is rather long (eq. 7). For the focal distance to be reduced an entrance aperture of the lens is made as small as possible and compound lenses with many refractive surfaces are used [29]. Also, X ray absorption in the material is of vital importance for refractive lenses. Thus, these lenses are more suitable for a synchrotron with its narrow X ray beams than for an X ray source with ion excitation[30].

Optical elements operating on interference basis consist of layers of materials with different dielectric permittivity. As X ray reflection from the layers is small, many layers with radiation in phase are applied for higher operation efficiency of such optical elements.

The principle of operation for zone plates and gratings is not different from that for the optical elements of visible light [27]. Manufacturing of a modern zone plate is a rather complicated engineering task. It should be mentioned that the first diffraction order in the zone plate gives the highest focused intensity, but even so, it is only about 10% efficient [30]. Optics of this type allows X ray microbeams of smaller spot size to be obtained in comparison with that for polycapillary optics.

Optical elements operating on interference and diffraction basis are all wavelength selective [30] . For incident angles less than the critical angle θ_c (eq. 8) the X rays are totally externally reflected from the surface.

$$\theta_c = \sqrt{\delta} \ ,$$

(8)

which is obtained from Snell's law.

The angle θ_c is small but the use of the curved capillary in which X rays are reflected multiple times from the inner capillary surface permits the X rays to be bent at a large angle.

The polycapillary optics is an array of a large number of small hollow bent glass tubes that is used for effective capturing of X rays from the given area. Note that a considerably higher X ray flux may be obtained in a spot with polycapillary optics than with zone plates. It

is known that such optics is characterized by a large solid angle of X ray [31] and high transmission (maybe over 50%) [30]; all that has determined the choice of polycapillary optics for the X ray quasi-monochromatic source based on the electrostatic accelerator.

5.   MEASUREMENTS ON THE PROTOTYPE X RAY QUASIMONOCHROMATIC SOURCE

A semiconductor X ray detector is placed in vacuum and is shielded by an absorbing foil to be protected from secondary and scattered particles.

The X ray spectrum from the prototype source (Fig. 7) was recorded with the collected charge of 10 µC; beam energy of 1.5 MeV. To construct an X ray source with a small-sized focal spot and high intensity two tasks should be solved: ion beam focusing and X ray focusing. These tasks would be handled in the prototype X ray source.

The X ray source with ion excitation comprises an ion source (electrostatic accelerator of the IAP NASU), ion-optical system, converters (targets generating the X rays), and X ray optical system. Matching of parameters of all the components is essential for the required characteristics to be obtained.
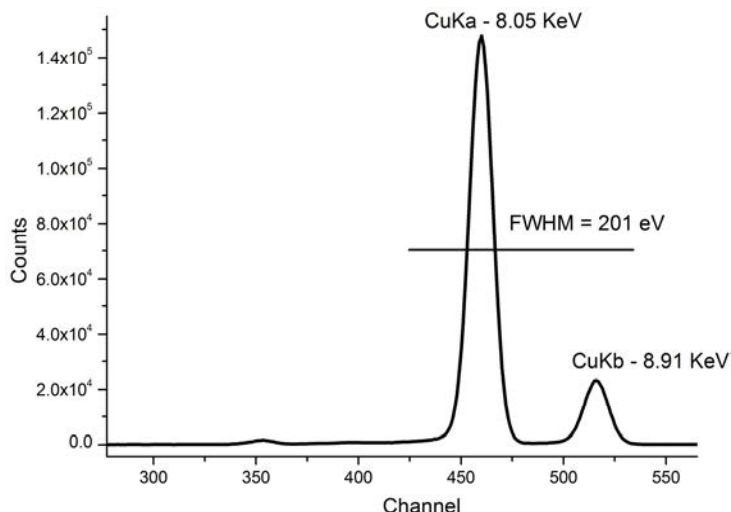

FIG. 7. X ray spectrum from a prototype source at 1.5 MeV proton beam energy.

The ion beam from the electrostatic accelerator passes through the ion-optical system and reaches a converter, generating quasimonochromatic X rays from a spot of certain size. Then the X rays pass through the X ray optical system to produce an X ray microbeam. In a polycapillary lens used as an X ray optical system, an effective focal spot size must be taken into account. This parameter has to be matched to the size of the radiation generating area on the converter. The latter size in turn depends on the emittance of the ion beam and on parameters of the ion-optical system.

6.   CONCLUSIONS

A prototype X ray quasimonochromatic source based on a 2 MeV electrostatic accelerator has been designed and constructed at the Institute of Applied Physics NASU. Proton beam focusing is performed by a doublet of electrostatic quadrupole lenses. X ray focusing is performed by a polycapillary lens positioned between the X ray generating target and an Amptek SDD detector. The K-yields calculated for Ti and Cu targets for 1.0-2.0 MeV

proton beam energy are in good agreement with experimental data [32]. The prototype X ray quasimonochromatic source is intended to be used in the investigations of radiation effects on single cells.

ACKNOWLEDGMENTS

REFERENCES

[1]   BROWNRIDGE, J.D., RABOY, S., Investigations of pyroelectric generation of X rays, J. Appl. Phys. **86** (1999) 640.

[2]   NAGAYCHENKO, V.I., SANIN, V.M., YEGOROV, A.M. SHCHAGIN, A.V., Spectra of pyroelectric X ray generator, Problems of atomic science and technology **2** (2004) 214.

[3]   RYMELL, U., MALMQVIST, L., BERGLUND, M., HERTZ, H.M., Liquid-jet target laser-plasma sources for EUV and X ray lithography, Microelectronic Engineering **46** (1999) 453.

[4]   YAMAGUCHI, N., TAKEMURA, Y., SHOYAMA, H., HARA, T., "Laser-plasma X ray source using ceramic target" (Proc. 8th Int. Conf. X ray Microscopy, Himeji City, Japan, 2005) 140-142.

[5]   FIEDOROWICZ, H., BARTNIK, A., SZCZUREK, M., DAIDO, H., SAKAYA, N., KMETIK, V., KATO, Y., SUZUKI, M., MASAI, Investigation of soft X ray emission from a gas puff target irradiated with a Nd:YAG Laser, Opt. Comm. **163** (1999) 103.

[6]   KANTSYREV, V.L., RUDAKOV, L.I., SAFRONOVA, A.S., ESAULOV, A.A., C HUVATIN, A.S., COVERDALE. C.A., DEENEY, C., WILLIAMSON, K.M., YILMAZ, M.F., SHRESTHA, I., OUART, N.D., OSOBORNE, G.C., Double planar wire array as a compact plasma radiation source, Phys. Plasmas **15** (2008) 030704.

[7]   OTENDAL, M., TUOHIMAA, T., VOGT, U., HERTZ, H.M., A 9 keV electron-impact liquid-gallium-jet X ray source, Rev. Sci. Instrum. **79** (2008) 016102.

[8]   HIRAI, T., YAMADA, H., SASAKI, M., HASEGAWA, D., MORITA, M., ODA, Y., TAKAKU, J., HANASHIMA, T., NITTA, N., TAKAHASHI, M., MURATA, K., Refraction contrast 11×-magnified X ray imaging of large objects by MIRRORCLE-type table-top synchrotron, J. Synchrotron Radiat. **13** (2006) 397.

[9]   SHABEL'NIKOV L.G., DENYSENKO V.L., ILJASHENKO M.V., STORIZHKO V.E., DROZDENKO A.A., VERSHYNSKYI S.A., Project of X ray quasi-monochromatic source on basis of proton-beam accelerator, supplied with the X ray focusing optical system, Metallofiz. Noveishie Tekhnol. **32** (2010) 1 (in Russian).

[10] GLADKIKH, P., KARNAUKOV, I., MYSTYKOV, A., SKYDRA, V., ZELINSKY, A., NESTOR facility injection conception, Problems of atomic science and technology **3** (2011) 75.

[11] KASHIWAGI, S., HAM, Y., ISHIKAWA, H., KAWAI, H., KURODA, R., MAEDA, K., NAGASAWA, H., OSHIMA, T., "Experiment of soft X ray generations using inverse Compton scattering at Waseda University" (Proc. of EPAC, Paris, France, 2002) 694-697.

[12] CHEN, J.G., XU, W., GUO, W., MA, Y.G. CAI, X.Z., WANG, H.W., LU, G.C., XU, Y., WANG, C.B., PAN, Q.Y., YUAN, R.Y., XU, J.Q., WEI, Z.Y., YAN, Z., SHEN, W.Q., An X ray source based on Compton backscattering of CO_2 laser and 100 MeV electrons, Nucl. Instrum. Meth. A **580** (2007) 1184.

[13] PARK, S. H., CHA, Y., JEONG, Y.U., LEE, B.C., LEE, K., "Compton X ray generation at the KAERI SC RF LINAC" (Proc. of the 27th International Free Electron Laser Conference, Stanford, California, 2005), 495.

[14] FOLKMANN, F., GAARDE, C., HUUS, T., KEMP, K., Proton induced X ray emission as a tool for trace element analysis, Nucl. Instrum. Meth. **116** (1974) 487.

[15] AVALDI, L., BASSI, S., CASTILGLIONI, M., MILAZZO, M., SILARI, B., WECKERMANN, B., Experimental results from high-intensity sources of monochromatic X rays generated by 10-38 MeV protons, Nucl. Instrum. Meth. A **299** (1990) 240.

[16] HARKEN, A.D., RANDERS-PEHRSON, G., JOHNSON, G.W., BRENNER, D.J., The Columbia University proton-induced soft X ray microbeam, Nucl. Instrum. Meth. B **269** (2011) 1992.

[17] STORIZHKO, V.E., DROZDENKO, A.A., MIROSHNICHENKO, V.I., PONOMAREV, A.G., "The microanalitical facility on the base of the compact electrostatic accelerator of IAP NAS of Ukraine" (Proc. Int. Conf. Current Problems Nucl. Phys. At. Energy, Kyiv, Ukraine, 2006) 745-753 (in Russian).

[18] STORIZHKO, V.E., PONOMAREV, A.G., REBROV, V.A., CHEMERIS, A.I., DROZDENKO, A.A., DUDNIK, A.B., MIROSHNICHENKO, V.I., SAYKO, N.A., PAVLENKO, P.A., The Sumy scanning nuclear microprobe: Design features and first tests, Nucl. Instrum. Meth. **260** (2007) 49.

[19] CAMPBELL, J.L., JOHANSSON, S.A.E., MALMQVIST, K.G.., Particle-induced X ray emission spectrometry (PIXE), Wiley-Interscience, New York (1995).

[20] COHEN, D.D., HARRIGAN, M., K- and L-shell ionization cross sections for protons and helium ions calculated in the ECPSSR theory, Atom. Data Nucl. Data **33** (1985) 255.

[21] PIA,. M.G., WEIDENSPOINTNER, G., AUGELLI, M., QUINTIERI, L., SARACCO, P., SUDHAKAR, M., YOGLAUER, A., PIXE simulation with Geant4, IEEE Trans. Nucl. Sci. **56** (2009) 3614-3649.

[22] SZILAGYI, M., Electron and ion optics, Plenum Press, New York and London (1988).

[23] DYMNIKOV, A.D., OSETINSKY, G.M., Forming systems of micron size proton beams, Physics of Elementary Particles and Atomic Nuclei **20** (1989) (in Russian) 694.

[24] PONOMAREV, A.G., et al., Parametric multiplets of magnetic quadrupole lenses: application prospects for probe-forming systems of nuclear microprobe, Nucl. Instrum. Meth. B **231** (2005) 86.

[25] VERSHYNSKYI, S.O., PONOMAREV., O.G., STORIZHKO, V.YU., DENYSENKO, V.L., ILJASHENKO, M.V., Optimization of ion-optics system for X ray quasi-monochromatic source on the basis of electrostatic accelerator, Nuclear Physics and Atomic Energy **11** (2010) (in Russian) 195.

[26] JAMES, R. W., The Optical Principles of the Diffraction of X rays, Cornell University Press, Ithaca, NY, (1965).

[27] DABAGOV, S.B., Channeling of neutral particles in micro- and nanocapillaries, Physics-Uspekhi **46** (2003) (in Russian) 1053.

[28] LENGELER, B., SCHROER, C., TUEMMLER, J., BENNER, B., RICHWIN, M., SNIGIREV, A., SNIGIREVA, I., DRAKOPOULOS, M., Imaging by parabolic refractive lenses in the hard X ray range, J. Synchrotron Rad. **6** (1999) 1153.

[29] SNIGIREV, A., KOHN, V., SNIGIREVA, I., SOUVOROV, A., LENGELER, B., Focusing high-energy X rays by compound refractive lenses, Appl. Optics **37** (1998) 653.

[30] "Handbook of Optics: Volume III Classical Optics, Vision Optics, X ray Optics" 2nd edn (BASS, M. Ed.) Mcgraw-hill Professional Publishing (2000) ISBN: 0071449310.

[31] KUMAKHOV, M.A., Capillary optics and their use in X ray analysis, X ray Spectrom. **29** (2000) 343.

[32] LOPES, J.S., JESUS, A.P., FERREIRA, F.B.G., X ray production in Ca, Sc, Ti, V, Cr, Mn and Fe by protons of 0.5–2 MeV energy, J. Phys B-At. Mol. Phys. **11** (1978) 2181

CONTRIBUTORS TO DRAFTING AND REVIEW

The report summarizes the results of discussions held on the aforementioned topics by the participants of a Technical meeting on Applications of Synchrotron radiation sources for Compositional and Structural Characterization of Objects in Cultural Heritage, Forensics and Materials Science (Vienna, Austria, October 17-21, 2011). Contributions to the drafting of this report were made by:

Cultural Heritage/Forensics Working Group

Prof Janssens, Koen	University of Antwerp, Belgium
Dr Bertrand, Loic	IPANEMA, Synchrotron SOLEIL, France
Dr Cotte, Marine	ESRF, Grenoble, France
Dr Dias, M. Isabel	InstitutoTechnologico Nuclear, Sacavem, Portugal
Dr Klysubun, Wantana	SLRI, Thailand
Dr Kempson, Ivan	University of South Australia, Australia

Materials Science Working Group

Prof Dr Streli, Christina	TU - Vienna, Austria
Dr Fu, Yanan	SSRF, Peoples Republic of China
Dr Beckhoff, Burkhard	PTB, Germany
Dr Menk, Ralf Hendrik	Sincrotrone Trieste, Italy
Dr Deb, Sudip	Indus, India
Dr Radisavljevic, Ivana	University of Belgrade, Serbia
Dr Sokaras, Dimosthenis	SLAC, USA
Prof Dr Storizhko, Volodymyr	University of Kiew, Ukraine

IAEA
International Atomic Energy Agency

ORDERING LOCALLY

In the following countries, IAEA priced publications may be purchased from the sources listed below or from major local booksellers.

Orders for unpriced publications should be made directly to the IAEA. The contact details are given at the end of this list.

BELGIUM
Jean de Lannoy
Avenue du Roi 202, 1190 Brussels, BELGIUM
Telephone: +32 2 5384 308 • Fax: +32 2 5380 841
Email: jean.de.lannoy@euronet.be • Web site: http://www.jean-de-lannoy.be

CANADA
Renouf Publishing Co. Ltd.
22-1010 Polytek Street, Ottawa, ON K1J 9J1, CANADA
Telephone: +1 613 745 2665 • Fax: +1 643 745 7660
Email: order@renoufbooks.com • Web site: http://www.renoufbooks.com

Bernan Associates
4501 Forbes Blvd., Suite 200, Lanham, MD 20706-4391, USA
Telephone: +1 800 865 3457 • Fax: +1 800 865 3450
Email: orders@bernan.com • Web site: http://www.bernan.com

CZECH REPUBLIC
Suweco CZ, s.r.o.
SESTUPNÁ 153/11, 162 00 Prague 6, CZECH REPUBLIC
Telephone: +420 242 459 205 • Fax: +420 284 821 646
Email: nakup@suweco.cz • Web site: http://www.suweco.cz

FRANCE
Form-Edit
5 rue Janssen, PO Box 25, 75921 Paris CEDEX, FRANCE
Telephone: +33 1 42 01 49 49 • Fax: +33 1 42 01 90 90
Email: fabien.boucard@formedit.fr • Web site: http://www.formedit.fr

Lavoisier SAS
14 rue de Provigny, 94236 Cachan CEDEX, FRANCE
Telephone: +33 1 47 40 67 00 • Fax: +33 1 47 40 67 02
Email: livres@lavoisier.fr • Web site: http://www.lavoisier.fr

L'Appel du livre
99 rue de Charonne, 75011 Paris, FRANCE
Telephone: +33 1 43 07 43 43 • Fax: +33 1 43 07 50 80
Email: livres@appeldulivre.fr • Web site: http://www.appeldulivre.fr

GERMANY
Goethe Buchhandlung Teubig GmbH
Schweitzer Fachinformationen
Willstätterstrasse 15, 40549 Düsseldorf, GERMANY
Telephone: +49 (0) 211 49 874 015 • Fax: +49 (0) 211 49 874 28
Email: kundenbetreuung.goethe@schweitzer-online.de • Web site: http://www.goethebuch.de

HUNGARY
Librotrade Ltd., Book Import
Pesti ut 237. 1173 Budapest, HUNGARY
Telephone: +36 1 254-0-269 • Fax: +36 1 254-0-274
Email: books@librotrade.hu • Web site: http://www.librotrade.hu

INDIA
Allied Publishers
1st Floor, Dubash House, 15, J.N. Heredi Marg, Ballard Estate, Mumbai 400001, INDIA
Telephone: +91 22 4212 6930/31/69 • Fax: +91 22 2261 7928
Email: alliedpl@vsnl.com • Web site: http://www.alliedpublishers.com

Bookwell
3/79 Nirankari, Delhi 110009, INDIA
Telephone: +91 11 2760 1283/4536
Email: bkwell@nde.vsnl.net.in • Web site: http://www.bookwellindia.com

ITALY
Libreria Scientifica "AEIOU"
Via Vincenzo Maria Coronelli 6, 20146 Milan, ITALY
Telephone: +39 02 48 95 45 52 • Fax: +39 02 48 95 45 48
Email: info@libreriaaeiou.eu • Web site: http://www.libreriaaeiou.eu

JAPAN
Maruzen-Yushodo Co., Ltd.
10-10, Yotsuyasakamachi, Shinjuku-ku, Tokyo 160-0002, JAPAN
Telephone: +81 3 4335 9312 • Fax: +81 3 4335 9364
Email: bookimport@maruzen.co.jp • Web site: http://maruzen.co.jp

RUSSIAN FEDERATION
Scientific and Engineering Centre for Nuclear and Radiation Safety
107140, Moscow, Malaya Krasnoselskaya st. 2/8, bld. 5, RUSSIAN FEDERATION
Telephone: +7 499 264 00 03 • Fax: +7 499 264 28 59
Email: secnrs@secnrs.ru • Web site: http://www.secnrs.ru

UNITED STATES OF AMERICA
Bernan Associates
4501 Forbes Blvd., Suite 200, Lanham, MD 20706-4391, USA
Telephone: +1 800 865 3457 • Fax: +1 800 865 3450
Email: orders@bernan.com • Web site: http://www.bernan.com

Renouf Publishing Co. Ltd.
812 Proctor Avenue, Ogdensburg, NY 13669-2205, USA
Telephone: +1 888 551 7470 • Fax: +1 888 551 7471
Email: orders@renoufbooks.com • Web site: http://www.renoufbooks.com

Orders for both priced and unpriced publications may be addressed directly to:

IAEA Publishing Section, Marketing and Sales Unit
International Atomic Energy Agency
Vienna International Centre, PO Box 100, 1400 Vienna, Austria
Telephone: +43 1 2600 22529 or 22530 • Fax: +43 1 2600 29302
Email: sales.publications@iaea.org • Web site: http://www.iaea.org/books